Aeolian sand transport processes, Part 1: model formulation and calibration

by Leo C. van Rijn; www.leovanrijn-sediment.com

1. Introduction

The wind-driven emission, transport, and deposition processes of sand and dust by wind are termed aeolian processes, after the Greek god Aeolus, the keeper of the winds. Aeolian processes occur wherever there is a supply of granular material and atmospheric winds of sufficient strength: in deserts, on beaches, and in other sparsely vegetated areas, such as dry lake beds. The blowing of sand and dust in these regions helps to shape the surface through the formation of sand dunes and ripples.

The terms dust and sand usually refer to solid particles that are created from the weathering of rocks. Sand is defined as mineral particles with diameters between 63 and 2,000 μm, whereas dust is defined as particles with diameters smaller than 63 μm.
Aeolian sand transport depends on:

- wind speed, direction and duration,
- sand composition (particle size and distribution),
- environmental conditions (moisture, vegetation, beach width, dune height, beach nourishment practices, type of coast: erosive, stabile or accretive).

Many descriptions of the present note are taken from the work of Nickling and Davidson-Arnott (1990), Kok et al. (2012) and Valance et al. (2015).
The author has published 3 papers on the subject Aeolian sand transport:

- L.C. van Rijn and G. Strypsteen, 2020, A fully predictive model for aeolian sand transport, Coastal Engineering, Vol. 156 (103600);
- L.C. van Rijn, 2022; A fully predictive model for aeolian sand transport, part 2: Description and calibration of models and effect of moisture and coarse materials; Coastal Engineering, Vol. 171 (104052);
- L.C. van Rijn, 2022; A fully predictive model for aeolian sand transport, part 3: Verification and application of model for natural beaches; Coastal Engineering, Vol. 171 (104051).

2. Physical processes and modes of wind-blown sand transport

2.1 Physics of wind-blown sand

Sand transport commences as soon as the threshold is exceeded. The transport of particles by wind can occur in several modes, which depend predominantly on particle size and wind speed.
The physics of aeolian saltation can be roughly divided into four main physical processes (**Figure 2.1.1**):

- the initiation of saltation by the aerodynamic lifting of surface particles (threshold/critical shear velocity),
- the subsequent trajectories of saltating particles,
- the splashing of surface particles into saltation by impacting saltators, and
- the modification of the wind profile by the drag of saltating particles.

The dominant mode of transport for sand particles in the size range of 100 to 300 μm is the saltation type of transport (small ballistic type of hops). As wind speed increases, sand particles of about 100 μm diameter are the first to be moved by fluid drag. After lifting, these particles hop along the surface in a process known as saltation. The impacts of saltating particles can also mobilize other particles. However, the acceleration of particles with diameters in excess of about 500 μm is strongly limited by their large inertia, and these particles generally do not saltate. Instead, they usually settle back to the soil after a short hop (< 10 mm) in a mode of

transport known as reptation. Alternatively, larger particles can roll or slide along the surface, driven by impacts of saltating particles and wind drag forces in a mode of transport known as creep and reptation.

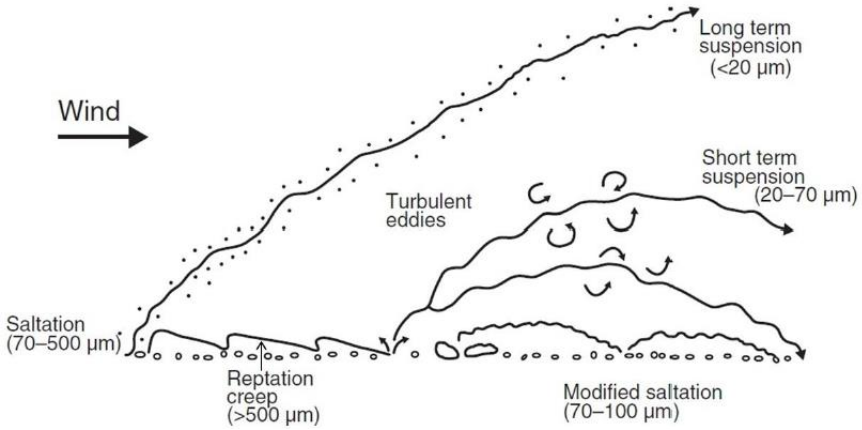

Figure 2.1.1 *Modes of wind-blown transport of sediment (Kok et al., 2012)*

These processes (creep, reptation and saltation; **Figure 2.1.1**) produce an exponential increase in the particle concentration, which leads to increasing drag on the wind, thereby retarding the wind speed in the saltation layer. It is this slowing of the wind that acts as a negative feedback by reducing particle speeds, and thus the splashing of new particles into saltation, which ultimately limits the number of saltating particles and thereby partially determines the characteristics of steady state saltation.
Very small particles are predominantly ejected from the soil by the impacts of saltating particles. Following ejection, dust particles are susceptible to turbulent fluctuations and thus usually enter short-term or long-term suspension. Very small particles (fine fraction) ranging from 63 to 100 µm are transported in suspension by turbulent eddies. Sand particles between 100 and 300 µm are mostly transported by making saltations (small hops). The largest particles (coarse fraction) ranging from 300 to 2000 µm are transported by sliding and rolling as surface creep. The transport of particles by rolling, sliding and small hops (saltations) can be defined as bed load transport of particles in more or less continuous contacts with the bed. Bed load transport of particles in a thin transport layer is the dominant mode of transport for sand particles (100 to 300 µm) in air. Observations in wind tunnels and in nature show that most of the transport occurs in a thin layer (< 0.05 m) above the sand surface (Ho, 2012.). In this thin transport layer, the particle velocity (averaged over the layer thickness) is almost insensitive to the external wind velocity above the transport layer and approximately equal to the 3 to 4 times the threshold bed shear velocity ($u_p \cong$ 3 to 4 $u_{*,cr}$). Particle concentration is so high that the wind velocity is strongly reduced to a value of the order of 0.8 to 1.2 m/s (Kok et al., 2012). An increase of the wind velocity results in an increase of the particle concentration which in turn leads to a decrease of the wind flow speed close to the bed such that the new equilibrium particle velocity remains almost unchanged (Valance et al., 2015).
Above the saltation layer, the suspended particle concentrations are much smaller, and the air flow is almost unaffected by the presence of the particle. As a result, the particle velocity above the saltation layer increases with increasing wind velocity (Valence et al., 2015).
A flat sand bed exposed to a wind strong enough to set grains into motion is unstable. That is, saltation over an initially flat sand bed results in the generation of two types of bedforms with distinct length scales: ripples with length scales of up to $1000d_{50}$ and dunes, which are typically 5 to 10 meters high but can reach lengths of 100 to 300 m. Dunes occur frequently as isolated objects moving on a firm ground (such as barchan dunes in a corridor) but also as multiple dunes evolving on a dense sand bed. Ripples appear most commonly on the surface of dunes as chains of small undulations that orient transversely to the wind trend. The physics governing the formation of ripples and dunes has been studied since the pioneering field works by Bagnold (1941, 1954). Many insights have been gained during the last few decades from computer modeling.

2.2 Details of saltation processes

After the saltation fluid threshold is exceeded, particles are lifted from the surface are quickly accelerated by the wind into ballistic trajectories and, after several hops, have sufficient momentum to splash surface particles. These newly ejected particles are themselves accelerated by wind and eject more particles when impacting the surface, causing an exponential increase in the horizontal saltation flux in the initial stages of saltation. This rapid increase in the particle concentration produces a corresponding increase in the drag of saltating particles on the fluid, thereby retarding the wind speed. This in turn reduces the speed of saltating particles, such that a steady state is reached when the speed of saltating particles is reduced to a value at which there is a single particle leaving the soil surface for each particle impacting it.

The distance required for saltation to reach steady state is characterized by the saturation length. Its value depends on several length scales in saltation, such as the length of a typical saltation hop, the length needed to accelerate a particle to the fluid speed, and the length required for the drag by saltating particles to retard the wind speed. The saturation distance is about 10 to 30 m for dry loose sand.
In addition to the saturation length, the adjustment distance is another characteristic length scale over which the horizontal saltation flux increases to a steady state. The corresponding adjustment effect arises because the atmospheric boundary layer flow adjusts to the increased roughness of the surface layer produced by saltation. The increased surface roughness acts as a greater sink of horizontal fluid momentum, which increases the downward flux of fluid momentum, thereby increasing the wind shear velocity for a given free stream wind speed in the atmospheric boundary layer. This process acts as a positive feedback on saltation and is termed the Owen effect. Field studies indicate that the adjustment distance for a flat field site is of the order of about 100 to 200 meters (Davidson-Arnott et al., 2008).
Saltation is in steady state when its primary characteristics, such as the horizontal mass flux and the concentration of saltating particles, are approximately constant with time and distance. Since wind speed can undergo substantial turbulent fluctuations, this is rarely true on timescales longer than minutes or often even seconds, causing saltation to be highly intermittent. In fact, a substantial fraction of sand transport occurs in aeolian streamers or sand snakes, which are probably produced by individual eddies of high-speed air. These streamers have typical widths of about 0.2 meters, thereby producing strong variability on short time and length scales.
The particle concentration in transport-limited saltation is in steady state when there is exactly one particle leaving the soil bed for each particle impacting it. An equivalent constraint is that for each saltating particle lost to the soil bed due to failure to rebound upon impact, another particle must be lifted from the soil bed and brought into saltation by either splash or aerodynamic entrainment.
Wind tunnel experiments show that particles are splashed at impact speeds typical of saltation (about 1 m/s for loose sand). Particle entrainment in steady state is dominated by splash, not by direct fluid lifting.

The splashing of surface particles by impacting particles is the main source of new saltators after saltation has been initiated. The particles strike the soil nearly horizontally and rebound at angles of about 40° from horizontal. The impact on the soil surface partially converts the saltator's horizontal momentum gained through wind drag into vertical momentum. This conversion is critical to replenish the vertical momentum dissipated through fluid drag.
The impact of a saltating particle on the soil bed can thus produce a rebounding particle as well as one or more splashed particles.

Numerical computer simulations show saltation heights of 15 to 30 mm and saltation lengths of 200 to 500 mm for particles in the range of 100 to 500 μm under a wind speed of about 10 m/s ($u_* \cong 0.4$ m/s). Saltation heights are about 50 mm for a wind speed of 25 m/s. These computed values are much smaller than observed values, see **Figures 4.2.2** and **4.2.4**.

The saltation height (δ_{sal}) of the sand particles in air scales with the particle size (d_{50}), and the excess shear velocity ($u_*-u_{*,th}$). Based on analysis of the measured data of Yang et al. (2019), a tentative relationship similar to that for the saltation height in water (Van Rijn 1987) is:

$$\delta_{sal}=\alpha_{sal}\,(d_{ref}/d_{50}^{0.5})\,(u_*-u_{*,th})/g^{0.5} \qquad (2.2.1)$$

with α_{sal} =150, d_{ref}=0.00025 m, $u_{*,th}$= threshold shear velocity (see Equation 3.1.4) being in the range of 0.16 to 0.36 m/s for particles in the range of 50 to 500 μm. Data are given in **Table 2.2.1**. Equation (2.2.1) has the correct dimension of length and shows a decreasing thickness of the transport layer for increasing particle size, see **Figure 2.2.2**.
The saltation length is given by:

$$L_{sal} = 20\,\delta_{sal} \qquad (2.2.2)$$

Shear velocity u_* (m/s)	**Saltation height δ_{sal} (m)**		**Saltation length $L_{saltation}$ (m)**	
	Computed	**Observed[1]**	**computed**	**observed**
0.4	0.08	0.1-0.2	1.6	-
0.6	0.23	0.2-0.3	4.6	-
0.8	0.36	0.3-0.4	7.2	-

[1]data of Han et al. (2012) and Yang et al. (2019)
Table 2.2.1 *Saltation height and length for sand particles of 0.3 mm*

Figures 2.2.1 and **2.2.2** show the saltation height (δ_{sal}) and distance (L_{sal}) for sand grains in the range of 20 to 500 μm based on Equations (2.2.1) and (2.2.2). The maximum saltation height and length of 50 μm-particles is about 1.5 m and 30 m during storm conditions (BF 9).
Observations in wind tunnels and in nature show that the particle velocity (averaged over the transport layer thickness) is almost insensitive to the external wind velocity above the transport layer and approximately equal to about $10(gd)^{0.5}$at the sand surface to about $40(gd)^{0.5}$ at the top of the transport layer (d=particle size). This range is approximately equal to 2 to 5 times the threshold bed shear velocity ($u_p\cong$ 2 to 5 $u_{*,th}$).
Particle concentration is so high that the wind velocity is strongly reduced to a value of the order of 1 (±0.5) m/s. An increase of the wind velocity results in an increase of the particle concentration which in turn leads to a decrease of the wind flow speed close to the bed such that the new equilibrium particle velocity remains almost unchanged (Valance et al., 2015). **Figure 2.2.3** shows particle velocity data.
Above the saltation layer, the particle concentration is much smaller and the air flow is almost unaffected by the presence of the particle. As a result, the particle velocity above the saltation layer increases with increasing wind velocity (Valence et al., 2015).
Summarizing: the speed of energetic particles moving mostly at the top of the transport layer increases with the bed-shear velocity u_*, whereas the speed of less energetic particles moving mostly close to the sand surface remains approximately constant.

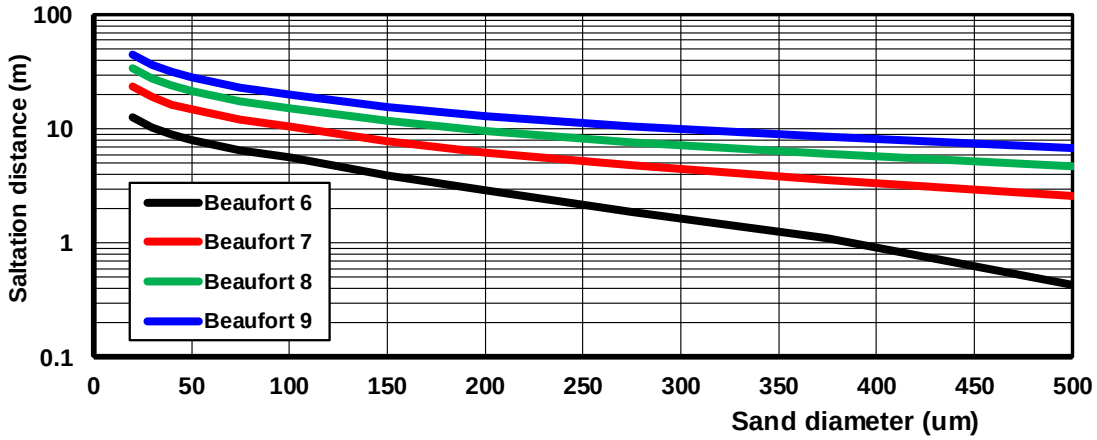

Figure 2.2.1 *Saltation distance as function of sand diameter and wind speed*

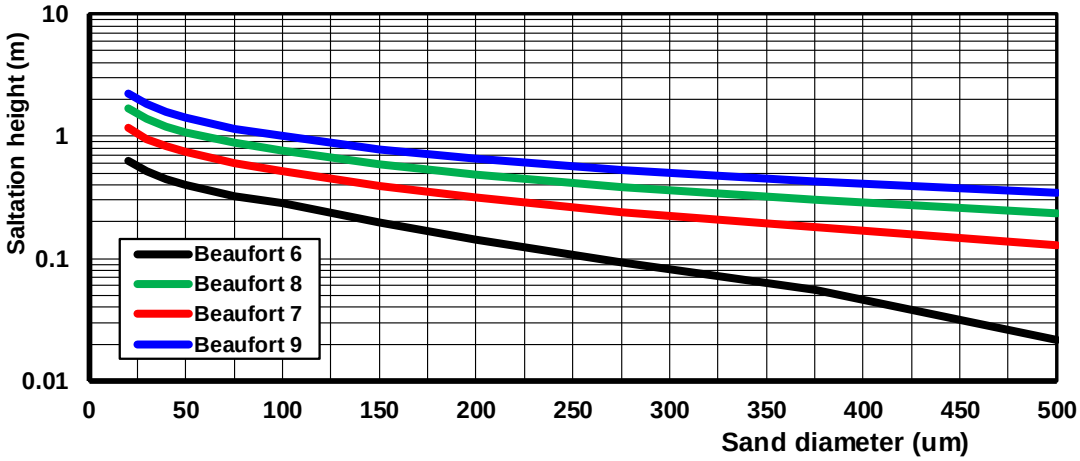

Figure 2.2.2 *Saltation height as function of sand diameter and wind speed*

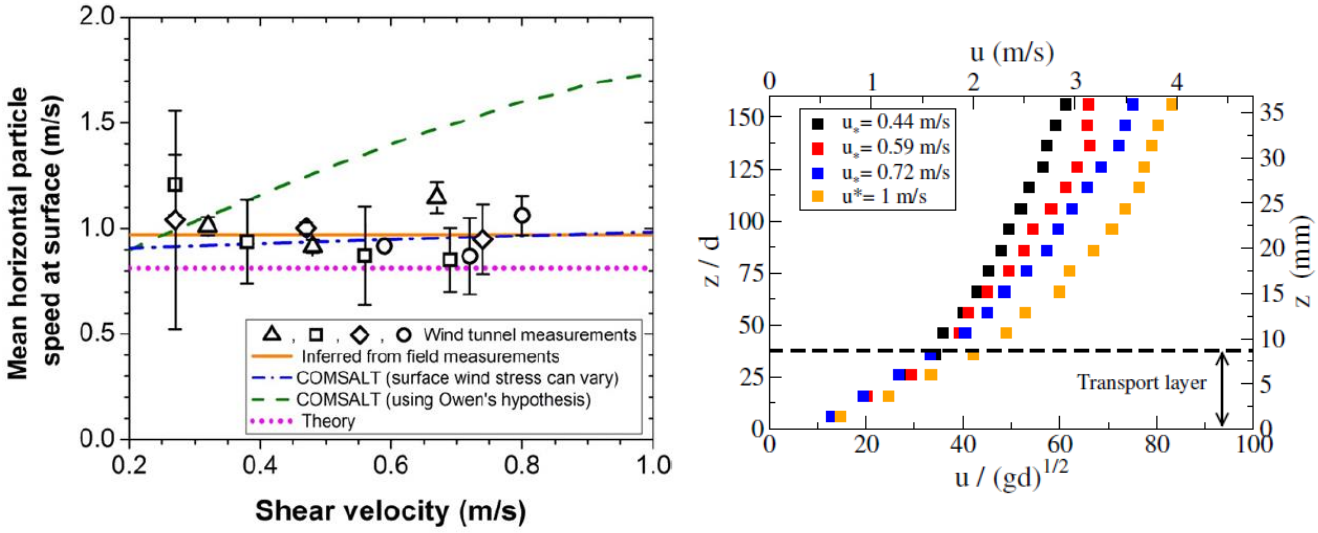

Figure 2.2.3 *Particle velocity data*
Left: Measured and computed mean horizontal particle velocity at surface (Kok et al., 2012)
Right: Measured particle velocity profiles for sand d_{50}=0.23 mm (Valance et al., 2015)

Summarizing, the transport of particles by wind can be crudely separated into several physical regimes:

- long-term suspension (< 20 µm),
- short-term suspension (20 - 63 µm),
- saltation (63 - 500 µm), and
- reptation and creep (> 500 µm).

Furthermore, we can distinguish between:

- transport-limited saltation, for which the amount of saltating sand is limited by the availability of wind momentum to transport the sand;
- supply-limited saltation, for which the amount of saltating sand is limited by the availability of loose soil particles that can participate in saltation, which can occur for crusted or wet soils.

2.3 Available instrumentation

Aeolian sand transport can be measured if accurate instrumentation is available. The most basic instruments are:

- wind velocity meter (vane or cup-type sensors);
- electronic grain impact sensors (saltiphones); piezo-electric sensor; laser-type sensor; high-frequency fluctuations can be detected/measured; able to resolve the HF spatial and temporal variability in saltation flux resulting from wind turbulence in the atmospheric boundary layer;
- trap type instruments (Leatherman trap; MCAW trap; BES trap; Streamer trap); one bulk sample over the test duration is obtained.

A saltiphone is a commercially available sampler which consists of a microphone installed in a stainless-steel tube mounted on a ball bearing (**Figure 2.3.1**; Poortinga et al., 2013). Sand particles that hit the microphone produce a high-frequency signal. Frequencies of about 8 Khz are amplified and used to determine saltation whereas other frequencies that are caused by rain and wind are reduced using a narrow band filter. Two output signals are provided: a digital pulse and an analogue voltage. The digital signal gives an output that is translated into number of counts. The analogue output signal also provides this information but has the additional option of measuring the intensity of particle impacts because it measures the energy of impact on the membrane. In this mode, the output signal represents the kinetic energy of the particles, and thus particle size and speed. Calibration is required to relate the output variables to sand transport rates. Calibration problems are the accuracy of input reference conditions (other trap-type sampler co-located beside the sensor), the saturation effects, the sensitivity of each microphone affecting the acoustic signal and the cleanliness of the output signal (noise ratio).
A similar type of sensor is the piezo-electric sensor which generates an electric pulse when a saltating particle hits the piezoelectric element.
Laser-based systems use a laser beam and photo sensors to detect sediment particles crossing the laser beam.
Various trap-type samplers are available (Poortinga et al., 2013). The original Wilson and Cooke trap consists of a bottle containing an inlet and outlet, whereby the trapped sediment is deposited in the bottle. In later studies, these bottles were mounted on a pole equipped with a sail to ensure that the inlet was always directed towards the wind (**Figure 2.3.1**). This extended setup is called the Modified Wilson and Cooke (MWAC) trap. The MWAC-traps showed good performance in a wind tunnel study (Poortinga et al. 2103). The MWAC- trap may be problematic to use at coastal beaches in strong winds with rain and salt sprays leading to blocking/clogging of the small intake openings (De Grande and De Moor, 2019). Bottles/traps close to beach surface may easily generate small scour holes and can therefore not be used close to the sand surface, where most of the sand is moving.

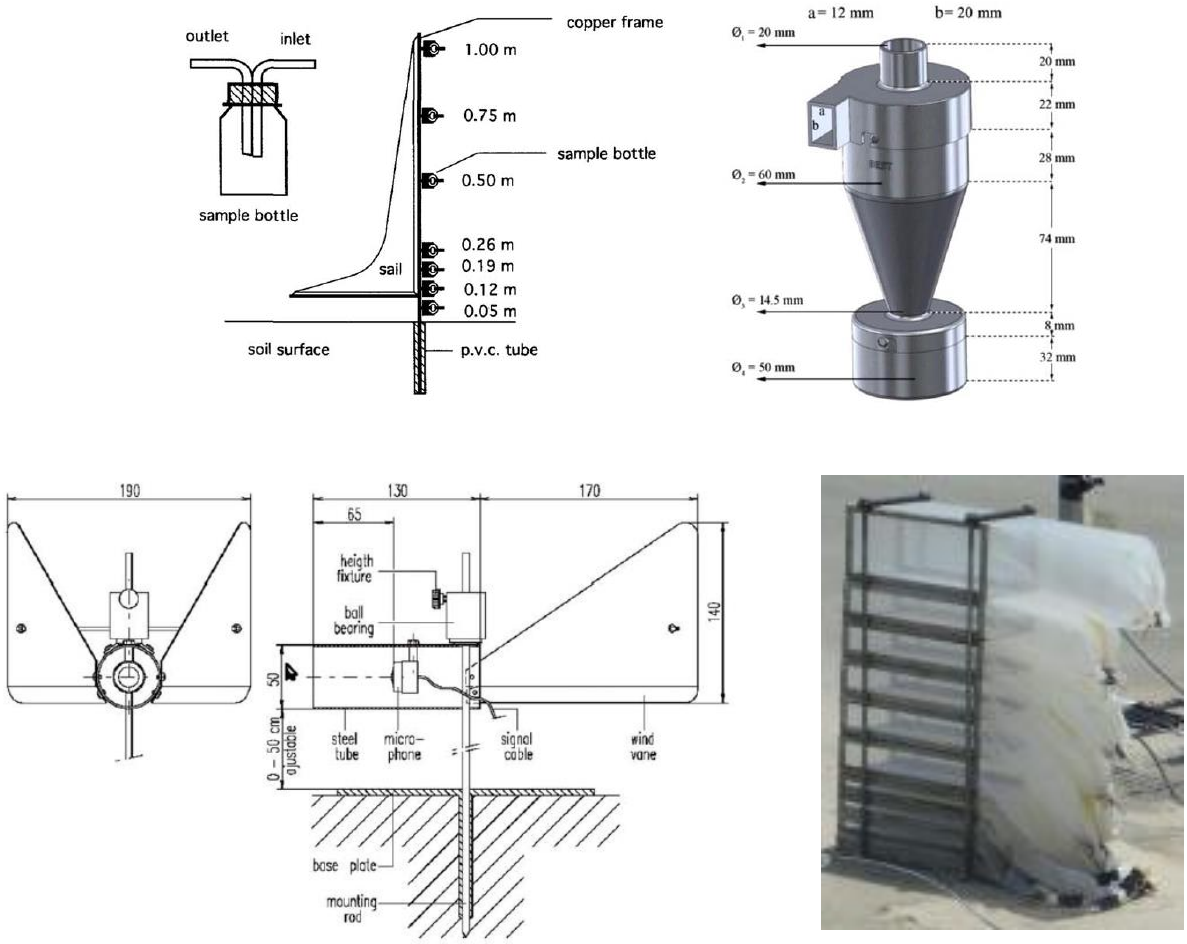

Figure 2.3.1 *Instrumentation for aeolian sand transport (Poortinga et al., 2013)*
Upper left: Modified Wilson-Cook trap (MWAC); Upper right: Basaran-Erpul Sediment trap (BEST)
Lower left: Saltiphone sensor; Lower right: Sherman Streamer trap (SST)

The trap of Basaran and Erpul (BEST) is a cyclone-type trap with a conical shape (**Figure 2.3.1**). Sediment enters the trap via an inlet and follows a circular trajectory within the cone. The heaviest particles will settle due to gravitational and centrifugal forces whereas the lightest particles will be evacuated through the outlet. The Sherman streamer trap (SST) is a simple trap with a nylon bag (50 or 63 µm) wherein the sand particles are trapped, see **Figure 2.3.1**. This trap system (Sherman et al., 2014) is comprised of a vertical stack of thin stainless-steel rectangular frames enclosed with nylon mesh that maximizes flow through the trap and minimizes flow distortion. The nylon mesh can be adhered to the thin metal frame via spray adhesive. This cost-effective set of traps is easy to use, quick to deploy, easy to retrieve samples in the field and have excellent efficiency (Sherman et al., 2014), (Farrell and Swan, 2016).
The efficiency and behavior of different sediment traps were reported in numerous studies. Most of these studies used the controlled environment of a wind-tunnel, but some also performed a relative calibration in the field (Poortinga et al., 2013).
Basaran et al. (2016) compared two trap-type samplers at a field site in Turkey: BEST and MWAC. They found that the BEST was able to trap both sand and dust size particles up to 1.20 m above soil surface. The MWAC was not able to adequately trap sand particles.

3. Sand transport model for saturated conditions

3.1 Modification of Bagnold-equation

Sand transport commences as soon as the threshold is exceeded. The dominant mode of transport for sand particles in the size range of 100 to 300 μm is the saltation type of transport (small ballistic type of hops). Very small particles (fine fraction) ranging from 63 to 100 μm are transported in suspension by turbulent eddies. The largest particles (coarse fraction) ranging from 300 to 2000 μm are transported by sliding and rolling as surface creep. The transport of particles by rolling, sliding and small hops (saltations) can be defined as bed load transport of particles in more or less continuous contacts with the bed. Bed load transport of particles in a thin transport layer is the dominant mode of transport for sand particles (100 to 300 μm) in air. Observations in wind tunnels and in nature show that most of the transport occurs in a thin layer (< 0.03 m) above the sand surface (Ho, 2012.). In this thin transport layer, the particle velocity (averaged over the layer thickness) is almost insensitive to the external wind velocity above the transport layer and approximately equal to 3 to 4 times the threshold bed shear velocity ($u_p \cong$ 3 to 4 $u_{*,th}$). Particle concentration is so high that the wind velocity is strongly reduced to a value of the order of 0.8 to 1.2 m/s (Kok et al., 2012). An increase of the wind velocity results in an increase of the particle concentration which in turn leads to a decrease of the wind flow speed close to the bed such that the new equilibrium particle velocity remains almost unchanged (Valance et al., 2015).
Above the saltation layer, the suspended particle concentration is much smaller and the air flow is almost unaffected by the presence of the particle. As a result, the particle velocity above the saltation layer increases with increasing wind velocity (Valence et al., 2015).

Many researchers have proposed models for aeolian sand transport under ideal conditions with uniform and steady wind obeying the law of the wall; with almost uniform (size, composition) and dry sand on a horizontal sand surface without vegetation and other obstacles. Uncertainties related non-ideal conditions as present at field sites are discussed by Sherman et al. (2013). One of the first models for ideal conditions has been formulated by Bagnold (1936) and is most widely used. Sherman et al. (1998, 2013) and Strypsteen (2019) have shown that the Bagnold-model performs reasonably well in predicting sand transport of high-quality data sets.
Herein, only the Bagnold-model with minor modifications is proposed to be used as a predictive model. Strypsteen et al. (2019) have given a detailed description of the modified Bagnold-model. This model for dry sand particles reads as:

Similar to sand transport in rivers, the sand transport of dry sand in air can be described by a set of dimensionless parameters, being:

- dimensionless transport rate $\phi = q_{s,mass}/(\rho_s\, s^{0.5}\, g^{0.5}\, d_{50}^{1.5})$;
- dimensionless grain size $D_* = [(s-1)\, g/\upsilon^2)]^{1/3}\, d_{50}$;
- dimensionless bed-shear stress $\theta = u_*^2/[(s-1)\, g\, d_{50}]$;
- dimensionless density $s = \rho_s/\rho_a$ and $s-1 \cong s$ for air;

with:

$q_{s,mass}$ = mass sand transport (in kg/m/s);
ρ_s = sediment density (2650 kg/m³);
ρ_a = air density (1.2 kg/m³);
d_{50} = median grain size (m);
υ = kinematic viscosity of air (1.33 10^{-5} m²/s for 0 °C and 1.5 10^{-5} m²/s for 20 °C);
u_* = bed-shear velocity (m/s).

The sand transport equation can be most generally formulated as:

$$\phi = \alpha_1 (D_*)^{\beta} (\theta-\theta_{th})^{\gamma} \qquad (3.1.1)$$

with: θ_{th} = dimensionless bed-shear stress at threshold conditions, α_1, β, γ = coefficients.
Following Bagnold (1941) for bed-load transport in air and Meyer-Peter and Mueller (1948) for bed-load transport in water, the best value is γ=1.5 and thus:

$$q_{s,mass} = \alpha_1 (D_*)^{\beta} \rho_s [s^{0.5} g^{0.5} d_{50}^{1.5}] [s^{-1.5} g^{-1.5} d_{50}^{-1.5})] [u_*^2-u_{*,th}^2]^{1.5}$$

$$q_{s,mass} = \alpha_1 (D_*)^{\beta} \rho_s s^{-1} g^{-1} [u_*^2-u_{*,th}^2]^{1.5}$$
$$q_{s,mass} = \alpha_1 (D_*)^{\beta} (\rho_a/g) [u_*^2-u_{*,th}^2]^{1.5}$$
$$q_{s,mass} = \alpha_2 (D_*)^{\beta} (\rho_a/g) [u_*^3-u_{*,th}^3]$$
$$q_{s,mass} = \alpha_2 [(s\, g/\upsilon^2)^{\beta/3} (d_{50,ref})^{\beta}] (d_{50}/d_{50,ref})^{\beta} (\rho_a/g) [u_*^3-u_{*,th}^3]$$

Using: s=2650/1.2=2208, υ=1.4 10^{-5} m^2/s, $d_{50,ref}$= 0.00025 m, β=0.5, it follows that

$$q_{s,mass} \cong 3.5\, \alpha_2 (d_{50}/d_{50,ref})^{0.5} (\rho_a/g) [u_*^3-u_{*,th}^3]$$
$$q_{s,mass} \cong \alpha_B (d_{50}/d_{50,ref})^{0.5} (\rho_a/g) [u_*^3-u_{*,th}^3]$$

which is a modified Bagnold-equation. Based on the work of Bagnold: $\alpha_B=3.5\alpha_2 \cong 2$

The modified Bagnold-equation for **dry** sand particles is herein given as:

Modified Bagnold (1941): $$q_{s,equilibrium}= \alpha_B\, \alpha_{ad}\, \alpha_{shell} (d_{50}/d_{50,ref})^{0.5} (\rho_{air}/g) [(u_*)^3- (u_{*,th})^3] \qquad (3.1.2)$$

Another expression is

Kok et al. (2012): $$q_{s,equilibrium}= \alpha_{DK}\, \alpha_{ad}\, \alpha_{shell} (\rho_{air}/g)\, u_{*,th} [(u_*)^2- (u_{*,th})^2] \qquad (3.1.3)$$

Threshold shear stress Bagnold (1941):

$$u_{*,th,B}= \alpha_{th} [(\rho_s/\rho_{air}-1)\, g\, d_{50}]^{0.5} \quad \text{for } d_{50}> 100\ \mu m \qquad (3.1.4a)$$
$$u_{*,th,B} = u_{*,th,100\ um} \quad \text{for } 32 < d_{50}< 100\ \mu m \qquad (3.1.4b)$$

Threshold shear stress and wind velocity including slope, turbulence and moisture effects:

$$u_{*,th}= \alpha_w\, \alpha_{slope}\, u_{*,th,B} \qquad (3.1.4c)$$
$$u_{w,th}= (u_{*,th}/\kappa) \ln(30z_w/k_s) \qquad (3.1.5)$$

Shear velocity:

$$u_* = \alpha_{veg}\, \alpha_{sh}\, \alpha_{acc}\, \kappa\, u_w/\ln(30z_w/k_s) \qquad (3.1.6)$$
$$u_{*,grain} = \alpha_{veg}\, \alpha_{sh}\, \alpha_{acc}\, \kappa\, u_w/\ln(30z_w/d_{90}) \qquad (3.1.7)$$

with:

$q_{s,equilibrium}$ = mass flux of sediment at equilibrium conditions (saturated transport);
d_{50} = particle size (m);
$d_{50,ref}$ =reference particle size = 250 10^{-6} m (0.25 mm; 250 μm);
ρ_{air} = density of air ($\cong$1.2 kg/m^3);
ρ_s = sediment density ($\cong$2650 kg/m^3);
g = acceleration of gravity (m/s^2);

u_* = surface shear velocity due to wind forces (m/s);
$u_{*,grain}$ = grain-related shear velocity (m/s);
$u_{*,th}$ = surface shear velocity at initiation of motion; threshold shear velocity (m/s);
k_s = equivalent roughness length scale of Nikuradse (m); and is related to the thickness of the transport layer and ripple height;
u_w = wind velocity at height z_w above the beach surface level (m/s);
z_w = height above the beach surface level at which wind velocity is defined;
κ = constant of Von Karman (=0.4);
α_B = Bagnold-coefficient for dry sand ($\cong$ 1.5 for uniform sand; $\cong$1.8 for naturally graded sand; $\cong$2.8 for widely graded sand);
α_{DK} = DK-coefficient ($\cong$ 5) for natural dry, loose sand particles;
α_{ad} = adjustment coefficient = $(L_{fetch}/L_{ad})^{0.6}$; (maximum 1);
α_{shell} = $(1-2p_{shell}/100)^2$= reduction coefficient related to the presence of shells;
α_{th} = 0.11 based on data of Shao-Lu (2000) and Han et al. (2011); $\cong$0.1 based on Bagnold (1941);
α_w = moisture coefficient =1+0.1(w_{20mm}); α_w=1 for dry sand (w_{20mm}=0%);
α_{veg} = vegetation coefficient=$[1-p_{veg}(\Delta_{veg}/\Delta_{veg,minimum})^{0.5}/100]^2$ with $\alpha_{veg,minimum}$=0.1;
Δ_{veg} = vegetation height; $\Delta_{veg,minimum}$= minimum vegetation height (= 0.1 m);
α_{sh} = sheltering coefficient (α_{sh}< 1 for sheltered sites; α_{sh}= 1 for exposed sites);
α_{acc} = coefficient related to wind acceleration for levels higher than beach level= 1+0.03h_s;
α_{slope} = coefficient for sand grains at a sloping surface= $[(1+\beta/\phi)^{0.75}(1+\gamma/\phi)^{0.37}]^{0.5}$;
w_{20mm} = moisture content of upper 20 mm= ratio of mass water and mass dry sand in sample x 100%;
p_{shell} = percentage of shells (0 to 30%);
p_{veg} = percentage of vegetation cover (%);
h_s = level above beach level (m); h_s= 0 = beach level;
L_{fetch} = fetch length at beach (input; about 10 to 100 m normal at beach);
L_{ad} = adjustment length scale of sand transport to equilibrium transport (input; about 100-200 m);
β = longitudinal slope angle (positive for upsloping windflow; negative for downsloping windflow);
γ = lateral slope angle and φ= angle of repose.

3.2 Initiation of saltation and threshold bed shear velocity

The value of the wind stress at which saltation is initiated is known as the static fluid threshold shear stress. This threshold depends not only on the properties of the fluid, but also on the gravitational and interparticle cohesion forces that oppose the fluid lifting. The fluid threshold is distinct from the dynamic or impact threshold, which is the lowest wind stress at which saltation can be sustained after it has been initiated. The impact threshold is smaller than the fluid threshold because the transfer of momentum to the surface through particle impacts is more efficient than through drag (Kok et al., 2012).
Herein, only the dynamic threshold shear velocity based on Equation (3.1.4) is used with α_{th}= 0.11 based on data of Shao-Lu (2000) and Han et al. (2011) whereas $\alpha_{th}\cong$0.1 based on Bagnold (1941). Experimental data (Kok et al., 2012) show that the measured threshold shear velocities of very fine sediment between 20 and 100 μm are scattered with values between 0.15 and 0.25 m/s. Equation (3.1.4a) underpredicts the measured values and therefore the shear velocity of fine sediment is herein assumed to be constant and equal to the threshold shear velocity of 100 μm-sand yielding a constant value of 0.16 m/s.
The transport processes for conditions around the threshold value are strongly dominated by the instantaneous turbulent fluctuations resulting in an intermittent transport process. For example, if the mean shear stress is equal to the threshold stress ($\tau_{mean}=\tau_{th}$), there still may a small net transport due the largest fluctuations ($\tau_{max}>\tau_{th}$). Basically, this can only be represented by using a stochastic approach (Davidson-Arnott et al., 2008).

When a grain is resting on a sloping surface, the threshold shear velocity is larger for upsloping wind flow and smaller for downsloping wind flow. A simple and fairly accurate is the method of Dey (2003), which has been slightly improved by the author: $\alpha_{slope}=u_{*,th,slope}/u_{*,th,o}=[(1+\beta/\varphi)^{0.75}(1+\gamma/\varphi)^{0.37}]^{0.5}$ with β=longitudinal slope angle (+ for upsloping flow; – for downsloping flow) , γ= lateral slope angle and φ= angle of repose.
Figure 3.2.1 shows the measured and computed data of Bagnold and others. Measurements of the fluid threshold for sand and dust are denoted by filled symbols, whereas measurements of the fluid threshold for materials other than sand and dust are denoted by open symbols.
Figure 3.2.2 shows the Bagnold-expression for particles in the range of 0.1 to 1 mm.

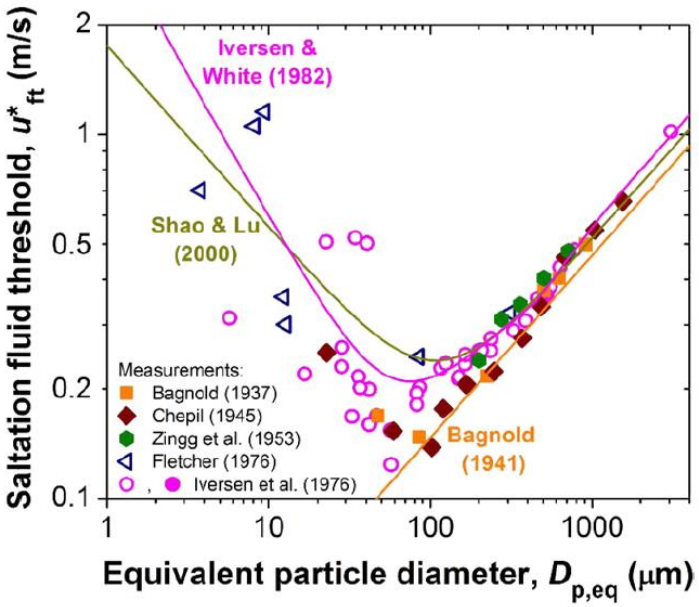

Figure 3.2.1 *Threshold shear velocity (Kok et al., 2012)*

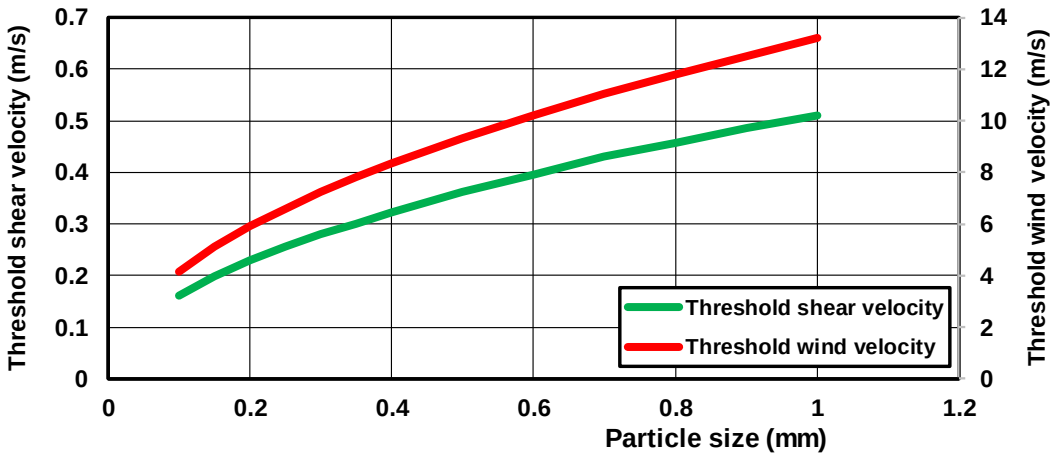

Figure 3.2.2 *Threshold shear velocity and wind velocity of dry, loose sand particles (k_s= 0.01 m, z_w= 10 m, κ=0.4, ρ_{air}=1.2 kg/m^3)*

3.3 Effect of grain size

Equation (3.1.2) has been used to compute the wind-induced sand transport.
In the case of dry sand with d_{50}= 300 μm= 0.0003 m; $u_{*,th}$= 0.28 m/s; α_{th}=0.11; the computed sand transport is:

u_*= 0.5 m/s:	$Q_{s,equilibrium,\ Bagnold}$	= $2x(300/300)^{0.5}$ (1.2/9.81) (0.5^3-0.28^3]	= 0.025 kg/m/s
	$Q_{s,equilibrium,\ DK}$	= $5x(1.2/9.81)x0.28x(0.5^2-0.28^2]$	= 0.029 kg/m/s
u_*= 1.0 m/s:	$Q_{s,equilibrium,\ Bagnold}$	= $2x(300/300)^{0.5}$ (1.2/9.81) (1^3-0.255^3]	= 0.24 kg/m/s
	$Q_{s,equilibrium,\ DK}$	= $5x(1.2/9.81)x0.28x(1^2-0.28^2]$	= 0.16 kg/m/s
u_*= 2.0 m/s:	$Q_{s,equilibrium,\ Bagnold}$	= $2x(300/300)^{0.5}$ (1.2/9.81) (2^3-0.255^3]	= 1.95 kg/m/s
	$Q_{s,equilibrium,\ DK}$	= $5x(1.2/9.81)x0.28x(2^2-0.28^2]$	= 0.67 kg/m/s

Figure 3.3.1 shows the wind-induced sand transport of dry, loose sand based on the formula of Bagnold for three sand diameters. It can be seen that the wind transport increases with grain diameter for wind speeds > 12 m/s (factor $d_{50}^{0.5}$ is dominant) and decreases with grain diameter for wind speeds < 12 m/s ($u_{*,th}$ is dominant).

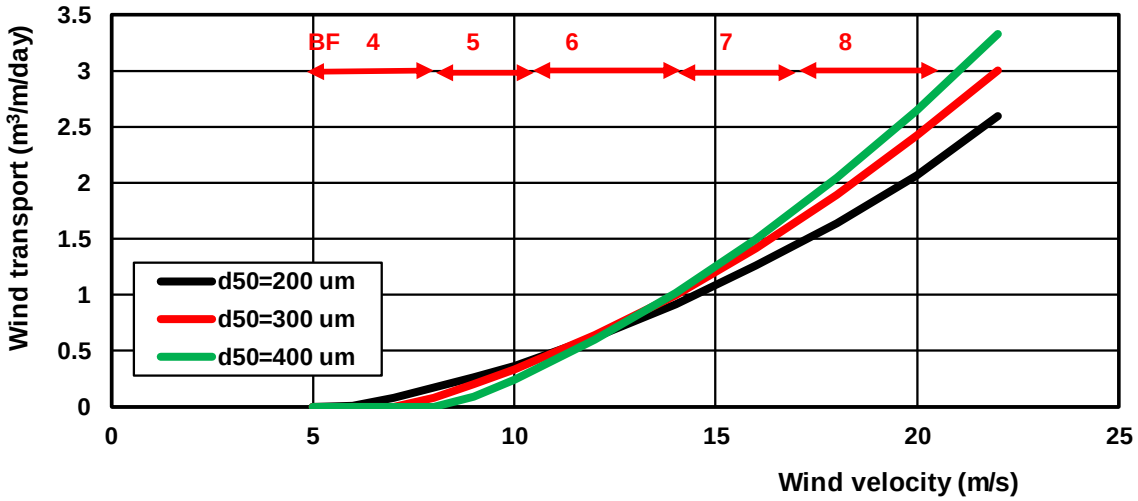

Figure 3.3.1 *Wind transport of dry, loose sand particles at beach based on Bagnold-equation. (k_s= 0.01 m, z_{wind}= 10 m, ρ_a= 1.2 kg/m³, α_B= 2; L_{fetch}=L_{ad}= 100 m)*

The ability of the modified Bagnold-equation to represent the effects of grain diameter and shear velocity is shown in **Figure 3.3.2** in comparison to the measured sand transport rates in the wind tunnel of Belly (1964) for three diameters (d_{50}=0.44, 0.3 and 0.145 mm). The coefficient of the modified Bagnold equation was set to 3.5 instead of 2 for optimum representation of the measured transport rates of 0.44 m-sand. This value of the coefficient was also used for 0.3 mm and 0.145 mm-sand. The measured values show that the sand transport rate of 0.145 mm-sand is much smaller than that of 0.44 mm and 0.3 mm-sand. The transport rate of 0.3 mm is smaller than that of 0.44 mm-sand form u_*>0.5 m/s, but larger for u_*<0.5 m/s. The modified Bagnold equation also shows this effect for u_*<0.4 m/s. The decrease of the transport rate for decreasing grain size is also shown by the Bagnold equation, but the effect is much too small for fine sand of 0.145 mm. The cubic relationship between the transport rate and the shear velocity is in good agreement with the measured values of the transport rate.

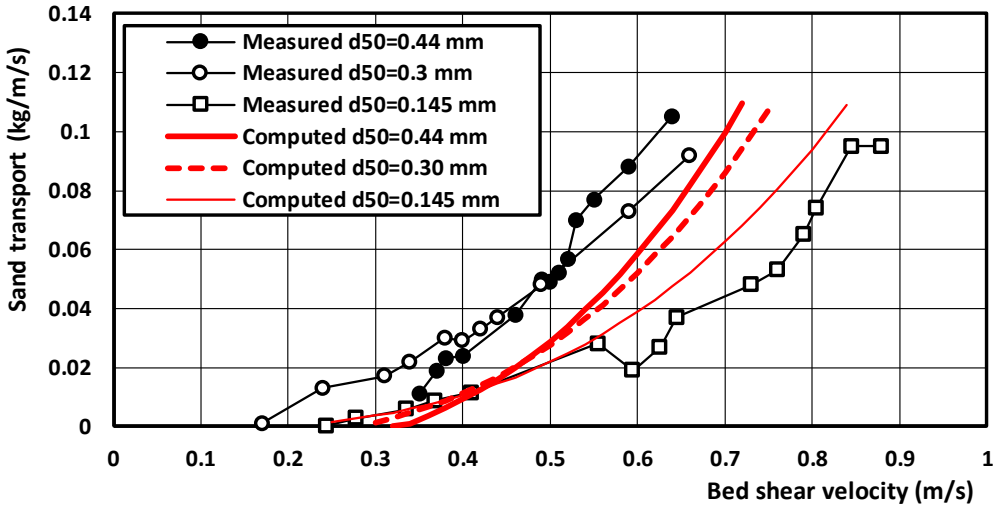

Figure 3.3.2 *Effect of grain diameter on transport of dry, loose sand particles based on modified Bagnold-equation; d_{50}=0.44, 0.3 and 0.145 mm; data of Belly (1964)*

The wind tunnel experiments of Han et al. (2011) and Yang et al. (2019) can be used to study the effect of grain diameter on the sand transport rate. Han et al. (2011) used a grain diameter of d_{50}=0.203 mm, while Yang et al. (2019) used a grain diameter of d_{50}=0.455 mm. The experiments were done in the same wind tunnel using the same sand trap sampler and wind speeds in the range of 8 to 22 m/s.
Figure 3.3.3 shows the measured sand transport rate as function of wind speed for two grain diameters. The accuracy of the sand transport rates is assumed to be about 30%. No effect of grain diameter can be observed for higher wind speeds >18 m/s, while the sand transport rate of the smaller grain diameter (fine sand) is larger for wind speeds <16 m/s. This latter is opposite to the grain diameter effect of the Bagnold-equation, which gives larger transport rates for larger diameters ($q_s \approx d_{50}^{0.5}$).

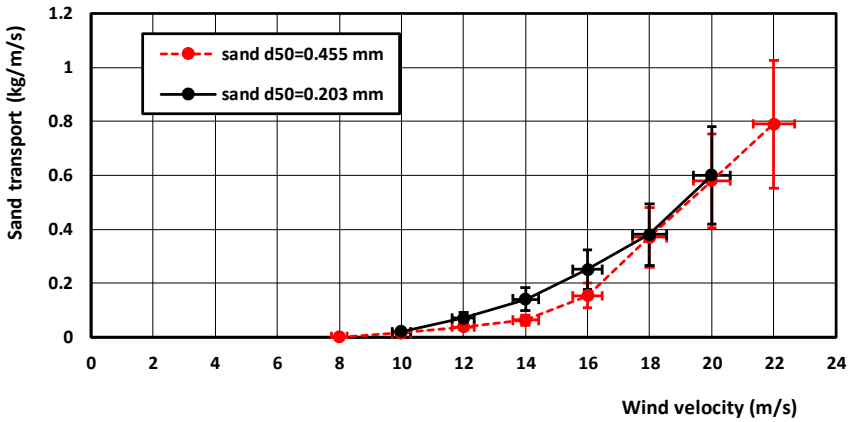

Figure 3.3.3 *Effect of grain diameter on sand transport; data of Han et al. (2011) and Yang et al. (2019)*

3.4 Bed roughness

3.4.1 Influencing parameters

The wind velocity in the near-bed region strongly depends on the effective or equivalent bed roughness (k_s) as defined by Nikuradse (see Equation 3.4.1). This roughness length (k_s) is defined as the equivalent grain roughness replacing any type of roughness yielding the same overall bed roughness (same velocity profile).
It is most logic to assume that the effective roughness (k_s) of the sandy beach surface is related to the:

- grain roughness effects of static and saltating particles (Owen, 1964; Farrell and Sherman, 2016; Field and Pelletier 2018);
- height of the micro bed morphology (ripples), (Pelletier and Field 2016, Field and Pelletier, 2018);
- size of shells or shell fragments/clusters which are sometimes abundantly available, particularly at nourished beaches.

The effective roughness length of an irregular sand surface is strongly related to the presence of flow separation, which is primarily controlled by the slopes, curvature and height of the irregularities. In particular, the roughness elements with the steepest slopes have the largest effect on the roughness length. Bed irregularities generate additional near-bed turbulent velocity fluctuations (turbulence) enhancing sand transport. In areas with abundant sand supply, the height and wavelength of aeolian ripples may increase with increasing shear velocity and increasing grain size. Little is known about the relative contribution of saltation processes and ripple formation to changes in roughness length (Field and Pelletier, 2018).
Most likely, the static and dynamic grain roughness are the most important components, but the role of form roughness is not yet fully clear. Both effects can be separated by the method of shear partitioning resulting in: $\tau=\tau^{/}+\tau^{//}$ with $\tau^{/}$= grain-related shear stress and $\tau^{//}$=form drag-related shear stress (Van Rijn 1993). Bed-load transport in water flow is mostly related to $\tau^{/}$, whereas suspended load transport is affected by both components ($\tau^{/}+\tau^{//}$). Wind tunnel experiments are required to evaluate the influence of form roughness on wind-blown sand transport (see also **Section 3.4.5**).
The field data sets of Sherman et al. (2013), described as a data set closely approaching ideal conditions for dry and unvegetated sand, were used to determine the roughness values required for perfect agreement of measured and computed sand transport rates using the modified Bagnold-equations (3.1.2) and (3.1.4) with $\alpha_B=2$ and $\alpha_{th}=0.11$ (and $\alpha_{ad}=\alpha_{shell}=\alpha_{veg}=1$). Thus, it is assumed that this equation is perfect and that discrepancies are only related to the uncertainties of the bed-shear velocity. The bed shear velocity is computed by using: $u_*=\kappa u_w/\ln(30z_w/k_s)$ with: u_w= measured wind velocity at height z_w=2 m above the surface, κ=0.4 and $k_{s,perfect}$=roughness height giving perfect agreement of measured and computed sand transport rates. The $k_{s,perfect}$-values were determined by trial and error until perfect agreement of measured and computed transport rates is obtained. This procedure was repeated using a smaller and larger transport coefficients $\alpha_B=1.5$ and $\alpha_B=2.5$ (range given by Bagnold) resulting in larger and smaller $k_{s,perfect}$-values (uncertainty range).
Figure 3.4.1 shows the ratio of the $k_{s,perfect}$ and $k_{s,measured}$ and the uncertainty range as function of the measured wind velocity at 2 m above the surface. Most values are smaller than 0.3, which suggest that the effective roughness required for sand transport is only a fraction of the overall roughness. When this effect is neglected and the overall roughness (measured shear velocity u_*) is used, the Bagnold-equation systematically overpredicts the measured sand transport rates of Sherman et al. (2013) by a factor of 2 to 5. Thus, most likely, the static and dynamic grain roughness (related to $\tau^{/}$) rather than the overall roughness are the dominant components for sand transport, similar to that for sand transport by flowing water (Van Rijn 1993). In **Section 3.4.4** a roughness predictor will be derived for the static and dynamic grain roughness.

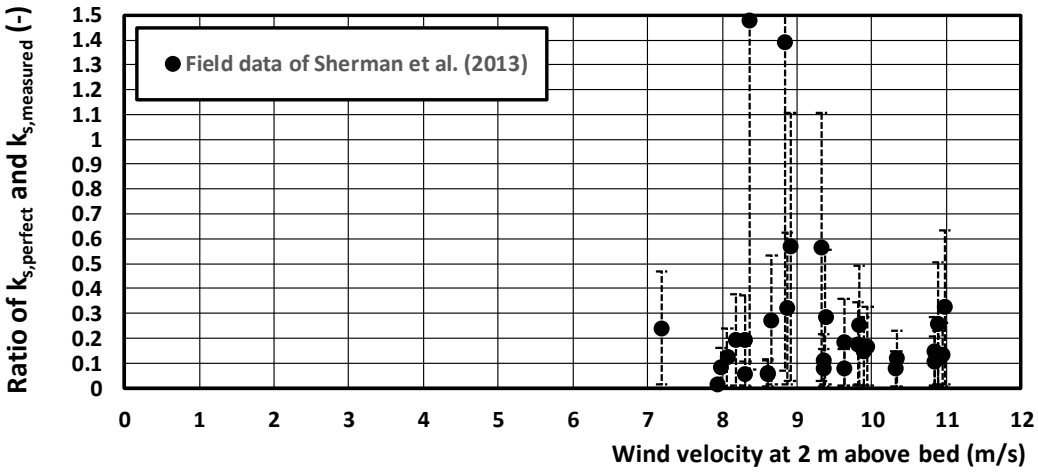

Figure 3.4.1 *Ratio of $k_{s,perfect}$ and $k_{s,measured}$ as function of the wind velocity*

3.4.2 Modification of near-surface wind velocity profile

The wind velocity without particles can be described by: $u_{wind,z} = (u_*/\kappa) \ln(z_w/z_o)$ (3.4.1)

where $\kappa = 0.40$ is von Kármán's constant, z_w= height above surface, z_o is the aerodynamic surface roughness, which denotes the height at which the logarithmic profile, when extrapolated to the surface, yields zero wind speed.

The large length scale of the atmospheric boundary layer in which saltation occurs causes the Reynolds number of the flow to be correspondingly large, typically in excess of 10^6 such that the flow in the boundary layer is turbulent. Since the horizontal fluid momentum higher up in the boundary layer exceeds that near the surface, eddies in the turbulent flow on average transport horizontal momentum downward through the fluid. Together with the much smaller contribution due to the viscous shearing of neighboring fluid layers, the resulting downward flux of horizontal momentum constitutes the fluid shear stress. Because the horizontal fluid momentum is transported downward through the fluid until it is dissipated at the surface, the shear stress is approximately constant with height above the surface for flat and homogeneous surfaces.

Equation (3.4.1) is based on the assumption that the shear stress in the surface layer is constant with height. This is a realistic approximation for flat, homogeneous surfaces, but can be unrealistic for other conditions, such as for surface with non-uniform surface roughness or substantial elevation changes. Furthermore, the drag by saltating particles reduces the horizontal momentum flux carried by the wind.

For small roughness-related Reynolds numbers (< 5), the roughness elements are too small to substantially perturb the viscous sublayer of about 0.4 mm, and the flow is known as aerodynamically smooth.
For large roughness-related Reynolds numbers (> 60), the roughness elements are so high that the viscous sublayer is substantially disrupted, and the flow is termed aerodynamically rough and $z_o=k_s/30$.
Aeolian saltation on earth takes place for roughness-related Reynolds numbers of 1 to 100 and thus usually occurs in the transition zone between the smooth and rough aerodynamic regimes. Since the roughness in the transition regime does not differ much from that in the aerodynamically rough regime, most studies have used $z_o=k_s/30$ to approximate the surface roughness.

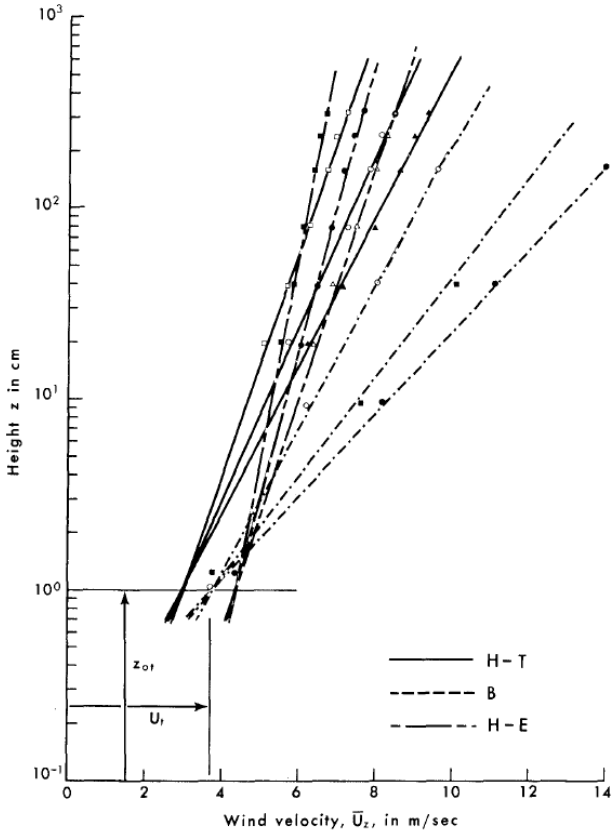

Figure 3.4.2 *Measured wind velocity profiles at three different sites (Hsu, 1974)*

The near-surface wind profile is modified through momentum transfer to saltating particles. Indeed, it is the retardation of the wind profile through drag by saltating particles that ultimately limits the number of particles that can be saltating under given conditions.
According to Bagnold (1941), the velocity profile in the near-bed layer is better described by:

$$u_{wind,z} - u_{wind,th} = (u_*/\kappa)\ \ln(z_w/z_{o,th}) \qquad (3.4.2)$$

with: $u_{wind,th}$= wind velocity at threshold conditions at level $z_w=z_{o,th}$ (see **Figure 3.4.2**).
Bagnold states that the wind velocity in the saltation layer is reduced by drag forces to wind velocity just beyond initiation of movement (threshold conditions).

Li et al. (2010) studied the variability of the apparent von Kármán parameter (κ_a) during aeolian saltation in a field experiment with dry sand in the range of 0.22 to 0.44 mm at Jericoacoara, Ceará, Brazil. To test this variability, velocity profiles, Reynolds stress and sand transport data were measured and analyzed. For a steady state, homogeneous turbulent boundary layer there is a constant stress layer within which: $\tau = -\rho \langle u'w' \rangle = \rho u_*^2$ with τ=shear stress, u' and w' = instantaneous horizontal and vertical velocity fluctuation components, ρ= density of air and <>=time-averaging.
The term $-\rho \langle u'w' \rangle$ represents the Reynolds stress. The time-averaged velocity profile data can be used to determine the bed-shear velocity as: $u_*= \kappa_a$ m, with m is the slope of the least squares line fit to the velocity profile by linear regression of ln(z) (independent variable) against u_z (dependent variable). This gives: $\kappa_a = [1/m]\ [\langle u'w' \rangle]^{0.5}$. The term $[\langle u'w' \rangle]$ was derived from the turbulent velocity measurements using an ultrasonic anemometer (R.M.Young 81000), with an internal sample rate of 160 Hz and 32 Hz output rate

over at least 2 minutes. The ultrasonic anemometer was mounted at 1 m above the bed and the sampling durations were 120 s or longer. To measure sediment transport rates and concentrations, vertical arrays of eight hose-style traps were deployed, with horizontal openings of 0.10 m and, from the surface up, vertical openings 0.025, 0.025, 0.050, 0.050, 0.050, 0.100, 0.100, and 0.100 m. The κ_a-parameter was found to be in the range of κ_a=0.25 for relatively large sand transport rate of 0.03 kg/m/s to about κ_a=0.4 for zero transport (17 data points).
The author has plotted the κ_a-parameter in **Figure 3.4.3** as function of a dimensionless transport parameter T (see Equation 3.4.8b), which is defined as: $T= [(u_{*,grain})^2 - (u_{*,th})^2]/(u_{*,th})^2$ with: $u_{*,grain}=\kappa u_w/(\ln(30z_w/d_{90})$, u_w = measured wind velocity at z_w=2 m, $u_{*,th}$= threshold bed-shear velocity based on Equation (3.1.4), κ=0.4 and $d_{90}=2d_{50}$.
The results can be represented by: $\kappa_a= \kappa_o e^{-0.25T}$ with κ_o=0.4, $\kappa_{minimum}$= 0.25 and T= transport parameter.

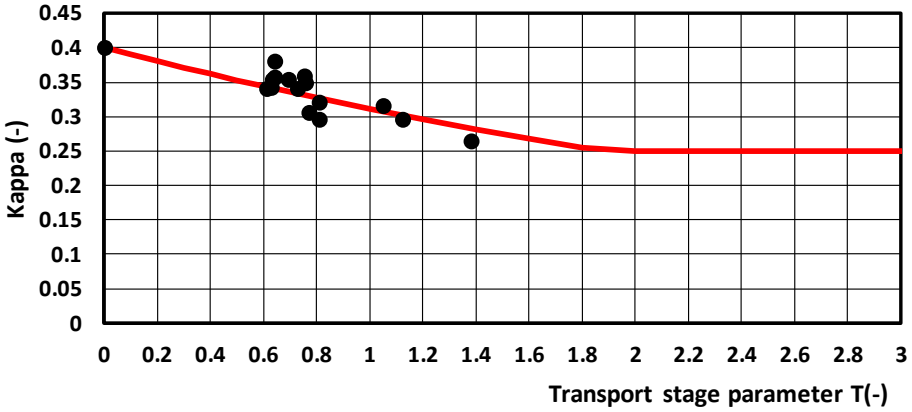

Figure 3.4.3 *κ_a-parameter as function of transport parameter T; data of Li et al. (2010)*

3.4.3 Effective bed roughness height (k_s)

Flat bed
Xian et al. (2002) studied the aerodynamic roughness length (z_o) values of various types of flat surfaces of coarse materials in a wind tunnel and in the Gobi desert in China. The Gobi desert surface is usually flat, unvegetated and covered with gravel. Wind erosion is active. Seven sites with a flat surface and free of vegetation were chosen. The site characteristics are (see also **Table 3.4.1**):

- site 1, 2, 3: mainly consists of gravel and cobblestone with a sandy matrix; wind-blown sand is minimum and the threshold velocity is 7 to 7.6 m/s (at a height of 0.4 m);
- Sites 4, 5: flat sand and gravel surface with active sand transport; the threshold velocity is 6.2 m/s (at the height of 0.4 m);
- sites 6, 7: sand surface with some tiny cobbles.

Measured static roughness parameters are given in **Table 3.4.1** based on wind velocity profile data (10 cup anemometers). The selected maximum wind speed was 7 m/s to avoid blown sand activity.
The field results show that the effective bed roughness is of the order of 5 to 10d for the gravel-type surfaces and about 100d for sand-type surfaces. The relatively large roughness values of the sand surfaces is most likely caused by the larger roughness elements (cobbles) resting on the bed. Soil moisture may also have a significant effect, see data of Site 4.

The wind tunnel experiments were conducted in a straight tunnel with length of 37 m (working section of 21 m long), width of 1.2 m and height of 1.2 m. The floor of the wind tunnel is made of aluminum alloy plates,

with an average aerodynamic roughness length of k_s=0.9 mm. The test beds (4 m long, 1.2 m wide) were located at 16 to 20 m downwind of the inlet of the working section. Each bed was covered with a layer of roughness elements. Five kinds of roughness elements were used: crushed gravel with percentage of coverage of 30%, 60% and 80% (sparse to close packing), smooth oblate shingle from the Yellow River, 5–10 mm cobblestone, 2–5 mm cobblestone and 0.5–2 mm coarse sand. The diameters of crushed gravel and smooth oblate (elongated) shingle were similar and both longer than 10 mm. The mean height of crushed gravel was 20 mm with maximum values up to about 50 mm. The mean height of shingle was only about 5 mm. The length, width and height of cobblestone were nearly identical.
The free stream velocity was varied in the range of 6 to 15 m/s. A Pitot tube for measuring wind profiles was installed in the middle of the test bed area at the 19.8 m mark of the working section and used to obtain profiles from 4 mm to 500 mm above the bed surface.

The main findings can be summarized (**Table 3.4.2**), as follows:

- the effective bed roughness of crushed gravel and oblate shingle is related to d_{max} and varies in the range of k_s/d_{max}= 0.5 to 10; the roughness increases for increasing percentage of coverage;
- the effective bed roughness of cobblestone 5-10 mm with coverage of 60% varies in the range of k_s/d_{max}= 5 to 10;
- the effective bed roughness of cobblestone 2-5 mm and coarse sand 0.5-2 mm with coverage of 60% varies in the range of k_s/d_{max}= 0.5 to 1.5;
- the shape of the roughness elements has not much effect on bed roughness; the roughness ratio k_s/d_{max} of smooth oblate shingle is almost the same as that of crushed gravel;
- the maximum height of the roughness element is the most influential parameter.

Site	Sediment coverage (%)	Average height of roughness elements d (mm)	Moisture condition	Roughness length		
				z_o (mm)	k_s (mm)	k_s/d (-)
1 Gravel	60	14.2	dry	1.9	57	4
2 Gravel	50	6.5	dry	1.5	45	7
3 Gravel	50	4.8	dry	0.7	21	4.4
4 Sand-Gravel	25	3.5	wet dry	1.1 0.05	33 1.5	9.4 0.4
5 Sand-Gravel	20	2.0	wet	0.5	15	7.5
6 Sand (fine powder sand with 50% clay and some tiny cobbles	10	≅0.1 (excl. tiny cobbles)	wet	0.4	12	≅ 100
7 Sand (fine powder sand with about 50% clay and with some tiny cobbles)	10	≅0.1 (excl. tiny cobbles)	dry	0.3	9	≅ 100

Table 3.4.1 *Measured roughness parameters for Gobi desert sites, China*

Type of sediment	Average height/diameter d (mm)	Maximum height/diameter d_{max} (mm)	Coverage (%)	Roughness parameters		
				z_o (mm)	k_s (mm)	k_s/d_{max} (-)
Crushed gravel	20.5	50	30	0.9-1.8	27-55	0.55-1.1
			60	2.6-3.4	78-102	1.6-2
			80	7.5-15	225-450	4.5-9
Oblate shingle	4.8	10	30	0.25-0.4	7.5-12	0.75-1.2
			60	0.7-1	21-30	2.1-3
			80	0.9-2.1	27-63	2.7-6.3
Cobblestone 5-10 mm	4.7	10	60	1.8-3.6	55-110	5.5-11
Cobblestone 2-5 mm	3.5	5	60	0.03-0.2	0.9-6	0.2-1.2
Coarse sand 0.5-2 mm	1.25	2	60	0.04-0.09	1.2-2.7	0.6-1.4

Table 3.4.2 *Measured roughness parameters for flat beds with sediment in wind tunnel*

Dong et al. (2002) performed wind tunnel experiments to determine the aerodynamic roughness length of spherical roughness elements of different size and coverage at free-stream wind velocities in the range of 4 to 22 m/s. The horizontal tunnel floor was covered with regular spherical roughness elements and varying percentages of coverage. Six diameters (D) in the range of 19 to 65 mm were used. The protrusion above the surrounding horizontal cement floor (D_h) was about 0.65D. The roughness elements were placed in diamond patterns on the smooth wind tunnel floor of the test section. The coverage is the ratio of total base area of the roughness elements and the area of tested tunnel floor.
The aerodynamic roughness is found to decrease for increasing free-stream wind velocity in the range of 4 to 10 m/s and is about constant for wind velocities > 10 m/s. The aerodynamic roughness increases with coverage for coverage values of 1% to 50 % and is about constant for coverage values > 50%. The author has used the data of Dong et al. to determine the effective bed roughness k_s in relation to the diameter D and D_h, see **Table 3.4.3**. If only a few isolated gravel particles are present (coverage< 1%), the measured bed roughness is almost completely determined by the roughness of the surrounding bottom (cement floor). For coverages > 10%, the bed roughness can be represented by:

- coverage 10%: $k_s/D \cong 0.1$ to 0.15;
- coverage 30%: $k_s/D \cong 0.3$ to 0.35;
- coverage > 50%: $k_s/D \cong 0.4$ to 0.5.

Gravel coverage	Gravel diameter D (mm) and gravel height H above the surface (mm)					
	D=19 mm **D_h=12 mm**	**29** **19**	**38** **24**	**47** **31**	**57** **37**	**65** **43**
1%	k_s=0.5-1 mm	k_s=0.5-1 mm	k_s=0.5-1 mm	k_s=0.5-1 mm	k_s=0.5-1 mm	k_s=0.5-1 mm
10%	k_s/D=0.15 k_s/D_h=0.25	0.15 0.25	0.15 0.25	0.10 0.15	0.10 0.15	0.10 0.17
30%	k_s/D=0.35 k_s/D_h=0.55	0.35 0.55	0.35 0.55	0.30 0.45	0.30 0.50	0.30 0.50
>50%	k_s/D=0.35 k_s/D_h=0.60	0.40 0.65	0.30 0.45	0.40 0.65	0.45 0.70	0.40 0.60

Table 3.4.3 *Effective roughness of gravel/pebble-type particles based on the data of Dong et al. (2002)*

Zhang et al. (2004) studied the surface roughness of cultivated soil by performing wind tunnel tests with five artificially prepared soil surfaces. Soil samples were taken from farmland in Guinan County of Qinghai Province in the semi-arid region of northwest China. Before that time, the farmland had been undisturbed soil covered with classic steppe vegetation. The soil is chestnut soil with 36% sand, 53% silt and 11% clay.
Five surface soil samples to the depth of 15 cm were taken in sample boxes (50 cm × 30 cm × 15 cm) that were in the form of shallow trays. The samples were dried to a moisture content of 2% and artificially prepared so that the diameters of the largest clods (D_{max}) are about 50, 25, 15, 10 and 1.5 mm. The samples were mixed so that different sized clods were approximately uniformly distributed on the soil surface, see **Figure 3.4.4**. The samples were tested at a constant free-stream wind velocity of 8 m/s. The percentage of coverage of the largest clods is estimated to be about 20% to 40%. The measured results are given in **Table 3.4.4**. The effective roughness of a flat bed with about 20% to 40% of large clods is found to be in the range of k_s/D_{max}=0.4 to 1.3.

Summarizing the results of Dong et al. (2002) and Zhang et al. (2004), it can be concluded that the static bed roughness of a flat, horizontal bed is determined by the diameter of the largest 10% of the grains/particles present on the surface. In the case of a flat sandy surface, the d_{90} is a good measure to represent the roughness of the surface. This is also valid for a subaqueous sand surface (Van Rijn 1993).

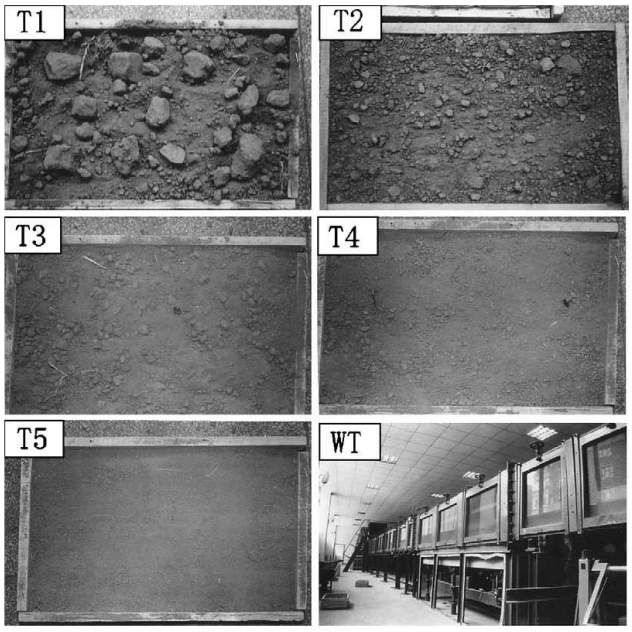

Figure 3.4.4 *Soil surfaces used by Zhang et al. (2004)*

Type of soil surface	Diameter of largest clods D_{max} (mm)	Roughness length z_o (mm)	Effective roughness k_s (mm)	Ratio k_s/D_{max} (-)
T1	50	2.5	75	0.67
T2	25	1.1	33	1.3
T3	15	0.47	14	0.93
T4	10	0.13	4	0.4
T5	1.5	0.05	1.5	1.0

Table 3.4.4 *Effective roughness of soil surface with large clods based on data of Zhang et al. (2004)*

Bed irregularities and bed forms

Owen (1964), based on analysis of field data, has found that the effective bed roughness of natural sandy surfaces with small-scale bed irregularities can be represented by:

$$z_o=\alpha_o\, u_*^2/2g \qquad (3.4.3)$$

$$k_s=30z_o=30\alpha_o\, u_*^2/2g$$

with: α_o= coefficient ($\cong$0.01). Thus, the bed roughness increases for increasing bed-shear velocity, either due to the increasing dynamic grain roughness (more saltating grains) and/or due to increasing bed forms (growing ripples). At very high wind velocities, the ripples will most likely disappear again.

Hsu (1974) analyzed various field data sets from a variety of environments with particles sizes between 0.2 and 0.3 mm, including those over beaches, tidal flats, and small dune fields in Barbados, Ecuador, Florida, and Texas and in the Libyan desert.
Based on these results, he proposed:

$$u_*=0.037\, u_{10m} \qquad (3.4.4a)$$

$$u_*=0.044\, u_{2m} \qquad (3.4.4b)$$

with: u_{2m}= wind velocity at z_w=2 m above bed and u_{10m}= wind velocity at z=10 m above bed.
Using: $u_{wind,z} = (u_*/\kappa)\ \ln(z_w/z_o)$ with κ=0.4 and z_w=2 m yields $u_{2m}/u_*=(1/\kappa)\ \ln(2/z_o)$ which is equivalent to

$$z_o=2/\exp(\kappa\, u_{2m}/u_*) \text{ or } k_s= 30z_o = 60/\exp(\kappa\, u_{2m}/u_*). \qquad (3.4.4c)$$

This yields: k_s= 0.0067 m (6.7 mm) for u_*=0.044 u_{2m} and κ=0.4. As bed form data are not reported by Hsu, it is not clear whether the effect of bed forms on the bed roughness is very small or that bed forms were just absent. In the latter case, the bed roughness will only be determined by the static and dynamic grain roughness.

Sherman (1982) and **Sherman and Farrell (2008)** proposed the following type of equation for natural sandy beds in wind tunnel and field conditions:

$$z_{o,dynamic}= z_{o,static} + (C_m/g)(u_*-u_{*,th})^2 \qquad (3.4.5a)$$

$$k_{s,dynamic}= k_{s,static} + (30C_m/g)(u_*-u_{*,th})^2 \qquad (3.4.5b)$$

with: c_m=coefficient and $k_{s,static}$= $2d_{50}$.
They found $C_m \cong 0.012$ for wind tunnel data sets and $C_m \cong 0.13$ for field data sets. The field and wind tunnel values are significantly different from each other by an order of magnitude. Limiting the maximum shear velocity u_* to less than 1.0 m/s, they found C_m = 0.023 for the wind tunnel data sets and $C_m \cong 0.15$ for the field data sets. Field and Pelletier (2018) found C_m=0.063 based on their field data. Using: $C_m\cong$0.1 for field sites, u_*=0.5 m/s and $u_{*,cr}$=0.25 m/s, it is found that $k_{s,dynamic} \cong$ 150 mm, which is so high that it can only be caused by form-related roughness. The precise types of beds are not described but most likely, the grain-related bed roughness is dominant in wind tunnel experiments, whereas the bed roughness in field conditions is dominated by small-scale bed forms (ripples).

Lancaster and Baas (1998) measured the bed roughness of a smooth, bare, wind-rippled sand surface at the western part of the former delta of the Owen River in eastern California, USA. The surface sand at the is coarse (median particle size of 500 to 1000 µm). The largest relief is of the order of 0.15 m. Bed form dimensions are not given, but most likely the average ripple heights are of the order of 50 mm. It was found that:

- k_s= 27 mm for wind conditions below the threshold condition (no sand transport);
- k_s= 38 mm for wind conditions with sand transport (saltating grains).

Strypsteen et al. 2017 and Strypsteen (2019) measured wind velocities (8 points up to 2.5 m above the bed) in 2016 at two Belgian beaches Mariakerke and Koksijde with sand in the range of 0.2 to 0.35 mm.
The beach of Mariakerke (d_{50}=0.31 mm) is somewhat flatter and contains some shell fragments due to regular nourishments (**Figure 3.4.5**), but the measurements were performed in the dry upper beach zone with not much shells. The bed roughness is relatively small < 10 mm, see **Table 4.2.11**.
The beach of Koksijde consists of sand (d_{50}=0.21 mm) with small-scale bed irregularities (ripples) and many shell fragments with height of the order of 30 mm, see **Figure 3.4.5**. The bed roughness is relatively high with values up to 45 mm, see **Table 4.2.12**.
Figure 3.4.6 shows the ratio u_*/u_{2m} against u_{2m} and the bed roughness height k_s against u_{2m}. The scatter due to turbulent velocity fluctuations is relatively large as values averaged over 20 s are shown.
The ratio u_*/u_{2m} is about 0.025 for wind conditions below the threshold value (< 4 m/s) increasing to 0.06 at a wind velocity of about 15 m/s.

The bed roughness height varies between 0.1 and 100 mm at beach Mariakerke and between10 and 100 mm at beach Koksijde. Analysis of time-averaged values over 15 to 30 min, yields (see also Tables 3.6.8 and 3.6.9) yields:

- roughness height (k_s) between 1 and 10 mm at beach Mariakerke for u_{2m}=2 to 10 m/s; which represents static and dynamic grain roughness;
- roughness height (k_s) between 10 and 100 mm at beach Koksijde for u_{2m}= 7 to 15 m/s; which represents roughness due to grains and small bed irregularities (ripples and shell fragments).

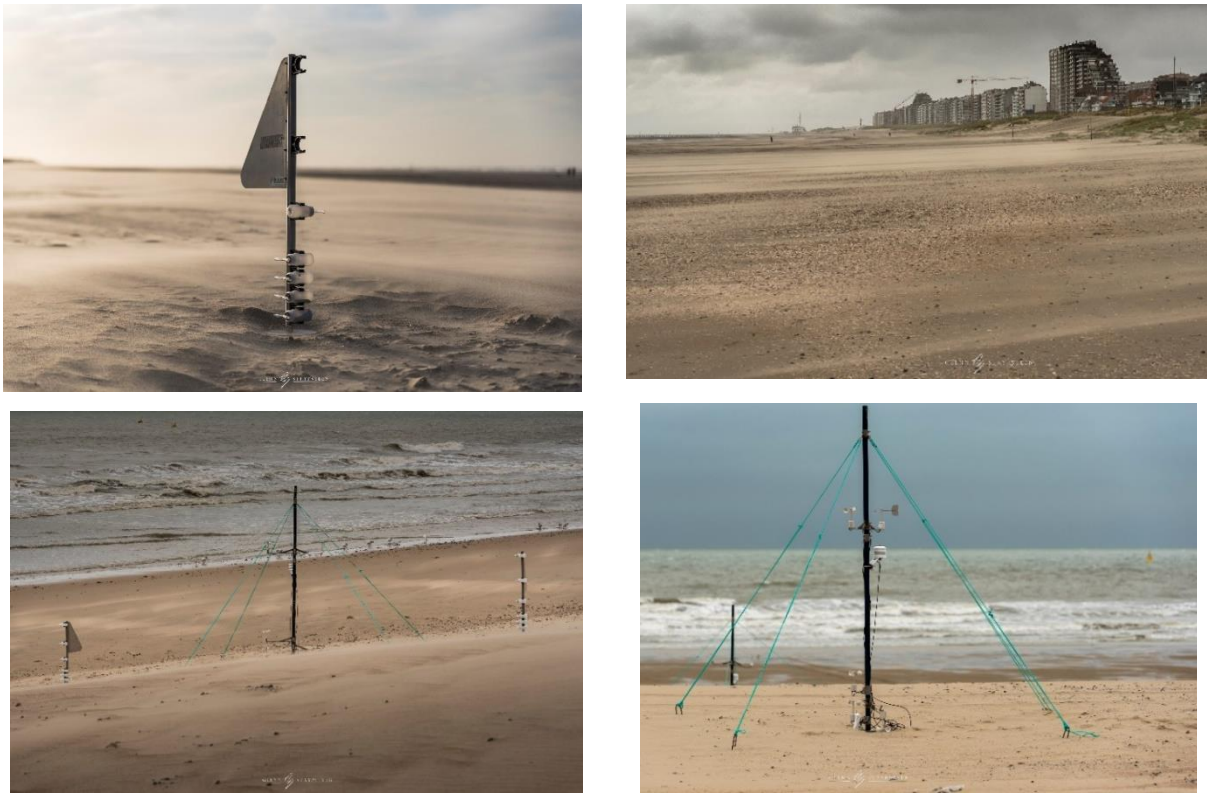

Figure 3.4.5 *Bed conditions during at Belgian coast*
Upper: beach Koksijde (d_{50}=0.22 mm); Lower: beach Mariakerke (d_{50}=0.31 mm), Belgium

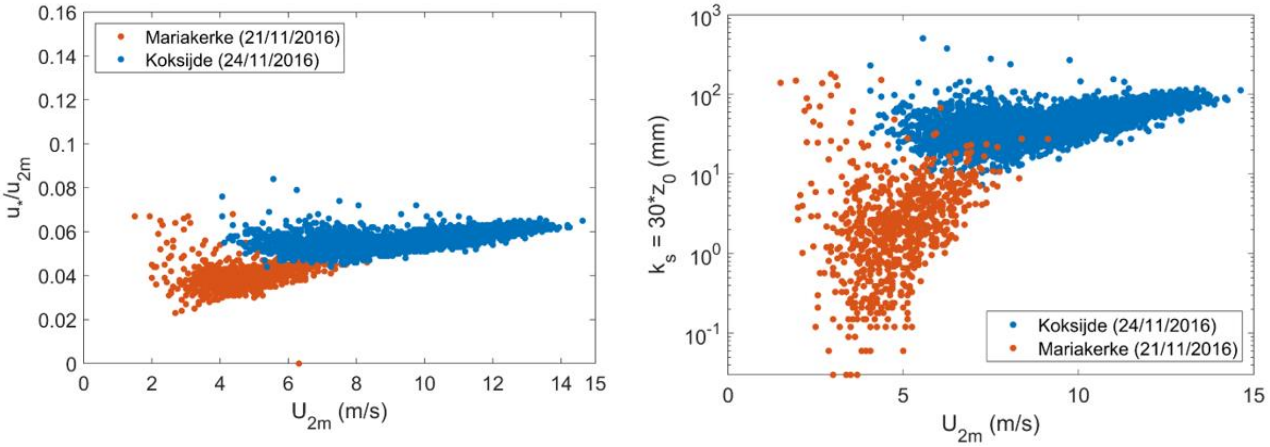

Figure 3.4.6 *Bed roughness for different wind velocities(Strypsteen, 2019)*
Left: u_*/u_{2m} against wind velocity U_{2m} at z=2 m; Right: k_s against u_{2m}

Pelletier and Field (2016) studied the roughness length of the microtopography of desert-type surfaces. They collected wind-velocity profiles and high-resolution topographic data using terrestrial laser scanning (TLS) from sites in the southwestern US during the spring of 2015. The scanner was mounted on a 3.5 m tripod to maximize the angle of incidence (low angles of incidence elongate the "shadows" or occlusions behind microtopographic highs in square areas of 10x10 m^2. The roughness length scale was quantified by the H_{RMSE}, the root-mean-squared deviation of elevation values measured at a sampling interval of 0.01 m using the TLS. The H_{rmse}-values varied in the range of 0.55 to 36 mm. The dominant wave lengths were in the range of 0.03 to 0.1; 0.1 to 1 and 1 to 3 m. In addition to the H_{rmse}, the average slope S_{av} was computed over a horizontal scale of 0.01 m, for each site. Values of S_{av} ranged from 0.01 to 0.159 m/m. Each study site was an area of at least 30m×30m with relatively uniform roughness. The surfaces studied were predominantly crusted and devoid of vegetation. No sediment transport was present during fast winds.
Wind speeds were measured at 1 s intervals and at seven heights above the surface (0.01, 0.035, 0.076, 0.16, 0.52, 1.22, and 2.80 m) using four Inspeed Vortex rotating cup anemometers and four AccuSense hot-wire anemometers (F900 series). The hot-wire sensors were secured to an L-shaped steel frame and placed above the surface such that the small opening in the sensor head was oriented as perpendicular to the wind direction as possible. The lowest cup and the highest hot-wire anemometers were positioned at the same height (0.16 m) above the sur-face to standardize measurements between the two types of wind sensors. The hot-wire sensor velocities were corrected as the sensors measured wind speeds that were approximately 10 % lower than the values obtained from the cup anemometers. During the data collection, the hot-wire sensors were moved to approximately 25 to 50 random locations within each site. The results showed that the lowest two hot-wire sensors (located 0.10 and 0.035 m above the ground) sometimes produced deviating results, because of the position of the sensors close to roughness elements. The measured velocity profiles were analyzed to extract the u_* and z_o-values. Mean values are given in **Table 3.4.5**.
Herein, it is assumed that the height (crest to trough) of the dominant bed irregularities is about in the range of 2 to 4 H_{rmse} (Δ_{ib}=2-4H_{rmse}). Using Δ_{ib}=3H_{rmse}, the ratio k_s/Δ_{ib} is given in **Table 3.4.5** showing values in the range of 0.04 to 7 depending on the bed slope/steepness.

Site	RMS-value of bed elevations H_{rmse} (mm)	Slope of bed elevations S_{av} (-)	Measured mean z_o (m)	Measured mean k_s (m)	Ratio k_s/H_{rmse} (-)	Ratio k_s/Δ_{ib} (-)
Death valley rough	34	0.144	23	690	20	7
Death valley intermediate	36	0.142	16	480	13	4
Death valley smooth	26	0.122	6.3	190	7	2.3
Soda Lake rough	14	0.159	7.6	230	16	5.3
Soda Lake smooth	11	0.154	4.6	140	13	4.3
Willcox rough	6.6	0.056	0.26	8	1.2	0.4
Willcox smooth	4.8	0.076	0.16	5	1.1	0.37
Lordsburg rough	1.3	0.032	0.047	1.4	1.1	0.37
Lordsburg intermediate	0.72	0.017	0.002	0.06	0.083	0.03
Lordsburg smooth	0.55	0.017	0.002	0.06	0.11	0.04

Table 3.4.5 *Bed roughness data of desert-type USA-sites (Pelletier and Field 2016)*

The effective bed roughness $k_{s,ib}$ of the irregular bed elevations can be represented by simple expressions, as follows:

Linear slope effect: $k_{s,ib} = 20\ \Delta_{ib}\ S$ (3.4.6a)

Quadratic slope effect: $k_{s,ib} = 150\ \Delta_{ib}\ S^2$ (3.4.6b)

with:

$\Delta_{ib} = 3H_{rmse}$ = height of dominant bed irregularities;

S= slope/steepness of dominant bed irregularities ($S \cong \Delta_{ib}/\lambda_{ib}$);

λ_{ib} = length of dominant bed irregularities.

Equations (3.4.6a,b) are shown in **Figure 3.4.7**. As can be seen, the effective bed roughness of the irregular bed elevations is strongly dependent on the bed slope. For steep bed slopes of about 0.15, the effective bed roughness is of the order $k_{s,ib} \cong 5\Delta_{ib}$. Equation (3.4.6a) is the same as that for the flow of water over a rippled bed (see Equation 6.2.15, Van Rijn 1993).

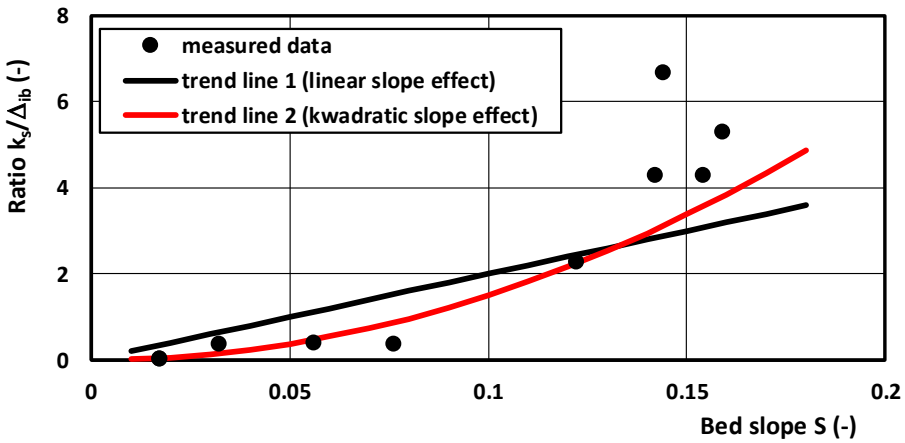

Figure 3.4.7 *Ratio of $k_{s,ib}/\Delta_{ib}$ as function of the bed slope S*

Field and Pelletier (2018) studied the contributing effects of micro-morphology (ripples) and saltation-related grain roughness to the overall bed roughness. They report field measurements of z_o-values derived from velocity profiles measured over an evolving sand ripples in field conditions (Salton Sea dune field near Salton City, California, USA). The ripple field had a bimodal grain-size distribution with the fine fraction ranging from 0.05 to 0.2 mm in diameter and the coarse fraction ranging from 0.5 to 1 mm in diameter. The topography was measured by terrestrial laser scanning and the saltation intensity was measured using a laser scanner-instrument (placed at about 0.185 m above the bed). Wind speeds were measured at 6 s intervals at four heights above the bedform (0.185 m, 0.52 m, 1.22 m, and 2.80 m) using standard cup anemometers. Average wind speed during the monitoring period was approximately 6.5 m/s at 1.22 m above the surface, with gusts commonly exceeding 12 m/s. Wind speeds were close to or exceeded the saltation threshold during the three monitoring periods. Measurements were only done during periods when the wind direction was uniform and perpendicular to the ripple field.
The sand ripple height (Δ) and length (λ) were in the range $\Delta \cong 0.01$-0.015 m; $\lambda \cong 0.15$-0.35 m for smaller shear velocities of 0.2 to 0.3 m/s increasing to $\Delta \cong 0.015$-0.03 m; $\lambda \cong 0.3$-0.5 m for larger shear velocities of 0.3 to 0.6 m/s. An example of the ripple field is shown in **Figure 3.4.8**. The observations indicate that at low shear velocity ripples can maintain a fairly constant height and spacing while migrating downwind without further growth or development.
The overall k_s-values derived from the data (Figure 7 of Field and Pelletier 2018) are roughly:

- k_s=0.5 to 5 mm for u_* <0.2 m/s (during conditions with static sand ripples and no saltation);
- k_s=1.5 to 15 mm for u_* =0.2 to 0.4 m/s (during conditions with saltation and evolving sand ripples);
- k_s= 5 to 50 mm for u_* = 0.4 to 0.6 m/s (during conditions with saltation and evolving sand ripples).

The roughness height during periods without saltation (u_*<0.2 m/s;) was measured to be $k_s \cong 0.5$ to 5 mm and represents the static grain roughness plus the form roughness of the sand ripples. These values are rather small, which may be related to the presence of fairly regular ripple patterns. The measurements indicate that the k_s-values during periods of saltation are approximately a factor of 5 to 10 greater than the values derived for conditions without saltation (static sand ripples). The maximum roughness values at the site with regular ripples of Field and Pelletier (2018) are up to 50 mm, where those of Pelletier and Field (2016) are up to 700 mm for a site with irregular bed forms. Hence, the form roughness of irregular bed forms may be substantially higher.

Figure 3.4.8 *Sand ripple field in Salton Sea desert near Salton City, California, USA (Field and Pelletier 2018)*

Summary

The effective grain roughness of a flat (static) sand bed without any grain movement is related to the size of the largest particles (d_{90}). Ideally, the static roughness of a flat bed can only be studied in a wind tunnel setup and even there it is almost impossible to make a perfectly flat bed. Usually, a type of scraper gliding over the edges of a tray is used to flatten/smooth the sand surface. Mostly, very small relict undulations remain to be present, particularly for the finer sands (0.1 to 0.3 mm). Van Rijn (1982) studied the effective roughness of flat sand beds in flumes and rivers. The effective bed roughness was found to be in the range of $k_{s,grain}$= 1 to 10 d_{90} with a mean value of $3d_{90}$. The relatively large experimental range expresses the effect of small irregularities related to preparation of laboratory beds. A perfectly flat bed in field conditions is hardly possible. Observations of flat beds often show the presence of small irregularities, isolated larger roughness elements (shells, stones, pebbles, cobbles, vegetation) or the presence of patches with finer and coarser materials in conditions with graded sediments.

Based on the available data (Xian et al. 2002, Dong et al. 2002 and Zhang et al, 2004), it is proposed to use $k_s=3d_{90}$ for static grain roughness of relatively fine sands (<0.5 mm) and $k_s=1d_{90}$ for coarse sand (>0.5 mm) and gravels. A minimum value of k_s=3 to 5 mm may be used for a static flat bed in field conditions.

The effective grain roughness of a flat (dynamic) sand bed with significant sand transport as sheet flow is related to the thickness of the saltation or sheet flow layer, which increases for increasing wind velocities. Observations show that the transport layer is as high as about 0.5 m above the sand surface. However, most of the sand transport occurs in a layer with a thickness of about 50 mm (Yang et al. 2018). The effective roughness of a flat sand surface during conditions with intense sand transport in the upper wind regime is not precisely known, as no field data for this regime are available, but most likely the roughness will be related to the thickness of the saltation layer (10 to 50 mm). Winterwerp et al. (1990) studied the dynamic grain roughness in the upper flow regime with a plane fine sand bed in a water flume and flow velocities up to 2 m/s resulting in a dynamic grain roughness of about 10 mm ($\cong 50d_{50}$). Similar experiments have not yet been done for aeolian transport. Therefore, generally accepted relationships to describe the effective bed roughness of a flat dynamic sand bed are not yet available.

Small-scale bed forms (ripples) or bed irregularities with height scales of 0.01 to 0.1 m and length scales of 0.1 to 1 mare mostly generated in the lower wind regime (< 10 m/s) and are gradually smoothed out in the transitional (10 to 15 m/s) and upper wind regimes (> 15 m/s). When ripples are present, the effective bed roughness (from roughness) increases significantly, depending on the height and steepness of the ripples.

The maximum effective bed roughness was found to be of the order of 5 times the bed form height (Pelletier and Field 2016). However, the data of Field and Pelletier (2018) show that the effect of form roughness is very minor with effective bed roughness values up to 50 mm. Similar values were found by Lancaster and Baas (1998). Based on the work of Owen (1964), Sherman and Farrell (2008) and Strypsteen (2019), the effective bed roughness (k_s) is in the range of 10 to 100 mm. As bed form information is lacking, it is not clear whether these roughness values are caused by the drag of saltating particles, the form drag of the bed forms or both. The effect of form drag on the sand transport process is not yet fully clear. The form roughness of ripples leads to: i) smaller wind velocities in the near-bed layer, ii) larger shear velocities and iii) more turbulence (larger fluctuations). Larger shear velocities and more turbulence most likely lead to more saltating particles (larger concentrations), but smaller velocities lead to smaller transport rates. Overall, the sand transport may be slightly increased by the effect of form roughness (presence of ripples). Wind-driven sand transport is more intensively related to shear stresses acting on the static and dynamic grains and to lesser extent related to form drag, similar as in water flow (Van Rijn 1993).

A major drawback of the roughness predictors proposed by Owen (1964) and Sherman and Farrell (2008) is that the bed roughness (k_s) is related to the overall bed-shear velocity u_*, which depends on the bed roughness (k_s) itself. Hence, an iterative method is required to determine the k_s-value.

3.4.4 General predictive model for effective bed roughness

The transport of particles by wind occurs in different transport regimes, which depend on the particle size and wind speed. Particles at a flat beach surface are set into motion if the wind speed exceeds the threshold value for initiation of motion. At low wind speed just beyond the threshold condition most particles will move by rolling, sliding and hopping along the sand surface. This transport regime is known as creep and reptation. For increasing wind speeds the particles are lifted from to bed to make ballistic trajectories which are known as saltations, primarily dominated by gravitational and aerodynamical forces. The impacts of the saltating particles with the sand surface may result in rebounds of grains, but the impacting grains may also mobilize and eject other particles into saltations. Saltating particles may be susceptible to turbulent velocity fluctuations in the near-bed layer, particularly when small-scale bed forms (ripples) are present or are developing along the sand surface. The powerful vortices developing in the lee zones behind the ripple crests may intensify the pickup of sand particles resulting in larger transport rates. Small particles (< 150 μm) may be continuously supported by turbulent motions and travel in suspension over longer distances. The processes with creep, reptation, saltations and developing ripples predominantly occur in the lower wind transport regime with wind speeds in the range of 5 to 10 m/s. Ripples will be gradually smoothed out in the upper transport regime with wind speeds larger than about 10 m/s as more and more particles are travelling in suspension.
The transport regimes can be identified by the transport stage parameter T which is defined (see Van Rijn 1984, 1993) as the grain-related bed-shear stress minus the threshold bed-shear stress divided by the threshold bed-shear stress ($T = (\tau_{grain}-\tau_{th})/\tau_{th} = (u_{*,grain}^2-u_{*,th}^2)/u_{*,th}^2$).
The bed roughness of relevance for sand transport strongly depends on the transport stage, as follows:

- Premature transport stage with rolling, sliding and hopping particles (T<0.5): mostly static grain roughness related to the larger particles (d_{90}) of the sand surface; additional static roughness due to larger roughness elements resting on the bed surface creating vortices in their lee zones (shells, stones, debris, etc.) may be present in all transport regimes;
- Lower transport stage with saltating particles and evolving bed ripples (0.5<T<1): dynamic grain roughness produced by small-scale vortices in the lee of the saltating particles due to the wind-particle velocity differences; additional form-related roughness due to the presence of small-scale bed forms (ripples) creating vortices in the lee zones behind the bed form crests enhancing the number of saltating grains;
- Transitional transport stage with saltating particles and smoothed-out ripples (1<T<3): dynamic grain roughness in combination with gradually disappearing form-related roughness;
- Upper transport regime with a thin sheet flow layer of saltating particles in contact with the surface and suspended transport layer (T>3): dynamic grain roughness.

It is proposed to represent the effective bed roughness for sand transport by the following expressions.

$$k_s = k_{s,ir} + k_{s,grain,st} + k_{s,grain,dyn} \quad (3.4.7)$$

$$k_s = k_{s,ir} + d_{90} + \alpha_1 \gamma_r d_{50} T^{\alpha 2} \quad (3.4.8a)$$

$$T = [(u_{*,grain})^2 - (u_{*,th})^2]/(u_{*,th})^2 \quad (3.4.8b)$$

$$u_{*,grain} = \alpha_{veg}\, \alpha_{sh}\, \alpha_{acc}\, \kappa\, u_w/\ln(30 z_w/d_{90}) \quad (3.4.8c)$$

$$u_* = \alpha_{veg}\, \alpha_{sh}\, \alpha_{acc}\, \kappa\, u_w/\ln(30 z_w/k_s) \quad (3.4.8d)$$

with:

u_w = measured wind velocity at height z above the bed (m/s);
$u_{*,th}$ = threshold bed-shear velocity based on Equation (3.1.4), (m/s);
u_* = bed shear velocity (m/s);
$k_{s,ir}$ = roughness due to irregularities (shells, stones, etc) producing additional turbulence (m);
T = transport stage parameter (-);
$k_{s,grain,st}$ = bed roughness height due to static grains (m);

$k_{s,grain,dyn}$ = bed roughness height due to dynamic grains (m);
d_{90} = grain diameter (90% smaller);
s = relative density=ρ_s/ρ_{air};
κ = 0.4; α_1 and α_2= coefficients.
γ_r = 1+1/T= ripple enhancement coefficient for the lower wind transport regime; values between 1 and 3 depending on the ripple steepness (maximum value=3).

The γ_r-coefficient is related to the T-parameter in a way that the effect reduces for increasing T-values as the ripples are gradually smoothed out. Data to calibrate this coefficient are not available. The coefficients are found to be α_1 = 15 and α_2= 1 for the data sets of Han et al. (2011) and Yang et al. (2019), see **Section 4.3**.
The d_{90} is roughly equal to d_{90}=2 to 3d_{50} for fairly uniform (narrow-graded) sand and may be as large as about d_{90}=10d_{50} for very wide-graded sand mixtures. When relatively large shells and other roughness elements are present on a flat sand bed, the roughness will increase considerably due to generation of extra turbulence depending on the size and coverage of the roughness elements (see **Section 3.4.3**) resulting in an increase of the sand transport capacity. The static roughness of shells may be in the range of 2 to 5 mm for small to large shells with a cover percentage of 5% to 10%. The roughness of shells can be neglected for cover percentages < 5% (see Dong et al., 2002). The bed roughness related to irregularities is most likely somewhat larger for coarse sand surfaces than for fine sand surfaces. Equation (3.4.8) is a first attempt to better describe the dynamic grain roughness related to the saltation process. Detailed experiments in wind tunnels are highly recommended to improve the coefficients involved.
It is noted that the bed roughness for sand transport may be substantially smaller than the bed roughness for the large-scale wind flow which is dominantly affected by macro-scale bed features (dunes, objects, etc.).

3.4.5 Future research on roughness

To extend the knowledge of the bed roughness of sand beaches, a limited number of wind tunnel and field experiments are proposed, see **Table 3.4.6**. The velocity profiles should be measured using an array of 6 to 8 wind velocity sensors over a height of maximum 1 m in the wind tunnel and maximum 2 m in field conditions (velocity averaging over at least 3 minutes to obtain reliable average values).

Test	Wind conditions	Type of measurements	Description of test
WT1	Low wind 5-7 m/s (no transport)	Velocity profiles	1. flat sand bed (two sands: 0.2 and 0.4 mm) 2. sand bed with ripples (artificially prepared) 3. flat sand bed with shells (p_{shell}=10%, 30%, 50%, 70%)
WT2	High wind 7-15 m/s (transport)	Velocity profiles and sand transport	1. flat sand bed (short duration tests of 1 to 10 minutes) 2. rippled bed (artificially prepared) 3. flat sand bed with shells (p_{shell}=10%, 30%, 50%, 70%)
Field1	Low wind 5-7 m/s parallel (no transport)	Velocity profiles	1. natural dry beach (remove debris as much as possible over area 30x10 m^2); measure vertical height of irregularities/bed forms by leveling instrument 2. flat dry beach over distance of 30 x10 m^2; use tractor and scraper to make a flat bed 3. beach with artificial ripples; use tractor and plough to make a rippled bed over an area of 30x10 m^2
Field2	High wind 7-15 m/s parallel (transport)	Velocity profiles and sand transport	1. natural dry beach (remove debris as much as possible over area 30x10 m^2); measure vertical height of irregularities/bed forms by leveling instrument 2. flat dry beach over distance of 30 x10 m^2; use tractor and scraper to make a flat bed

Table 3.4.6 *Proposal wind tunnel (WT) and field tests related to bed roughness*

3.5 Saturation length scale

Saturated or equilibrium sand transport may differ from the actual transport due to: i) limited fetch length; ii) horizontal variations of roughness, moisture, shells, vegetation and grain size/composition (see overview of Delgado-Fernandez, 2010). Fetch length (F_w) is the distance over which wind blows along the sand surface. Saturation length or adjustment length (L_{ad}) is the distance which is required for approaching saturated or equilibrium transport. This length scale is also known as the critical fetch length ($F_{w,cr}=L_{ad}$). Supply-limited conditions are present if the fetch length is smaller than the adjustment length ($F_w<L_{ad}$). Similarly, when transport conditions change due to horizontal variation of sand and surface conditions, the transport rate adjusts/adapts to the new conditions within the saturation distance, which depends on the thickness of the sand transport layer, the wind speed and the mixing capacity (turbulence and roughness) and wind speed. Experiments in wind tunnels with dry, loose sand surfaces have shown that the transport layer including the saltation layer and the suspended layer is of the order of 0.1 to 0.5 m for low to high wind velocities and grain diameters between 0.2 and 0.45 mm. Most of the transport takes place in a layer of about 0.05 m (Han et al, 2011; Yang et al. 2019). The adjustment of the boundary layer flow over a rough surface can be described by $\delta \cong 0.2x^{0.6}$ (Granger et al., 2006). Hence, the adjustment length scale for the air flow to adjust over the height of the transport layer of δ=0.5 m is about 5 to 10 m. Given near-surface wind speeds of the order of 5 m/s, the adjustment time scale is about 1 to 2 s. Basically, the adjustment length scale to approach equilibrium conditions in air and in water (Van Rijn 1987) depends on the shear velocity (u_*), the particle diameter (d_{50}) or fall velocity (w_s) expressing the gravity effect and the thickness of the transport layer (δ_s). A classic problem in water is the adjustment of sand transport in a channel with a fine sand bed downstream of a rigid bed channel. The adjustment from zero transport at the entrance of the sand bed to the new equilibrium sand transport value takes about 50 to 100 times the water depth (Van Rijn 1987). Hence, a conservative estimate for sand transport in water and air is: $L_{ad}=100\ \delta_s$ (Van Rijn 1987).
The thickness of the transport layer (δ_{sal}) in air is assumed to be equal to the saltation height of the sand particles and scales with the particle size (d_{50}), and the excess shear velocity ($u_*-u_{*,th}$). Based on analysis of the data of Yang et al. (2019), a tentative relationship similar to that for the saltation height in water (Van Rijn 1987) is:

$$\delta_{sal}=\alpha_s\ (d_{ref}/d_{50}^{0.5})\ (u_*-u_{*,th})/g^{0.5} \qquad (3.5.1)$$

with α_s =150, d_{ref}=0.00025 m and $u_{*,th}$= threshold shear velocity (m/s). Data are given in **Table 3.5.1**. Equation (3.5.1) has the correct dimension of length and shows a decreasing thickness of the transport layer for increasing particle size.
The saturation length is defined to be:

$$L_{ad}=100\ \delta_{sal}=2\ 10^4\ (d_{ref}/d_{50}^{0.5})(u_*-u_{*,th})/g^{0.5} \qquad (3.5.2)$$

Very accurate data of the saturation length scale for saltation type of sand transport are not really available, but the wind tunnel data of Han et al. (2012) and Yang et al. (2019) and the field data of Davidson-Arnott et al. (2008) at a Canadian beach with sand of 0.26 mm; Jackson and Cooper (1999) at Benone beach, Northern Ireland; Zhang et al. (2012) and Dong et al. (2012) in China deserts suggest values in the range of 10 to 100 m. **Table 3.5.1** shows computed and measured values of the saturation length for a particle of 0.0003 m (0.3 mm) with threshold shear velocity $u_{*,th}$= 0.28 m/s.
Equilibrium sand transport conditions also depend on various limiting effects (small or wide grain size composition; moisture content; armor effects). The adjustment length scale of dry sand is different from that of wet sand. Relatively high transport rates were measured by Davidson-Arnott et al. (2008) in conditions with offshore winds when sand supplied from the dry upper beach was transported over a damp, hard surface on the lower foreshore. Thus, the transport rate may exceed that for dry sand if the sand supply

comes from a dry upwind zone and the sand particles are transported over a moist and hardpacked surface, see **Figure 3.5.1**. These high transport rates are probably caused by the lower drag losses for sand grains impacting with the hard surface. Where surface moisture is very high, some saltating grains may adhere to the surface on impact resulting in smaller transport rates. Where bedforms such as ripples or low dunes are present on a wet sand surface, grains resting on the surface in the lee of the bed forms may become wet resulting in higher threshold values leading to smaller transport rates. In these conditions the transport rate will be smaller than for dry sand. If surface moisture is lower, sufficient dry sand may accumulate where the fetch is long enough (e.g. for highly oblique winds) that the transport rate will eventually equal that for dry sand.
A consequence of this is that the spatiotemporal behavior of the limiting factors must be part of the prediction model (process-based approach, see De Vries and Hoonhout 2017 and Hoonhout and De Vries 2019).

Shear velocity u_* (m/s)	**Saturation length L_{ad} (m)**	
	computed	**observed**[1]
0.4	8	≅10 (wind tunnel)
0.6	23	≅10-50
0.8	36	≅50-100 (field)

[1]wind tunnel data of Han et al. (2012) and Yang et al. (2019); the field data of Davidson-Arnott et al. (2008) at a Canadian beach with sand of 0.26 mm; Jackson and Cooper (1999) at Benone beach, Northern Ireland; Zhang et al. (2012) and Dong et al. (2012) in China deserts

Table 3.5.1 *Saturation length for sand particles of 0.3 mm*

A simple approach to deal with adjustment effects due to limited fetch is the use of an adjustment coefficient in Equation (3.1.2):

$$q_s = \alpha_{ad}\, q_{s,equilibrium} \qquad (3.5.3a)$$

$$\alpha_{ad} = (L_{fetch}/L_{ad})^{0.6} \text{ with } \alpha_{ad} = 1 \text{ for } L_{fetch} > L_{ad} \qquad (3.5.3b)$$

The power is taken as 0.6 similar to that of air flow layer adjustment (Granger et al., 2006). Using Equation (3.5.3), the adjustment process proceeds in a progressive way; the sand transport is about 70% of the equilibrium value after 50% of the total adjustment length (L_{fetch}/L_{ad}=0.5). If the dry zone of the beach is wider than about 100 m, the adjustment coefficient can be safely neglected.

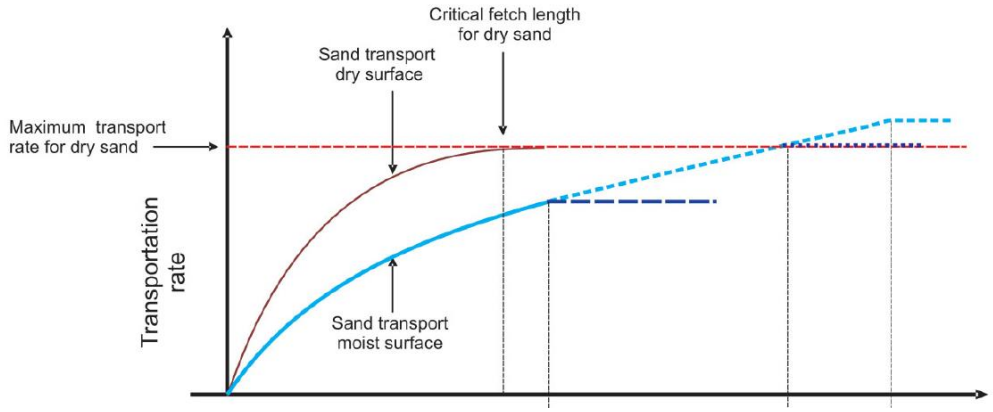

Figure 3.5.1 *Sketch of adjustment length scale for dry and moist sand (Davidson-Arnott et al. 2008)*

4. Sand transport for saturated conditions based on predicted shear velocity

4.1 Roughness predictor

To compute the sand transport rate (Equation 3.1.2), the bed shear velocity (u_*) and thus the bed roughness height (k_s) are required as input parameters. If measured velocity profile data is available, these parameters can be derived from the measured data. If only one wind velocity from a nearby weather station is available, the bed roughness parameter (k_s) must be predicted and can then be used to compute the bed-shear velocity. Various expressions are available to predict the k_s-value (Equations 3.4.3 to 3.4.5).
A major drawback of these equations is that the bed roughness (k_s) is related to u_*, which depends on the bed roughness (k_s) itself. Hence, an iterative method is required to determine the k_s-value. A non-iterative prediction method is given by Equation (3.4.8), as follows:

4.2 Data sets used

Various data sets from wind tunnel experiments and field sites have been used for calibration and verification of the predictive model. Only data sets with shear velocities which are more than 5% larger than the threshold shear velocity have been selected ($u_* > 1.05\ u_{*,th}$).

4.2.1 Wind tunnel experiments in USA by Belly (1964)

Belly (1964) has performed detailed wind tunnel experiments with sand diameters of 0.44, 0.3 and 0.145 mm. Sand transport rates were measured in tests with and without sand feed.

Sand d_{50}=0.44 mm			**Sand d_{50}=0.3 mm**			**Sand d_{50}=0.145 mm**		
Measured wind velocity at z=0.3 m above surface (m/s)	**Measured shear velocity (m/s)**	**Measured sand transport (kg/m/s)**	**Measured wind velocity at z=0.3 m above surface (m/s)**	**Measured shear velocity (m/s)**	**Measured sand transport (kg/m/s)**	**Measured wind velocity at z=0.3 m above surface (m/s)**	**Measured shear velocity (m/s)**	**Measured sand transport (kg/m/s)**
7.6	0.38	0.023	**5.5**	0.24	0.013	4.5	0.24	0.00017
7.8	0.40	0.024	6.1	0.31	0.017	4.9	0.28	0.0028
8.7	0.46	0.038	6.7	0.34	0.022	5.5	0.34	0.0059
9.0	0.49	0.050	7.5	0.38	0.030	5.9	0.37	0.0088
9.2	0.50	0.049	7.8	0.40	0.029	6.4	0.41	0.0114
9.4	0.51	0.052	8.0	0.42	0.033	8.1	0.56	0.028
9.5	0.52	0.057	8.2	0.44	0.037	8.5	0.60	0.019
9.8	0.53	0.070	8.6	0.49	0.048	8.9	0.63	0.027
10.1	0.55	0.077	10	0.59	0.073	9.2	0.65	0.037
10.7	0.59	0.088	11	0.66	0.092	10.1	0.73	0.048
11.4	0.64	0.0105				10.4	0.76	0.053
						10.8	0.79	0.065
						11.0	0.81	0.074
						11.4	0.85	0.095
						11.9	0.88	0.095

Table 4.2.1 *Measured sand transport rates; d_{50}=0.44, 0.3 and 0.145 mm; Belly 1964*

The wind velocity was measured by a pitot tube mounted in the wind tunnel (length=30 m; width=1.2 m; height=0.8 m). The wind tunnel had a sand feed system at the entrance. The sand bed had a length of 20 m and thickness of about 0.05 m. Sand transport was measured by a trap sampler at the end of the sand bed. The sand transport data are given in tables for 0.44 mm-sand (26 data points) and 0.145 mm sand (15 data points). The plots of Belly for 0.44 m sand only shows 13 data points, which are herein used (extracted from the plots). The data for 0.3 mm-sand were also extracted by the author from plots (11 data points) given by Belly. The measured wind velocities were not given by Belly (1964) and were therefore derived by the author from the plot of u_* against u_{wind} at 1 foot above the surface using the data of 0.455 mm-sand. The run times were in the range of 5 to 30 minutes depending on the wind velocity. Ripples were observed for wind velocities in the range of 7 to 10 m/s. Ripples were smoothed out for velocities > 10 m/s. The bed-shear velocity was derived from measured wind velocity profiles and given in tables for 0.44 mm and 0.145 mm-sand. The measured wind velocity at 0.3 m above the surface was used as input data for the Bagnold-equation. The measured sand transport rates of the three types of sand used in this study are shown in **Table 4.2.1** and in **Figure 3.3.2**.

4.2.2 Field experiments at Inch Spit beach in Ireland, Sherman et al. (1998)

The Inch Spit data were obtained along the beach and back beach profile seaward of the foredune in April 1994. The Inch site is part of a morphodynamically dissipative system in Dingle Bay, on the south-western coast of Ireland. Fetch distances perpendicular to the shoreline varied from 100 to almost 250 m, depending on the tide and wave conditions. Blowing sand was captured using Leatherman/Rosen type cylindrical traps with openings 40 mm wide and 450 mm high, and the bottom of the opening flush with the sand surface.
The data representing the mean values of tower 1 and 2 (situated in the upper beach area with relatively dry sand without vegetation) are given in **Table 4.2.2**.

Date	Run	Bed shear velocity u_*(m/s)	Wind velocity at 2 m a.b. U_{2m} (m/s)	Bed roughness k_s (mm)	Sand transport q_s (kg/m/min)
24/04/1994	1	0.49	8.9	42	0.46
24/04/1994	2	0.49	8.8	44	0.40
24/04/1994	3	0.41	8.2	20	0.43
24/04/1994	4	0.61	10.0	83	0.75
26/04/1994	5	0.55	9.6	57	0.58
26/04/1994	6	0.59	9.9	75	0.47
26/04/1994	7	0.54	9.3	63	0.27
28/04/1994	9	0.41	8.1	23	0.21
28/04/1994	10	0.41	8.6	14	0.17
28/04/1994	11	0.43	8.6	21	0.41
28/04/1994	12	0.41	8.2	21	0.28

Table 4.2.2 *Field data sand transport (mean values of tower 1 and 2 with almost dry sand) at Inch Spit beach, Dingle Bay, Ireland; almost horizontal, wide beach (slope <1°); d_{50}=0.17 mm; $p_{shell}\cong$2% (Sherman et al., 1998)*

4.2.3 Field experiments at three sites in Ireland, Portugal and Brazil of Sherman et al. (2013)

Data were obtained from field experiments conducted at three sites (see **Table 4.2.3**). Chronologically, the experiments were at Inch Spit, Ireland, Esposende, Portugal and Jericoacoara, Brazil. The original Inch data were obtained along the beach and back beach profile seaward of the foredune in April 1994. The Inch site is part of a morphodynamically dissipative system in Dingle Bay, on the south-western coast of Ireland. Fetch distances perpendicular to the shoreline varied from 100 to almost 250 m, depending on the tide and wave conditions. Blowing sand was captured using Leatherman/Rosen type cylindrical traps with openings 40 mm wide and 450 mm high, and the bottom of the opening flush with the sand surface.

Run	Run time (s)	Sand diameter d_{50} (mm)	Bed-shear velocity u_* (m/s)	Wind velocity at 2 m a.b (m/s)	Roughness height z_o (mm)	Slope fit parameter m	Sand transport (kg/m/s)
I1	1020	0.17	0.4	12.3	0.27	0.99	0.0068
I2	1020	0.17	0.45	11.8	1.73	1.12	0.0019
I3	1020	0.17	0.36	11.1	0.28	0.9	0.0019
I4	1020	0.17	0.31	10.8	0.052	0.76	0.0014
I5	1020	0.17	0.45	12.1	1.24	1.12	0.0048
E1	600	0.31	0.49	13.5	0.96	1.23	0.0087
E2	600	0.31	0.49	13.5	0.96	1.23	0.0073
E3	900	0.31	0.41	12.1	0.45	1.03	0.0016
E4	900	0.3	0.41	12.1	0.45	1.03	0.0017
E5	360	0.32	0.51	14	1.05	1.28	0.0086
E6	360	0.32	0.51	14	1.05	1.28	0.0093
E7	900	0.35	0.41	12.3	0.36	1.03	0.0144
E8	600	0.34	0.35	11.3	0.14	0.88	0.0062
E9	600	0.33	0.38	11.9	0.22	0.95	0.0033
E10	600	0.33	0.39	11.6	0.4	0.98	0.0026
E11	900	0.28	0.32	9.9	0.25	0.8	0.0003
E12	600	0.27	0.38	11.3	0.41	0.95	0.0024
J1	120	0.3	0.68	16.6	3.4	1.69	0.032
J2	180	0.22	0.66	16	3.8	1.66	0.024
J3	180	0.22	0.71	17	4.2	1.78	0.032
J4	213	0.23	0.68	16.1	4.6	1.69	0.022
J5	170	0.3	0.66	16.5	2.8	1.65	0.026
J6	240	0.29	0.58	14.9	2.1	1.46	0.0204
J7	240	0.28	0.56	14.6	1.8	1.41	0.018
J8	240	0.28	0.55	14.6	1.5	1.38	0.016
J9	240	0.3	0.5	13.6	1.1	1.26	0.015
J10	240	0.3	0.53	14.3	1.2	1.34	0.018
J11	240	0.25	0.54	13.9	2	1.35	0.0263
J12	300	0.27	0.54	13.5	2.8	1.35	0.020
J13	240	0.33	0.56	15.6	0.84	1.4	0.023
J14	299	0.43	0.57	15.7	0.96	1.43	0.0164
J15	240	0.44	0.57	15.8	0.9	1.44	0.0273

Table 4.2.3 *Summary of data from three field sites; dry sand; no vegetation; κ=0.4 (Sherman et al., 2013)*

The field site at Esposende, along the northern coast of Portugal, was near the downwind end of a parabolic dune trough (May and June 2006). The upwind surface was flat and unobstructed and almost horizontal near the sand traps. During the experiments the sand surface was dry, and winds blew parallel to the trough with a fetch of approximately 80 m. Blowing sand was trapped using vertical arrays of hose-type traps. Samples for grain size analyses were obtained from sand caught in the traps.
Located on the north-eastern coast of Brazil, the Jericoacoara site was also near the downwind end of a parabolic dune trough, but at a location approximately 500 m from the shoreline. The upwind surface was flat and unobstructed, with a fetch of approximately 100 m, and the surface was almost horizontal near the traps. During the experiments, the wind blew parallel to the trough and the surface sediments were dry. Sand transport rates were measured with vertical hose-type trap arrays and grain size samples were obtained from the trapped sands.
In order to estimate shear velocity using the cup anemometer data, wind speeds were averaged over time intervals coincident with those for sand trap data. Regression analysis was used to obtain log-linear best fit lines, the slopes, m, of which were used to solve $u_* = \kappa m$. Samples for grain size analysis were washed, dried, and sieved. Samples for moisture content analysis were weighed, dried, and then reweighed. Weight differences were used to estimate percent water content by weight.
The number of data was reduced to 32 data sets (5 for Inch Spit; 12 for Esposende and 15 for Jericoacoara) by selecting: i) only those wind profiles with a best-fit line r^2 exceeding 98%, ii) only those data for which the sand moisture content was less than 2% and iii) data sets with sand transport rates larger than about 0.3 g/m/s (1 kg/m/hour).

4.2.4 Wind tunnel experiments in China by Han et al. (2011)

Han et al. (2011) studied the effect of moisture content on sand transport by wind in a wind tunnel (length=37m, width=1.2m, height=1.2 m) in China, see **Figure 4.2.1**. Sand trap measurements were done at the end of a sand tray with length of 4 m. The bed consisted of sand with d_{50}=0.203 mm. The sand trap (efficiency of 90% for particles >0.1 mm) had a height of 0.6 m and was sectionalized in 60 openings with height of 10 mm and width of 5 mm. The lowest opening is flush with the sand surface. The wind velocity was measured at z_w=0.6 m above the flat sand surface using a Pitot-tube method. The moisture content (ratio of mass of water and mass of dry sandx100%) of the sand bed was varied in the range of 0.14% to 2.7%. The moisture content of the sand bed was prepared just before the experiment using distilled water. Each experiment was run over only 90 s to prevent a change of the moisture content. Five bed surface samples with thickness of **1 mm** were taken after each experiment to determine the moisture content again.

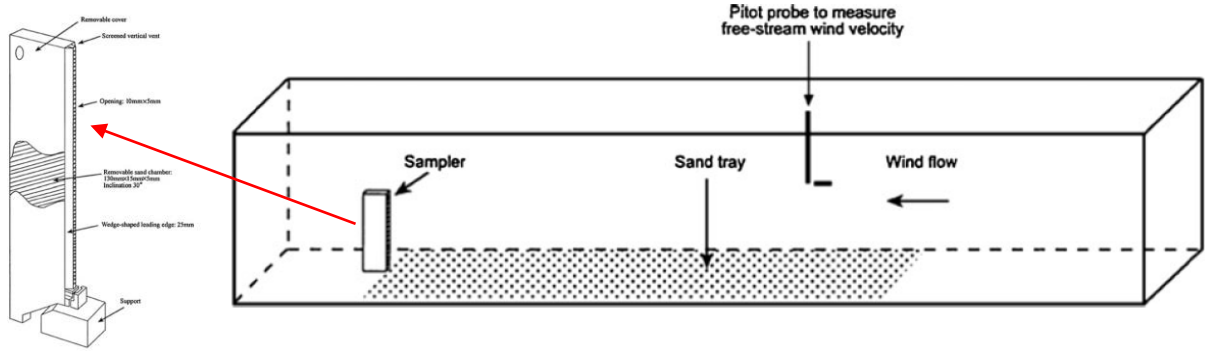

Figure 4.2.1 *Experimental setup in wind tunnel and sand trap sampler (Han et al. 2011)*

The measured results show that most of the sand transport is taken place in a layer with height of about 0.2 to 0.4 m above the sand surface depending on the wind velocity (10 to 20 m/s), see **Figure 4.2.2**.

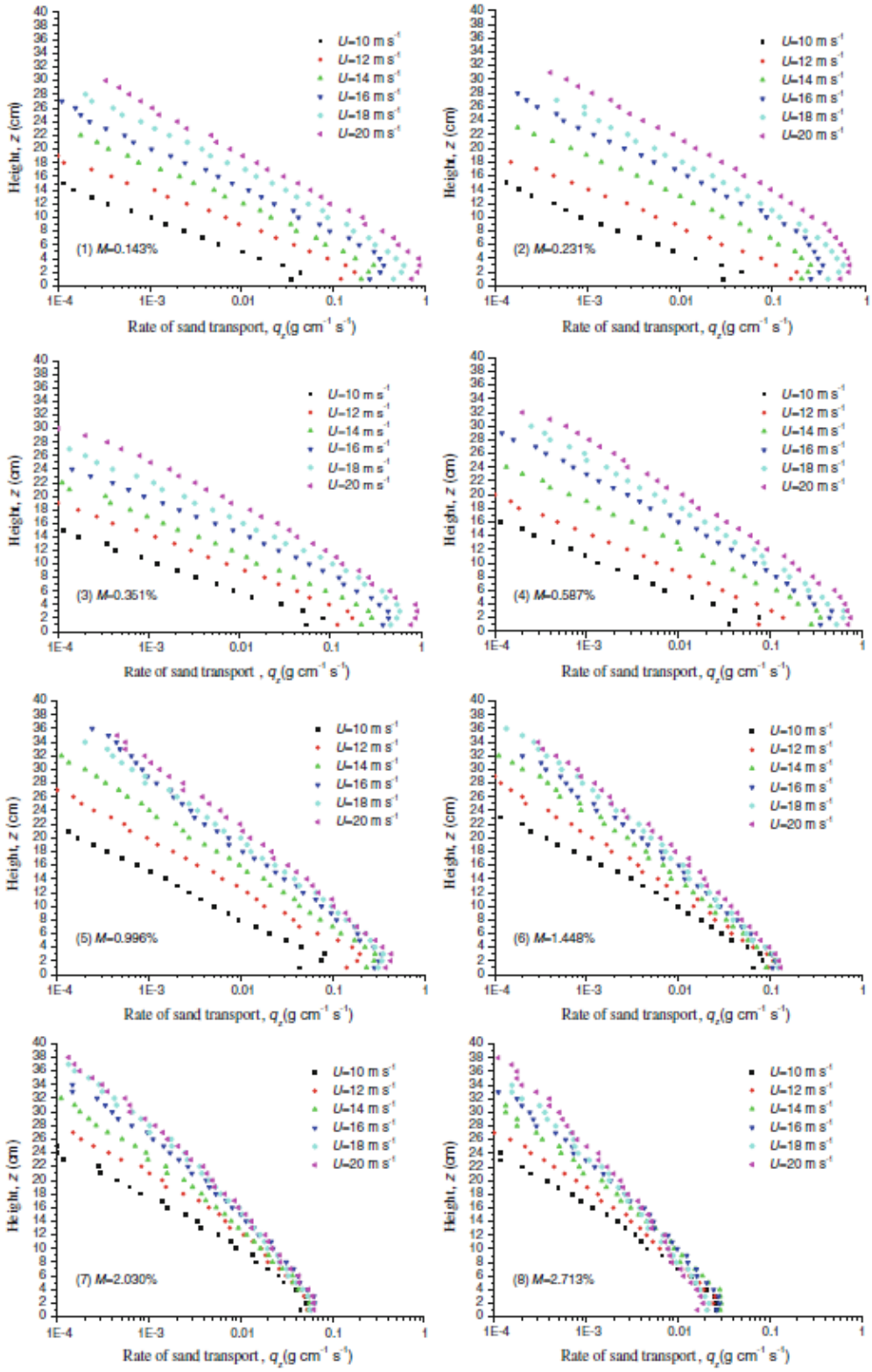

Figure 4.2.2 *Sand flux profiles for various moisture contents and wind velocities (sand flux in gram/cm²/s; height in cm); (Han et al. 2011)*

The moisture content has almost no effect on the height of the transport layer. The sand transport rates integrated over the transport layer are given in **Table 4.2.4**.
The most important results of Han et al. (2011) can be summarized, as follows:

- sand flux profiles show an almost constant flux in the lowest 5 cm; some profiles show bending slightly backwards (deceasing values close to sand surface) which may be related to the generation of small scour holes around the lowest intake opening of the sampler (measuring errors);
- sand flux profiles can be represented by an exponential distribution of the type $q_z=q_o\exp(-kz)$;
- sand transport integrated over the transport layer strongly increases for increasing wind velocity (**Table 4.2.4** column2 and 3; factor 30 for wind velocity increasing from 10 to 20 m/s; $q_s \approx u_w^5$);
- sand transport rate strongly decreases (see **Figure 4.2.3**) for increasing moisture content (w):
  w_{1mm}< 0.25%: sand is almost dry and sand transport tis fairly constant;
  w_{1mm}=0.25-1.5%: sand transport is fairly constant for u_w=10-14 m/s;
  sand transport is significantly reduced for u_w=14-20 m/s;
  w_{1mm}>1.5%: sand transport is very small (factor 10 to 20) smaller than that for dry sand;
- sand surface is relatively hard with higher erosion resistance for w_{1mm}>1.5% (transition point when a thin water film can be present around each sand grain, see **Section 5.4**) resulting in stronger rebounds of saltating particles (larger particle velocity and rebound angle).

Wind velocity at z=0.6 m above sand surface (m/s)	**Depth-integrated sand transport (in kg/m/s) for different moisture content (in %)**							
	mc_{1mm}= 0.14%	**0.23**	**0.35**	**0.59**	**1.0**	**1.45**	**2.03**	**2.71**
10	q_s=0.015	0.014	0.025	0.021	0.035	0.044	0.033	0.018
12	q_s=0.067	0.066	0.073	0.052	0.10	0.06	0.042	0.019
14	q_s=0.13	0.15	0.14	0.17	0.17	0.07	0.045	0.025
16	q_s=0.22	0.26	0.26	0.26	0.23	0.082	0.056	0.025
18	q_s=0.36	0.4	0.38	0.38	0.27	0.087	0.052	0.02
20	q_s=0.61	0.61	0.57	0.55	0.31	0.1	0.057	0.019

Table 4.2.4 *Depth-integrated sand transport in wind tunnel; d_{50}=0.203 mm (Han et al., 2011)*

Table 4.2.5 shows a comparison of measured and computed sand transport rates for the case of a dry sand bed (moisture content w_{1mm}< 0.25%). The α_{th}-value of the threshold shear velocity is set to 0.11. The bed roughness is set to k_s=5 mm, typical for a flat surface with a sheet-like bed load transport layer. The Bagnold-equation and the DK-equation produce values which are very reasonable for a wind velocity of 10 and 12 m/s but are much too small (factor 3) for higher wind velocities.

Wind velocity at z=0.6 m above sand surface (m/s)	**Sand transport for dry sand bed (kg/m/s)**		
	Measured	Computed Bagnold model (α_B=2; α_{th}=0.11; $k_{s,grain}$= 5 mm)	Computed DK-model (α_{DK}=5; α_{th}= 0.11; $k_{s,grain}$=5 mm)
10	0.015	0.023	0.026
12	0.065	0.042	0.041
14	0.14	0.068	0.058
16	0.25	0.10	0.079
18	0.38	0.15	0.101
20	0.60	0.20	0.127

Table 4.2.5 *Comparison of measured and computed depth-integrated sand transport; dry sand d_{50}= 0.203 mm (moisture content w_{1mm}<0.25%)*

Table 4.2.6 shows a comparison of measured and computed sand transport rates for moisture sand (w_{1mm}=1, 2 and 2.7%). The α_{th}-value of the threshold shear velocity is set to 0.11. The bed roughness is set to $k_{s,grain}$=5 mm, typical for a flat surface with a sheet-like bed load transport layer. The Bagnold-equation including the effect of moisture produces values which are of the right order of magnitude; particularly for higher wind speeds. The computed values are zero for lower wind speeds due to the increase of the threshold bed-shear velocities for increasing moisture content.

Wind velocity at z_w=0.6 m above sand surface (m/s)	**Sand transport for dry sand bed (kg/m/s)**					
	Measured			Computed Bagnold model (α_B=2; α_{th}=0.11; $k_{s,grain}$= 5 mm)		
	w_{1mm}=1%	w_{1mm}=2%	w_{1mm}=2.7%	w_{1mm}=1%	w_{1mm}=2%	w_{1mm}=2.7%
10	0.035	0.033	0.018	0.	0.0	0.
12	0.10	0.042	0.019	0.013	0.0	0.
14	0.17	0.045	0.025	0.039	0.006	0.
16	0.23	0.056	0.025	0.074	0.04	0.034
18	0.27	0.052	0.02	0.12	0.085	0.078
20	0.31	0.057	0.019	0.17	0.14	0.13

Table 4.2.6 *Comparison of measured and computed depth-integrated sand transport; moisture sand d_{50}= 0.203 mm (moisture content w_{1mm}= 1% to 2.7%)*

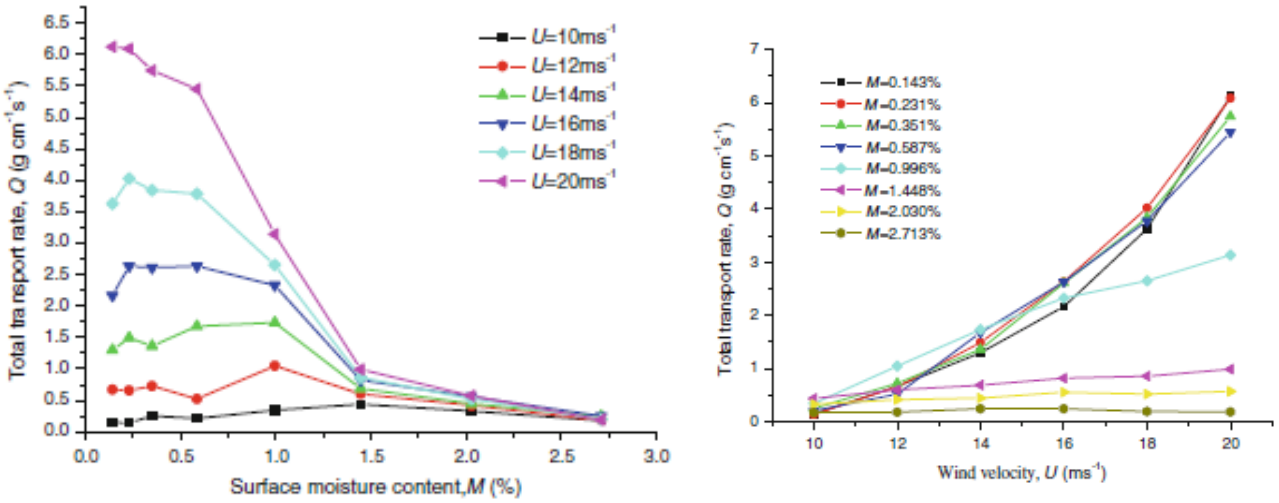

Figure 4.2.3 *Depth-integrated sand transport as function of wind velocity and moisture content (Han et al., 2011)*

4.2.5 Wind tunnel experiments in China by Yang et al. (2019)

Yang et al. (2018) studied the grain size distribution of the saltating particles for wind velocities in the range of 8 to 22 m/s, see **Figure 4.2.4**. The sand used for the wind tunnel experiments was typical dune sand collected from the southern margin of the Tengger Desert in China. The mean sand grain size is 455 μm. Before performing the blown sand experiments, free-stream wind velocities were determined at a height of 0.3 m above the center line of the working section of the wind tunnel using a pitot tube. The sand beds were 1 m wide, 0.1 m deep and 8 m long, and this ensured that the blown sand flux reached the saturation state

at all measured wind velocities. The sand in the bed at each wind velocity was replaced for each experiment. A passive segmented sand trap with height of 0.5 m (see **Figure 4.2.1**) was used to collect the sand grains in the saltation layer and was located on the center line 12 m downward from the entrance of the working section of the tunnel. The duration of each experiment was 480, 360, 180, 90, 65, 30, 20 and 10 sec for the wind velocity range of 8 to 22 m/s. The following features can be observed from Figures (Yang et al., 2019):

- the mass percentage of the very fine and fine sand fractions decrease for increasing wind speeds, whereas the mass percentages of both coarse fractions increase for increasing wind speeds (**Figure 4.2.5right**);
- the sand transport varies with wind velocity to the power 5 for the coarse fractions to power 7 for the very fine fraction (**Figure 4.2.5left**);
- the mean grain size of the saltating particles varies from about 300 μm (0.3 mm) for a wind speed of 8 m/s to about 420 μm (0.42 mm) for a wind speed of 22 m/s (**Figure 4.6.6left**); more coarse particles are moving/saltating at higher wind speeds;
- the mean grain size decreases with height above the sand bed up to a level of 0.1 to 0.2 m and increases again at higher levels above the bed (**Figure 4.2.6right**); the proportion of the finer fractions (very fine sand and fine sand) initially increases above the sand bed and then decreases slightly with height, while that of the coarser fractions (medium and coarse sand) shows the opposite trend.

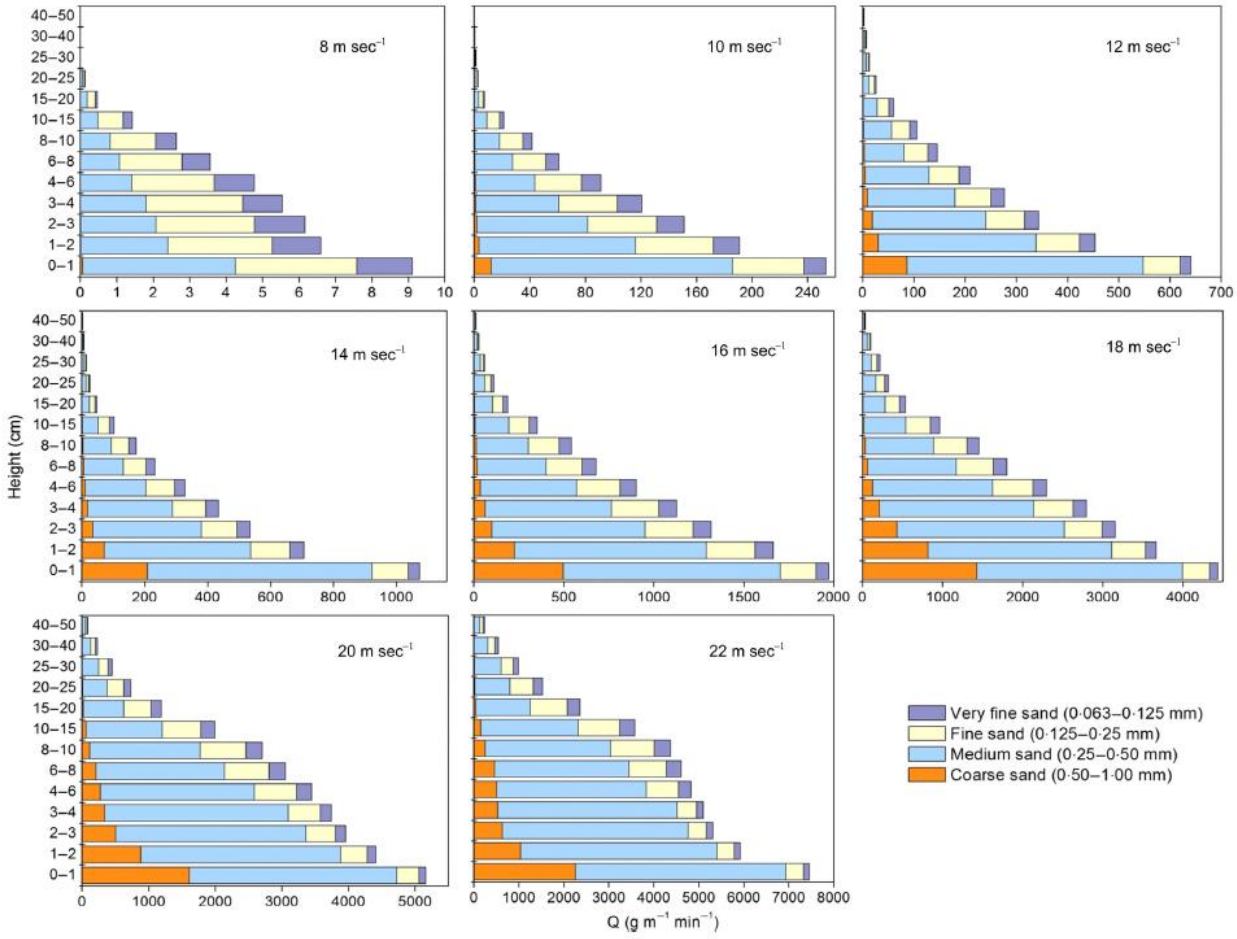

Figure 4.2.4 *Vertical distribution of horizontal sand flux for 4 sand fractions and wind speeds of 8 to 22 m/s; $d_{50,bed}$=0.455 mm (Yang et al., 2019)*

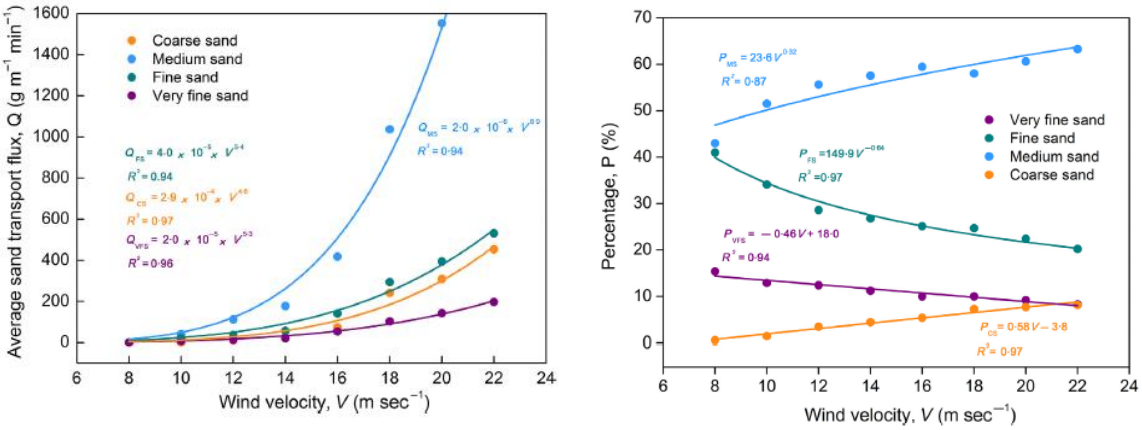

Figure 4.2.5 *Left: sand transport per fraction as function of wind speed; $d_{50,bed}$=0.455 mm, Right: mass percentage of each fraction as function of wind speed; $d_{50,bed}$=0.455 mm*

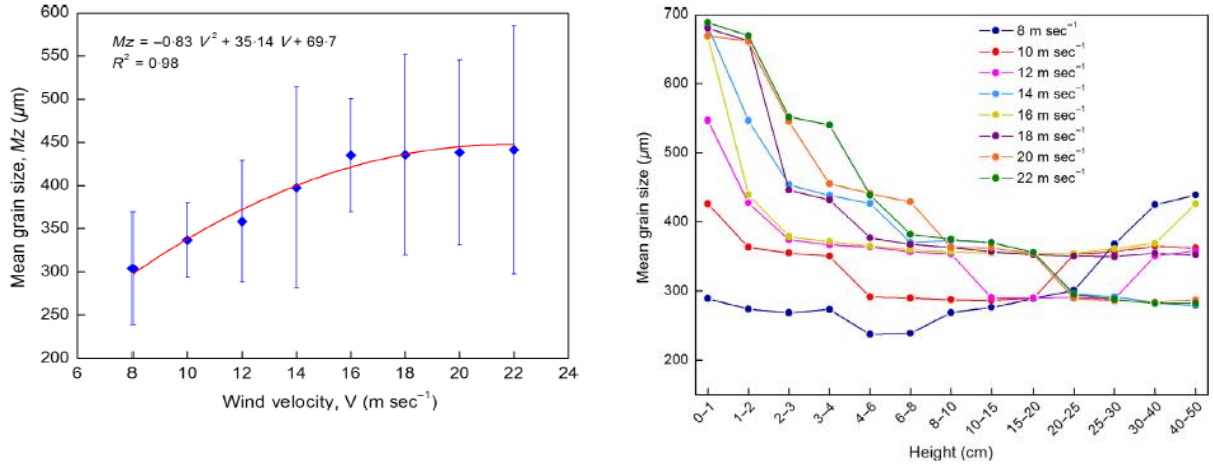

Figure 4.2.6 *Left: mean grain size as function of wind speed; $d_{50,bed}$=0.455 mm (Yang et al., 2019) Right: vertical distribution of mean grain size; $d_{50,bed}$=0.455 mm (Yang et al., 2019)*

Table 4.2.7 presents the sand transport rates derived from **Figure 4.2.4**. Computed values based on the Bagnold-equation and the DK-equation are also presented for a constant roughness of k_s=5 mm. The computed values are of the right order of magnitude for wind speeds > 16 m/s, but are systematically too large for wind speeds < 14 m/s. Most likely, the bed roughness is overestimated using k_s=5 mm for wind speeds < 14 m/s.

Wind velocity at z_w=0.3 m above sand surface (m/s)	Sand transport for dry sand bed (kg/m/s)		
	Measured	Computed Bagnold model (α_B=2; α_{th}=0.11; $k_{s,grain}$= 5 mm)	Computed DK-model (α_{DK}=5; α_{th}= 0.11; $k_{s,grain}$=5 mm)
8	0.00067	0.012	0.013
10	0.015	0.036	0.035
12	0.038	0.073	0.061
14	0.063	0.124	0.093
16	0.153	0.191	0.13
18	0.37	0.28	0.17
20	0.58	0.39	0.22
22	0.79	0.52	0.27

Table 4.2.7 *Comparison of measured and computed depth-integrated sand transport; dry sand d_{50}= 0.455 mm; data of Yang et al. (2019)*

4.2.6 Field experiment in southeastern part of Tengger desert in China by Dong et al. (2012)

Dong et al. (2012) performed a field experiment in desert conditions. This area is a typical shifting dune field free of any vegetation and dominated by dunes. The primary ridges of the dunes are 3 to 20 m tall, spaced at 30 to 170 m, and aligned in a NE-SW direction. The subsidiary ridges are 1 to 6 m tall, spaced at 20 to 70 m, and aligned in a NW-SE direction. Annual precipitation is about 180 mm, most of which falls in the summer and autumn. An area of 600 x 800 m² was flattened to permit observations of aeolian transport (2005).

Three plots of 80x80 m² were established within the area (**Figure 4.2.7**):

a) an area of open shifting sand was flattened without further treatment to ensure that sediment transport came from both outside and inside the plot;
b) an enclosed plot of shifting sand was surrounded by 20 m wide straw checkerboard barriers on all four sides to ensure that sediment transport came primarily from inside the plot;
c) a gravel-covered plot was established by creating a 30-mm-thick layer of gravel with a mean diameter of 3 mm that completely covered the sand surface to ensure that sediment transport came exclusively from outside the plot.

The three plots (dry sand with d_{50}=0.19 mm) were aligned perpendicular to the primary NW wind.
Wind data (free-stream wind velocity) was acquired from a meteorological tower at the center of the site at eight heights (1, 2, 4, 8, 16, 24, 32, and 48 m above the surface) using wind sensors connected to a data logger. The wind data acquisition system was set to record wind velocity averaged at 1-min intervals. The aeolian transport observation plots were 100 to 300 m upwind from the central meteorological tower.
Sediment transport was measured in April and May 2008 using vertical segmented sediment samplers (LDDSEG samplers) designed by the Key Laboratory of Desert and Desertification, Chinese Academy of Sciences. This sampler is about 1 m tall and is divided into 50 openings (each 20 mm □ 20 mm) to collect the horizontally transported wind-eroded sediment at 50 heights at 20-mm intervals. Each opening is connected to a sediment chamber that is inclined downward at an angle of 30° with respect to the horizontal, and the chamber is removed after each observation period. The sampler was evaluated in a wind tunnel before using it at the study site. Sampling efficiency of the samplers defined in wind tunnel tests for dune sand from this area ranged from 72 to 87%. An overall sampling efficiency of 80% (the average sampling efficiency) was adopted to correct the transport data. Simultaneous sediment transport observations were conducted in the three plots using one LDDSEG sampler per plot, installed at the downwind edge of each plot. **Table 4.2.8**

shows 5 characteristic data of the measured sand transport data of Dong et al. (2012) for the open sand plot. The variability of the measured data is relatively large (factor 2 to 3 for each wind velocity class) due to wind velocity fluctuations. The measured transport rates of the enclosed sand plot were

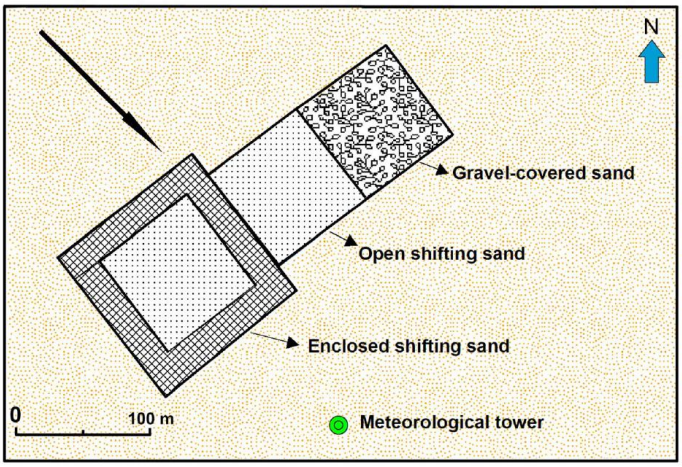

Figure 4.2.7 *Experimental setup (Dong et al., 2012)*

The plot with enclosed shifting sand and the gravel-covered plot had similar transport rates that were lower (factor 2) than that above the plot with open shifting sand. These differences suggest that sediment availability is an important factor in determining the transport rate. Given the horizontal dimension of about 80 m, the adjustment length scale for dry sand is of the order of 50 m.
Flux density profiles above all three plots were expressed well by an exponential decay function to describe the saltation flux density profiles.
The computed transport rates of the Bagnold-equation and the DK-equation based on a bed roughness of ks=5 mm are much too small (factor 2 to 3), see **Table 4.2.8**.

Wind velocity at z_w=16 m above the sand surface (m/s)	**Effective thickness of sand transport layer (m)**	**Measured sand transport (kg/m/hour)**	**(kg/m/s)**	**Computed sand transport Bagnold α_B=2 (kg/m/s)**	**DK α_{DK}=5 (kg/m/s)**
5.5 (±0.5)	0.25	2	0.00055	0.	0.
6.5 (±0.5)	0.3	5	0.0014	0.00011	0.00021
7.5 (±0.5)	0.35	15	0.0042	0.0014	0.0025
8.5 (±0.5)	0.4	30	0.0083	0.0032	0.0052
10 (±0.5)	0.5	70	0.019	0.0067	0.0097

Table 4.2.8 *Measured sand transport events; plot open shifting sand; dry sand d_{50}=0.19 mm; data of Dong et al. (2012)*

4.2.7 Field experiment at Texel beach 2013, The Netherlands

A small-scale field experiment was done by the author at the beach of Texel (The Netherlands) in July 2013; beach sand of about 0.2 to 0.25 mm (dry, loose particles). A strong wind was blowing parallel to the water line at a wind speed of about u_{wind10}= 8 to 10 m/s (Beaufort 5 to 6).

The beach particles were moving by sliding, rolling and saltating in a thin layer of 2 to 3 mm thick with a speed of about 0.2 to 0.4 m/s (carpet-type of transport). About 10% of the surface was moving and wind gusts were very important resulting in intermittent transport processes.
Small-scale ripples were present (height of 0.01 to 0.03 m, length of 0.2 to 0.3 m).
A small trench (length=0.1 m; width=0.1 m) was made normal to the wind. The trench was completely filled in about 30 minutes yielding a transport rate of about q_s= 0.01 kg/m/s (bulk density of 1600 kg/m^3).
Using: α_B=2; α_{DK}=5; d_{50}= 0.225 mm, k_s= 30 mm (including ripple related bed roughness), u_{wind10}= 9 m/s, yields:
$u_{*,th}$= 0.282 m/s, u_*= 0.39 m/s;
$q_{s,bagnold}$= 2x(0.225/0.3)$^{0.5}$x(1.2/9.81)x[0.39^3-0.242^3] = 0.010 kg/m/s
$q_{s,kok}$= 5x(1.2/9.81)x0.242x[0.39^2-0.242^2] = 0.014 kg/m/s
Both values are in good agreement to the measured value of 0.01 kg/m/s.

4.2.8 Field experiments at Koksijde and Mariakerke beaches 2016-2018, Belgium

A field experiment was done by Campos (2018) at the beach of Koksijde in Belgium. The measurement location was the dry beach outside the wet intertidal beach zone. The beach sand has a d_{50}=0.22 mm. Wind-induced sand transport was measured by using 6 streamer type traps on top of each other (**Figure 4.2.8**). Each trap has a length of 25 cm; an opening with vertical size of 5 cm; horizontal size of 10 cm. The sand particles are trapped in a nylon bag (length of 50 cm to 75 cm for the lowest trap) with mesh size of 50 μm. The sand trap data are presented in **Table 4.2.9.** The mass of sand in the lowest trap varies between 6%5 and 75% of the total mass. Hence, about 70% of the sand transport occurs in the lowest 5 cm of the transport layer. The sand transport is computed as the total trap mass divided by the duration and the mouth width (=0.1 m). The data can be summarized into three different cases (see **Table 4.2.10**). Computed values of the Bagnold-equation and the DK-equation using a bed roughness of k_s= 5 mm are somewhat too small (factor 1.5 to 2).

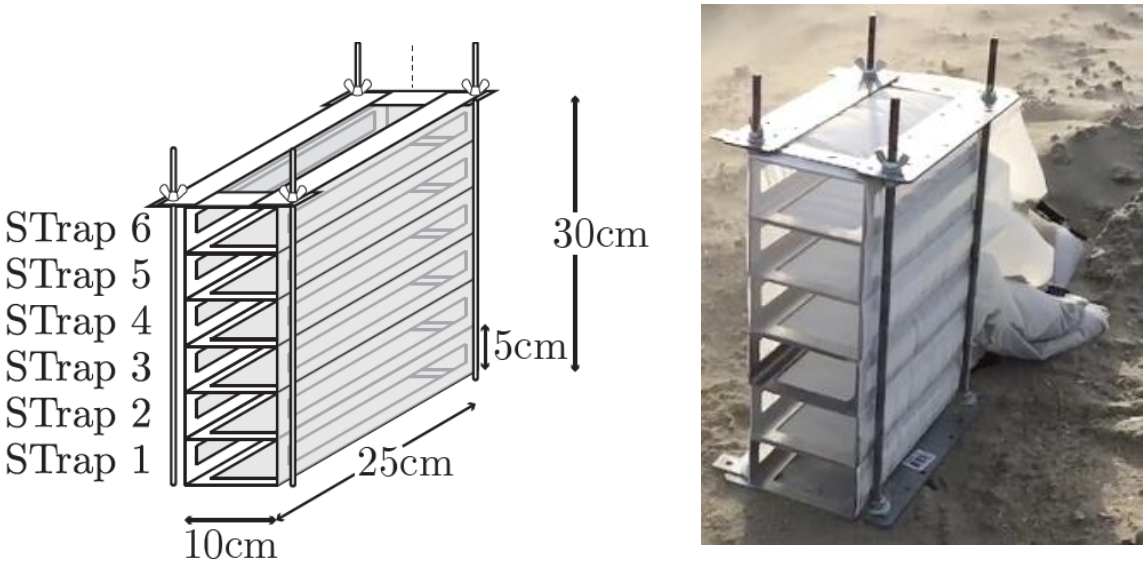

Figure 4.2.8 *Streamer type sand traps (Campos, 2018)*

Wind velocity at z_w=0.5 m above surface	Duration of event (s)	Sand transport trapped (in grams)							Sand transport (kg/m/s)
		Trap 1 0-5 cm	Trap 2 5-10 cm	Trap 3 10-15 cm	Trap 4 15-20 cm	Trap 5 20-25 cm	Trap 6 25-30 cm	Total	
7.2	2200	1968	655	145	50	14	5	2826	0.013
8.4	960	1498	448	133	45	17	9	2150	0.022
8.7	1050	1508	560	169	61	26	13	2337	0.022
9.2	1440	2938	907	301	106	45	22	4319	0.03
9.2	1080	2178	693	226	92	39	18	3246	0.03
9.1	1440	2687	605	186	68	30	16	3592	0.025
9.2	1320	2439	730	248	101	45	20	3583	0.027
9.2	2250	3529	1045	352	140	61	32	5159	0.023

Table 4.2.9 *Sand trap data Koksijde beach, Belgium (Campos, 2018)*

Wind velocity at z_w=0.5 m above the sand surface (m/s)	Effective thickness of sand transport layer (m)	Measured sand transport (kg/m/s)	Computed sand transport (k_s=5 mm) Bagnold α_B=2 (kg/m/s)	DK α_{DK}=5 (kg/m/s)
7.2 (±0.3)	0.3	0.013	0.007	0.01
8.5 (±0.3)	0.3	0.022	0.013	0.017
9.2 (±0.3)	0.3	0.026	0.018	0.021

Table 4.2.10 *Measured and computed sand transport; dry sand d_{50}=0.22 mm; Koksijde beach Belgium (data of Campos, 2018)*

Strypsteen (2019) and **Strypsteen et al. (2019)** conducted field experiments at the beaches of Mariakerke and Koksijde in Belgium. Between 2016 and 2018, simultaneous monitoring of meteorological variables and aeolian transport (using MWAC sand traps) of dry sand with d_{50} in the range of 0.22 to 0.31 mm was carried out on the subaerial beach of two study sites in Belgium. The bed consists of beach sand with small-scale bed forms (ripples) and bed irregularities with height of the order of 50 mm. The basic data used by Strypsteen et al. (2019) are shown in **Tables 4.2.11** and **4.2.12**. The wind velocity (u_{2m}) at z_w=2 m above the bed, the bed-shear velocity (u_*) and the bed roughness (k_s) are related by the equation: $u_{2m}=(u_*/\kappa)\ \ln(60/k_s)$ with κ=0.4.
The beach of Mariakerke (d_{50}=0.31 mm) is somewhat flatter and contains some shell fragments due to regular nourishments, but the measurements were performed in the dry upper beach zone without much shells. The bed roughness is smaller than 10 mm, see **Table 4.2.11**.
The beach of Koksijde consists of sand (d_{50}=0.21 mm) with small-scale bed irregularities (ripples) and many shell fragments with height of the order of 50 mm, see **Figure 3.4.5, 3.4.6**. The bed roughness is relatively high with values up to 45 mm, see **Table 4.2.12**.
The results of various aeolian transport models were compared to the measured data of two beaches along the Belgian coast. The shear velocities were calculated from measured wind profile data. Mean shear velocities ranged from 0.25 to 0.6 m/s. Transport rates of dry sand ranged from 0.002 to 0.037 kg/m/s. The modified Bagnold model of Equation (3.1.2) was found to yield the best score (Strypsteen et al., 2019). The DK-model (Equation 3.1.3) was close second best.

Date	Run	Bed shear velocity u_*(m/s)	Wind velocity at z_w=2 m a.b. u_{2m} (m/s)	Bed roughness k_s (mm)	Sand transport q_s (kg/m/s)
13/05/2016	1	0.39	8.9	6	0.006
17/03/2017	1	0.32	7.3	7	0.00383
18/03/2017	1	0.42	9.4	7	0.0065
19/03/2017	1	0.44	10.1	6	0.0265
	2	0.47	10.8	6	0.0262
	3	0.45	10.1	7	0.0268
	4	0.43	9.7	7	0.0157
21/03/2017	2	0.36	8.2	7	0.0041
12/11/2017	1	0.56	12.7	7	0.023
25/04/2018	1	0.39	8.9	6	0.0065
	2	0.41	9.4	6	0.0073
26/04/2018	1	0.38	8.7	6	0.0088
	2	0.37	8.3	7	0.0075
27/04/2018	1	0.34	7.8	6	0.0122

Table 4.2.11 *Field data sand transport at Mariakerke beach, Belgium (2016-2018); run duration= 15 to 30 min; d_{50}=0.31 mm; $p_{shell} \cong 5\%$ (Strypsteen et al., 2019)*

Date	Run	Bed shear velocity u_*(m/s)	Wind velocity at z_w=2 m a.b. u_{2m} (m/s)	Bed roughness k_s (mm)	Sand transport q_s (kg/m/s)
19/10/2016	1	0.45	9.1	19	0.0069
	2	0.41	8.2	20	0.0035
24/11/2016	1	0.47	8.5	43	0.021
	2	0.52	9.4	44	0.0245
	3	0.45	8.1	44	0.0139
	4	0.49	8.9	42	0.02
	5	0.52	9.4	43	0.0282
	6	0.54	9.8	43	0.0338
29/01/2018	1	0.51	12.0	5	0.019
	2	0.45	11.6	2	0.021
	3	0.53	10.6	20	0.037

Table 4.2.12 *Field data sand transport at Koksijde beach, Belgium (201-2018); run duration=15 to 30 min; d_{50}=0.22 mm; $p_{shell} \cong 10\%$ to 15% (Strypsteen et al., 2019)*

4.3 Calibration of predictive model

The coefficients α_1 and α_2 of Equation (3.4.8) are found to be α_1 =15 and α_2= 1 for the wind tunnel data sets of Han et al. (2011) and Yang et al. (2019). These experiments refer to a flat sand bed without shells (γ_r = 1; d_{90}=2d_{50}). The predicted grain roughness values are in the range of 3 to 20 mm depending on the wind velocity between 8 and 22 m/s. Measured values of the roughness are not given by Han et al. (2011) and Yang et al. (2019). However, the computed roughness values are of the right order of magnitude compared to the range of 1 to 10 mm found by Strypsteen et at. (2019) for the flat beach of Mariakerke (Belgium).
The computed sand transport rates are all within a factor 2 of the measured values for 0.2 mm-sand used by Han et al. (2011) but are systematically too large (factor 2) for the 0.455 mm-sand of Yang et al. (2019). see **Tables 4.3.1** and **4.3.2** and **Figure 4.3.1**.

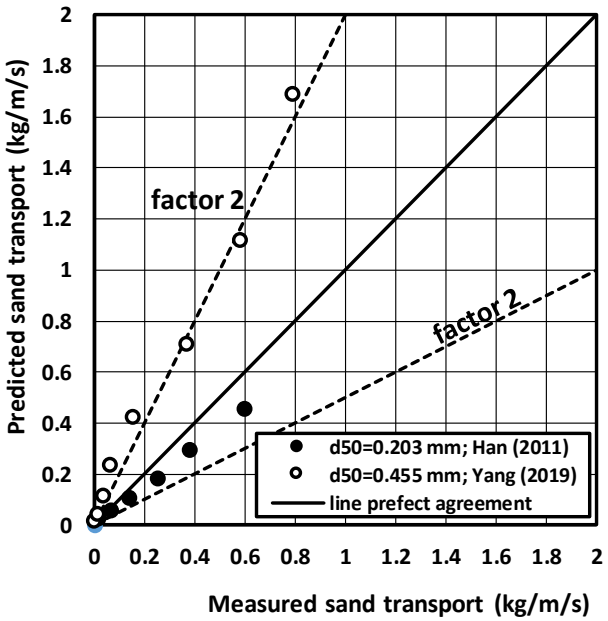

Figure 4.3.1 *Comparison of measured and computed sand transport; α_B=2; α_{th}=0.11; d_{90}=2d_{50} data of Han et al. (2018) and Yang et al. (2019)*

Wind velocity at z_w=0.6 m above sand surface (m/s)	**Sand transport for dry sand bed; modified Bagnold-model** (α_B=2; α_{th}=0.11)		
	Measured	Computed (α_1= 15; α_2=1; d_{90}=2d_{50})	
		Roughness height $k_{s,grain}$ (mm)	Sand transport (kg/m/s
10	0.015	6.4	0.026
12	0.065	10.5	0.056
14	0.14	15.2	0.107
16	0.25	20.7	0.184
18	0.38	26.9	0.296
20	0.60	33.8	0.453

Table 4.3.1 *Comparison of measured and computed sand transport; dry sand d_{50}= 0.203 mm; $u_{*,th}$=0.23 m/s; data of Han et al. (2011)*

Wind velocity at z_w=0.3 m above sand surface (m/s)	**Sand transport for dry sand bed; modified Bagnold-model** (α_B=2; α_{th}=0.11)		
	Measured	Computed (α_1= 15; α_2=1; d_{90}=2d_{50})	
		Roughness height $k_{s,grain}$ (mm)	Sand transport (kg/m/s
8	0.00067	6.9	0.0156
10	0.015	6.7	0.043
12	0.038	12.3	0.113
14	0.063	18.8	0.233
16	0.153	26.4	0.422
18	0.37	35.0	0.707
20	0.58	44.6	1.12
22	0.79	55.2	1.69

Table 4.3.2 *Comparison of measured and computed sand transport; dry sand d_{50}= 0.455 mm; $u_{*,cr}$=0.345 m/s; data of Yang et al. (2018)*

4.4 Verification of predictive model

The predictive model consisting of Equations (3.1.2, 3.1.4 and 3.4.8) has been verified using the data sets of Belly (1964), Sherman et al. (1998, 2013) and Strypsteen et al. (2019). In all, 105 high-quality data sets have been used.
The input data are the measured wind velocity at z_w=2 m, the d_{50} and d_{90}-values, see **Table 4.4.1.** For all field data, it is assumed that d_{90}=3d_{50}.
The roughness related to background irregularities is varied between 1 and 15 mm depending on the presence of shells and other irregularities. No information is available for the field sites of Portugal and Brazil. As relatively coarse sand is present at these sites, the background roughness is set to 2 mm.
The background roughness is set to 2 mm for the data of Mariakerke beach where minor shells and other irregularities were observed and to 15 mm for the data of Koksijde beach where large patches of shells and shell fragments/hash were observed. McKenna et al. (2012) found k_s-values in the range of 1 to 6 mm for a surface with many shells in a wind tunnel. In field conditions these values will somewhat larger due the presence of shell clusters.

The computation procedure for dry sand is as follows:

1) specify wind velocity u_w at one height;
2) specify d_{50} and d_{90} of sand;
3) specify longitudinal and lateral slope angles (= 0 for horizontal surface);
4) specify background roughness of irregularities $k_{s,ir}$;
5) compute static grain roughness $u_{*,grain}$ by Eq. (3.4.8c);
6) compute threshold shear velocity $u_{*,th}$ by Eq. (3.1.4);
7) compute T-parameter by Eq. (3.4.8b);
8) compute bed roughness k_s by Eq. (3.4.8a),
9) compute shear velocity u_* by Eq. (3.4.8d);
10) compute sand transport q_s by Eq. (3.1.2).

Other parameters are: κ=0.4; ρ_{air}=1.2 kg/m^3; ρ_{sand}=2650 kg/m^3;α_B=2; α_{cth}=0.11; $d_{50,ref}$= 0.00025 m.

Figure 4.4.1 the comparison of measured and computed sand transport rates for all available 118 data points. (1998). Most (73%) of the predicted data are within a factor of 2 of the measured values. Similar scores were obtained by Van Rijn (1984) for sand transport by water flow. Given all variabilities and non-uniformities involved and the problem of measuring under extreme wind conditions, it may be almost impossible to predict the sand transport with an accuracy less than a factor of 2. The predicted values are sometimes too large at conditions near the threshold value, which is an inherent effect of a deterministic approach. This is, however, not important for engineering practice as the transport rates involved are very small. The predicted values are somewhat too small for higher wind velocities. The model underprediction may be related to the underprediction of the dynamic grain roughness ($k_{s,grain,dyn}$), as only a few laboratory data of Han et al. (2011) and Yang et al. (2018) were used to calibrate the dynamic grain roughness (Equation 3.4.8). This can be improved by using results from new wind tunnel tests with flat mobile beds (future research). According to Sherman et al. (2013), the measured transport rates at their field sites may be slightly too small, as minor moisture may have been present in the sand surface raising the threshold values slightly. Most likely, measured transport in field conditions are somewhat too small rather than too large given the relatively low efficiencies of most trap samplers. Sherman et al. (2013) noticed significant overprediction (factor 2 to 3) of the original Bagnold-equation with measured shear velocities as input (κ=0.4). The overprediction is substantially reduced by using smaller bed-shear velocities taking only grain-related roughness into account (Equation 3.4.8).

Data set	Number of data points	Wind velocity (m/s)	Grain size		Roughness of irregularities $k_{s,ir}$ (mm)
			d_{50} (mm)	d_{90} (mm)	
Wind tunnel experiments (Belly 1964)	36	5-12	0.44, 0.3, 0.145	$3d_{50}$	0
Wind tunnel experiments (Han et al. 2011)	6	10-20	0.203	$2d_{50}$	0
Wind tunnel experiments (Yang et al. 2019)	8	8-22	0.455	$2d_{50}$	0
Inch spit beach, Ireland (Sherman et al. 1998, 2013)	17	5-10	0.17	$3d_{50}$	1 (minor shell < 2%)
Esponsende site, North Portugal (Sherman et al., 2013)	12	10-14	0.27-0.35	$3d_{50}$	2
Jericoacoara site, 500 m from shoreline, north-eastern coast of Brazil (Sherman et al., 2013)	15	13-17	0.22-0.44	$3d_{50}$	2
Mariakerke beach Belgium (Strypsteen et al., 2019)	14	6-11	0.31	$3d_{50}$	2 (minor shell < 5%)
Koksijde beach Belgium (Strypsteen et al., 2019)	11	8-12	0.22	$3d_{50}$	15 (many patches of shells and shell hash; 10%-15%)

Table 4.4.1 *Grain size and roughness input parameters of calibration and verification data*

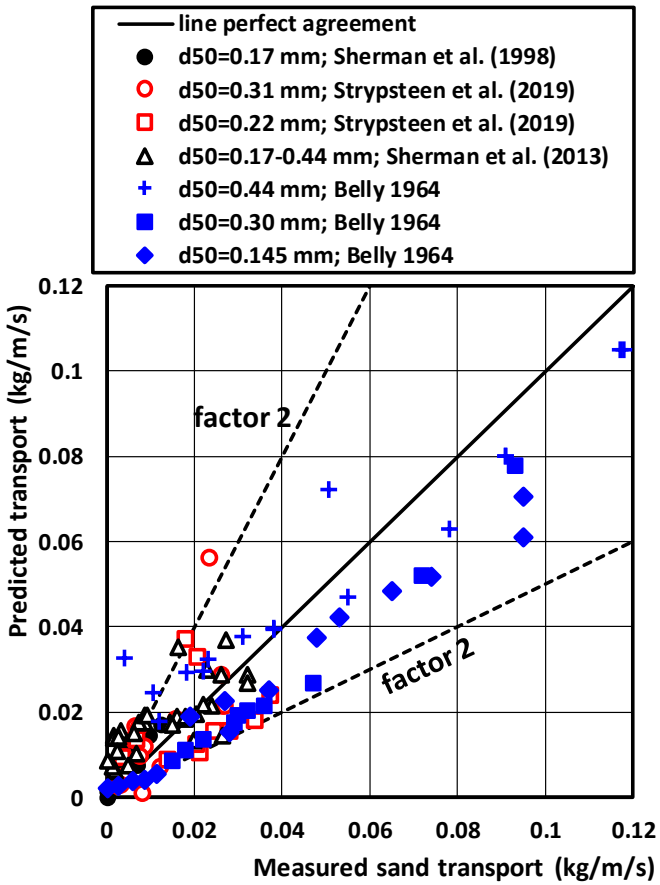

Figure 4.4.1 *Comparison of measured and computed sand transport*

5. Processes affecting sand transport

5.1 General

A fully predictive model must include the effects of varying moisture content, vegetation and shells. Herein, it is proposed to represent these effects by simple coefficients acting on the bed-shear velocity, the threshold velocity or on the sand transport rate. The proposed coefficients are derived from reliable data in the opinion of the authors and can be seen as first estimates for engineering purposes. Further research is required to improve and extend the knowledge. Some processes can be studied in wind tunnels (effect of bed slope, moisture and shells), but other processes can be better studied at field sites (vegetation, saturation). Given time and budget, the proposed coefficients can be gradually improved as more data become available.

5.2 Moisture content and cohesion

Wind-induced sand transport is strongly affected (reduction factor of 2 to 10) by moisture content of the sand surface (upper 1 to 3 mm) and related cohesion/adhesion effects, particularly for lower wind velocities < 20 m/s (Hotta et al., 1984). Moisture contents up to 8% had much less effect (< factor 2) for high wind velocities in the range of 20 to 30 m/s in a wind tunnel (Hotta et al., 1984).
Cohesion and adhesion between particles increase the surface resistance against erosion (threshold shear velocity). Cohesion and adhesion effects may result from the presence of moisture, salt, algae, clay, organic matter and calcareous materials. Even low levels of moisture may effectively reduce the transport rate of dry sand. However, intensive rainfall may also increase the sand transport rate by splash effects promoting saltation processes. Moisture content (w) may be the direct result of precipitation, water spray, wave uprush near the water line or capillary action (adhesive forces; surface tension forces).
Moisture fraction is generally defined as: w= mass water of sample/mass dry sand of sample (moisture content is moisture fraction x 100%). Moisture content of a saturated sample can be computed by the expression $w_{saturated}=[\varepsilon/(1-\varepsilon)][\rho/\rho_s]x100\%$ with ε= porosity factor (0.35-0.45 for sand); ρ= water density ($\cong$1000 kg/m^3); ρ_s= sand density ($\cong$2650 kg/m^3), yielding $w_{saturated}$= 20%-30%. Generally, moisture contents are in the range of 0 to 10%, as the pores are not fully saturated with water.
Let us assume that a sand particle with diameter D is covered by a thin water film with thickness δ except at the particle contact points; any other pore water is absent.
The volume of the water film is: $V_{wf} = 1.33\pi\ [(0.5D+\delta)^3-(0.5D)^3]$ and the mass is: $M_{wf}=\rho V_{wf}$.
The volume of the sand particle is: $V_{sand}=1.33\pi(0.5D)^3$ and the mass is $M_{sand}=\rho_s V_{sand}$.
The mass ratio of water and dry sand defined as the moisture fraction is:
$w= M_{wf}/M_{sand}= \rho[(0.5D+\delta)^3-(0.5D)^3]/[\rho_s(0.5D)^3]$.
Using: D=200 μm for sand, δ=0.01D=2 μm, it follows that: $w \cong 0.025$ (2.5%).
Thus, a thin water film with thickness equal to 2 μm surrounding a sand particle of 200 μm yields a moisture content of about 2.5%. A water film of 1 μm yields a moisture content of 1%. Dry sand has a moisture content < 0.25% (Han et al., 2011). In conditions with a moisture content > 2.5%, the sand transport rate is strongly reduced to a very small value. In conditions with w=10% (near the water line), the surface is so saturated that aeolian transport reduces to almost zero even under very strong winds.

Small amounts of moisture are characteristic of beach sediments with moisture being created from a variety of sources, including wave uprush, capillary rise from the subsoil water table, wave spray and precipitation (rain fall). Field experiments (Davidson-Arnott, 2008) show that the moisture content at a certain location and thus the threshold shear velocity can change over a period of minutes to hours through drainage as the beach water table falls or drying by wind and solar radiation. Surface moisture can limit the rate of release of sediment from the surface, even when sediment transport is continuous, and that it is probably the primary control on the observed adjustment effects on beaches. Even low levels of moisture may effectively

reduce the maximum transport rate, i.e. the final transport rate may never reach levels predicted for dry sand. Based on this, the wind-driven sediment transport is highly variable in space and usually intermittent in time. Moisture increases the resistance of the sand particles against lift and drag, due to cohesive forces of the adsorbed water films surrounding them. Intense rainfall increases the moisture content and thus the cohesion between the beach surface particles, but it may also enhance the sand transport rate by combined splash and saltation processes. On sandy beaches, the splash process is significant over short time intervals during high-intensity rain events, but this effect is, in terms of quantity, of secondary importance. The cohesion effect of residual moisture resulting from rainfall lasts over longer time spans and is of crucial importance yielding a significant reduction of the threshold shear velocity and hence sediment transport.

Various authors have studied the influence of moisture on the threshold shear velocity of sand particles by wind in wind tunnel conditions (Chepil, 1956; Belly, 1964; Hotta et al., 1984; Saleh and Fryrear, 1995; Cornelis and Gabriels, 2003 and Han et al., 2011) and in field conditions (Davidson-Arnott et al., 2005, 2008; Udo et al., 2008).

Moisture content of upper 1 to 2 mm (%)	**Measured threshold shear velocity (m/s)**
0.12	0.35
0.15	0.37
0.22	0.4
0.3	0.42
0.5	0.47
0.8	0.52
1.3	0.55
3	0.58

Table 5.2.1 *Measured threshold values as function of moisture content; d_{50}=0.44 mm (Belly 1964)*

Belly (1964) studied the effect of moisture on the threshold shear velocity in a wind tunnel with a sand surface (d_{50}=0.44 mm). Two conditions were studied: i) winds of various humidity values were blown over the sand for a sufficiently long time to dampen the sand surface and ii) adding water directly to the sand surface in combination wind saturated with water to prevent drying of the sand surface. It was very difficult to keep the air at a particular humidity during the tests, because the water vapor condensed on the wall of the tunnel and around the fan when air is circulating in the tunnel. It was decided to take account only of the ultimate threshold being the lowest wind strength which gives a general movement of the sand. This was defined as occurring when the sand transport rate was 0.04 gram/cm/sec. The results of Belly (1964) are shown in **Table 5.2.1**. and in **Figure 5.2.3**.
Belly proposed the following function: $u_{*,th,wet}/u_{*,th,o}=1.8+0.6\log(w_{2mm})$ with w_{2mm}= moisture content op topmost 2 mm of the sand surface (%), see **Figure 5.2.3.**

Hotta et al. (1984) observed a constant threshold increase of 0.075 m/s for each 1%-increase of moisture (w_{5mm}) up to w_{5mm}=8%.

Cornelis and Gabriels (2003) studied the effect of moisture on the threshold shear velocity in a wind tunnel with a sand surface (d_{50}= 0.25 mm). Wind-tunnel experiments were conducted on pre-wetted dune sand with moisture contents ranging from 0 to 4%. Sand samples were exposed to different wind speeds for 2 min. Moisture content (in kg/kg) was determined gravimetrically before and after each experiment, and the saltation of sand particles was recorded electronically with a saltiphone. Shear velocities were derived from

the wind speed profiles. For each moisture content, the experiments were repeated at different shear velocities, with the threshold shear velocity being determined by least-squares analysis of the relationships between particle number rates and shear velocity.
The sand was prewetted by mixing with a known amount of demineralized water. The pre-wetted samples were kept in closed plastic bags for 24 h in order to obtain a homogeneous distributed moisture content. The samples were placed in a tray (0.9x0.4x0.02 m), which was located at a distance of 6 m downwind from the entrance of the wind-tunnel working section. The sample surface was smoothed and levelled to the test section false floor by drawing a straight beam across the sand surface.
Moisture content was determined gravimetrically in three replicates before and after each test on small samples taken down to 3 mm by scraping with a sharp knife. The wet sand was exposed to the wind at different shear velocities for 2 min. Before each run, the wet sand tray was covered with a Perspex sheet that was removed once the desired shear velocity was reached, which took a maximum of about 1 min for the highest shear velocities. The relative humidity was almost constant during the experiments, as measured at with a humidity probe with capacitive sensor and ranged from 31% to 34%.
The initiation of sand movement was determined by measuring, at each moisture content, the sand transport (i) near the sand surface at different shear velocities using a saltiphone. An equation of the type $I = c(u_*^3 - u_{*,th}^3)$ was fitted to the saltiphone data sets for the different moisture contents to determine the $u_{*,th}$-parameter.
Although the run time of each test was relatively short (2 min), the moisture content appeared to decrease rather rapidly as can be seen from the initial and final moisture content, see **Table 5.2.2**. The high wind velocities are most likely able to dry the uppermost surface layer rather quickly and, consequently, the drier layer that is thus formed is subjected to erosion. As a shallow but dry surface layer has now been removed, the 'new' surface has a higher moisture content compared with the layer removed. This 'new' surface thus has to dry out again before particle erosion will occur, and so on. As a consequence of these temporal changes in surface moisture content due to drying and removal of drier surface layers, the surface moisture content determined at the end of each test run is not necessarily the moisture content at threshold. It is possible that the dry layer was already partly removed at the end of the experiment. Moisture content can therefore be slightly higher and, hence, the final moisture content can be somewhat overestimated, particularly at high shear velocities. The relevance of the initial moisture content values is as follows. The sand layer that is subject to drying is probably about 1 mm thick only. Once it is dry enough, it will be removed before the drying process proceeds to the underlying layer. The initial moisture content can therefore be considered as an average value for the top layer, say a few centimeters thick.

Moisture content w_{2mm} (%)			**Threshold shear velocity (m/s)**
initial value before test	**final value after test**	**average value**	
0	0	0	0.28
0.3	0.1	0.2	0.328
1.2	0.2	0.7	0.34
0.8	0.2	0.5	0.382
1.4	0.4	0.9	0.385
1.8	0.7	1.25	0.457
3.4	1.5	2.45	0.479
2.5	2.0	2.25	0.484
4.0	2.1	3.05	0.483

Table 5.2.2 *Measured threshold values as function of moisture content; d_{50}=0.25 mm (Cornelis and Gabriels 2003)*

Han et al. (2011) studied the effect of moisture content on the threshold shear velocity in a wind tunnel with various sand beds (0.11, 0.175, 0.25, 0.35 and 0.45 mm), see **Figure 5.2.1**. The effect of moisture is negligibly

small for moisture content w_{1mm}< 0.25%. **Table 5.2.3** shows the threshold shear velocity values for dry sand and low values of the moisture content (w=0.25% and 0.5%). The results of Han et al. (2011) for almost dry sand with w_{1mm}=0.25% are slightly larger (factor 1.1 to 1.3) than that of Bagnold (1941). Sand with w_{1mm}=0.5% has a significant higher threshold shear velocity (factor 1.5 to 2). For w=2.5% the threshold shear velocity is factor of 3 higher than that for w_{1mm}=0.25%., see **Figure 5.2.1**.

Davidson-Arnott et al. (2008) studied the effect of moisture of the upper 20 mm on sand transport processes at a Canadian beach with sand of 0.26 mm. Large variations of the threshold wind speeds were observed: $U_{wind,cr,min}$= 5 m/s (lowest wind speed with sediment transport) and $U_{wind,cr,max}$= 9 m/s (highest wind speed without sediment transport) mainly due to variations of the moisture content. The mean threshold wind speed is equal to about ≅0.5($U_{wind,cr,min}$+ $U_{wind,cr,max}$) and is found to increase with moisture content w_{20mm} (about 30% for a moisture content increasing from 0 to 4%).

Particle size (μm)	Threshold shear velocity based on Bagnold (1941) dry sand (m/s)	Threshold shear velocity (m/s) based on Han et al. (2011)	
		w_{1mm}=0.25% (almost dry sand)	w_{1mm}=0.5%
110	0.17	0.23	0.38
140	0.19	0.25	0.40
175	0.21	0.27	0.42
250	0.26	0.30	0.52
350	0.30	0.35	0.65
450	0.34	0.35	0.67

Table 5.2.3 *Comparison of threshold shear velocities of Bagnold (1941) and Han et al. (2011) for dry sand and sand with low moisture contents*

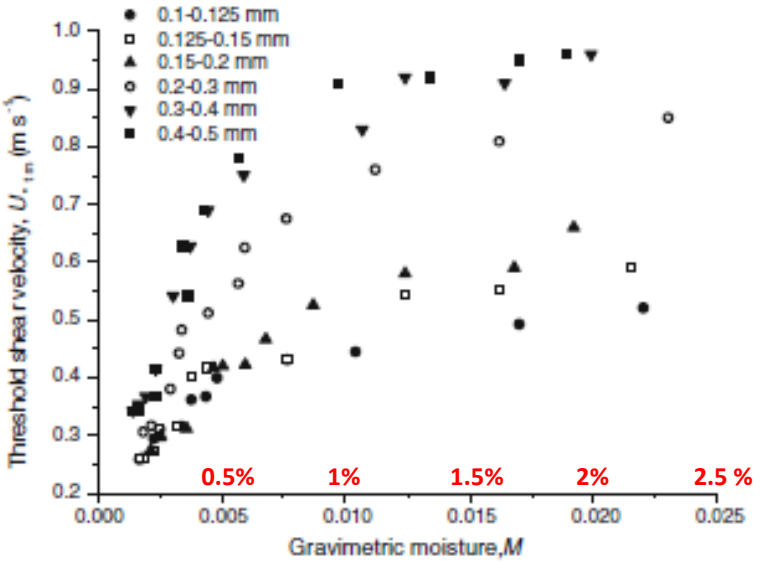

Figure 5.2.1 *Threshold shear velocity as function of grain diameter and moisture content (Han et al., 2011)*

Davidson-Arnott et al. (2008) have proposed to consider a distribution of threshold wind velocity values (rather than a single value) with $u_{cr,min}$ and $u_{cr,max}$ as the extremes for dry and moist sand (**Figure 5.2.2**). When the beach is dry, the distribution would probably reflect in some way the particle size distribution. When the beach surface is quite moist the whole distribution will shift towards much higher threshold wind speeds and the shape of the distribution may change to include the influence of cohesion processes. The shape of the distribution for the moist surface should also reflect the potential for surface drying. Incident winds also fluctuate in strength and thus have their own probability distribution, as shown in **Figure 5.2.2**. The resulting temporal pattern of sediment entrainment thus reflects the relationship between the two probability curves: one for wind speed and the other for the entrainment threshold. In **Figure 5.2.2** the threshold distribution for relatively dry sand lies mostly below that of the wind-speed distribution resulting in only a small fraction of time when the speed dropped below the threshold (nearly continuous sediment transport). However, with a relatively moist surface, entrainment will take place only when there is coincidence between higher wind gusts and surface drying shown by the small area of overlap between the two curves on the right-hand side of **Figure 5.2.2** (only occasional sediment transport).

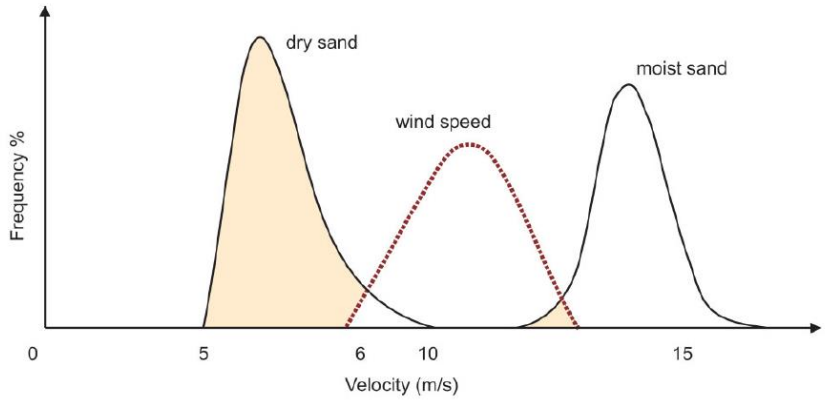

Figure 5.2.2 *Sketch of probability distribution of the threshold wind speed for dry and moist sand (Davidson-Arnott et al. 2008)*

Available data of Belly (1964), Cornelis and Gabriels (2003) and Han et al. (2011) are shown in **Figure 5.2.3**. The effect of moisture is negligibly small for moisture content w_{1mm}< 0.25% (Han et al. 2011). The threshold shear velocity increases for increasing moisture content. Sand with w_{1mm}=0.5% has a significant higher threshold shear velocity (factor 1.5 to 2) than that of dry sand. The scatter and error ranges are relatively large, which is most likely caused by the different definitions and measuring method used by the various researchers. A basic problem is the rapid decrease of the moisture content due to the blowing wind, even for very short run times (< 2 min, Cornelis and Gabriels, 2003). Field data also show considerable scatter.
Available laboratory data of Belly (1964), Hotta et al. (1984), Cornelis and Gabriels (2003) and Han et al. (2011) are shown in **Figure 5.2.3**. The effect of moisture is negligibly small for moisture content < 0.25% (Han et al. 2011). The threshold shear velocity increases for increasing moisture content. Sand with w=0.5% has a significant higher threshold shear velocity (factor 1.5 to 2) than that of dry sand. The scatter and error ranges are relatively large, which is most likely caused by the different definitions and measuring method used by the various researchers. The wind tunnel data of Belly refer to the upper 1 mm of the surface, as he used a moist air flow. The wind tunnel data of Hotta et al. refer to a layer of 5 mm as samples with thickness of 5 mm were taken from the surface. The wind tunnel data of Cornelis and Gabriels and Han et al. refer to a layer of 1 to 3 mm.
A basic problem is the rapid decrease of the moisture content due to the blowing wind, even for very short run times (< 2 min, Cornelis and Gabriels, 2003). Davidson-Arnott et al. (2008) report an increase of the threshold wind speed and shear velocity of only 20% for 0.26 mm-sand in the case of an increase of the moisture content of the upper 20 mm of the sand surface from 1 to 4% in field conditions, see **Figure 5.2.3**.

Udo et al. (2008) found an increase of a factor of 2 for 0.18 mm-sand in the case of an increase of the moisture content from 0 to 10% in the upper 20 mm.

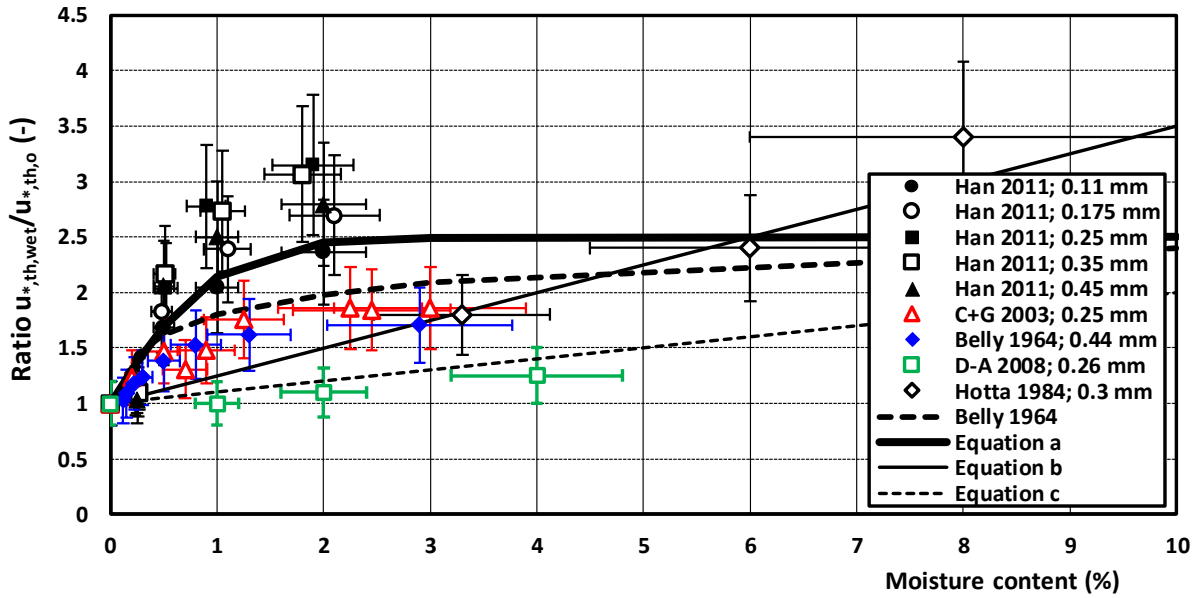

Figure 5.2.3 *Threshold shear velocity as function of particle diameter and moisture content; laboratory data (Han et al. 2011; Cornelis and Gabriels 2008; Belly 1964) and field data (Davidson-Arnott et al. 2008)*

The field results show a large discrepancy compared to those for wind tunnel conditions. Most likely, this is caused by the thickness of the top layer in which the moisture content is measured. The field data are valid for a top layer with a thickness of about 20 mm, whereas the laboratory data refer to the topmost layer of 1 to 5 mm. The moisture content of the thin top layer of 1 to 5 mm in field conditions will be much lower than the average value over a layer of 20 mm. The field experiments (Davidson-Arnott, 2008) also show that the moisture content at a certain location and thus the critical shear velocity can change rapidly over a period of minutes to hours due to drainage and/or drying by wind and sun. Large variations of the critical wind speeds were observed: $u_{w,min}$= 5 m/s (lowest wind speed with sediment transport) and $u_{w,max}$= 9 m/s (highest wind speed without sediment transport) mainly due to variations of the moisture content. Based on this, the wind-driven sediment transport is highly variable in space and usually intermittent in time. Delgado-Fernandez (2011) found that the moisture conditions of natural beaches can be crudely classified into three categories: a) dry with w_{20mm}<2% and a fully developed saltation system; b) medium with w_{20mm}=2 to 10% and restricted sand transport and c) wet with w_{20mm}>10% and sand transport is completely prevented.

The effect of the moisture content on the threshold shear velocity is herein represented by: $u_{*,th,wet}=\alpha_w u_{*,th,B}$ with

$$\alpha_{w,2mm} = 1+2\tanh(w_{2mm}) \quad (5.2.1a)$$

$$\alpha_{w,5mm} = 1+0.25w_{5mm}) \quad (5.2.1b)$$

$$\alpha_{w,20mm} = 1+0.1w_{20mm} \quad (5.2.1c)$$

with: w_{2mm}= moisture content in upper 2 mm of surface (in %), w_{5mm}= moisture content in upper 5 mm of surface and w_{20mm}=moisture content in upper 20 mm of surface. Equations (5.2.1a,b.c) and that of Belly are shown in **Figure 5.2.3**. Equation (5.2.1a) and that of Belly (1964) are both in reasonable agreement with the laboratory results, but largely overpredict for field conditions. Equation (5.2.1b) is very close to the data and the empirical equation of Hotta et al. (1984). Equation (5.2.1c) represents the field data of Davidson-Arnott (2008) and is advised for field conditions provided that the moisture content of the topmost 20 mm is measured

(input value). Application of Equation (5.2.1c) requires input data of the moisture content of the topmost 20 mm of the sand bed, either from measurements or from a prediction model for the moisture content. Brakenhoff et al. (2019) have studied the moisture content in cross-shore direction from the low tide water line to the upper dry beach and developed a prediction model for the surface moisture content calibrated with data from a mesotidal beach in The Netherlands. The length of the intertidal beach was about 60 m. Their results show that the lower 30% of the intertidal beach is always saturated with water and w_{20mm}> 20%. Higher up the tidal beach up to the high tide line, the moisture content is between 5% and 20% depending on the tidal stage; drying rates were found to be 50% in 2.5 hours. Above the high tide line, the moisture content decreased from about 5% at the high tide line to about 2% at about 30 m beyond the high tide line in conditions without rainfall. This latter zone is the transition zone to the dry beach, where the moisture content solely depends on precipitation (rainfall). In the Netherlands, there is a total rainfall time of about 500 hours or about 20 days per year in which windblown transport in the 'dry' beach zone is almost absent (wet conditions w_{20mm}>10%), about 45 days with restricted conditions (medium w_{20mm}=2% to 10%) and 300 days with dry conditions (w_{20mm}<2%). Drying times of the topmost layer of 3 mm after rainfall are found to be fairly short (< 3 hours, Hotta et al., 1984). This means that effect of precipitation on wind transport in the dry beach zone is meaningful, but not dominant. Most of the time (at least 80%), the dry beach zone is really dry.
De Vries et al. (2014) have found that the transition zone of about 30 m seaward and landward of the high tide line in which the moisture content reduces from about 5% to 2% is an important source of sand for the gradual pickup (entrainment) of sand, as other supply-limiting factors (shells, vegetation) are absent in that zone. The pickup process will continue in the dry beach zone if supply-limiting factors are absent (shell lag deposits, vegetation).

5.3 Vegetation

Wind-blown sand transport is substantially reduced if numerous roughness elements are present on a sand surface, as shown in a fundamental study by Gillies et al. (2006). Sand transport was measured between plastic buckets (4 different configurations) resting on a flat horizontal sand surface. Results of these tests indicate that sediment transport rates through patches of roughness are controlled by the roughness density depending on the dimensions (width, height) and number of elements. Sand transport reductions based on comparison with upwind trap results were as large as 90%.

The effects of vegetation on wind-blown sand can be described as (Wolfe and Nickling 1993):

- vegetation extracts momentum from the air flow resulting in larger roughness;
- vegetation elements are obstacles for saltating sand grains;
- vegetation reduces part of the surface where sand transport takes place.

Vegetation leads to an increase of the aerodynamic roughness length (z_o), and to an increase of the friction velocity above the vegetation layer. Vegetation is herein identified as grass-type plants with a maximum height of about 0.5 m. In the layer with vegetation, momentum is extracted from the air flow and turbulence is produced at the lee side of the roughness elements. The friction velocity (u_*) depends on the vegetation physiography, and on the density and spatial configuration of the plants/stems, which can be described by a reduction factor acting on the shear velocity. The shear velocity can be determined from wind velocity measurements outside the roughness layer (say 2 times the plant height) to eliminate the local velocity variations occurring between the plants. Both the shear velocity and overall effective bed roughness will increase due to the presence of the vegetation.
Two approaches are possible to account for the effect of vegetation on the sand transport rate:

- increase of the threshold value as the sand grains are hiding between the vegetation and the application of the total bed-shear velocity for sand transport (Musick and Gillette, 1990; Musick et al., 1996; Raupach et al., 1993);
- reduction of bed-shear velocity acting on the sand grains between the vegetation and the application of the standard threshold shear velocity (Raupach 1992).

The latter approach requires partitioning of the bed shear stress ($\tau=\tau'+\tau''$) into a component related to grain roughness (τ') and another component related to form drag of the vegetation (τ''). The stress component τ' represents the averaged stress on the exposed surface. This approach has been formulated in great detail by Raupach (1992), Brown et al. (2008), Shao et al. (2015). Raupach assumed that the surface consists of randomly distributed cylinders uniform in size, each having a frontal area of a_f and n is the number density (number unit area) of the roughness elements (roughtons). The frontal area index of the roughtons is $\lambda=n\ a_f$. The ratio of roughton basal area to frontal area is $\sigma=a_b/a_f$ and the exposed percentage of the surface subject to wind velocity is $p_s=(1-\sigma\lambda)100$ and the cover percentage $p_v=\sigma\lambda 100$.
The shear stress on the exposed surface can be expressed as: $\tau'/\tau=[1-\sigma\lambda]^{-1}[1+\beta\lambda]^{-1}$ with $\beta=C_r/C_s$ and C_s= frictional drag coefficient and C_r= pressure drag coefficient.
Raupach et al. (1993) formulated a correction factor for the threshold friction velocity in the presence of roughness elements: $u_{*,th}=u_{*,th,o}\ [(1-m\sigma\lambda)(1+m\beta\lambda)]^{0.5}$ with m=coefficient < 1.
For example: n=10 dune plants per m^2; $a_b=0.01\ m^2$; $a_f=0.03\ m^2$; $\beta=10$ and m=0.5, then $\lambda=n\ a_f=0.3$ and $\sigma=a_b/a_f=0.33$ and $p_s=(1-0.3x0.033)100=99\%$ and $p_v=1\%$ and thus: $\tau'/\tau=[1-\sigma\lambda]^{-1}\ [1+\beta\lambda]^{-1}\cong 0.3$ and $u_{*,cr}\cong 1.5\ u_{*,cr,o}$.
The approach of Raupach is most scientific, but it contains many coefficients and parameter to be specified, as the vegetation roughness is of complex nature with many influential parameters (stem diameter, stem height, number of stems per bundle; bundle porosity, bundle configuration, heterogenous clustering, etc). Herein, a simpler approach is proposed for engineering practices by using a correction coefficient based on percentage of cover and on the vegetation height and acting on the shear velocity (see Equation 3.1.6).
Various researchers have studied the effect of vegetation on wind-blown sand transport in wind tunnels (Buckley, 1987; Burri et al., 2011; Youssef et al., 2012; Hesp et al., 2019) and at field sites (Wasson and Nanninga, 1985; Lancaster and Baas 1998; Arens et al., 2001; Hupy 2003; Hesse and Simpson, 2006; Davidson-Arnott et al., 2012).
Buckley (1987) studied the effect of sparse vegetation on wind-blown dune sand (0.15 mm) in a wind tunnel. Three plant types were used, corresponding to characteristic shapes of common small herbaceous dune plants; Type F: erect and spreading, 10 cm high and 12 cm across; Type G: graminiform, 12 cm high and 9 cm across; and Type R: rounded, 5 cm high and 7 cm across. The plants were mounted in narrow copper tubes soldered to moveable baseplates under the same bed. Plants were distributed in 7 contiguous 1 m squares in the central segment of the test section, with the same density (n) in each square. Densities of 0, 1, 2, 3, 4, 5, 7, 10 and 15 plants per square meter were tested for each plant type, representing projected cover percentage of 0-17% for type F, 0-10% for type G and 0-4% for type R. Sand transport was measured with three high precision vertical profile traps 50 cm downstream of the vegetated area: one in the center of the tunnel, and one 20 cm in from each edge. Each trap consists of a knife-edged vertical slot 1 cm across, divided into 1 cm square orifices leading to independent collectors under the tunnel.
The effect of plant cover on sand transport rate at constant wind velocity for type F is, as follows:

- cover 1%: reduction of sand transport by 8% for wind velocity of 10 m/s and 7% for 15 m/s;
- cover 5%: reduction of sand transport by 35% for wind velocity of 10 m/s and 30% for 15 m/s;
- cover 10%: reduction of sand transport by 60% for wind velocity of 10 m/s and 50% for 15 m/s;
- cover 20%: reduction of sand transport by 90%; for wind velocity of 10 m/s and 85% for 15 m/s.

The results of Buckley (1987) are shown in **Figure 5.3.3**.

Lancaster and Baas (1998) studied the effect of vegetation on the bed roughness and the sand transport process at the western part of the former delta of the Owen River in eastern California, USA. The surface

sand at the site is coarse (median particle size of 500 to 1000µm). The sand sheets are vegetated with salt grass with a cover that ranges from zero to about 30 per cent and which increases northwards, see **Table 5.3.1**. Four 40 m by 15 m plots (A,B,C,D) were selected with a cover density from bare to moderate, see **Figure 5.3.1**. The maximum relief on each of the plots was less than 1 m and ranged between 0·15 m at Site A to 0·80 m at Sites C and D.

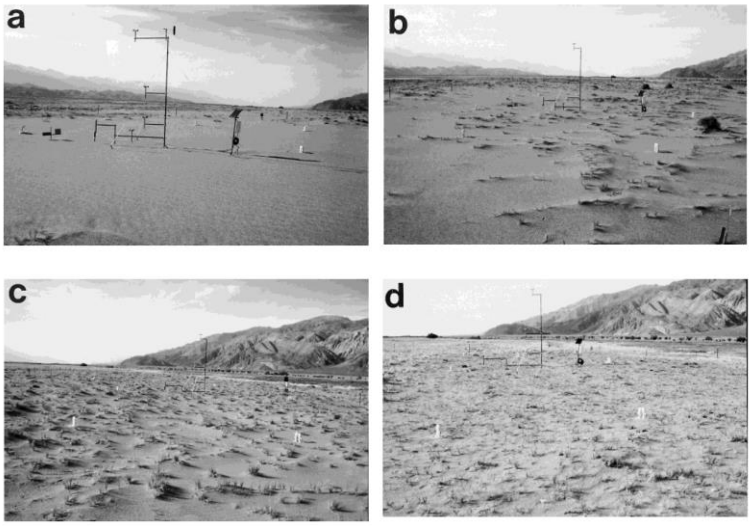

Figure 5.3.1 *Study sites Owens Lake, California, USA (Lancaster and Baas, 1998)*

Sites	Median particle size (mm)	Height vege tation (mm)	Cover vege tation (%)	Bed roughness (mm)		Thres hold shear velo city (m/s)	Sand flux at 0.1 to 0.2 m above bed and averaged over all events (g/m²/s)	
				static (no tran sport)	dynamic (tran sport)		wind from NW (10 events)	Wind from South (6 events)
A. smooth, bare, wind-rippled sand bed; relief 0.14 m	0.5-1	0	0	27	20-40	0.42	0.6	0.5
B. within a wide blowout	0.5-1	100	4.2	100	60-90	0.45	0.3	0.5
C. relief with small (0.30–0.50 m high) sand mounds around clumps of salt grass	0.5-1	90	12	325	240-600	0.75	0.14	0.3
D. broad undulations 0.2m to 0.6m high.	0.5-1	110	26.3	440	400-530	0.81	0.04	0.02

Table 5.3.1 *Basic data based on Lancaster and Baas (1998)*

Each plot was instrumented from early November 1995 to May 1996 with eight bidirectional sand collectors at a height of 0.1 m; a mast with four Met One cup anemometers at heights of 0.5, 1.0, 2.0 and 4.0 m; a piezo-electric sensor to detect the onset of transport at height of 0.2m, and a BSNE sand trap at 0.2 m height. The vegetation cover was determined as: $p_{veg}=(1/A)\sum(w\ b)x100\%$ with w= length of vegetation plant along longest axis and b= length of vegetation plant along perpendicular axis and A= total area considered.
The threshold wind shear velocity for sediment transport was determined by identifying the 5 min intervals at which the impact sensor started and ended recording particle movement. The u_* value for these intervals was considered to be the threshold shear velocity at the start and end of sand transport. The value for the bare sand site compares well with the value for threshold velocity calculated using the equation of Bagnold

(1941), which is 0·49 m/s for a sand with a modal diameter of 1 mm. The threshold values were found to increase for increasing vegetation cover, see **Table 5.3.1**. The sand flux measured at 0.1 to 0.2 m above the bed was largest at the sites A and B with a vegetation cover < 5%, see **Table 5.3.1**. The sand flux strongly decreases for increasing values of the vegetation cover. **Figure 5.3.3** shows the normalized sand transport rates (compared to upwind transport rates) for increasing cover values. A vegetation cover of 10% already gives a reduction of 50%. The reduction is about 90% for a cover of about 25%.

Arens et al. (2001) studied the effect of vegetation density on aeolian sediment transport and deposition in the area of foredunes. Reed stems are planted as a surrogate for vegetation at the frontal side of the foredune. Three plots were planted with 4, 2 and 1 bundles per m^2. Each bundle consists of 15 stems; bundle diameter is 0.17 m; porosity of bundle is about 50%. Profile changes were measured between May 1996 and April 1997. When the stems had been completely buried, differences in profile evolution vanished. After a second planting of reed stems in January 1997 the process was repeated. The study site is located near the Hague; Dutch North Sea coast, The Netherlands. The beach was nourished in 1995. The height of the foredune is around 12 m above mean sea level. The top and the landward side of the foredune are densely covered with marram grass, but the seaward dune front is bare. This is the zone where reed stems are commonly planted to trap sand. The beach is wide and dissipative, with an average tidal range of 2 m. The dry beach width is about 50 to 60 m. The seaward front of the foredune was partitioned into three plots, each 100 m long along the foredune and 10 m wide over the cross-shore. The height of the stems is approximately 0.5 m immediately after planting and gradually decreases due to sand burial. The number of bundles is 1 per m^2 at distance of 1 m in plot N1, 2 per m^2 at distance of 0.7 m in plot N2 and 4 per m^2 at distance of 0.5 m in Plot N4, see **Figure 5.3.2**.

Sediment transport measurements were performed in February 1997. Transport rates were measured using omnidirectional, vertical sand traps, consisting of six to ten trays that are stacked at 5 cm intervals. Traps were placed on three locations: the beach, near the dune foot and in the plots at about 8 m from the seaward boundary of the plot. The influence of reed stem density can be clearly observed from **Figure 5.3.2**.
Plot N4: Deposition starts at the first row, and a steep, small dune is developed. The back of this dune gradually migrates upslope over time. Once a row of bundles is filled up completely, sand is transported further landward, and deposition starts within the next row.
Plot N1: Deposition occurs simultaneously over almost the entire depth of the plot. Strongest deposition does not occur at the first row, but at some distance from the seaward boundary of the bundles. A more gentle and wide dune develops and deposition is spread out over a number of rows. Some deposition also occurs behind the zone of reed stems.

Figure 5.3.2 *Plots N1 and N4 (Arens et al. 2001)*

Plot N2 shows an intermediate type development which, however, resembles Plot N1 more than Plot N4.
In May 1997, all plots had gained a sand volume of about 12 m^3/m, indicating that the sediment budget is relatively constant, regardless of the particular profile evolution.
Analysis of all sand trap data (wind velocity between 10 and 12 m/s) shows roughly (see also **Figure 5.3.3**):

- plot N1 with cover= 2.3%; sand transport ≅ 60% of upwind sand transport without reed;
- plot N2 with cover= 4.5%; sand transport ≅ 30% of upwind sand transport without reed;
- plot N4 with cover= 9.1%; sand transport ≅ 0.1% of upwind sand transport without reed.

Burri et al. (2011) performed a windtunnel study of wind-blown sand with live plant canopies: three canopy densities (cover 4%, 16% and 47%) of Perennial Ryegrass (h=6 cm) and bare sand surfaces (d_{50}≅0.6 mm). Experiments were performed with three canopy densities of Perennial Ryegrass and with bare sand surfaces. The results suggest that the total sediment mass flux decreased rapidly with increasing canopy density, as follows:

- large-density canopy (frontal area index λ = 0.58; cover 47%): reduction of transport compared to unplanted configuration by about 99%;
- medium-density canopy (λ = 0.16; cover 16%); reduction of transport by about 90%;
- small-density canopy (λ = 0.03; cover 4%), increase of transport by about 20%, which is attributed to elevated shear stress on the sand bed caused by flow acceleration and turbulence produced by the plant elements; the grasses were observed to trigger erosion by oscillating movements at the surface.

Davidson-Arnott et al. (2012) reported a 99%-reduction of sand transport at a vegetated foredune (stations 6,10) with cover percentages of 15 to 25% compared with sand transport at the beach (stations 1,3,4; d_{50}=0.26 mm) during an event with wind velocities of about 10 to 11 m/s. Sand transport reduced from about 50±30 kg/m/hr to about 0.35±0.25 kg/m/hr. These results are in line with the values presented in **Figure 5.3.3**.

All available data are shown in **Figure 5.3.3**. It can be clearly seen that high reed bundles (h=50 cm) of Arens et al. (2001) have a greater reducing effect on the sand transport rate than the lower plants (h=10cm) used by Buckley (1987) and Lancaster and Baas (1998). Hupy (2003) found that sand transport was much larger in areas of loose sand and at sites directly downwind from loose sand than in areas containing heavy crusting, gravel, or a forb/grass cover. Differences between sites with gravel surfaces and those with forb/grass cover were, however, insignificant. Thus, the cover percentage seems to the dominant factor rather than the type of cover. Hesse and Simpson (2006) also conclude that sand movement along desert dunes is primarily controlled by vegetation cover. Sand movement responds to short-term variations in vegetation cover (including crust). A simple threshold of vegetation cover below which sand transport begins was not found.

The data of **Figure 5.3.3** can be crudely represented by an engineering expression, as follows:

$$\alpha_{veg}=[1-(\Delta_{veg}/\Delta_{veg,minimum})^{0.5}p_{veg}/100]^2 \qquad (5.3.1)$$

with: p_{veg}=percentage of vegetation cover (%); Δ_{veg} = height of vegetation which is of order of 0.1 to 0.5 m; $\Delta_{veg,mimimum}$ = minimum height of vegetation (about 0.1 m).
Computed results are shown in **Figure 5.3.3** for wind velocity=12 m/s at z_w=2 m and d_{50}=0.3 mm, d_{90}=0.5 mm. This approach yields a reduction of the sand transport rate by about 80% for p_{veg}=25% and $\Delta_{veg}/\Delta_{veg,minimum}$=1. Lancaster and Baas (1998) found a reduction of almost 95% for a vegetation cover of about 25%. The agreement is not perfect, but the general trends are well represented. More field research is required to extend the knowledge of the vegetation effect.

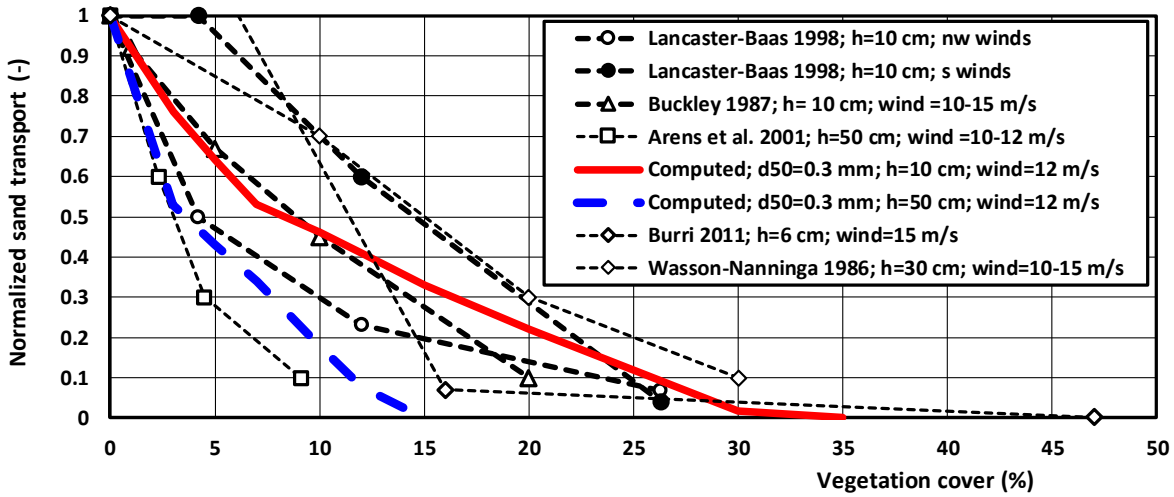

Figure 5.3.3 *Normalized sand transport (ratio of transport and upwind transport) as function of vegetation cover based on various field data*

5.4 Shells

Wind-induced sand transport is strongly reduced when the surface is covered with high amounts of shells, shell fragments and gravels, which are known as aeolian shell-gravel pavements (Carter 1976, Carter and Rihan, 1978). These transport limitations are caused by the presence of non-erodible roughness elements within the surface sediments. When a surface consists of normally graded sand-sized material mixed with a smaller fraction of coarse sand, the sediment flux is initially governed by the transport capacity of the wind and the grain diameter of the mobile fraction. However, as erosion proceeds the larger, non-erodible fraction becomes more exposed and remains at the surface as a deflation lag deposit, limiting the transport to almost zero at given wind-induced stress. Initially, the sand transport increases slightly for low exposure of the coarser grains due to creation of additional turbulence and local velocity accelerations around the immobile coarse grains. Eventually, the sand transport reduces significantly for a very large exposure height of the coarse grains. In that case the shear stress exerted on the smaller grains between the larger coarse grains is significantly reduced to below the threshold shear stress for entrainment (transport-limited conditions). A higher wind-induced stress is required for further erosion of the smaller grains. Lag deposit surfaces can be observed at agricultural fields (Chepil and Woodruff, 1963; Lyles et al., 1974)

Various wind tunnel studies on the effect of non-erodible coarse grains on aeolian transport have been done in the past. The effect of non-erodible roughness elements on a surface of erodible particles was studied by Gillete and Stockton (1989). An approximately 1 cm deep layer of erodible spheres was poured onto the wind tunnel floor, and the non-erodible spheres were placed on the surface in such a manner that the non-erodible spheres were half buried. The larger elements shelter part of erodible surface particles requiring larger shear stresses for erosion. Similar tests were done by Nickling and McKenna Neuman (1995). They studied the development of deflation lag deposits with a series of wind tunnel tests. Glass spheres (18 mm in diameter) were placed along the complete length of the wind tunnel working section in regular staggered arrays using three different spacings (d=18, 30 and 60 mm) and completely covered with erodible sand of 0.27 mm. The free stream velocity was 8 m/s above the surface and the sediment transport measured using a wedge-shaped trap with an electronic balance. Test results indicate that lag development has a profound effect on both the sediment flux and wind profile characteristics. Initially, there is an increase in sediment flux above that for a rippled sand bed because of increased erosion around the emerging roughness elements. As the roughness elements are more exposed (higher emergence), the sediment flux decreases rapidly, tending towards zero.

Information of the effect of gravel on sand transport can be obtained from a study of Tan et al. (2013). They studied the change in sand transport from a pure sand bed to a bed covered with gravel (20 to 55 mm) using a mobile wind tunnel operated in the Gobi Desert in China. The sand transport was reduced by about 20% for a gravel coverage of 10%, about 40% for a gravel coverage of 20%. The maximum reduction was about 50% for gravel coverage of 30% up to 70%. The basic cause the sand transport reduction is the decrease of the wind velocities in the lowest layer of 50 to 100 mm above the sand surface (measured by thin Pitot-tubes) due to the presence of the large gravel particles. As a consequence of the reduced sand transport rates, deposition of sand was observed at the bed covered with gravel particles. Similar findings are given by Gillies et al. (2006). Wind-blown sand transport is substantially reduced if numerous roughness elements are present on a sand surface. Sand transport was measured between plastic buckets (4 different configurations) resting on a flat horizontal sand surface. Results of these tests indicate that sediment transport rates through patches of roughness are controlled by the roughness density depending on the dimensions (width, height) and number of elements. Sand transport reductions based on comparison with upwind trap results were as large as 90%.

Various field studies of beach armouring studies are available, but very few studies have produced quantitative results of aeolian transport rates. Beach armouring was oberved at two nourished beach sites south of The Hague, The Netherlands (De Vries et al. 2014; Hoonhout and De Vries, 2017; De Vries and Hoonhout, 2019). Sand transport processes were measured in December 2010 at Vlugtenburg beach after nourishment which has resulted in an artificial beach, dune and foreshore. The nourished sand contains a relatively large amount of shell fragments. Due to sorting processes over time, the shell fragments form lag deposits at the upper beach, but the lag deposits are continuously reworked in the intertidal zone resulting in patchers of finer and coarser sediments. A significant gradient in sediment transport over the beach was observed during periods with onshore winds. Sediment transport increases in the direction of the wind until a certain distance. A strong increase of sediment transport is found at the lower beach during low tide. At the upper beach there is no significant increase of sediment trans due to the presence of lag deposits on the upper beach. These lag deposits limit sediment supply at the upper beach and create a spatially varying sediment supply.
Lag deposits were also formed at the Sand Motor beach south of The Hague, which is a large-scale artificial beach plain (nourishment 2011) with sand surface level at +5 m above mean sea level (Hoonhout and De Vries, 2017; De Vries and Hoonhout, 2019). The nourished sand had a d_{50} of about 0.35 mm with about 5% of coarse sediments and shells > 2 mm based samples from a depth of 0.5 m below the surface. Over time the percentage of coarse materials of the top layer gradually increased to about 20% due to winnowing of finer sand blown away in downdrift directions. This beach surface armouring process resulted in significant limitations of the sand transport rates of finer sediment compared to the transport capacity. As the beach plain is at a level of +5 m, the surface is not reworked by the action of tides and waves resulting in a very stabile armour layer except during an extreme storm wind event in combination with high surge water levels. The armour layer is absent in the intertidal zone where tides and waves are continuously reworking the top layers.

Van der Wal (1998) studied the effect of shells on the wind-induced transport rate of beach sand. Beach sand samples were taken from 5 sites along the Dutch coast and tested in a wind tunnel. The d_{50} varied in the range of 0.21 to 0.35 mm. The percentage of coarse materials consisting of gravel, stones and shells (> 2 mm) varied in the range 7% to 32%. A tray with (length=1.22m; width=0.33 m; height=0.03m) was filled with weighed oven-dried sand and placed in the middle of the test section. The sample surface was smoothed and levelled to the tray edges. The wind speed was gradually increased over one minute to about 11 m/s and kept at this speed for another minute. Then, the wind speed was gradually returned to zero over one minute. After the experiment, the sand was reweighed. The percentage of sand blown off during the test was calculated for each of the experiments. The sand transport rate without shells was reduced by about 40% for

a shell percentage of 7% and about 80% to 85% for a shell percentage of 18% to 32%. Shell pavements were formed during the wind tunnel experiments with shell-rich beach samples.

McKenna et al. (2012) conducted a wind tunnel study on the effect of various types of shells on the erosion of sand with a total area of about 10 m². They have observed in their wind tunnel experiments that the shells are not operating independently, but rather display some degree of spatial organization resulting in shell clusters of partly interlocking shells of different sizes. Shells are sometimes rolling coming to rest against others downwind resulting in clusters. Corridors of lower shell coverage are generated at the sand surface. Wind velocities were in the lower range of 8 to 12 m/s (BF<7). Three types of shells were used (**Figure 5.4.1**): crushed shells with cover percentages between 12% and 22% (heights 1.1 to 1.6 mm); small shells < 12.7 mm with cover percentages between 17% and 43% (heights 2.6 to 5.7 mm) and large shells > 12.7 mm with cover percentages between 14% and 30% (heights 7 to 9.2 mm), see **Table 5.4.1**. The freestream velocity was gradually increased until the cumulative number of particle counts recorded by a piezoelectric impact sensing device began to increase continuously. A sediment trap at the downwind end was used to collect sand particles eroded from between the shells. The test was terminated when bed the transport rate dropped to a negligible value (<0.05 g/cm/s). It was observed that the shells were organized into chains and clusters with the long axis of many of the shells appearing to be aligned with the wind flow. The threshold wind velocity and shear velocity is found to increase by about 15% to 25% for a cover of 15% and about 35% to 50% for a cover of 43%, see **Figure 5.4.2**.
The amount of erosion after the test (in kg/m^2) was recorded showing almost no erosion for the largest cover values of 40% both for small and large shells. Erosion is reduced by a factor of 5 to 10 by increasing the cover of shell from about 15% to about 30-40%, see **Figure 5.4.3**. Crushed shells are less effective than small/large shells.

Types of beds	**Height of shells above surface** (mm)	**Ratio volume shell to volume sand** (-)	**Cover** (%)	**Threshold values (m/s)**		**Bed roughness k_s** (mm)	**Erosion of sand from between shells in about 1 to 2 hours (kg/m²)**	
				Wind velocity	Shear velocity		Wind velocity =10 m/s	Wind velocity = 13 m/s
sand d_{50}=0.28 mm	-	-	-	5.5	0.26	1.2	-	-
sand+ crushed shells	1.1-1	0.125	12	6.2	0.32	1.8	4	10
		0.25	22	6.8	0.42	6.0	2	4
sand +small shells < 12.7mm	2.6-5.7	0.25	17	6.6	0.37	0.3	2.5	5
		0.5	43	7.6	0.52	1.8	0.5	0.5
Sand+ large shells > 12.7 mm	7-9.2	0.25	14	6.4	0.41	1.8	3	10
		0.5	30	7.1	0.56	4.8	0.5	1

Table 5.4.1 *Data of wind tunnel experiments on the effect of shells on wind transport; McKenna et al. (2012)*

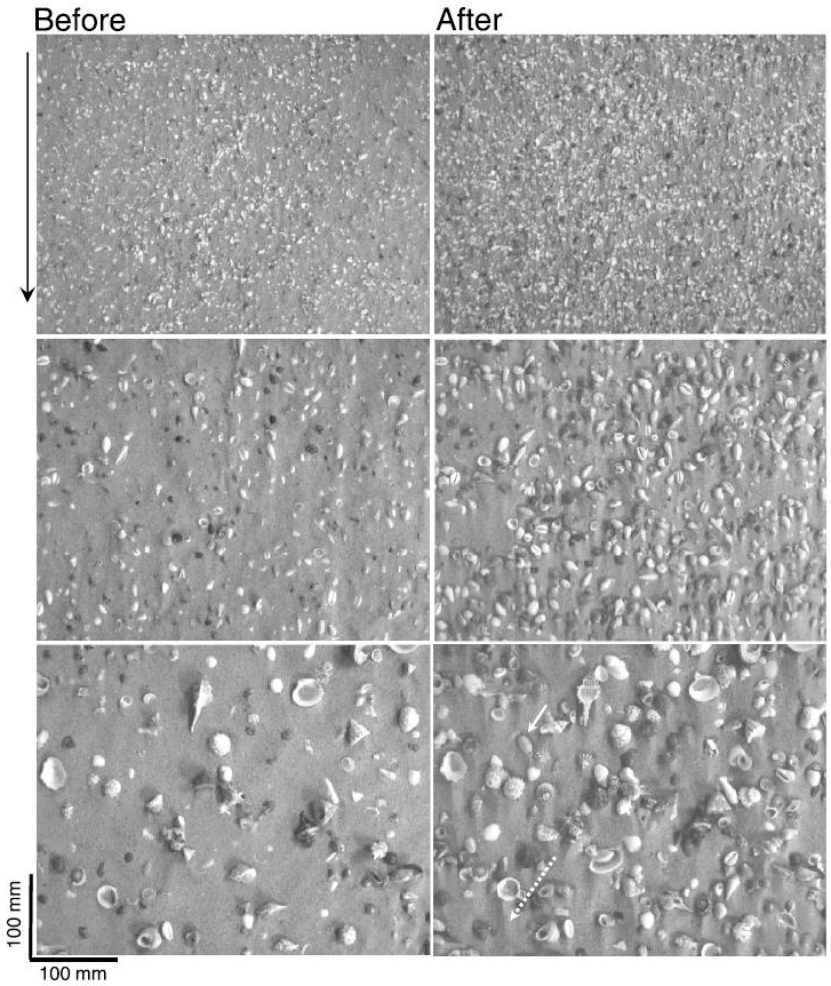

Figure 5.4.1 *Images of bed surface before and after the tests; McKenna et al. (2012)*
Top: crushed shells 22%; Middle: small shells 43%; Bottom: large shells 30%

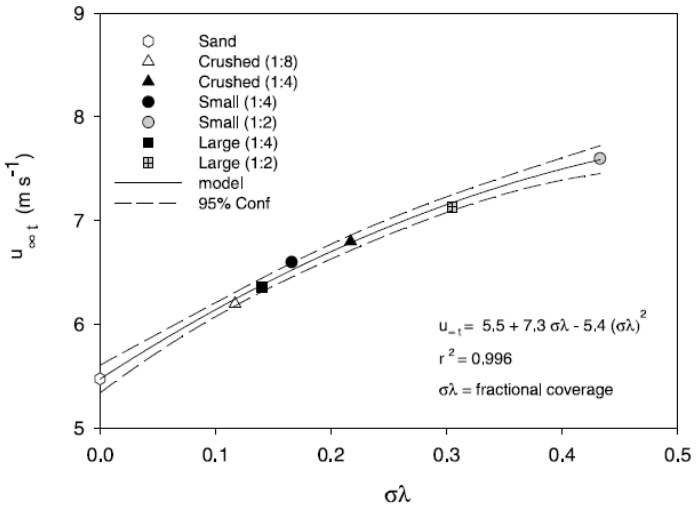

Figure 5.4.2 *Threshold wind velocity as function of fractional cover; McKenna et al. (2012)*

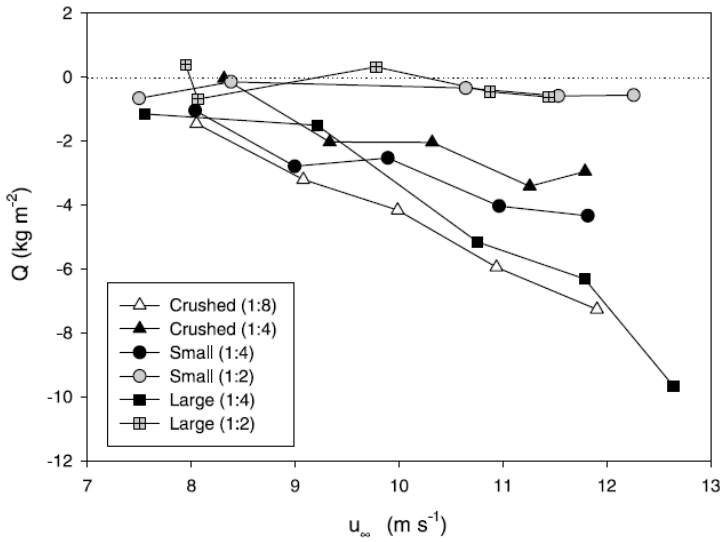

Figure 5.4.3 *Net eroded mass of sand as function of wind velocity; McKenna et al. (2012)*

Cadée (1992) has done observations of aeolian transport of large shells (Mya shells) along the Prins Hendrik sea dike on the island of Texel (The Netherlands) during and after storm events with wind velocities > Beaufort 10.
His observations are summarized, as follows:

- storm event from South with wind velocities > 30 m/s (BF 12) on 25 January 1990: large quantities of Mya-shells (lengths of 30 to 110 mm; mean length of 60 mm) were transported from the narrow beach on the seaside across the dike and were deposited on the landward side of the dike.
- storm event from Southwest with wind velocities > 30 m/s (BF 12) on 26 February 1990: Mya-shells and other shells were transported over the narrow beach parallel to the dike through saltations with maximum height of 1 m and maximum length of 10 m; shells lying with their hollow side to the beach surface (convex upward) were very stabile and hardly movable; shells with their rounded side to the beach (convex downward) were very mobile.
- storm event from South in January 1991 with wind velocities of 24 to 27 m/s (BF 10): Mya-shells were transported across the dike.

Based on this, it can be concluded that large shells can only be transported in appreciable quantities during storm events with relatively high wind speeds (BF > 10). The threshold wind speed at the onset of motion of large Mya-shells is about 20 m/s ($u_{*,th}$=0.75 m/s).

Effect on transport rate

Shells (calcium carbonate) can protect the beach surface against erosion of the sand particles. Large percentages of shell are mostly found on the upper part of natural beaches outside the wave action zone and on beaches with nourished sand. Literature on this topic is rather scarce and mostly qualitative. The two main effects of shells on the sand transport process are: i) shells cover a certain area of the bed which is not available for sand particle erosion and ii) sand particles in the direct vicinity of shells are less exposed to the wind forces (hiding effect). Observations in wind tunnels and field conditions show that shells of different sizes tend to interlock and form clusters (spatial organization; Mckenna et al., 2012; Strypsteen 2019).
McKenna et al. (2012) have observed in their wind tunnel experiments that the shells are not operating independently, but rather display some degree of spatial organization resulting in shell clusters of partly interlocking shells of different sizes. Shells are sometimes rolling coming to rest against others downwind

resulting in clusters. Corridors of lower shell coverage are generated at the sand surface. This justifies the use of a simple transport-limiting coefficient for engineering practices.
At the Dutch sand motor site (see Section 6.2) with shell cover values up to 20%, sufficient sand particles were winnowed from the shelly bed to give appreciable erosion and deposition volumes of sand.

Important parameters appear to be the fetch length and the uniformity of the shell cover. In wind tunnel experiments, the fetch length is relatively small (1 to 8 m in the studies discussed herein) and the initial shell cover is quite uniform in space. In field conditions, the fetch length is often larger than 50 m and the shells are not uniformly distributed over the beach surface. Shell clusters are pronounced features at natural beaches (Strypsteen 2019).

Based on available observations, it is herein assumed that the effects of shells on the sand transport process can be best represented for engineering purposes by a simple reduction coefficient acting on the transport rate.
The reduction effects based on the tests of Van der Wal (1998) and Mckenna et al. (2012) are simply represented in Equation (3.1.2) by a reduction factor acting on the transport rate:

$$\alpha_{shell}=(1-2p_{shell}/100)^2 \qquad (5.4.1)$$

with p_{shell}=percentage of shell (<30%). The sand transport rate as affected by shells was not measured directly in the studies considered herein (van der Wal, 1998; Mckenna et al., 2012; Hoonhout and De Vries, 2017) and thus Equation (3.8) could not be tested against measured transport rates.

Equation (3.8), which is only valid for a shell cover < 30%, is herein used as a supply-limiting factor acting on the sand transport rate to obtain a quick engineering scan of the effect of shells in reducing sand transport on nourished shelly beaches. The gradual development of an armor layer in time cannot be represented in this way, as it requires a more detailed approach. Basically, the simulation of sand transport in conditions with a relatively wide grain size distribution (d_{90}/d_{10}> 10) and significant shell cover values (10% to 30%) requires an approach with multiple fractions including a book-keeping process for each grid cell and vertical sand layer. Hiding and exposure effects must be included as well as roughness variation effects (Raupach 1992; Van Rijn 2007). The present model can be extended to a fractional approach (Van Rijn 2007). Using such an approach, the changes in surface conditions can be simulated both in space and time. Hoonhout and De Vries (2017) used a fractional model to study the windblown sand transport at a large-scale mega-nourishment (sand motor in The Netherlands). They found that the intertidal zone and the transition zone where shells were absent were the dominant sources of sand for windblown sand. The dry beach plain with abundant shell cover (5% to 15%) developed a beach armor layer suppressing the pickup of sand particles to some degree. However, such an approach is far more complex with many coefficients and calibrations involved and may be a bridge too far for engineering purposes (see detailed discussion by McKenna et al., 2012). Equation (3.8) yields meaningful results for the Dutch sand motor site which is a shelly beach plain/nourishment site. Model improvements based on detailed research in wind tunnels and at field sites focusing on the sand transport processes with wide grain size distributions including/excluding shells are highly recommended.

5.5 Dust transport

5.5.1 Erosion and emission of dust

Soils without vegetation and low moisture content and consisting of fine sediments are most sensitive to wind erosion and dust emission. The most substantial sources of fine dust-type sediments are deserts and dry lake beds (Kok et al., 2012). A dust storm is the result of strong turbulent winds entraining large quantities of dust particles, reducing visibility.
Very fine (dust-type) particles that can be transported thousands of kilometers from their source regions predominantly have diameters smaller than 20 µm (Kok et al., 2012). Dust particles in soils occurs mostly as:

- coatings on larger sand particles;
- part of soil aggregates with a typical size in the range of 20 to 300 µm.

Dust particles are emitted naturally through three distinct processes (Kok et al., 2012)

- direct aerodynamic lifting;
- ejection of dust from soil aggregates by impacting saltating particles (rupturing the bonds between individual constituents of the aggregates);
- ejection of dust from soil aggregates that are participating in saltation.

The emission of dust-type sediments from either soil aggregates or saltating dust aggregates is thus initiated by wind speeds exceeding the fluid threshold for saltation. Direct aerodynamic lifting of dust requires wind speeds somewhat larger than the saltation threshold (see **Figure 3.2.1**). Consequently, direct aerodynamic lifting is a less important source of dust than impact-induced emission from dust aggregates in the soil or in saltation. Dust can also be emitted through human activities.
Since dust emission is primarily due to saltation bombardment and subsequent sandblasting, the threshold wind speed above which dust emission occurs is about equal to the saltation threshold. Factors increasing the threshold velocity are cohesive (moisture) effects and hiding effects (fines sediments in between larger roughness elements such as pebbles and stones). The presence of larger roughness elements reduces the wind shear stress on the intervening bare soil and increases the total threshold wind stress required to initiate saltation and dust emission.
The presence of soil moisture can create substantial interparticle forces that inhibit the initiation of saltation, especially for sandy soils. For low relative humidities (below 65%), these interparticle forces are produced primarily by bonding of adjacent adsorbed water layers (hygroscopic forces), whereas for high relative humidities (above 65%) this occurs primarily through the formation of water wedges around points of contact (capillary forces). Water adsorption is governed by electrostatic interactions of the mineral surface with the water molecules. Since sandy soils generally contain a lower density of net electric charges, substantially less water can be adsorbed onto sandy soils than onto clayey soils. Consequently, water bridges form in sandy soils at a relatively low soil moisture content, thereby producing substantial capillary forces.
Often, the vertical dust flux is related to the horizontal saltation flux, as follows: $E_{dust}=\alpha\ q_s$, with: α= dust emission efficiency factor in the range of 0.01 to 0.0001, q_s= equilibrium sand transport rate.
The α-coefficient strongly depends on soil properties such as the clay content, the bonding strength of soil dust aggregates, the dry aggregate size distribution and the presence of soil crusts.

5.5.2 Deposition of dust

After emission, mineral dust particles are removed from the atmosphere by either dry deposition or wet deposition. Dry deposition is due to the combined action of gravitational settling with turbulent diffusion in the atmospheric boundary layer and molecular diffusion in the laminar sublayer near surfaces, such as vegetation canopies. Wet deposition includes both in-cloud scavenging, in which dust serve as cloud

condensation or ice nuclei and subsequently precipitate, and below-cloud scavenging, in which precipitating raindrops collect dust aerosols. Wet deposition generally dominates for aerosols smaller than about 5 µm in diameter, whereas dry deposition dominates for aerosols larger than about 5 µm. The resulting lifetime of a dust particle decreases with its size and ranges from about 1 to 2 weeks for clay particles (with diameter <2 µm), to several hours or days for silt particles (>2 µm). Consequently, only dust particles smaller than about 20 µm in diameter remain suspended in the atmosphere for sufficient time periods to substantially affect weather and climate.

6. Wind-blown sand transport on beaches

6.1 Sand transport processes in beach-dune systems

Erosive coasts
The primary dune row is continuously eroded and sand is available for aeolian transport in the downwind direction. Sand is blown into the dune field behind the primary dune row which may result in white dunes (sand covering vegetation). Transgressive dunes can be formed moving landwards. Sand dunes are generally highest and without much vegetation along erosive coasts bordering tidal inlets.

Accretive coasts
The supply of sand is so large that a large buffer of sand is present in front of the primary dune row (wide beach plains) resulting in the generation of new embryonal dunes, dune growth and seaward migration of dunes. Vegetation can generally keep up with aeolian transport.

Stabile coasts
New dunes may be generated at the dune toe and in the upper beach zone. Periodic storm erosion by high tides in combination with wind surges can remove the young dunes after which the cycle is repeated. Vegetation can survive as the aeolian transport is not high enough. The height of the primary dune row may grow slowly.

Annual aeolian sand transport along Holland coast
Based on analysis of sounding data, the net annual aeolian transport at the Holland coast between Hoek van Holland and Den Helder (distance of 110 km) is about 2 to 4 m^3/m/year in landward direction across the crest of the primary dune row (De Ruig, 1989).
Arens (2009) has studied the effect of beach nourishment on dune growth. About 55 million m^3 of sand (40% in beach zone and 60% in surf zone) was supplied at the Holland coast (Hoek van Holland-Den Helder; 110 km; The Netherlands) between 1997 and 2007. The dune growth volume was found to be about 22% (12 million m^3) of the total beach nourishment volume, which is equivalent with an annual dune volume growth of about 10 m^3/m/year.

6.2 Example applications of the predictive sand transport model

The proposed model can be applied in a rather straightforward way for loose, dry sand without shells and vegetation. For moist beach and dune systems including shells and vegetation, the estimation of these parameters requires detailed attention. The percentage of shells can be determined from samples taken over the upper 20 cm of the sand surface at the site or from samples taken at the offshore borrow (source) area in the case of beach nourishment. Vegetation height and cover can be estimated from sites similar to the site studied. Guidelines for the estimation of moisture can be given by distinguishing three ranges (Delgado-Fernandez, 2011): i) almost dry sand for moisture values w_{20mm}< 2% during 70% to 80 % of the time, ii) transition range with a drying sand surface and w_{20mm}=2% to 10% during 3 hours after each rainfall event and iii) wet sand for w_{20mm}> 10% during rainfall conditions preventing sand transport.
Two example cases are studied: i) sand transport at a horizontal beach parallel to the shoreline with effects of moisture and vegetation and ii) sand transport from the beach normal to the dune crest.

6.2.1 Sand transport at beach parallel to shoreline

The predictive model for wind-blown sand transport has been used to predict the sand transport rate for a range of conditions. **Figure 6.2.1** shows computed values for dry sand with d_{50}=0.3 mm and d_{90}=0.5 mm. The predicted transport rates for dry sand (solid bold curve) show a continuously increasing transport rate for increasing wind velocity. The effects of moisture (5.2.1c) and vegetation cover (Equation 5.3.1) are also shown. The moisture content increases the threshold shear velocity significantly and reduces the dynamic grain roughness (smaller T-parameter and thus smaller $k_{s,grain}$), resulting in almost zero transport for a wind velocity of 8.5 to 14.5 m/s for w_{20mm}-values of 2% to 10% of the topmost 20 mm of the beach sand surface. Once, the threshold value is exceeded the transport rate is much smaller. The reduction effects are largest for wind velocities < 18 m/s. The reduction effect diminishes for higher wind velocities further away from the threshold value. For a high wind velocity of 30 m/s (Beaufort scale 11), the reduction effect is about 20% for w_{20mm}=2% to about 50% for w_{20mm}=10%.
Vegetation (plant height=0.3 m) with covers of 5% to 15% reduces the effective shear velocity of the wind resulting in almost zero transport for wind velocities smaller than 6.5 to 8.5 m/s. Vegetation has a strong effect on the sand transport rate for wind velocities < 12 m/s. A vegetation cover of 15% consisting of plants of 0.3 m high reduces the sand transport rates by a factor of 2 to 3 for wind velocities > 12 m/s.

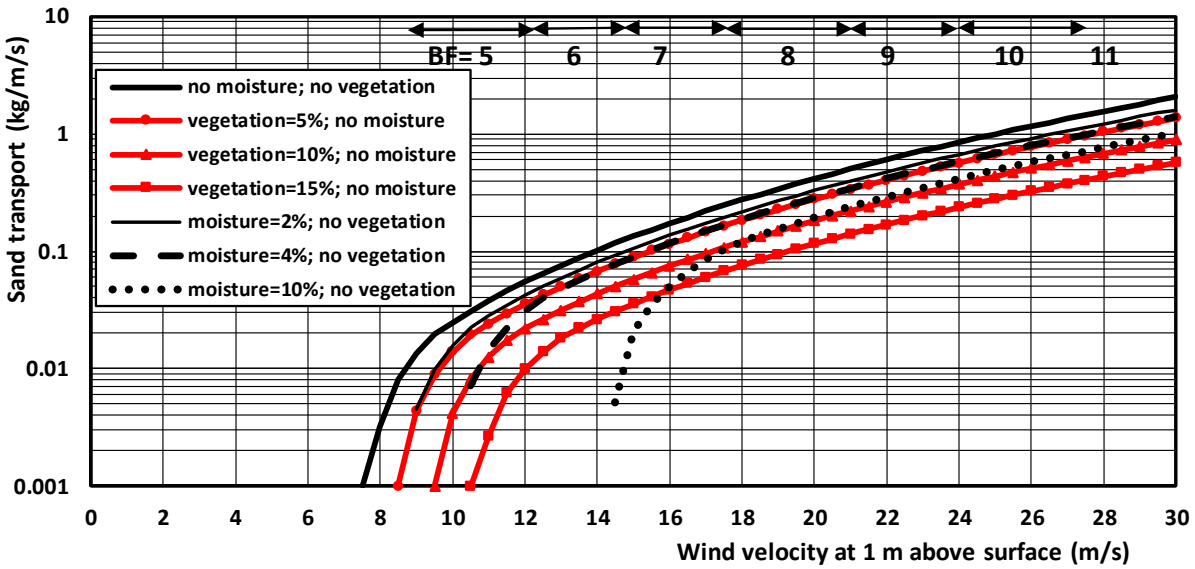

Figure 6.2.1 *Wind transport of sand based on predictive model (modified Bagnold-equation) (d_{50}=0.3 mm; d_{90}=0.5 mm; α_B= 2; α_{th}= 0.11)*

A very interesting test case for the predictive model is the windblown sand transport at the Dutch sand motor site, which is a mega-nourishment of about 21 Mm³ (De Vries and Hoonhout, 2018; Hoonhout and De Vries 2019). The dominant wind direction is parallel to the fore dunes. Measured deposition/erosion volumes are 300,000±100,000 m³ for a period of 4 years (2011-2015) in the windblown beach plain area. Based on this, the annual-mean sand transport is about 75,000±25,000 m³/year. The beach width normal to the coast is about 750 m in the middle zone of the site resulting in an annual-mean sand transport rate per unit width of about 100±35 m³/m/year passing from the updrift half on the southwest side to the downwind half on the northeast side of the beach plain area. The large beach plain at a level of 5 m above mean sea level consists of shelly sand with d_{50}=0.335 mm and a shell cover in the range of 5% to 15%. The tidal range is about 2 m. The dominant wind direction is from southwest approximately parallel to the foredune row. During about 30% of the time, the wind speeds are below 8 m/s (BF3) without transport. During 70% of the time, the

annual-mean wind speed representative for sand transport is about 10 to 11 m/s (BF5) at a height of 10 m above the beach surface. **Table 6.2.1** shows measured and computed annual-mean transport values for three cases. The computed value is about 50% too large for ideal conditions with dry sand, no shells and no moisture. Fairly accurate results are obtained for a shell cover of 10% and minor moisture of 1% to 2% (supply limiting factors). Most likely, shells are more important than moisture effects, as the beach plain is very flat and infiltration of rainfall is rapid due to the relatively high beach level. Hoonhout and De Vries (2019) have used a much more complex sand transport model (Aeolis) including beach armoring due to presence of shells and a beach drying model in the intertidal zone. Detailed model calibration was required to represent the measured erosion and deposition patterns in the windblown zone. They used the term $(u_*-u_{*,th})^3$ in the Bagnold-equation, which yields much too small transport rates (Strypsteen 2019; Strypsteen et al. 2019). As windblown transport rates were not successfully measured by mechanical traps at the sand motor site, the coefficients of the transport model could not be calibrated separately. The transport model and the detailed beach armoring model were all calibrated in one procedure, which may easily obscure the deficiencies of each component. It is concluded that the sand motor data with a shell cover < 15% and mostly dry sand can be represented by a fairly simple model approach as proposed in this paper.

Cases	Computed annual-mean sand transport (m^3/m/year)	Measured annual-mean sand transport (m^3/m/year)
1. Wind speed= 10-11 m/s; dry sand d_{50}=0.335mm; d_{90}=1-3 mm; no shells; no moisture	140±70	100±35
2. Wind speed= 11 m/s dry sand d_{50}=0.335mm; d_{90}=2 mm; shells=5%-15%; no moisture	130±30	
3. Wind speed= 10-11 m/s; moist sand d_{50}=0.335mm; d_{90}=2mm; shells=10%; moisture w_{20mm}=1%-2%	60±30	

Table 6.2.1 *Measured and computed sand transport rates; sand motor site The Netherlands*

6.2.2 Sand transport normal to dune

Wind flow from the beach across the foredune profile involves acceleration and deceleration effects over a non-uniform sand surface. If vegetation is present along part of the dune front, the surface roughness may also vary horizontally (non-uniform roughness). The wind speed at the sloping dune surface can be determined by various methods:

- measurements at the sloping surface (wind speed masts);
- wind flow computations using a mathematical model (open foam CFD-model);
- empirical coefficients relating local wind speed to the upwind velocity ($u_{w,x}=\alpha_x u_{w,o}$).

Wind normal to the beach accelerates along the slope of the foredune and is maximum at the dune crest level, see **Figures 6.2.2** and **6.2.3**. The influence of topography on wind speed is prominent. The speedup effect increases with height of the foredune. An increase in height from the beach to the dune crest of about 10 m causes an increase in windspeed of about 20% to 40% (Arens et al., 1995) with respect to the wind speed measured at the beach (reference value)**.** A further increase in foredune height > 10 m appears to have limited influence, probably because the increase in height (acceleration) is compensated by an increase in roughness due to the presence of irregularities at the dune crest.
The sand transport at the sloping surface of the dune front is affected in various ways: i) increase of the wind velocity enhancing the sand transport rate, ii) increase of the threshold shear velocity for upsloping wind flow reducing the sand transport rate and iii) decrease of the particle velocity during upward part of the saltation

trajectory related to the counteracting gravity component reducing the transport rate. Another effect is the generation of upward wind velocities enhancing suspension processes. During strong onshore winds, the upward wind velocities may exceed the fall velocity of grains of 0.2 to 0.3 mm (0.8 to 1.5 m/s). Suspension effects are herein neglected. It is assumed that saltation is the dominant mode of transport.

Field data

Arens et al. (1995) studied the wind speedup effects at the front of the foredune at three coastal sites (sand of 0.17 to 0.26 mm) in the Netherlands. The dune height was in the range of 6 to 23 m. The beach width was in the range of 80 to 600 m. Three to five masts with cup-anemometers were placed at the beach, in the dune zone (corner zone) and at the dune crest. The wind speedup effects are shown in **Table 6.2.2** for conditions with wind flow normal to the dune (purely onshore winds). Wind deceleration occurs in the dune toe zone (corner zone), where the wind speed is reduced by about 10%-20% (site 1, 2) for small dunes with heights up to 10 m to about 50% for large dune with height of about 20 m (site 3). Wind acceleration is most strong at near the dune crest, where the wind speed is increased by 10% for small dunes to 50% for larger dunes (8 to 22 m). An increase in foredune height up to 10 m leads to an increase of the speed-up near the dune crest of about 50% during onshore wind, but a further increase of foredune height from 10 to 20 m has little effect, most likely due to increased roughness and deflection of flow. The wind speedup effect is maximal between 1 and 2 m above the surface. During strong onshore wind, sand is lifted near the dune foot and moves over the foredune in suspension. During weaker winds, vertical wind velocities do not exceed fall velocities of the sand grains, and most of the sand is deposited near the dune foot.

Location	**Beach-dune sites**				
	Schiermonnikoog (Arens et al., 1995)	**Groote Keeten** (Arens et al., 1995)	**Nieuw Haamstede** (Arens et al., 1995)	**Articial dune** (Smyth and Hesp 2015)	**Sand dune in desert and wind tunnel** (Wiggs et al., 1996)
Dune dimensions	dune height= 5 m dune slope 1 to 7	10 m 1 to 4	22 m 1 to 15 and 1 to 3	1 to 1.5	10 m 1 to 10
Corner	$u_z/u_{z,o}$=0.8 (about 1 m above beach level)	$u_z/u_{z,o}$=0.9 (about 2 m above beach level)	$u_z/u_{z,o}$=0.55-0.8 (about 3 to 7 m above beach level)	$u_*/u_{*,o}$=0.5	$u_*/u_{*,o}$= 0.8-1
Mid front	-	-	-	$u_*/u_{*,o}$=1.0-1.1	$u_*/u_{*,o}$= 1.2-1.3
Crest	$u_z/u_{z,o}$=1.1 (at 4 m above beach level)	$u_z/u_{z,o}$=1.3-1.5 (at 6 m above beach level)	$u_z/u_{z,o}$=1.3-1.5 (about 20 m above beach level)	$u_*/u_{*,o}$=1.7	$u_*/u_{*,o}$= 1.5-1.7 (just before crest)

Table 6.2.2 *Relative wind speed and shear velocity ($u_z/u_{z,o}$; $u_*/u_{*,o}$) in at corner, front and crest of dune during conditions with wind flow normal to dune*

Wiggs et al. (1996) studied the wind velocity distribution across an unvegetated desert dune (10 m high; 100 m long) in Oman and across an artificial dune (scale model 1 to 200) in a wind tunnel. Both the field and wind tunnel data demonstrate similar patterns of wind and shear velocity over the dune, confirming significant flow deceleration upwind of and at the toe of the dune, acceleration of flow up the windward slope (see **Table 6.2.2**). The field data show a decrease of the shear velocity at the dune toe, but this was not observed in the wind tunnel based on shear velocity data derived from turbulence measurements. Such a reduction in shear velocity in the dune toe zone should result in a reduction in sand transport and subsequent sand deposition. This is not observed in the field. Wind tunnel measurements using a special high-frequency wire probe suggests that the field method of shear velocity derivation is inadequate. The wind tunnel results

exhibit no reduction in shear velocity upwind of or at the toe of the dune. Evidence provided by measured Reynolds stress profiles and turbulence intensities measured in the wind tunnel suggest that this maintenance of upwind shear stress may be the result of slightly diverging streamline curvature producing additional turbulence, which are not recorded by the techniques used in the field measurements.

Smyth and Hesp (2015) studied the wind flow over a small artificial dune of sand (0.25 mm) with trapezoidal cross-section made at the landward end of a beach. The dune height is 3 m; the length of the dune front is 4 m; the dune front slope is 1 to 1.5 (angle=34°). The beach has a slope of 3°. A computational fluid dynamic model (CFD) has been used to compute the wind flow across the dune and the shear velocity along the surface for an onshore wind velocity of 8 m/s at z=1 m above the beach surface (inlet x=0). The surface roughness applied is k_s=15 mm. The results clearly show a reduction in shear velocity at the foot of the dune, see **Figure 6.2.2**. The wind velocity decreases in the upwind corner zone and lee zone of the dune. The wind velocity strongly increases at the crest. The relative shear velocity values at the dune foot, at mid-front and at the crest are shown in **Table 6.2.2**. The deceleration and acceleration effects at the toe and near the crest computed by Smyth and Hesp (2015) are much stronger than the effects measured by Arens et al. (1995), which is most like caused by the sharp transitions in the profile of the artificial dune. In field conditions these transitions will be smoother resulting in less strong deceleration/acceleration effects.

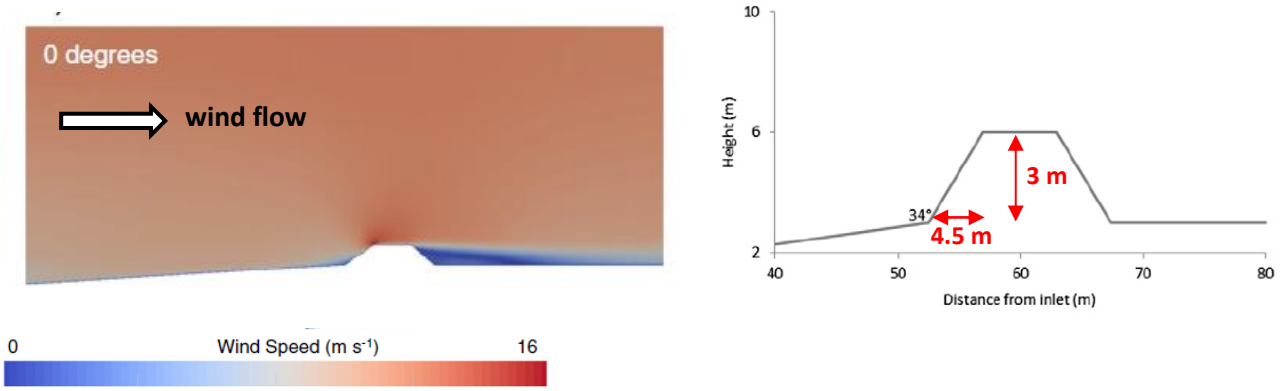

Figure 6.2.2A *Wind velocity field across an artificial dune; wind velocity at inlet =8 m/s at 1 m above surface (Smyth and Hesp, 2015)*

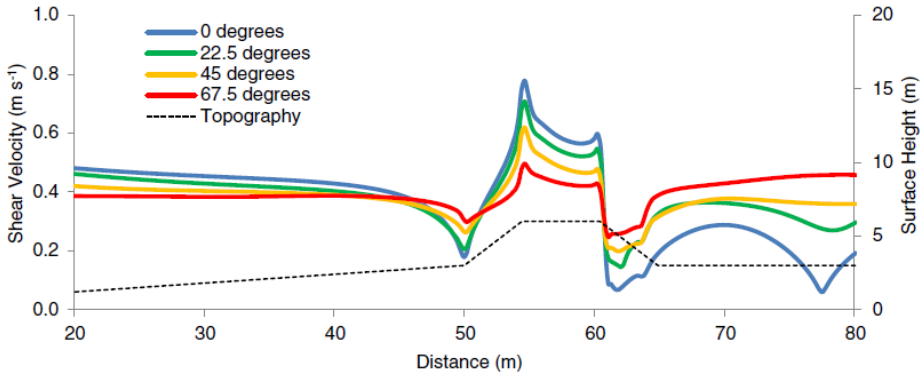

Figure 6.2.2B *Shear velocity across an artificial dune for 4 wind directions; shear velocity at inlet ≅0.45 m/s 1 m above surface (Smyth and Hesp, 2015)*

All available information on the distribution of the shear velocity along the dune front including the variation ranges is summarized in **Figure 6.2.3**. The variation range of the shear velocity is relatively large in the dune toe zone, which is related to the varying surface slope in this zone. The shear velocity is considerably reduced (factor 2) in a corner zone with a sharp transition in slopes (Smyth and Hesp 2015), but the reduction in the dune toe zone is much smaller for field cases with a smoother transition in slope. The variation range in the crest zone is much smaller than in the dune toe zone.

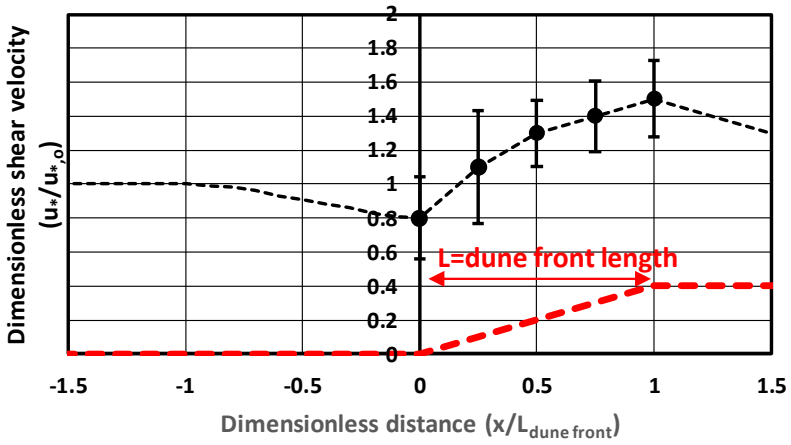

Figure 6.2.3 *Dimensionless shear velocity along dune front based on available data*

Model computations

The predictive modified Bagnold-equation has been used to compute the sand transport rates at the beach and across the dune front up the crest for wind flow normal to the dune. The beach is assumed be sufficiently wide to ensure saturated sand transport conditions. The upwind velocity is defined at 1 m above the beach level and varied in the range of 7 to 30 m/s. Two cases for dry sand are considered, see **Table 6.2.3**. The dune of Case 1 has a relatively sharp transition in the dune toe zone, whereas the dune of Case 2 is a natural dune taken from the data of Davidson-Arnott et al. (2012), see **Figure 6.2.4**.
In both cases it is assumed that the median grain size is about constant along the beach and dune faces based on the detailed sampling analysis work of Hallin et al. (2019) for beaches in Sweden.

Parameters	Case 1	Case 2
Sand diameters d_{50}, d_{90} (mm)	0.3; 0.5	0.26; 0.5
Angle of repose (°)	35	35
Dune height above beach (m)	10	10
Slope angle dune toe zone (°)	35	12
Slope angle dune front zone (°)	35	22
Threshold shear velocity at beach, dune toe zone and dune front (m/s)	0.28; 0.35	0.26; 0.29; 0.31
Coefficient wind modification at +2 m above beach level (dune toe)	0.9	1.0
Coefficient wind modification at +3 m above beach level (dune toe)	1.0	1.2
Coefficient wind modification at +5 m above beach level (mid-front)	1.2	1.3
Coefficient wind modification at +10 m above beach level (crest)	1.5	1.5

Table 6.2.3 *Dune dimensions and parameters of Case 1 and 2*

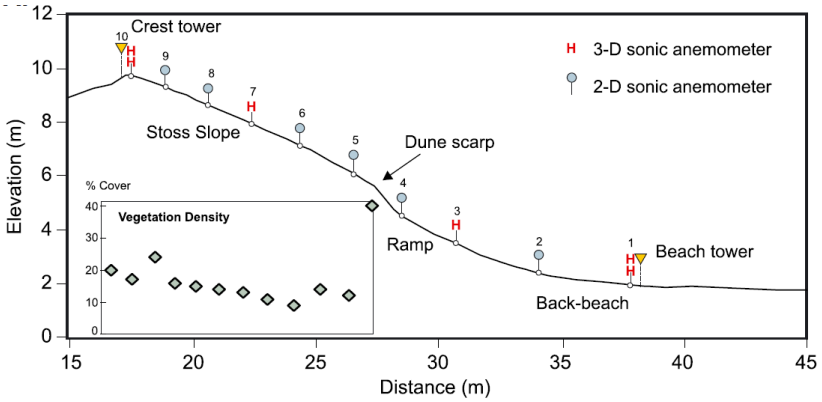

Figure 6.2.4 *Dune profile (April-May 2010); Greenwich dunes, Prince Edward Island National Park, Canada (Davidson-Arnott et al., 2012)*

The sand transport is computed at levels of 2 m and 3 m in the dune toe zone, at 5 m (mid-front), and at the dune crest of 10 m above the beach level. The wind speed modification across the dune front ($u_{wind,local}=\alpha_{local}$ $u_{w,o}$) is derived from the available field and wind tunnel measurements (**Table 6.2.2** and **Figure 6.2.3**) and are given in **Table 6.2.3**. The values for Case 1 are slightly smaller than those of Case 2, which has a smoother natural profile in the dune toe zone resulting in higher velocities.

Case 1

Figure 6.2.5 shows the computed aeolian sand transport rates at 4 levels for wind flow normal to the dune front. The wind velocity is given at the beach. The sand transport rates in the dune toe zone (levels of 2 to 3 m) are smaller than the sand transport rates at the beach for all conditions resulting in deposition which is mainly caused by the slight reduction of the wind speed in this zone and the increase of the threshold shear velocity. The sand transport rates at a level of 5 m (mid-front) are higher than those at 3 m resulting in erosion. The sand transport rates at the crest (10 m above beach level) are much higher than those at 5m resulting in major erosion. Most of the eroded sediments are deposited beyond the dune crest where the shear velocities are rapidly decreasing (Smyth and Hesp, 2015). When vegetation with cover percentage of 10% and grass plant height of 0.3 m is present along the dune front (above level of 3 m), the sand transport rates in this zone are reduced to values which are below or slightly above (near the crest) those at a level of 3 m resulting in accretion along the upper part of the dune front. Minor erosion may occur near the crest. Summarizing, there is a tendency for accretion in the dune toe zone for all conditions. Erosion will mainly occur above the dune toe zone up to the crest (without vegetation). When vegetation is present in the upper dune zone, accretion is promoted by trapping of sand between the grass plants.

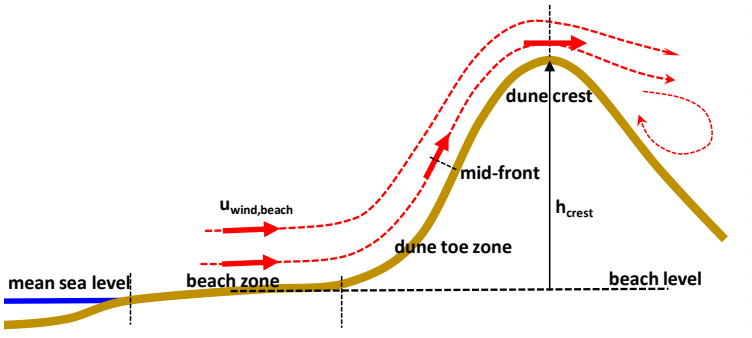

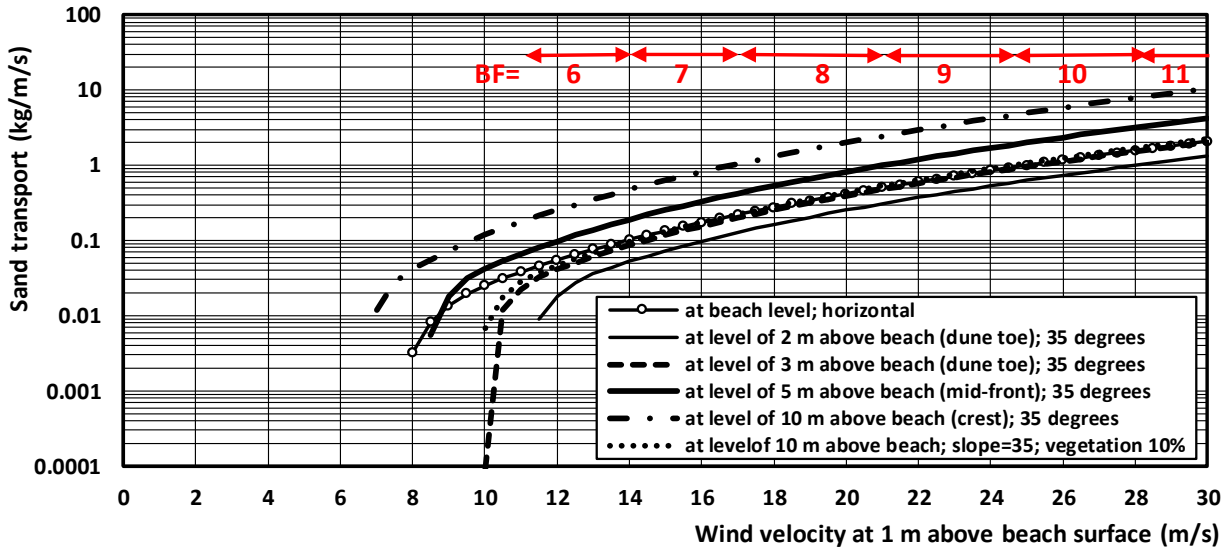

Figure 6.2.5 *Case 1: Aeolian sand transport at beach level and at higher levels along dune front; d_{50}= 0.3 mm; including effects of wind modification, slope on threshold shear velocity and vegetation*

Case 2

Figure 6.2.6 shows the computed aeolian sand transport rates at 4 levels for conditions with wind flow normal to the dune front. The wind velocity is given at the beach. The sand transport rates (dry sand) in the dune toe zone at level of 2 m is about the same as that on the beach except for relatively small wind speeds < 10 m/s. The sand transport rates at level of 3 and 5 m are larger (factor 1.5 to 3) than those at level or 2 m. The sand transport rates at level of 10 m (crest) are a factor of 5 larger than those at level of 2 m. The increase of the sand transport rates between levels of 2 and 10 m will lead to erosion if vegetation is absent. The sand transport rates are also computed for conditions with vegetation (plant height=0.3 m; cover=15%) resulting in a significant reduction (factor of 10).

These computed results are compared to the measured results of Davidson-Arnott et al. (2012). They report measured transport rates during oblique onshore winds of about 10 to 11 m/s (at dune crest): about 0.0055 kg/m/s at a level of 2 m and 0.018 (±0.003) kg/m/s at levels of 3 to 5 m. Assuming a smaller wind velocity of about 9 m/s (20% lower than at the crest), the computed sand transport rate is of the order of 0.01 kg/m/s at level of 2 m and about 0.03 to 0.04 kg/m/s at level of 3 to 5 m. These computed values are a factor of 2 to 2.5 larger than the measured values, which is a very reasonable results as the measured values are valid for moist sand (rain fall) reducing the transport rates. Sand transport rates in crest zone with vegetation were also measured by Davidson-Arnott et al. (2012). The vegetation cover of marram grass was measured in contiguous 1 m square quadrats along a profile parallel to the instrument line and was highly variable, ranging from about 20% near the crest to about 9% near the top of the scarp and 40% right at the scarp crest. The measured sand transport rates in the crest zone (levels of 9 to 10 m) are almost zero (smaller than 0.00015 kg/m/s; factor 50 smaller than at level of 2 m). The model predicts zero transport for a vegetation cover of 15% (plant height=0.3 m) for wind velocities < 11.5 m/s.

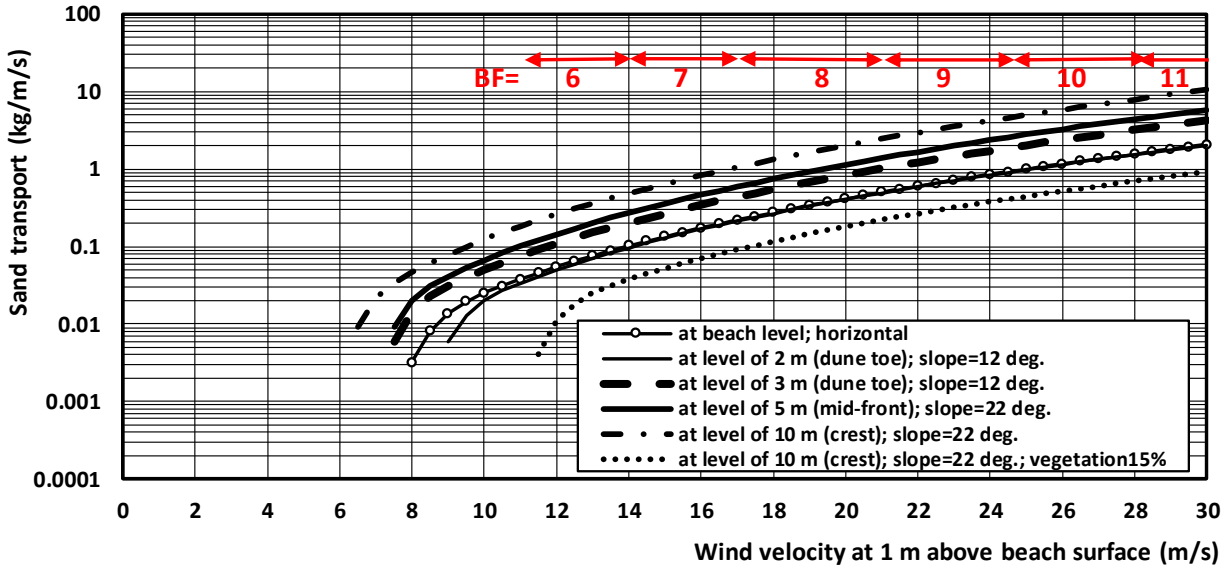

Figure 6.2.6 *Case 2: Aeolian sand transport at beach level and at higher levels along dune front; d_{50}= 0.26 mm; including effects of wind modification, slope on threshold shear velocity and vegetation*

6.2.3 Sand transport at beach for year-round conditions

Example 1

The modified sand transport equation of Bagnold has been used to compute the aeolian transport along a wide beach consisting of dry, loose sand of 0.2 and 0.35mm (k_s= 0.01 m, ρ_s=2650 kg/m^3, α_B= 2, α_v= 1, α_w=1, L_{ad}=100 m; L_{fetch}=100 m; no moisture and no vegetation).

Wind speed (m/s)	Number of days	Wind direction to North	Coast normal to North	Windtransport Bagnold d_{50}=0.2 mm (m^3/m)		Windtransport Bagnold d_{50}=0.35 mm (m^3/m)	
				normal to shore	parallel to shore	normal to shore	parallel to shore
9 (BF 5)	25	15° (195°)	45°	7.8	-4.5	5.0	-2.9
12 (BF 6)	7	15° (195°)	45°	6.4	-3.7	6.9	-4.0
15 (BF 7)	5	15° (195°)	45°	9.5	-5.5	11.5	-6.6
9	30	45° (225°)	45°	10.8	0	6.9	0
12	10	45° (225°)	45°	10.5	0	11.4	0
15	5	45° (225°)	45°	10.9	0	13.2	0
9	30	75° (255°)	45°	9.4	5.4	6.0	3.5
12	10	75° (255°)	45°	9.1	5.3	9.9	5.7
15	5	75° (255°)	45°	9.5	5.5	11.5	6.6
Totaal	**125**			**84 m^3/m**	**2.5 m^3/m**	**82.4 m^3/m**	**2.3 m^3/m**

75°=wind direction to which the waves are going; (195°)= wind direction from which the waves are coming

Table 6.2.4 *Windtransport during 125 days of onshore wind*

Table 6.2.4 yields the annual wind transport of sand at a beach with wind from the sectors 180°-210°, 210°-240° en 240°-270° (southwest to northwest). The wind transport (summed over 125 days) is not much affected by particle size.
In practice, the landward transport of sand towards the dune row is a factor of 10 smaller due to moisture and adjustment effects reducing the transport rates (non-saturated transport).
Using: α_{ad}= 0.5 (supply-limited conditions due to presence of small beach), α_w= 1.5 (mopisture effect), the windtransport reduces to 13.5 m^3/m (normal) and 1.1 m^3/m (parallel).

Example 2
Beach sand: d_{50}=0.3 mm; longitudinal beach/dune axis makes an angle of 40 degrees with North (**Figure 6.2.7** and **Table 6.2.5**).
The wind rose is divided in 4 quadrants (with respect to the longitudinal axis of the dune, see **Figure 6.2.7**.
Each quadrant has 3 sectors of 30°, as follows:

Quadrant I (SW-NW):	sectors 9, 10, 11;	total 120 days
Quadrant II (NW-NE):	sectors 12, 1, 2;	total 74 days;
Quadrant III (NE-SE):	sectors 3, 4, 5;	total 75 days;
Quadrant IV (SE-SW):	sectors 6, 7, 8;	total 97 days;
All quadrants:		total 366 days

Computation results based on AEOLIANTRANSPORT.xls (see Table 6.2.5)
The computed sand transport rates (in m^3/m/year) can be summarized, as:

- wind from quadrants I and IV: transport rates are relatively high (dominant);
- wind from quadrant I (120 days)
  normal to SE: 35 m^3/m/year for dry sand decreasing to 1 m^3/m/year for wet sand with vegetation;
  parallel to NE: 75 m^3/m/year for dry sand decreasing to 1 m^3/m/year for wet sand with vegetation;
- wind from quadrant IV (97 days):
  normal to NW: 26 m^3/m/year for dry sand decreasing to 4 m^3/m/year for wet sand with vegetation;
  parallel to NE: 110 m^3/m/year for dry sand decreasing to 20 m^3/m/year for wet sand with vegetation;
- wind from quadrants II and III (149 days): relatively small transport values between 10 and 1 normal to crest; sand transport decreases significantly (factor 5 to 10) due to presence of vegetation;
- sand transport increases/decreases by 10% for smaller grain diameter (0.25 mm) and larger diameter (0.4 mm);
- based on the computed sand transport rates, the erosion of sand at the dune crest (covered with vegetation) is estimated to be about 10 to 15 m^3/m/year at the edges of the dune crest, **Figure 6.2.8**.

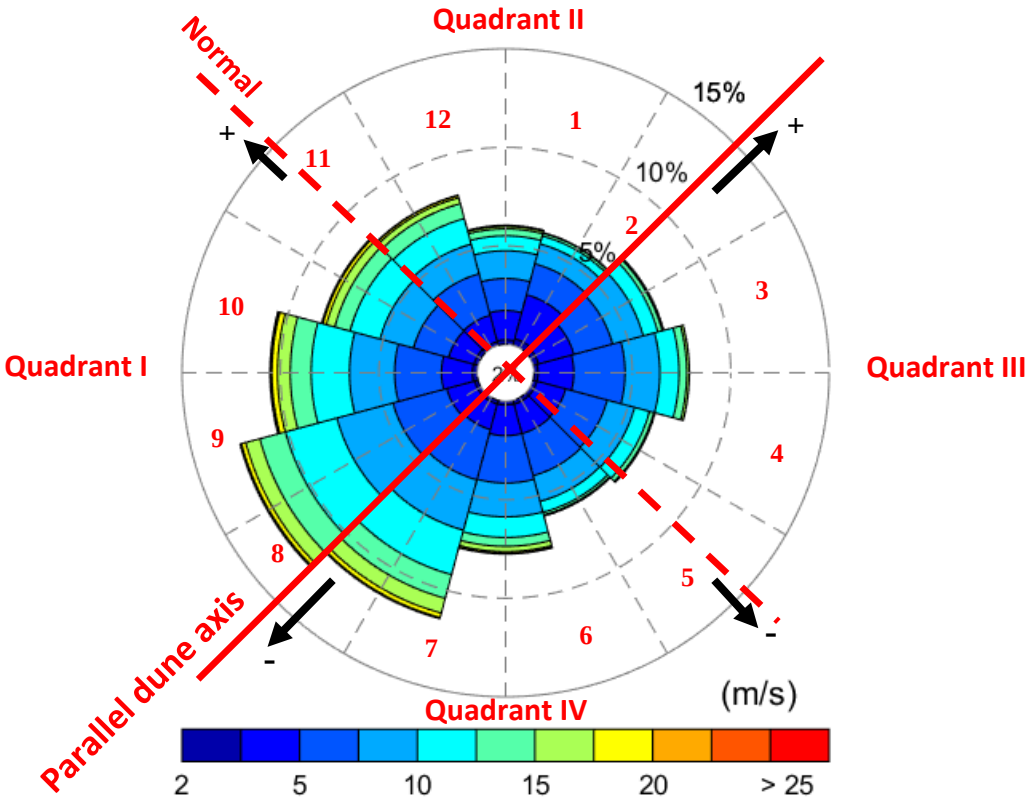

Figure 6.2.7 *Windrose with 4 quadrants and 12 sectors; Sand transport directions (+ or -; black arrows) Parallel dune axis = red line (angle 40° to North); normal to dune axis= dashed red line*

Scenarios	Wind transport (m^3/m/year including pores)									
	Quadrant I (α_{sh}=0.8)		Quadrant II (α_{sh}=0.8)		Quadrant III (α_{sh}=1)		Quadrant IV (α_{sh}=1)		All Quadrants	
	normal	parallel	normal	parallel	normal	parallel	normal	parallel	normal	parallel
Dry loose sand, d_{50}=0.3 mm No vegetation (α_v=1) No moisture (α_w=1)	-35	75	-9	-10	11	-37	26	110	-7	138
Wet sand, d_{50}=0.3 mm No vegetation (α_v=1) Moisture (α_w=1.3)	-6	11	-4	-4	6	-20	17	80	13	67
Dry loose sand, d_{50}=0.3 mm Vegetation (α_v=0.8) No moisture (α_w=1)	-4	7	-2	-2	3	-3	9	40	6	42
Wet sand, d_{50}= 0.3 mm Vegetation (α_v=0.8) Moisture ((α_w=1.3)	-1	1	0	0	1	-3	4	20	4	18

ρ_{air}=1.2 kg/m^3; ρ_{sand}=2650 kg/m^3;
Dry bulk density sand= 1600 kg/m^3; adjustment length sand transport = 100 m; surface roughness k_s=0.01 m
α_v= vegetation coefficient; α_w= moisture coefficient; α_{sh}= sheltering coefficient (reduced wind)
Normal: - = sand transport normal to dune crest in direction south-east; + = in direction north-west
Parallel: - = sand transport parallel to dune crest in direction south-west; + = in direction north-east

Table 6.2.5 *Wind transport at sand dune*

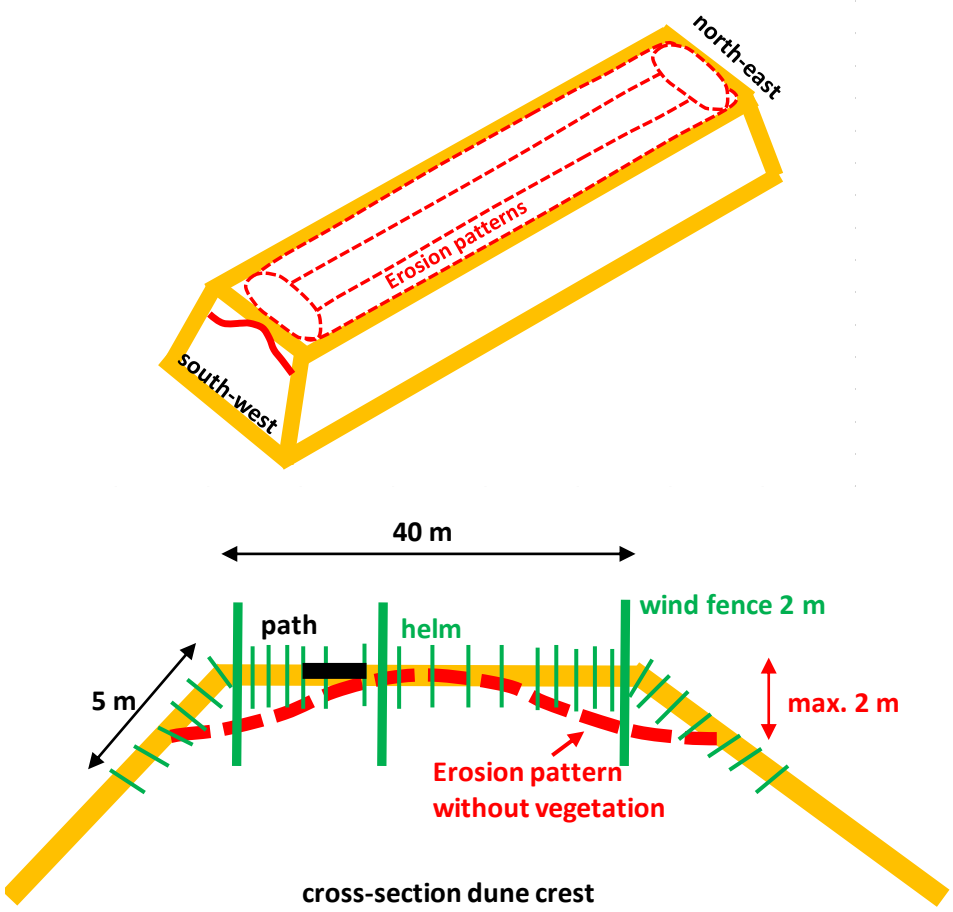

Figure 6.2.8 *Wind erosion at dune crest and preventive measures (vegetation and wind fences)*

6.3 Preventive measures to reduce erosion

Erosion due to wind can be reduced to less than 5 $m^3/m/year$ by taking the following measures:

- grass-type vegetation (spinifex; 9 to 10 plants per m^2);
- temporary wind screens/fences (brushwood; lengths of 2 to 2.5 m);
- paper pulp can be sprayed (thin layer) on dry loose sand to reduce erosion (temporary) at dune surfaces without vegetation.

The most effective measure is to plant grass-type vegetation. Usually, it is sufficient to use about 10 plants per m^2. The plants are manually pushed into small holes made in the dry sand. A team of 5 to 10 men can make a production of about 5000 m^2 per day. Machinery (tractors) can be used at flat surfaces. Planting is done in seasons with some rain, as the plants need some water for growth. After a few years the root system of the plants is penetrated into the sand body over a length of 1 to 3 m.

7. References

Arens, 2009. Effects of nourishments on dune development (in Dutch). Report 2009.02, Amsterdam
Arens, S.M., Van kaam-Peters, H.M.E. and Van Boxel, J.H., 1995. Air flow over foredunes and implications for sand transport. Earth Surface Processes and Landforms, Vol. 20, 315-332
Arens, S.M., Baas, A.C.W., Van Boxel, J.H., and Kalkman, C., 2001. Influence of reed stem density on foredune development. Earth Surface Processes and Landforms, Vol. 26, 1161-1176. Doi: 10.1002/esp.257
Bagnold, RA., 1936. The Movement of Desert Sand. Proc. Royal Soc. London, Series A 157, 594-620.
Bagnold, R.A. 1941, 1954. The physics of blown sand and desert dunes. Methuen, New York.
Basaran, M, Uzun, O. and Erpul, G., 2017. Evaluation of field performance of BEST aeolian sediment catcher in sandy-loam soil of arid zone of Turkey. Soil and Water Res., Vol. 12, 96-105
Belly, P.Y., 1964. Sand Movement by Wind. U.S. Army Corps of Engineers, Technical Memorandum No 1, CERC, Washington, DC.
Brakenhoff, L.B., Smit, Y., Donker, J.J.A. and Ruessink, G., 2019. Tide-indiced variability in beach surface moisture: observations and modelling. Earth Surface Processes and Landforms, Vol. 44, 317-330
Brown, S., Nickling, W.G. and Gillies, J.A., 2008. A wind tunnel examination of shear stress partitioning for an assortment of surface roughness distributions. Journal of Geophysical Research Vol. 113. F02S06. Doi: 10.1029/2007JF000790
Buckley, R.C., 1987. The effect of sparse vegetation on the transport of dune sand by wind. Letters to Nature, Vol. 325, 426-428
Burri, K., Lehning, M, Gromke, C, Graf, K., 2011. Aeolian sediment transport over vegetation canopies; a wind tunnel study with live plants. Aeolian Research Vol. 3 (2), 205-213. Doi: 10.1016/j.aeolia.2011.01.003
Cadée, G. 1992. Eolian transport of Mya shells, Palaios, Vol. 7.
Campos, L.D., 2018. Quantification methods for aeolian sand transport on beaches. Doctoral Thesis, University of Twente, The Netherlands
Carter, R., 1976. Formation, maintenance and geomorphological significance of an aeolian shell pavement, J. Sediment. Res. 46 (2), Doi: 10.1306/ 212F6F8C-2B24-11D7-8648000102C1865D.
Carter, R. and Rihan, C., 1978. Shell and pebble pavements on beaches: examples from the north coast of Ireland, Catena 5 (3–4), 365–374. Doi: 10.1016/ 0341-8162(78)90019-X.
Chepil, W.S., 1956. Influence of moisture on erodibility of soil by wind. Proc. Soil Sci. Soc. Am., 20, 288–292.
Chepil, W. S. and Woodruff, N. P. (1963). The physics of wind erosion and its control. Adv. Agronomy, 15, 211-302.
Cohn, N., Hoonhout, B.M., Goldstein, E.B. and De Vries, S., 2019. Exploring marine and aeolian controls on coastal foredune growth using a coupled model. Journal of Marine Science and Engineering, Vol. 7, 1-25, doi:.org/10.3390/jmse7010013
Cornelis, W.M., Gabriels, D., 2003. The effect of surface moisture on the entrainment of dune sand wind: an evaluation of selected models. Sedimentology Vol. 50, 771–790.
Davidson-Arnott, R.G.D., Bauer, B.O., Ollerhead, J., Hesp, P.A., Namikas, S. and Walker, I.J., 2005. Moisture and fetch effects on aeolian sediment transport rates during a fall storm, Greenwich dunes, Prince Edward Island. Canadian Coastal Conference.
Davidson-Arnott, R.G.D., Yang, Y., Ollerhead, J., Hesp., P.A. and Walker, I.J., 2008. The effects of surface moisture on aeolian sediment transport threshold and mass flux on a beach. Earth Surface Processes and Landforms, Vol. 33, 55-74. Doi:10.1002/esp.1527
Davidson-Arnott, R.G.D., Walker, I.J., Hesp, P.A., Ollerhead and Chapman, C., 2012. High-frequency sediment transport responses on vegetated foredune. Earth Surface Processes and Landforms, Vol. 37, 1227-1241
Delgado-Fernandez, I., 2010. A review of the application of the fetch effect to modelling sand supply to coastal foredunes. Aeolian Research Vol. 2 (2-3), 61-70

Delgado-Fernandez, I., 2011. Meso-scale modelling of aelian sediment input to coastal dunes. Geomorphology Vol.130, 230-243
De Grande, E. and De Moor, T., 2019. Influence of meteorological and environmental effects on aeolian transport (in Dutch). MSc. Thesis, KU Leuven, Belgium
De Ruig, J.H.M., 1989. Sediment balance of Holland coast 1963-1986 (in Dutch). Rapport GWAO-89.016. Dienst Getijdewateren, Rijkswaterstaat, Den Haag
De Vries, S., Arens, S.M., De Schipper, M.A., and Ranasinghe, R., 2014. Aeolian sediment transport on a beach with a varying sediment supply. Aeolian Research Vol. 15, 235-244
De Vries, S. and Hoonhout, B., 2017. Field measurements on spatial variations in aeolian sediment availability at the sand motor mega nourishment. Aeolian Research Vo. 24, 93-104
Hoonhout, B. and De Vries, S., 2019. Simulating spatiotemporal aeolian sediment supply at a mega nourishment. Coastal Engineering Vol. 145, 21-35
Dey, S., 2003. Threshold of sediment motion on combined transverse and longitudinal sloping beds. Journal of Hydraulic Research, Vol. 41, No. 4, 405-415.
Dong, Z., Liu, X. and Wang, X., 2002. Aerodynamic roughness of gravel surfaces. Geomorphology Vol 4, 17-31
Dong, Z., Lu, P., Zhang, Z. and Qian, G., 2012. Aeolian transport in the field: a comparison of the effects of different surface treatments. Journal of Geophysical Research Atmosphere, Doi: 10.1029/2012JD017538
Farrell, E.J. and Swann, C. 2016. Geomorphological Techniques. Chapter 3.1.4. British society for Geomorphology
Farrell, E.J. and Sherman, D.J., 2016. Process-scaling issues for aeolian transport modelling in field and wind tunnel experiments: roughness length and mass flux distributions. Journal of Coastal Research, SI19, 384-389.
Field, J.P. and Pelletier, J.D., 2018. Controlls on the aerodynamic roughness length and the grain size dependence of aeolian sediment transport. Earth Surface Processes and Landforms Vol. 43, 2616-2626. Doi: 10.1002/esp.4420
Gillies, J.A., Nickling, W.G. and King, J., 2006. Aeolian sediment transport through large patches of roughess in the atmospheric inertial layer. Journal of Geophysical Research Vol. 111, F02006. Doi: 10.1029/2005JF000434
Graf, W.H. and Pazis, C.G., 1977. Deposion and erosion phenomena in an alluvial channel (in French). Journal of Hydraulic Research Vol. 15, No. 2
Granger, R.J., Essery, R., Pomeroy, J.W., 2006. Boundary-layer growth over snow and soil patches: field observations. Hydrological Processes 20, 943–951.
Hallin, C., Larson, M., and Hanson, H., 2019. A process-based model for aeolian sediment transport and spatiotemporal varying sediment availability. Journal of Geophysical Research, Earth Surface, Vol. 121, doi:10.1002/2015JF003692
Han, Q., Qu, J., Liao, K., Zhu, S., Zhang, K., Zu, R. and Niu, Q., 2011. A wind tunnel study of aeolian sand transport on a wetted surface using sands from tropical humid coastal southern China. Environmental Earth Sciences, Vol. 64, 1375-1385; DOI 10.1007/s12665-011-0962-7
Hesp, P.A., Dong, Y., Cheng, H., and Booth, J.L., 2019. Wind flow and sedimentation in artificial vegetation: Field and wind tunnel experiments. Geomorhology Vol. 337, 165-182
Hesse, P., and Simpson, R.L., 2006. Variable vegetation cover and episodic sand movement on longitudinal desert sand dunes. Geomorphology Vol. 81, 276-291
Ho, T., 2012. Experimental study of saltating particles in a turbulent boundary layer. Doctoral Thesis, University of Rennes, France
Hoonhout, B. and De Vries, S., 2019. Simulating spatiotemporal aeolian sediment supply at a mega nourishment. Coastal Engineering Vol. 145, 21-35
Horikawa, K., Hotta, S. and Kraus, N.C., 1986. Literature review of sand transport by wind on a dry sand surface. Coastal Engineering 9, 503–526.

Hotta, S., Kubota, S., Katori, S., Horikawa, K., 1984. Sand transport by wind on a wet sand surface. Proceedings 19th Coastal Engineering Conference. ASCE, New York, 1265–1281.
Hsu, S.A., 1974. Computing eolian sand transport from routine weather data. Chapter 94, Proc. International Conference Coastal Engineering, Copenhagen
Hupy, J.P., 2003. Influence of vegetation cover and crust type on wind-blown sediment in a semi-arid climate. Journal of Arid Environments Vol. 58, 167-179
Jackson, N.L. and Nordstrom, K.F., 1997. Effects of time-dependent moisture content of surface sediments on aeolian transport rates across a beach, Wildwood, New yersey, USA. Earth Surface Processes and Landforms Vol. 22, 611-621
Jackson, D., Cooper, J., 1999. Beach fetch distance and aeolian sediment transport. Sedimentology, 517–522.
Kok, J.F., Parteli, E.J.R., Michaels, T.I. and Karam, D.B.., 2012. The physics of wind-blown sand and dust. Rep. Prog. Phys. Vol. 75, Doi:10.1088/0034-4885/75/10/106901
Lancaster, N. and Baas, A., 1998. Influence of vegetation cover on sand transport by wind; field studies at Owens Lake, California. Earth surface processes and Landforms Vol. 23, 69-82
Li, B., Ellis, J.T. and Sherman, D., 2010. Variability of the apparent Von Karman constant during aeolian transport. Geophysical Letters. Doi. 10.1029/2010GL044068
Liu, X., Dong, Z., Wang, X., 2006. Wind tunnel modeling and measurements of the flux of wind-blown sand. Journal of Arid Environments Vol. 66, 657–672.
Lyles, L., Schrandt, R. and Schmeidler, N. (1974) How aerodynamic Roughness elements control sand movement. Trans. Am. Soc. Agricultural Engrs, 17, 134-139.
McKenna Neuman, C., Li, B. and Nash, D., 2012. Micro-topographic analysis of shell pavements formed by aeolian transport in a wind tunnel simulation. Journal of Geophysical Research Vol. 117, F04003. Doi: 10.1029/2012JF002381
Meyer-Peter, E. and Mueller, R., 1948. Formulas for bed load transport. 2nd IAHR Congress, Stockholm, Sweden
Musick, H.B. and Gillette, D.A. 1990. Field evaluation of relationships between a vegetation structural parameter and sheltering against wind erosion. Land Degradation and Rehabilitation Vol. 2, 87–94.
Musick, H.B., Trujillo, S.M. and Truman, C.R., 1996. Wind-tunnel modelling of the influence of vegetation structure on saltation threshold. Earth Surface Processes and Landforms Vol. 21, 589–605.
Nickling, W.G. and Davidson-Arnott, R.G.D., 1990. Aeolian sediment transport on beaches and coastal dunes. Proc. Canadian Symposium on coastal sand dunes
Nickling, W.G. and McKenna Neuman, C., 1995. Development of deflation lag surfaces. Sedimentology 42, 403-414
Owen, P.R., 1964. Saltation of uniform grains in air. Journal of Fluid Mechanics, Vol. 20, 225-242
Pelletier, J.D. and Field, J.P., 2016 Predicting the roughness length of turbulent flows over landscapes with multi-scale microtopography. Earth Surface Dynamics Vol. 4, 391-404. Doi: 10.5194/esurf-4-391-2016
Poortinga, A, Van Minnen, J., Keijsers, J., Riksen, M., Goossens, D. and Seeger, M., 2013. Measuring fast-temporal sediment fluxes with an analogue acoustic sensor: a wind tunnel study. Plos One, Volume 8, Issue 9, www.plosone.org
Raupach, M.R., 1992. Drag and drag partition on rough surfaces. Boundary Layer Meteorology Vol. 60, 375–395.
Raupach, M.R., Gillette, D.A., Leys, J.F., 1993. The effect of roughness elements on wind erosion threshold. Journal Geophysical Research Vol. 98, 3023–3029.
Saleh, A. and Fryrear, D.W., 1995. Threshold wind velocities of wet soils as affected by wind-blown sand. Soil Sci., 160, 304–309.
Shao, Y. P. and Lu, H., 2000 A simple expression for wind erosion threshold friction velocity Journal Geophysical Research Vol. 105, 22437–43

Shao, Y. et al., 2015. A tribute to M.R. Raupach for contributions to aeolian fluid dynamics. Aeolian Research Vol. 19, 37-54
Sherman, D.J., 1992. An equilibrium relationship for shear velocity and apparent roughness length in aeolian saltation. Geomorphology, Vol. 5, 419–431.
Sherman, D.J. and Farrell, E.J. 2008. Aerodynamic roughness lengths over movable beds: comparison of wind tunnel and field data. Journal of Geophysical Research: Earth Surface Vol. 113; doi.org/ 10.1029/2007JF000784.
Sherman, D. J., Jackson, D. W. T., Namikas, S. L., and Wang, J., 1998. Wind-blown sand on beaches: An evaluation of models. Geomorphology, Vol. 22(2), 113–133. Doi: 10.1016/S0169-555X(97)00062-7
Sherman, D., Ellis, J.T., Li, B., Farrell, E.J., Maia, P. and Granja, H.M., 2013. Recalibrating aeolian sand transport models. Earth Surface and Landforms, Vol. 38, 169-178. Doi: 10.1002/esp.3310
Sherman, D.J., Swann, C. and Barron, J.D., 2014. A low-cost aeolian sand trap. Aeolian Research, Vol. 13, 31-34.
Smyth, T.A.G. and Hesp, P.A., 2015. Aeolian dynamics of beach scraped ridge and dyke structures. Coastal Engineering Vol. 99, 38-45
Strypsteen, G., 2019. Monitoring and modelling aeolian sand transport at the Belgian coast. Doctoral Thesis, KU Leuven, Belgium.
Strypsteen, G., Montreuil, A.L. and Rauwoens, P., 2017. Aeolian sand transport at the Belgian coast; field campaigns and first results. Paper 117. Coastal Dynamics.
Strypsteen, G., Van Rijn, L.C. and Rauwoens, P., 2019. On the relation between predicted and observed aeolian sand transport rates: a field study at the Belgian coast. Submitted to Journal of Aeolian Research
Tan, L., Zhang, W., Qu, J., Zhang, K., An, Z. and Wang, X., 2013. Aeolian sand transport over Gobi with different gravel coverages under limited sand supply: a mobile wind tunnel investigation. Aeolian Research 11, 67-74
Udo, K., Kuriyama, Y. and Jackson, D.W.T., 2008. Observations of wind-blown sand under various meteorological conditions at a beach. Journal of Geophysical Research Vol. 113, F04008. Doi: 10.1029/2007JF00936
Valance, A., Rasmussen, K.R., Moctar, A.O.E and Dupont, P., 2015. The physics of aeolian sand transport. Comptes Rendus Physique, Elsevier Masson, Vol. 16 (1), 1-13. Doi: 10.1016/j.crhy.2015.01.006
Van der Wal, D. 1998. The impact of the grain-size distribution of nourishment sand on aeolian transport. Journal of Coastal Research Vol. 14 (2), 620-631
Van Dijk, P. M., Stroosnijder, L. and De Lima, J.L.M.P., 1996. The influence of rainfall on transport of beach sand by wind. Earth Surface Processes and Landforms, Vol. 21, 341-352.
Van Dijk, P.M., Van Boxel, J. and Arens, S.M., 1999. Aeolian processes across transverse dunes, part II. Modelling the sediment transport and profile development. Earth Surf. Process. Landforms. Vol. 24, 319-333
Van Rijn, L.C., 1982. Equivalent roughness of alluvial bed. Journal of Hydraulics Division, ASCE, Vol. 108, Hy 10, 1215-1218.
Van Rijn, L.C., 1984. Sediment Transport, Part III: Bed Forms and Alluvial Roughness. Journal of Hydraulic Engineering, ASCE, Vol. 110, No. 12.
Van Rijn, L.C., 1987. Mathematical modelling of morphological processes in the case of suspended sediment transport. Doctoral Thesis, Civil Engineering Department, Delft University of Technology, Delft, The Netherlands
Van Rijn, L.C., 1993. Principles of sediment transport in rivers, estuaries and coastal seas. AquaPublications, The Netherlands (www.aquapublications.nl)
Van Rijn, L.C., 2006. Principles of sediment transport in rivers, estuaries and coastal seas, Part II. AquaPublications, The Netherlands (www.aquapublications.nl)
Van Rijn, L.C., 2007. Unified view of sediment transport by currents and waves, I: Initiation of motion, bed roughness, and bed-load transport. Journal of Hydraulic Engineering, 133(6), 649-667.

Van Rijn, L.C., 2007. Unified view of sediment transport by currents and waves, II: Suspended transport. Journal of Hydraulic Engineering, 133(6), 668-389.
Van Rijn, L.C., 2007. Unified view of sediment transport by currents and waves, III: Graded beds. Journal of Hydraulic Engineering, 133(7), 761-775.
Wasson, R.J. and Nanninga. P.M., 1986. Estimating wind transport of sand on vegetated surfaces. Earth Surface Processes and Landforms. Vol. 11, 505-514
Wiggs, G.F.S., Livingstone, I. and Warren, A., 1996. The role of streamline curvature in sand dune dynamics: evidence from field and wind tunnel measurements. Geomorphology Vol. 17, 29-46
Winterwerp, J.C., De Groot, M.B., Mastbergen, D.R. and Verwoert, H., 1990. Hyper-concentrated sand-water mixture flows over flat bed. Journal of Hydraulic Engineering, ASCE, Vol. 116, No.1
Wolfe, S.A. and Nickling, W.G., 1993. The protective role of sparse vegetation in wind erosion. Progress in Physical Geography 17, 50–68.
Xian, X., Tao, W., Qingwei, S. and Weimin, Z., 2002. Field and wind-tunnel studies of aerodynamic roughness length. Boundary-Layer Meteorology, Vol. 104, 151-163
Yang, Y, Liu, L., Shi, P., Zhang, G., Xiong, Y., Lyu, Y., Guo, L., Liang, B., Zhao, M., Dai, J., Zuo, X, and Han, X., 2019. Aerodynamic grain-size distribution of blown sand. Sedimentology, Vol. 66, 590-603
Youssef, F., Visser, S.M., Karssenberg, D., Erpul, G., Cornelis, W.M., Gabriels, D. and Poortinga, A., 2012. The effect of vegetation patterns on wind-blown mass transport at the regional scale: A wind tunnel experiment. Geomorphology Vol. 159-160, 178-188
Zhang, C.L., Zou, X.Y., Gong, J.R., Liu, J.R. and Liu, Y.Z., 2004. Aerodynamic roughness of cultivated soil and its influences on soil erosion by wind in a wind tunnel. Soil and Tillage Research Vol. 75, 53-59

Aeolian sand transport processes, Part 2: field measurements and model predictions for dry and moist beaches

Aeolian sand transport processes, Part 2; field measurements and model predictions for dry and moist sand

1. Introduction

This study is a continuation of earlier work on the development of the complete theory for the prediction of aeolian transport over dry and moist beaches of sand and coarse materials (Van Rijn, 2019; Van Rijn and Strypsteen 2020).
The author has published 3 papers on the subject Aeolian sand transport:

- L.C. van Rijn and G. Strypsteen, 2020, A fully predictive model for aeolian sand transport, Coastal Engineering, Vol. 156 (103600);
- L.C. van Rijn, 2022; A fully predictive model for aeolian sand transport, part 2: Description and calibration of models and effect of moisture and coarse materials; Coastal Engineering, Vol. 171 (104052);
- L.C. van Rijn, 2022; A fully predictive model for aeolian sand transport, part 3: Verification and application of model for natural beaches; Coastal Engineering, Vol. 171 (104051).

Moisture effects

The movement of sand particles by wind is strongly affected by rainfall and by shells lying on the sand surface. Relatively large moisture variations between 8% and 0% may occur over short spatial and time scales as result of rainfall and subsequent drying of the sand surface. Rainfall has two main, but opposing effects on the movement of sand particles at beach sites: a) initiation of splash-type of entrainment and saltation processes due to the impact of rain drops on the sand surface resulting in appreciable sand transport during rainfall events, particularly when the peak rainfall intensity coincides with the peak wind velocity and b) increase of the threshold shear stress/velocity due to cohesive and adhesive forces of very fine particles and water films surrounding the sand particles including crust forming at the surface resulting a higher resistance against entrainment and less sand transport, particularly for higher moisture contents. In general, rainfall and moisture variations can be seen as severe supply limiting effects.

Shells and gravels

Another transport limiting effect is the presence of shells on the sand surface. Shells (calcium carbonate) can protect the beach surface against erosion of the sand particles. Large percentages of shell are mostly found on the upper part of natural beaches outside the wave action zone and on beaches with nourished sand. Literature on this topic is rather scarce and mostly qualitative. The two main effects of shells on the sand transport process are: i) shells cover a certain area of the bed which is not available for sand particle erosion and ii) sand particles in the direct vicinity of shells are less exposed to the wind forces (hiding effect). Observations in wind tunnels and field conditions show that shells of different sizes tend to interlock and form clusters. At the Dutch sand motor site with shell cover values up to 20%, sufficient sand particles were winnowed from the shelly bed to give appreciable erosion and deposition volumes of sand.

Salt crusts

Field observations have show that bonding agents such as organic residues and soluble salts can significantly reduce the sand transport rates (Nickling and Ecclestone, 1981). Wind tunnel tests were carried out by Nickling mand Ecclestone (1981) to study the effects of two soluble salts (NaCl and KCl) on the threshold shear velocity of a well-sorted, fine sand. Results indicate that even small amounts of soluble salt can significantly increase the threshold velocity of the sand because of cement-like bonds formed between grains that tend to hold individual

particles in place. The measured critical shear velocity showed an increase from about 0.21 m/s to 0.35 m/s for a salt increase from 0 to 5 mg/g for 0.18 mm sand. It was found that the salt crystal growth causes the initially smooth sand surface to develop an irregular frothy texture for increasing salt concentration which also directly affects the threshold shear velocity. When a moist sand surface is exposed to relatively dry air with moderate wind velocities the surface will begin to dry by evaporation. Moisture lost from the surface will be replaced by capillary water drawn from some depth below the surface. However, if the evaporation rate exceeds the rate of capillary rise of water the surface may dry sufficiently to allow sediment transport to begin despite the fact that the sediment a few millimeters below the surface is too moist to be entrained at the given shear velocity. Sediment transport will continue if wind velocities remain above threshold, and evaporation exceeds the rate at which capillary water can move to the surface. The continued evaporation of capillary water, however, in many cases leads to the pre-cipitation of dissolved salts near the surface. Thus the rather transient stabilizing effect of surface moisture may be replaced over the long term by more perma-nent salt bonds that can significantly affect threshold velocities and the sediment transport rate. These salts tend to be rather stable over the long term because often they can only be removed slowly by a considerable degree of leaching through rainwater, snowmelt or inundation. In some cases, however, the effect of salt bonding can be removed or reduced by the break-up and erosion of the salt crust by wind. Once the destruction of the crust is initiated, exposing more easily entrained sediment, saltating grains from the exposed areas may 'lead to the gradual destruction of the crust (Nickling and Ecclestone, 1981).

Field data

Although sand transport by wind is easily observable, reliable and accurate data sets of sand transport rates are still scarcely available due to measuring difficulties. Sherman et al. (2013) have presented a high-quality dataset of 32 points, but not much more tabulated data based on well-defined parameters can be found in the literature. Therefore, new equipment for the measurement of aeolian transport has been developed and used at many dry and wet beach sites in Belgium and The Netherlands in conditions with wind up to Beaufort scale 9. In addition, new mini wind tunnels have been developed and used to study the effect of moisture and coarse materials on the transport of sand by wind. The results of the new and extensive studies are presented and discussed in this study.

The applied models for sand transport are presented in Section 2. Laboratory and field instrumentation and sites are explained in Section 3. The effects of moisture and coarse materials on the sand transport processes are discussed in Sections 4 and 5. Field data of sand transport and the verification of the proposed equations are given in Sections 6 and 7. Finally, the proposed equations are applied for long term transport in Section 8.

2. Sand transport model

2.1 Sand transport equations

2.2.1 Single fraction approach

Sand transport occurs when the threshold for motion is exceeded. The dominant mode of transport for sand particles in the size range of 70 to 500 μm is saltation ballistic trajectories. Very fine sand smaller than 70 μm is mostly transported in suspension by turbulent eddies. The coarse sand particles (> 500 μm) are transported by sliding and rolling as surface creep for wind velocities of 12 to 20 m/s (Yang et al., 2019). Very coarse particles can be transported as saltating particles during extreme wind velocities > 20 m/s. Observations in wind tunnels and in nature show that most of the transport occurs in a thin layer (< 0.03 m) above the bed surface (Bagnold, 1937; Ho, 2012; Han et al., 2011). In this thin transport layer, the layer-averaged particle velocity is almost insensitive to the external wind velocity above the transport layer. Particle concentration is so high that the wind velocity is strongly reduced (Kok et al., 2012). An increase of the wind velocity results in an increase of the particle concentration which in turn leads to a decrease of the wind flow speed close to the bed such that the new equilibrium particle velocity remains almost unchanged (Valance et al., 2015). Excellent reviews are given by Durán et al. (2011) and Kok et al. (2012).
Field observations on flat beaches show that sand transport by wind occurs in transversely coherent streamers (or transport lanes). As the response time of saltation to instantaneous wind velocities is relatively fast (within 1 s), the saltation process is most likely close to steady state (equilibrium) within each streamer lane. Field observations also show that wind blown sand transport within a streamer is variable on small spatial (bed forms, depressions, undulations) and short temporal scales related to turbulence and gusts (Barchyn et al., 2014). This causes a measurement problem as instruments producing high-resolution and spatio-temporal data are not yet available. Most electronic sensors are intrusive point-measuring instruments which produce particle counts rather than fluxes. Many sensors are required for integration of data over vertical and horizontal scales (saltation transport layer and surface irregularities) to deal with spatial variations. It is noted that most high-frequency sensors typically provide only relative, not absolute, measures of the aeolian saltation flux. Typically, these type of sensors produce data in counts per second, which require a conversion to physically meaningful quantities using time-integrated sand trap data (Martin et al., 2018). HF sensors can resolve saltation responses to turbulence, but their ability to provide absolute mass fluxes is questionable. Martin et al. (2018) describe a new methodology to generate reliable high-resolution time series of the total (vertically-integrated) saltation mass flux. They have used absolute low-frequency measurements from sediment traps to calibrate relative high-frequency measurements from optical particle counters and provide a systematic development, testing, and explanation for a calibration-based methodology of flux profiles and total saltation fluxes based on data from 3 filed sits (Brazil, USA).

At present stage of research, the simple mechanical trap-type samplers intercepting the moving particles of the saltation layer are the most reliable instruments to obtain field data for calibration of transport models. Sampling times should be sufficiently long (say 10 minutes) to integrate over fluctuations due to turbulence and wind gusts. Many samplings should be done at the “same” location to reduce variability due to small transverse and streamwise gradients. Similarly, the driving parameters (wind velocity, shear velocity) should be averaged over the same sampling period.
Longer averaging durations of wind velocity and sand transport give improved statistical convergence and more complete inclusion of all turbulent fluctuations, but short-term intermittency is obscured. Various researchers have studied the effects of time-averaging on measured aeolian transport (saltation flux). Guo et al. (2012) found systematic variations in fluxes of 1 to 60 minutes, especially when wind speeds were near threshold of motion. Martin et al. (2013) collected coupled high-frequency wind speed data (ultrasonic anemometer) and saltation

flux data (Wenglor sensors) during intermittent sand transport conditions on a sand dune. The time-averaged sand flux was found to show variations beyond a time scale of 5 minutes. These latter researchers believe that an averaging time scale of 10 min may provide a good balance between short-term variability and long-term meteorological variability.

Many analytical equations for wind blown transport of sand with a narrow size grading ($d_{90}/d_{10}< 5$) are available in the Literature. The most classic equation is that proposed by Bagnold (1941,1954). The simple analytical transport equations cannot deal with variability and can thus not fully represent the physics of wind blown sand transport processes. This can be partly overcome by using empirical coefficients to match measured transport data. Many transport equations were evaluated by Sherman et al. (1998, 2013) and by Strypsteen et al. (2021).

Recently, detailed numerical sand transport models have been developed that represent the entire range of grain motions, including grains that roll and/or slide along the bed, by periodic saltation motions with rebounds of a grain after colliding with the bed (Pähtz and Durán, 2018**;** Pähtz et al., 2021).

Herein, a new and simple deterministic approach is explored. The sand transport of dry sand close to the bed in both water and air can be described by a set of dimensionless parameters (Yalin, 1977; Van Rijn, 1993; Van Rijn, 2018), being:

- dimensionless sand transport: $\phi=q_{s,eq}/[\rho_s\,(s-1)^{0.5}g^{0.5}\,d_{50}^{1.5}]$; (2.1)
- dimensionless particle size: $D_*=[(s-1)g/\upsilon^2]^{1/3}\,d_{50}$; (2.2)
- dimensionless particle mobility parameter (Shields parameter): $\theta = u_{*,gr}^2/[(s-1)gd_{50}]$; (2.3a)
- dimensionless threshold particle mobility parameter (Shields parameter): $\theta_{th}= u_{*,th}^2/[(s-1)gd_{50}]$; (2.3b)
- dimension sediment density: $s=\rho_s/\rho_{air}$. (2.3c)

with:
$q_{s,eq}$ = equilibrium (saturated) mass sand transport (in kg/m/s);
ρ_s =sediment density (2650 kg/m³);
ρ_{air} =air density (1.2 kg/m³); $s\cong s-1$ for air;
d_{50}= median grain size (in m);
υ= kinematic viscosity of air ($1.33\cdot10^{-5}$ m²/s for 0 °C and $1.5\cdot10^{-5}$ m²/s for 20 °C);
$u_{*,gr}$ = grain-related bed-shear velocity (in m/s);
$u_{*,th}$ = threshold bed-shear velocity (in m/s).

The dimensionless sand transport equation can be formulated as (Yalin, 1977; Van Rijn, 1993):

$$\phi=\alpha\,[D_*]^{\beta}\,[\theta-\theta_{th}]^{\gamma} \qquad (2.4)$$

with α, β and γ being coefficients to be determined by calibration. Equation (2.4) is a universal equation for sand transport in water based on dimension analysis (Yalin, 1977; Van Rijn, 1993). Herein, it is assumed that Equation (2.4) is also valid for sand transport in air. Meyer-Peter & Müller (1948) have found that bed load transport of very coarse sand particles in water is independent of grain size ($\beta = 0$). Van Rijn (2007) has found that bed load transport of finer sand particles in water is related to $(d_{50})^{0.5}$; thus $\beta = 0.5$. Bagnold (1941) has found a similar power for wind-blown sand transport taking place in a very thin layer close to bed. Thus, the β-parameter is in the range of 0 to 0.5.
The classical models of Bagnold (1941) for sand transport in air and Meyer-Peter & Müller (1948) for sand transport in water close to the bed have a nonlinear relationship between transport and shear stress ($\gamma \cong 1.5$),

which is based on the assumption that the particle speed scales with the shear velocity (u_*), supported by the work of Kawamura (1951) and Owen (1964). However, recent studies based on numerical modelling of saltation characteristics suggest that the saltation height and speed are almost constant and independent of the shear velocity resulting in a linear relationship between wind-driven sand transport and shear stress (γ=1) for the low shear stress range with intermittent to continuous saltation transport (Ungar and Haff, 1987; Duran et al., 2011; Kok et al. 2012; Martin et al., 2013; Martin and Kok, 2018). The dimensionless saltation height (δ_s/d_{50}) was found to be in the range 140 to 220 and independent of u_*. The sand flux equation can be approximated by: $q_s=u_{eff}\, M_{load}$ with u_{eff}= effective streamwise speed of the saltating particles (m/s) and M_{load}= mass load of particles in motion per unit area (kg/m^2). Two regimes are distinguished (Durán et al, 2011; Pähtz and Durán, 2020), as follows:

- low shear velocity regime (u_*<1.5 to 2$u_{*,th,c}$): $u_{eff}=C_1 u_{*,th,c}$ and $M_{load}=C_2(\tau-\tau_{th,c})$ giving $q_s=C_3\, u_{*,th,c}\,(\tau-\tau_{th,c})$;
- high shear velocity regime (u_*>1.5 to 2$u_{*,th,c}$): $u_{eff}=C_4\, u_{*,}$ and $M_{load}=C_5(\tau-\tau_{th,c})$ giving $q_s=C_6\, u_*(\tau-\tau_{th,c}) \cong C_7(\tau)^{1.5}$;

with: q_s= equilibrium sand transport (kg/m/s) $\tau_{th,c}$ = $\rho_a u_{*,th,c}^2$=cessation (impact) threshold shear stress= shear stress at cessation of transport (Pa), ρ_a= air density (kg/m^3), C= calibration coefficient, C_3= calibration factor of the order of 5 to 8 based on field data (Kok et al., 2012; Martin and Kok, 2017). Based on this, the sand transport is found to be linearly related to the excess shear in the lower shear stress range and nonlinearly related with power 1.5 in the high shear stress range. This model approach with splash-dominated particle entrainment and constant saltation characteristics in the lower shear stress range is supported by measured saltation fluxes at various field sites (Martin et al. 2013; Martin and Kok, 2018). Measured fluxes at high shear stresses (storms, τ>0.45 Pa; fluxes > 60 g/m/s) are still missing. The data of Martin et al. (2013) suggest a linear relationship (γ=1) between transport and shear stress in the lower shear stress range near initiation of motion (015-0.25 Pa), but a nonlinear relationship (γ=1.5) is also plausible in this shear stress range.

Equation (2.4) is based on the shear stress at the sand surface, which can be derived from measured wind velocity profiles (if available, otherwise the bed roughness must be known or estimated).
Assuming logarithmic velocity profiles, the shear stress is defined by :

$$u_z=(u_*/\kappa)\ln(z/z_o) \qquad (2.5a)$$

with: u=wind velocity at height z above surface, u_*= shear velocity, z_o=zero velocity level ($\cong k_s/30$), k_s= bed roughness height.
Bagnold (1941) has found that the streamwise wind velocity at a "focal height ($z_f\cong$ 2 to 20 mm based on Bagnold and others) "converges to a constant time-averaged focal velocity (u_f) irrespective of the free-stream wind velocity. Above the near-bed region (20 mm) with intense saltation and constant wind speed, the wind velocity profile are unaffected and retain the logarithmic velocity distribution as if under "clean air" conditions, except that now the entire profile is shifted upward based on the focal height and can be described as:

$$u_z=u_f+(u_*/\kappa)\ln(z/z_f) \qquad (2.5b)$$

Martin et al. (2013) have used Equation (2.5a) for clean air conditions ($u_*<u_{*,ith}$) and Equation (2.5b) for active saltation conditions ($u_*>u_{*,th,cessation}$) at a field site in California (USA). Based on this approach, they found: $u_{*,ith}$=0.22 m/s being the threshold value at cessation of saltation, z_f=1.4 10^{-3} m (1.4 mm) and z_o=1.5 10^{-6} m (0.0015 mm) resulting in k_s=30x0.0015=0.045 mm which is much smaller than the median grain size at the field site (d_{50}=0.416 mm). The fluid threshold shear velocity for initiation of saltation $u_{*,th,initiation}$ was estimated to be 0.27 m/s ($u_{*,th,cessation}/u_{*,th,initiation}\cong$0.76).

It is noted that Equation (2.4) is a deterministic equation, which is by definition not accurate around threshold conditions with intermittent transport of rolling, sliding and saltating particles (Paintal, 1971; Grass, 1973; Stout and Zobeck, 1997 and others).
Sand transport in turbulent wind conditions around the threshold for initiation of motion is an intermittent process with the wind velocity often falling below the threshold wind speed. Stout and Zobeack (1997) measured instantaneous wind velocity and saltation intensity (number of particles impacting the sensor per s) close to the surface and determined the intermittency factor (γ_p) defined as the fraction of time with saltating particles ($o<\gamma_p<1$). This intermittency-factor equals 1 for conditions with continuous transport. They showed that turbulent wind around threshold conditions at a field site in the USA had an almost perfect normal (Gaussian) probability distribution with a standard deviation equal to about 15% of the mean wind speed ($\sigma_u \cong 0.15\ u_{mean}$; 5-minute data records). The threshold wind velocity (u_{th}) was defined as the mean wind speed giving an intermittency factor $\gamma_p=0.5$. This means that sand transport occurs during 50% of the time when the wind speed > u_{th} and no sand transport occurs during the other 50% of the time when the wind speed < u_{th}. Thus, sand transport occurs when the mean wind speed (or shear stress) is equal to the threshold wind speed (or threshold shear stress). This cannot be represented by a deterministic sand transport equation which always gives zero transport for $u=u_{th}$. Based on the work of Stout and Zobeck (1997), sand transport is almost zero ($\gamma_p<0.05$) for a mean wind speed of about $0.7u_{th}$; sand transport is continuous ($\gamma_p=0.9$) for a mean wind speed of about $1.3\ u_{th}$. Using a lower threshold value (impact or cessation threshold value) in a deterministic sand transport equation improves the predicting ability (Durán et al. 2011, Kok et al. 2012). Gomola et al. (2019) have tried to overcome the problem by introducing an intermittency factor in a deterministic transport equation, which, however, requires information of the cumulative probability density function of the wind speed around threshold conditions. Using this approach, the fractions of time with no, intermittent or continuous transport can be inferred. They have applied this detailed and fairly complicated method based on normally distributed wind speeds to available wind data (over 35 years) at 3 field sites. It was found that saltation type of transport is highly intermittent in months with relatively low wind speeds (2 to 6 m/s).
Another approach is the application of fully stochastic sand transport formulations to estimate the sand transport at conditions with intermittent particle motions (Kalinske, 1947; Einstein, 1950; ; Van Rijn 1993).

Van Rijn-equation

Substitution of Equations (2.1), (2.3) and (2.4) in Equation (2.5) and $s-1 \cong s$ for sand in air, it follows that:

$$q_{s,eq,VR} = \alpha_{VR}\,(\rho_{air}/g)\,(D_*)^{\beta}\,[(u_{*,grain})^2 - (u_{*,th})^2]^{1.5} \qquad (2.6a)$$

$$q_{s,eq,VR} = \alpha_{VR}\,\alpha_{ad}\,\alpha_{cf}\,(\rho_{air}/g)\,(D_*)^{\beta}\,[(u_{*,grain})^3 - (u_{*,th})^3] \qquad (2.6b)$$

with:
α_{VR} = calibration coefficient;
α_{ad} = adjustment coefficient for short fetch length (range 0 to 1; default=1 for a long fetch);
α_{cf} = reduction coefficient accounting for coarse materials (range 0 to 1; default =1 no effect).

Equation (2.6a) includes the term $(u_*^2-u_{*,th}^2)^{1.5}$ which can be replaced by the term $(u_*^3-u_{*,th}^3)$ as the error involved is fairly small for most practical wind velocities not close to initiation of movement. Around threshold conditions, the results of Equation (2.6a) can deviate significantly (factor 5 to 10), but these transport rates are extremely small and not very important in practice. Furthermore, the transport rates just beyond initiation of motion cannot be represented accurately by a deterministic equation with a constant power (Grass 1970, Paintal 1971, Van Rijn 1993). Basically, a stochastic approach is required to deal with this problem (Van Rijn, 1993, 2012). Although there is no physical reason to prefer Equation (2.6b) above Equation (2.6a), it has been found that Equation (2.6b) gives a slightly better overall fit to the transport data of Belly (1964) for 3 particle diameters (Section 2.3). Therefore, Equation (2.6b) is preferred and used in this study.

The threshold shear velocity is described by the Bagnold-equation (2.9).

Modified Bagnold-equation

Substitution of Equations (2.1), (2.2), (2.3)and (2.4) in Equation (2.5) and s-1 ≅ s for sand in air, and using: s = 2650/1.2 = 2208, $\upsilon = 1.4\ 10^{-5}$ m^2/s, D = 250 μm, β = 0.5, it follows that:

$$q_{s,eq,MB} = 3.5\ \alpha\ (d_{50}/D)^{0.5}\ (\rho_{air}/g)\ [u_*^2 - u_{*,th}^2]^{1.5} \quad (2.7a)$$

$$q_{s,eq,MB} \cong 3.5\ \alpha\ (d_{50}/D)^{0.5}\ (\rho_{air}/g)\ [u_*^3 - u_{*,th}^3] \quad (2.7b)$$

which is a modified Bagnold-equation for saturated (equilibrium) transport of dry sand in air.
Based on the work of Bagnold: $\alpha_B = 3.5\alpha \cong 2$. This derivation shows that a modified Bagnold model can be derived from general dimensional analysis. Strypsteen et al. (2020) have shown that the predictive ability of the modified Bagnold-equation (2.7) with $\alpha_B = 2$ is excellent for dry sand.

The modified Bagnold-equation for the transport of dry sand (see also Strypsteen et al., 2021) is given by:

Saturated/equilibrium transport:

$$q_{s,eq,MB} = \alpha_B\ \alpha_{ad}\ \alpha_{cf}\ (d_{50}/d_{50,ref})^{0.5}\ (\rho_{air}/g)\ [(u_{*,grain})^3 - (u_{*,th})^3] \quad (2.8)$$

Threshold shear velocity:

$$u_{*,th} = \alpha_w\ \alpha_{slope}\ u_{*,th,B} \quad (2.9a)$$

$$u_{*,th,B} = \alpha_{th}\ [(\rho_s/\rho_{air} - 1)\ g\ d_{50}]^{0.5} \quad \text{for } d_{50} > 100\ \mu m \quad (2.9b)$$

$$u_{*,th,B} = u_{*,fth,100\ um} \quad \text{for } 32 < d_{50} < 100\ \mu m \quad (2.9c)$$

Grain-related shear velocity:

$$u_{*,gr} = \kappa\ \alpha_{veg}\ f_{ob}\ \alpha_{gust}\ U_w/\ln(30 z_{wind}/k_{s,grain}) \quad (2.10)$$

with:

$q_{s,eq}$ = mass flux of sediment at equilibrium conditions (saturated transport, kg/m/s);
d_{50} = particle size (m);
$d_{50,ref}$ =reference particle size = (250 10^{-6} m; 250 μm);
ρ_{air} = density of air (≅1.2 kg/m^3);
ρ_s = density of sediment (≅2650 kg/m^3);
s =ρ_s/ρ_{air}= relative density,
υ =kinematic viscosity coefficient (m^2/s),
g = acceleration of gravity (m/s^2);
$u_{*,grain}$ = shear velocity related to the dynamic grains (m/s);
$u_{*,th}$ =surface shear velocity at initiation of motion; threshold shear velocity (m/s);
$k_{s,grain}$ = equivalent roughness length scale of Nikuradse (m) related to dynamic grains;
U_w = local wind velocity at height z_{wind} above the sand surface (m/s);
κ = constant of Von Karman (=0.4 for conditions without transport);
α_B = Bagnold-coefficient for dry sand ≅ 1.5 for uniform sand; ≅1.8 for naturally graded sand; ≅2.8 for widely graded sand (Bagnold, 1941); herein the value of 2 is used as default value: α_B= 2;
α_{ad} = adjustment coefficient related to fetch=[0.5b/(0.1+cosα)L_{ad}]$^{0.6}$; b= dry beach width; α=wind incidence angle to shore normal; L_{ad}= maximum adjustment distance (=100 m); $\alpha_{ad,max}$=1;
α_{cf} = reduction coefficient related to the presence of coare fraction (gravel and shells);
α_{th} = threshold coefficient ($\alpha_{th,initiation}$ =0.1-0.12 for the fluid threshold at initiation of motion of graded sand to coarse sand and $\alpha_{th,cessation}$=0.075 to 0.8 for the cessation (impact) threshold of fine to medium sand;
α_{slope} = coefficient for sand grains at a sloping surface (Van Rijn and Strypsteen, 2020; Dey 2003);

α_w = moisture coefficient (=1 for dry sand);
α_{veg} = vegetation coefficient (=1 for conditions without vegetation);
α_{gust} = wind gust effect =1.05 to 1.1 for field sites and 1 for wind tunnels (optional coefficient);
b = dry beach width.

It is recommended to apply a wind gust coefficient (α_{gust}) for wind transport at field sites to account for the effect of wind gust, which is a typical phenomenon in field conditions. Short-period wind gusts (time scale of 1 minute) intensify the sand transport process due to the non-linear relationship between transport and wind velocity. Wind velocity variations also occur in a wind tunnel, but these variations are caused by turbulence-related vortices, which are very different from macro-scale wind gusts. Implementation of this gust coefficient requires more research.

Initiation of motion

Laboratory and field experiments show that sand particles are still in motion when the shear velocity is smaller than the threshold value for initiation (fluid threshold shear velocity $u_{*,th,initiation}$) and only stops when the shear velocity is lower than the threshold for cessation of motion (impact threshold or cessation threshold shear velocity $u_{*,th,cessation}$). This suggests the coexistence of distinct fluid and impact thresholds for the initiation of aeolian saltation.

The value of the wind shear velocity at which particle motion by rolling, sliding and/or saltating is initiated is known as the (static) fluid threshold shear velocity ($u_{*,th,initiation}$), (Bagnold, 1941). This threshold depends not only on the properties of the fluid, but also on the gravitational and interparticle cohesion forces that oppose the fluid lifting. The fluid threshold is distinct from the dynamic or impact threshold velocity ($u_{*,th,initiation}$) which is the lowest wind shear velocity at which saltation can be sustained after it has been initiated. The particle impact or particle cessation threshold is lower than the fluid threshold because moving particles can bring other resting particles into motion more easy through particle impacts (Kok et al., 2012; Martin and kok, 2018).

Bagnold (1937, 1941) has found that $\alpha_{th,initiation} \cong 0.1\text{-}0.11$ (fluid threshold) and $\alpha_{th,cessation} \cong 0.8\ \alpha_{th,initiation}$ for the impact threshold. The data of Shao-Lu (2000) and Han et al. (2011) point to a fluid threshold coefficient of $\alpha_{th,initiation}=0.1$.

Other researchers have impact threshold values in the range of $\alpha_{th,cessation}/\alpha_{th,initiation} \cong 0.7$ to 0.8 based on analysis of field data (Martin et al., 2013; Martin and Kok, 2017, Martin and Kok, 2018; Comola et al., 2019). Martin et al. (2013) defined initiation (cessation) as transport (no transport) occurring after at least 1 second of transport=0 (transport > 0) and found $u_{*,th,cessation}/u_{*,th,initiation}=0.76$ based on analysis of measured wind velocity profiles around threshold conditions for a field site in USA. At this site the wind velocity reached a peak value of $U_{initiation} \cong 8.7$ m/s for initiation of motion, then declined toward a steady state of about 8.0 m/s for continued sustenance of transport. For cessation, wind velocity decreased gradually toward a minimum value of $U_{cessation} \cong$ 6.8 m/s at the time when transport ceased.

Martin and Kok (2017) determined the impact or cessation threshold value from the zero-intercept of the linear fit to saltation flux versus shear stress resulting in threshold shear velocity in the range 0.28 to 0.34 m/s for sand of d50=0.4 to 0.53 mm, which threshold shear are slightly smaller (10%) than the fluid shear velocity based on Bagnold (Equation 2.9b).

Martin and Kok (2018) have used a statistical method to derive the fluid and impact thresholds from high-frequency wind and saltation measurements at three field sites resulting in $u_{*,th,cessation}/u_{*,th,initiation}=0.81$, 0.86 and 0.84 for three field sites in Brazil and USA. Their measurements show that when saltation is mostly inactive, its instantaneous occurrence is governed primarily by wind exceedance of the fluid threshold. It is found that the time-averaged saltation flux is primarily governed by the impact threshold.

The transport data of Belly (1964) for uniform sand at very small shear velocities can be best represented by using the cessation (impact) threshold shear velocity $u_{*,th,cessation}$ ($\alpha_{th,cessation}$=0.08, see Section 2.3), which is very close to the value given by Bagnold (1937, 1941).
At sites with more graded sediment (d_{90}/d_{10}> 5) and a relatively large coarse fraction> 2 mm (about 10% or more), the initiation threshold coefficient will be much higher, as the finer particles are partly sheltered by the coarser materials. Lemmer beach in The Netherlands is an artificial inland recreational beach with graded beach sand (d_{10}=0.15 mm; d_{50}=0.3 mm, d_{90}=0.9 mm, $p_{coarse>2\ mm}$=10%). On 23 May 2020, the lowest wind speed at which moving particles were observed, was about 8 m/s at 1 m above the surface ($u_{*,th,initiation}\cong$0.3 m/s). Using d_{50}=0.3 mm and $u_{*,th,initiation}\cong$0.3 m/s , it follows from Equation (2.9b) that $\alpha_{th,initiation}$=0.12.
Experimental data (Kok et al., 2012) show that the measured threshold shear velocities of very fine sediment between 20 and 100 μm are scattered with values between 0.15 and 0.25 m/s. Equation (2.9b) underpredicts the measured values and therefore the shear velocity of fine sediment is herein assumed to be constant and equal to the threshold shear velocity of 100 μm-sand yielding a constant value of 0.16 m/s (Equation 2.9c).
The transport processes for conditions around the threshold value are strongly dominated by the instantaneous turbulent fluctuations resulting in an intermittent transport process. For example, if the mean near-bed velocity is equal to the initiation threshold velocity ($u_{mean}=u_{th,initiation}$), there is a small net transport due the largest fluctuations ($u_{max}>u_{th,initiation}$). Basically, this can be more accurately represented by using a stochastic approach (Davidson-Arnott et al., 2008).

Transport-limiting and supply-limiting effects

Aeolian sand transport across beaches is so complex due to many influential parameters such as grain size, grain sorting, armour layers, bed roughness, beach slope, moisture content and vegetation cover, that the transport is mostly smaller than the equilibrium transport (or transport capacity) of dry sand.
Sand transport is limited by two main effects: transport-limiting effects and supply-limiting effects.
Transport-limiting effects are effects (wind speed, grain size, roughness) which strongly modify/limit the equilibrium transport capacity. The transport capacity increases for increasing wind speed and decreasing grain size.
Supply-limiting effect are effects (bed state, fetch distance) which modify/limit the supply of sediment into the air flow. An important supply-limiting effect is the state of the bed surface as modified by moisture, salt crusts, vegetation cover and other bonding agents. This limiting effect partly depends on the strength of the wind speed. Moist particles and/or coarse armour layers consisting of gravels and shells may be immobile at low wind speeds, but may be rather mobile during storm events with high wind speeds. The reduction of sand transport over a moist surface can be determined to some extent by modifying the critical bed-shear velocity.
Another important supply-limiting effect is the fetch distance, which is the distance over which the beach is exposed to wind. The fetch distance is almost infinite for wind parallel to the beach and equal to the beach width beyond the HW-mark for wind normal to the beach. In conditions with onshore wind, there is a progressive increase in sand transport with downwind distance from a zone of no transport at the HW-mark towards the dune zone. In the case of a constant wind speed above the threshold value for initiation of motion, the development of sand transport to the equilibrium (saturated) value for dry sand primarily depends on the upwind fetch distance. The critical fetch distance is the minimum fetch distance to obtain equilibrium sand transport or sand transport capacity of dry sand. The critical fetch distance for dry sand may also be influenced by moisture, shells and vegetation. Based on field data, the critical fetch distance is found the be about 20 to 100 m, depending on the strength and direction of the wind (Jackson-Cooper 1999; Davidson-Arnott et al., 2005; Delgado-Fernandez, 2010). The critical fetch distance is fairly small (<50 m) for low wind speeds.

If the beach is small in comparison to the critical fetch distance, the transport is smaller than the equilibrium transport anywhere on the beach. This implies that most equilibrium models of sediment transport will typically overpredict the amount of sand transport.
If the beach is sufficiently wide or the wind approach angle is highly oblique, the fetch distance may exceed the critical fetch distance and the transport is equal to the equilibrium transport at locations beyond the critical fetch distance.
The effect of supply-limiting effects is demonstrated by three field experiments of Jackson and Cooper (1999), Bauer et al. (2009) and De Vries et al (2014)

Jackson and Cooper (1999) conducted an experiment to examine the influence of fetch distance on aeolian sediment transport on a natural sand beach at Benone Strand, County Londonderry, Northern Ireland. The site consisted of a wide dissipative beach (150 m wide at low tide and 80 m wide during high tide). An abundant dry sediment supply (d_{50}=0.17 mm) was available during the experiment. Wind velocity measured at 0.6 m above the sand surface ranged from 2 to 8 m/s. The fetch was in the range of 10 to 60 m. A circular trap (diameter 0.25 m; effective square diameter=0.22 m) coplanar with the sand surface was used to measure the sand transport rate. A fetch of about 15 to 20 m was required to get equilibrium sand transport for wind velocities up to 8 m/s. Their field data show sand transport rates of about 5, 10, 15 g/m/s for wind velocities of 6, 7 and 8 m/s (their rates are given in g/s for the circular trap which are converted herein to transport rates per unit width in g/m/s by dividing through an effective trap width of 0.22 m).
Bauer et al. (2009) conducted field experiments at Greenwich Dunes, Prince Edward Island National Park, Canada, which comprise about 4 km of shallow sandy beach and dunes overlying relatively weak sandstone bedrock. The study site was located about 1 km east of the mouth of the St. Peter's Bay estuary where the beach is 30 to 40 m wide and the foredune is about 8 m high. The area is micro-tidal with a mixed semi-diurnal regime and a maximum range at spring tides of about 1 m. The beach sediments are dominantly quartz sand with a mean diameter of 0.26 mm. Measurements of total sediment flux over an interval of about 10 minutes were made using five vertical traps over a cross-shore distance of about 30 m between the HW-mark and the dune foot. The moisture content of the upper 20 mm of the sand surface was measured using an electronic probe. On 11 October 2004, the wind of a storm event with wind speeds at 8 m up to 28 m/s was highly oblique to the beach. The moisture content at the upper beach was in the range of 3% to 6% . The transport rate was almost zero at the lower beach beyond the HW-mark and increased in landward direction. The maximum transport occurred at the two mid-beach locations where the fetch distances was about 50 to 150 m. The transport close to the dune foot was slightly lower due to the presence of vegetation and decreasing wind speed caused by the presence of the high foredune. Thus, sediment was stripped from the foreshore throughout the day and subsequently transported across the mid-beach and deposited on the upper beach. It was concluded that substantial moisture content in the surface sediments reduces the transport rate except when the wind speed is particularly intense. The angle of wind approach is critical to understanding the transport distribution across beaches because the fetch distance is relatively large in conditions with highly oblique winds.

De Vries et al. (2014) conducted field measurements from 6 to 10 December 2010 at Vlugtenburg beach located on the south west of the Holland coast (south of The Hague, The Netherlands) in conditions with mostly onshore wind in the range between 8 and 11 m/s at 2 m above the surface. The beach slope was 1 to 40 and the grain size was in the range of 0.2 to 0.3 mm. The beach is regularly nourished with sand from offshore resulting in a somewhat artificial beach-dune system with lag deposits on the beach due to shell clustering and coarse materials. The tide is semi diurnal with a neap-, spring-tidal range of 1.2 to 2.2 m. The cross-shore excursion of the waterline due to the tide is around 60 to 100 m. The width of the dry beach beyond the HW-mark is about 70 m. The tide creates a significant variability of beach width. To measure transport gradients in cross shore direction, the saltiphones were placed on the beach over a cross-shore distance of about 70 m. The most seaward saltiphone was placed just beyond the HW-mark. The most landward saltiphone was close to the dune foot.

The measured data in conditions with onshore wind show that the transport at mid-beach was much higher during the low tide when the fetch distance was relatively large. It was observed that the beach zone beyond the HW-mark was a dominant sediment source for landward sand transport. Sand transport at mid-beach was higher during the day with a drier sand surface than during the night. During another event, some of the saltiphones were placed in the intertidal zone. No transport was measured by the saltiphone in the intertidal zone. The transport was maximum at mid-beach at about 40 m from the HW-mark. The transport was slightly lower at the dune foot location, most likely due to slightly smaller wind speeds at that location due to the presence of the high foredune. It was concluded that the aeolian sediment transport over the beach originates from the beach zone just beyond the HW-mark and increases towards the mid-beach zone and the dune foot zone. The transport at the lower beach beyond the HW-mark is smaller than the equilibrium transport due to supply-limiting effects in conditions with onshore winds.

The results of these three field experiments in supply-limiting conditions show that the transport rate adjusts/adapts to the new conditions within a certain adjustment distance. This adjustment distance depends on the thickness of the transport layer, the wind speed and the mixing capacity (turbulence and roughness) and is in the range of 20 to 100 m form field conditions (Van Rijn and Strypsteen, 2020). Two types of upwind supply conditions are possible: underload or overload conditions. A typical example of underload conditions (supply-limited conditions) is the entrainment of sand at the lower beach (underload) in conditions with onshore wind at the lower beach (underload) as long as the fetch length is smaller than the adjustment length ($L_{fetch}<L_{ad}$). An example of overload conditions is the transition from an upwind site with a rough bed (high shear velocity) to a flat, smooth downwind surface (lower shear velocity) or the transition to a more sheltered site.
A simple approach to deal with adjustment effects in overload and underload conditions is given by (Van Rijn and Strypsteen, 2020):

$$q_{s,x}=q_{s,eq,up} - (x/L_{ad})^{0.6} (q_{s,eq,up}- q_{s,eq,down}) \qquad (2.11)$$

with: $q_{s,x}$= actual transport at location x, $q_{s,eq,up}$= equilibrium transport at upwind location (x=0) and $q_{s,eq,down}$= equilibrium transport at downwind location ($x=L_{ad}$). For underload conditions due to limited fetch ($x=L_{fetch}$ and $q_{s,eq,up}=0$), this yields: $q_{s,x}=\alpha_{ad}\, q_{s,eq,down}$ with $\alpha_{ad}= (L_{fetch}/L_{ad})^{0.6}$ and α_{ad} =1 for $L_{fetch} > L_{ad}$. The fetch distance is $L_{fetch}= (0.5b_w)/\cos\theta_w$ = fetch length to the mid-beach point and b_w= width of upper beach beyond uprush limit (input), θ_w= angle of wind incidence to shore normal.
The power of the adjustment process is taken as 0.6 similar to that of air flow layer adjustment (Granger et al., 2006). The adjustment process proceeds in a progressive way; the sand transport is about 70% of the equilibrium value after 50% of the total adjustment length ($L_{fetch}/L_{ad}=0.5$). If the dry zone of the beach is wider than about 100 m, the adjustment coefficient can be safely neglected. Research is recommended to improve the proposed equations.
The available prediction equations for the sand transport capacity of dry sand will significantly overestimate the actual sand transport capacity in conditions with moisture, shells and vegetation, if the supply-limiting effects are not taken into account (Mckenna Neuman et al., 2012; Van Dijk et al., 1996, Davidson-Arnott et al., 2005).
Generally-accepted methods for inclusion of supply-limiting effects are not yet available. Mostly, it is done in a pragmatic way by using empirical coefficients derived from fitting of field data.

2.1.2 Multi fraction approach

In some cases, the beach material has a relatively wide size grading ($(d_{90}/d_{10}>5$). Examples are nourished beaches, artificial beaches and gravel/shingle beaches. Due to sorting process over time, the coarse fractions including shells and shell fragments will form a lag deposit at the upper beach beyond the high water line resulting in an armour layer. The sand transport above the armour layer is strongly reduced, even for a long fetch distance.

At beaches with an armour layer, the intertidal zone where the armour layer is mostly absent due to wave action, may be a source of sediment for wind transport. The moisture level in this intertidal zone varies over the tidal cycle. In daytime, the beach sand in this zone will gradually become drier depending on solar radiation and wind strength which may result in sand transport if the wind is strong enough (De Vries et al., 2014; De Vries and Hoonhout, 2017; Hoonhout and De Vries, 2019).

In 2018, an artificial dune and beach system (Prins Hendrik sand dike) is made on the island of Texel (The Netherlands). Sand dredged at a borrow site in the North Sea was placed against the old dike to get a more natural appearance of the traditional dike. To reduce the maintenance cost due to erosion by wind and water, the beach was covered with a relatively coarse layer of sand, gravel and shells ($d_{90}/d_{10}\cong$10 to 15). Sand transport predictions for these cases require the application of the multi fraction approach, which was explored by Van Rijn (2007). Based on this, Equations (2.6b) and (2.8) can be represented as:

$$q_{s,eq,VR} = \alpha_{VR}\,\alpha_{ad}\,\alpha_{cf}\,(\rho_{air}/g)\,\sum_{i=1}^{i=N} f_i\,(D_{*,i})^{\beta}\,[(u_{*,grain})^3 - (\zeta_i\,u_{*,th})^3] \qquad (2.12a)$$

$$q_{s,eq,MB} = \alpha_{B}\,\alpha_{ad}\,\alpha_{cf}\,(\rho_{air}/g)\,\sum_{i=1}^{i=N} f_i\,(d_i/d_{50,ref})^{0.5}\,[(u_{*,grain})^3 - (\zeta_i\,u_{*,th})^3] \qquad (2.12b)$$

with: N= number of fractions, d_i= mean particle size of fraction I, f_i= fraction value (<1; $\sum f_i$=1) , ζ_i= hiding-exposure factor (finer particles are shielded by the larger particles and are more difficult to erode), $u_{*,th}$= threshold shear velocity of fraction i.
The hiding-exposure factor is tentatively expressed by (Van Rijn 2007):

$$\zeta_l = (d_{50}/d_i)^n \text{ with minimum value } \zeta_{l,minimum=1}=1 \qquad (2.13)$$

with: n=0.5 to 1.
If shells are present, it is assumed that each fraction is affected in the same way. Sediment particles under the shells do not participate in the transport process, which is taken into account by the percentage of shells (p_{shell}) per unit weight. Particles in the lee of the shells experience lower wind speeds and are thus less mobile. This effect is taken into account by a reduction coefficient acting on the transport rate (Van Rijn and Strypsteen 2020). Exploratory computations based on the multi fraction method are given in **Section 5.3**.

2.2 Dynamic grain roughness

The effective grain roughness of a flat (static) sand bed without any grain movement is related to the size of the largest particles (d_{90}), (Van Rijn, 1982, 1984, 1987, 1993, 2007). The effective bed roughness was found to be in the range of $k_{s,grain}$= 1 to 10 d_{90} with a mean value of $3d_{90}$. The relatively large experimental range expresses the effect of small irregularities related to preparation of laboratory beds. Observations of flat beds often show the presence of small irregularities, isolated larger roughness elements (shells, stones, pebbles, cobbles, vegetation) or the presence of patches with finer and coarser materials in conditions with graded sediments.
Based on the available data, it is proposed to use $k_s=3d_{90}$ for static grain roughness of relatively fine sands (<0.5 mm) and $k_s=1d_{90}$ for coarse sand (>0.5 mm) and gravels.
The effective grain roughness of a flat, dynamic sand bed with significant sand transport as sheet flow is related to the thickness of the saltation or sheet flow layer, which increases for increasing wind velocities. Most of the sand transport occurs in a layer with a thickness of about 50 mm (Yang et al. 2019). The effective roughness of a flat sand surface during conditions with intense sand transport in the upper wind regime is not precisely known, as no field data for this regime are available, but most likely the roughness will be related to the thickness of the saltation layer (10 to 50 mm).

Small-scale bed forms (ripples) or bed irregularities with height scales of 0.01 to 0.1 m and length scales of 0.1 to 1 m are mostly generated in the lower wind regime (< 10 m/s) and are gradually smoothed out in the transitional (10 to 15 m/s) and upper wind regimes (> 15 m/s; Belly 1964). When ripples are present, the effective bed roughness (form roughness) increases significantly, depending on the height and steepness of the ripples.
The maximum effective bed roughness of ripple-type bed forms was found to be of the order of 5 times the bed form height (Pelletier and Field 2016). However, the data of Field and Pelletier (2018) show that the effect of form roughness is very minor with effective bed roughness values up to 50 mm. Based on the work of Owen (1964), Sherman (1992), Sherman and Farrell (2008) and Strypsteen (2019), the effective bed roughness (k_s) is in the range of 10 to 100 mm. As bed form information is lacking, it is not clear whether these roughness values are caused by the drag of saltating particles, the form drag of the bed forms or both. The form roughness of ripples leads to: i) smaller wind velocities in the near-bed layer, ii) larger shear velocities and iii) more turbulence (larger fluctuations). Wind-driven sand transport is more intensively related to shear stresses acting on the static and dynamic grains and to lesser extent related to form drag-related turbulence, similar as in water flow (Van Rijn 1993).
Herein, a simple and straightforward roughness predictor (Van Rijn and Strypsteen, 2020) is used which primarily depends on the static and dynamic grain roughness parameters. Various transport regimes with different roughness parameters are distinguished based on the transport stage parameter T which is defined (see Van Rijn 1984, 1993) as the grain-related bed-shear stress minus the threshold bed-shear stress divided by the threshold bed-shear stress: $T=(\tau_{grain,}-\tau_{th})/\tau_{th}$.
The transport regimes and associated bed roughness parameters are:

- Premature transport stage with rolling, sliding and hopping particles (T<0.5): mostly static grain roughness related to the larger particles (d_{90}) of the sand surface;
- Lower transport stage with saltating particles and evolving bed ripples (0.5<T<1): dynamic grain roughness produced by small-scale vortices in the lee of the saltating particles due to the differences of the wind and particle velocities;
- Transitional transport stage with saltating particles and smoothed-out ripples (1<T<5): dynamic grain roughness in combination with gradually disappearing form-related roughness;
- Upper transport regime with a thin sheet flow layer of saltating particles in contact with the surface and suspended transport layer (T>5): dynamic grain roughness.

It is proposed to represent the effective bed roughness for sand transport in the lower, transitional and upper regime by the following expressions:

$$k_{s,grain} = k_{s,grain,\,st} + k_{s,grain,\,dyn} \quad (2.14a)$$

$$k_{s,grain} = d_{90} + \alpha_1\,\gamma_r\,d_{50}\,T^{\alpha 2} \quad (2.14b)$$

$$T = [\{u_{*,grain,st}\}^2 - \{\alpha_{slope}(0.5\alpha_w+0.5)u_{*,th,B}\}^2]/(u_{*,th,B})^2 \quad (2.14c)$$

$$u_{*,grain,st} = \alpha_{veg}\,\kappa U_{w,z}/(\ln(30z_w/d_{90}) \quad (2.14d)$$

$$u_{*,grain} = \alpha_{veg}\,\kappa\,U_{w,z}/(\ln(30z_w/k_{s,grain}) \quad (2.14e)$$

with:

$k_{s,ir}$ = roughness due to irregularities (shells, stones, etc) producing additional turbulence (m);
T = transport stage parameter (-);
$u_{*,th,B}$ = threshold shear velocity according to Bagnold;
$k_{s,grain,st}$ = bed roughness height due to static grains (m);
$k_{s,grain}$ = bed roughness height due to static and dynamic grains (m);
d_{90} = grain diameter (90% smaller);
α_w = moisture coefficient (=1 for dry sand);
$\gamma_r = 1+1/T$ = ripple enhancement coefficient factor;
κ=0.4; α_1 and α_2= coefficients.

The term $(0.5\alpha_w+0.5)u_{*,th,B}$ in Equation (2.14c) represents the average value of threshold shear velocity in dry and moist conditions.

The γ_r-coefficient is the ripple enhancement coefficient for the lower wind transport regime with values between 1 and 3 depending on the ripple steepness (-). It is related to the T-parameter in a way that the effect reduces for increasing T-values as the ripples are gradually smoothed out. The default coefficients α_1 and α_2 are found to be α_1 = 15 and α_2= 1 for the data sets of Han et al. (2011) and Yang et al. (2019), (Van Rijn and Strypsteen, 2020).

The d_{90} is roughly equal to d_{90}=2 to 3d_{50} for fairly uniform (narrow-graded) sand and may be as large as about d_{90}=10d_{50} for very wide-graded sand mixtures. When relatively large shells and other roughness elements are present on a flat sand bed, the effective roughness will increase considerably due to generation of extra turbulence depending on the size and cover of the roughness elements resulting in an increase of the sand transport capacity. The static roughness of shells may be in the range of 1 to 5 mm for small to large shells with a cover percentage of 5% to 10% (McKenna et al., 2012). The roughness of shells can be neglected for cover percentages < 5% (see Dong et al., 2002; McKenna et al., 2012). The bed roughness related to irregularities is most likely somewhat larger for coarse sand surfaces than for fine sand surfaces. Equation (2.14) produces dynamic grain roughness values in the range of 5 to 10 mm for wind speeds of 10 to 15 m/s, which is of the right order of magnitude compared to the field data of Davidson-Arnott et al. (2005) and Strypsteen (2019) for a flat bed without much irregularities (no shells, no ripples). Equation (2.8) is a first attempt to better describe the dynamic grain roughness related to the saltation process. Detailed experiments in wind tunnels are highly recommended to improve the coefficients involved. It is noted that the bed roughness for sand transport may be substantially smaller than the bed roughness for the large-scale wind flow which is dominantly affected by macro-scale bed features (dunes, objects, etc.).

Using the multi fraction approach, Equation (2.14) is proposed to be based on the d_{50} and d_{90} of the mixture.

2.3 Calibration of transport equations for dry sand in wind tunnel

Belly (1964) has measured wind blown sand transport in a wind tunnel using three fairly uniform diameters (d_{50}=0.44 mm, 0.3 mm and 0.145 mm). The data of Belly (39 data points) have been used to calibrate the modified Bagnold-equation and the Van Rijn-equation (single fraction method). Equation (2.14) was used for the grain-related shear velocity.

Van Rijn-equation

Figure 2.3.1 shows the measured sand transport data of Belly (1964) as function of the wind velocity at z=0.3 m above the sand surface. It can be observed that the sand transport strongly increases for increasing wind velocities. The measured transport rates also increase for increasing particle diameter between 0.145 mm and 0.3 mm. The measured transport rate of sand with d_{50}=0.3 mm is about 50% higher than of sand with d_{50}=0.145 mm. The sand transport of sand with d_{50}=0.3 and 0.44 mm is about the same. The two measured transport values at very low velocities of 4 and 4.5 m/s are doubtful as these values are well below generally accepted threshold conditions of Bagnold for 0.3 and 0.44 mm. The computed results show that the excess shear velocity to the power of 3 closely yields a curve which closely follows the measured values.

Equation (2.6b) was calibrated by varying three coefficients: α_{VR}, β and α_{th}. The best agreement of measured and computed transport rates was found for α_{VR}=1.8, β=0.1 and α_{th}=0.08, see **Figure 2.3.1(upper)**. Using these values, 92% of the computed transport rates are within a factor of 2 of the measured values (36 out of 39 data points).
The threshold shear velocity is best represented by the impact or cessation threshold ($\alpha_{th,cessation}$=0.08 instead of α_{fth}=0.1, see Equation (2.9)) to obtain the best agreement for low wind speeds. Using a value of $\alpha_{th,cessation}$ =0.08, the winnowing effect of fines from naturally graded sand at low wind velocities resulting in higher transport rates can be better represented. This coefficient may be significantly (0.1 to 0.12) larger for sand with a relatively coarse fraction shielding the finer particles.

Figure 2.3.1(lower) shows that the predicted transport rates using value $\alpha_{th,cessation}$=0.1 are too high at relatively low velocities < 8 m/s. Most likely, the measured transport rates are relatively high at low velocities because the finer fractions of the bed material are winnowed, which cannot be accurately represented by the median grain size (d_{50}). This can be corrected by slightly reducing the threshold value of the median grain size. The sand processes at low velocities are also discussed in Section 2.4.
The grain size effect is best represented by β=0.1, which means a weak increase of the transport rate for an increasing grain size. The value β=0.1 is assumed to be valid for particle sizes up to about 0.5 mm. For particles coarser than about 0.5 mm ($D_* \cong 20$), it is more logic to assume that the transport rate decreases for increasing particle size (D_*). Yang et al. (2019) have found that the transport strongly decreases for coarse sand (0.5 to 1 mm). Herein, a tentative equation β=-0.001D_*+0.12 is explored to represent the decrease of the transport rate for coarse sand. This equation yields a β-coefficient equal to 0.1 for D_*=20 and a decreasing β-coefficient from 0.1 to -0.3 for D_* > 20, see **Figure 2.3.2**.
The effect of grain size on the sand transport rate based on Equation (2.6b) with constant β=0.1 is shown in **Figure 2.3.3Upper**. The grain size is varied in the range of 0.2 to 10 mm. The sand transport rate is plotted as function of the wind velocity at 1 m above the surface. The sand transport rate of coarse materials is strongly affected by the threshold velocity. The sand transport rate slightly increases for increasing grain sizes (due to β=0.1) if the wind velocity is far beyond the threshold velocity.
Most likely, the coefficient β=0.1 is not really valid for coarse materials > 0.5 mm. It is more logic that β<0.1 for coarser grains resulting in a decreasing transport rate for increasing sizes.
Figure 2.3.3Lower shows the same plot for β=0.1 if D_*< 20 and β=-0.001D_*+0.12 for D*>20. Now, the transport rates of gravel with 2, 4 and 10 mm is much smaller. More research with very coarse and gravel is required to evaluate whether these results are meaningful.

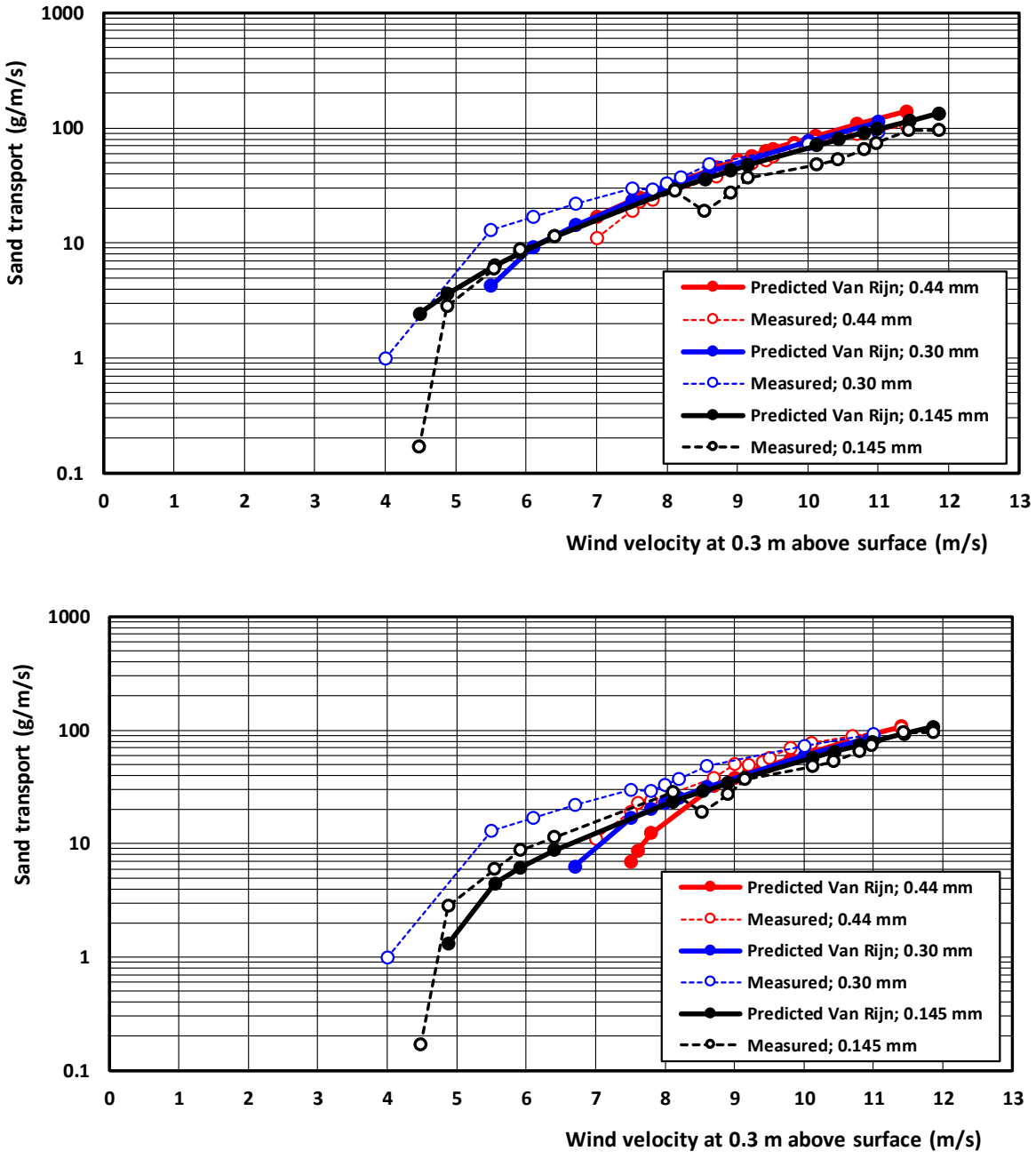

Figure 2.3.1 *Predicted and measured wind-blown sand transport; wind tunnel data of Belly (1964) and Van Rijn-equation (2.6b) α_{VR}=1.8; β=0.1 and $\alpha_{th,cessation}$=0.08 (upper) and $\alpha_{th,cessation}$=0.1 (lower)*

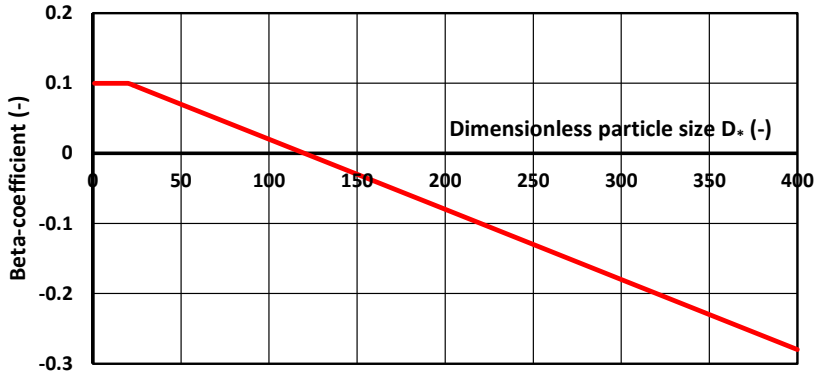

Figure 2.3.2 *β-coefficient as function of D**

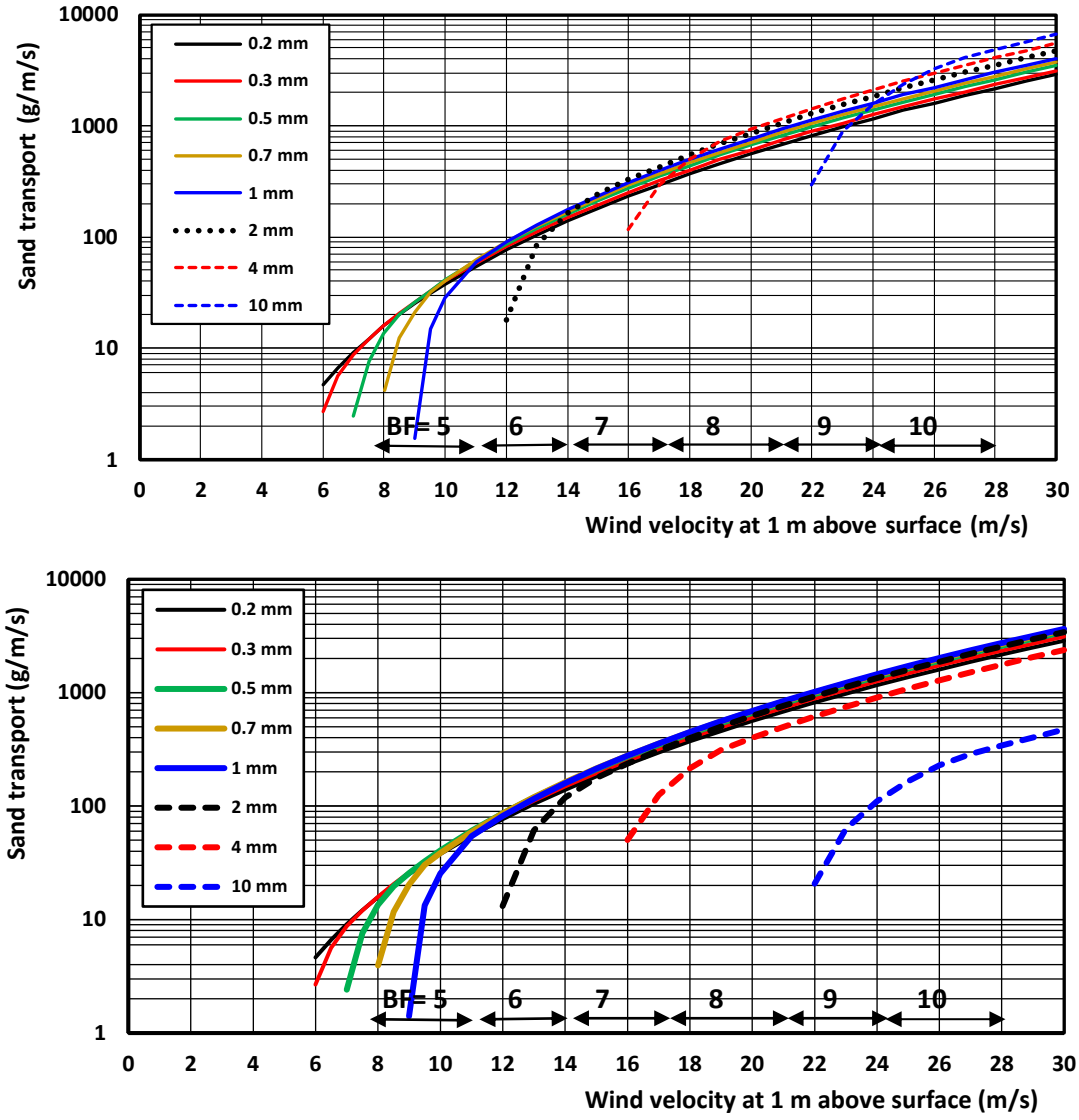

Figure 2.3.3 *Effect of grain size on predicted wind-blown sand transport; VR-equation*
Upper: β=0.1; Lower: β=0.1 for D< 20 and β=-0.001D*+0.12 for D*>20*

Modified Bagnold-equation

Equation (2.6b) was calibrated by varying two coefficients: α_B, and α_{th}. The β-coefficient representing the grain size effect was set to β=0.5 as proposed by Bagnold. The best agreement of measured and computed transport rates was found for α_B=2 and α_{th}=0.08, see **Figure 2.3.4(upper)**. Using these values, 90% of the computed transport rates are within a factor of 2 of the measured values (35 out of 39 data points).

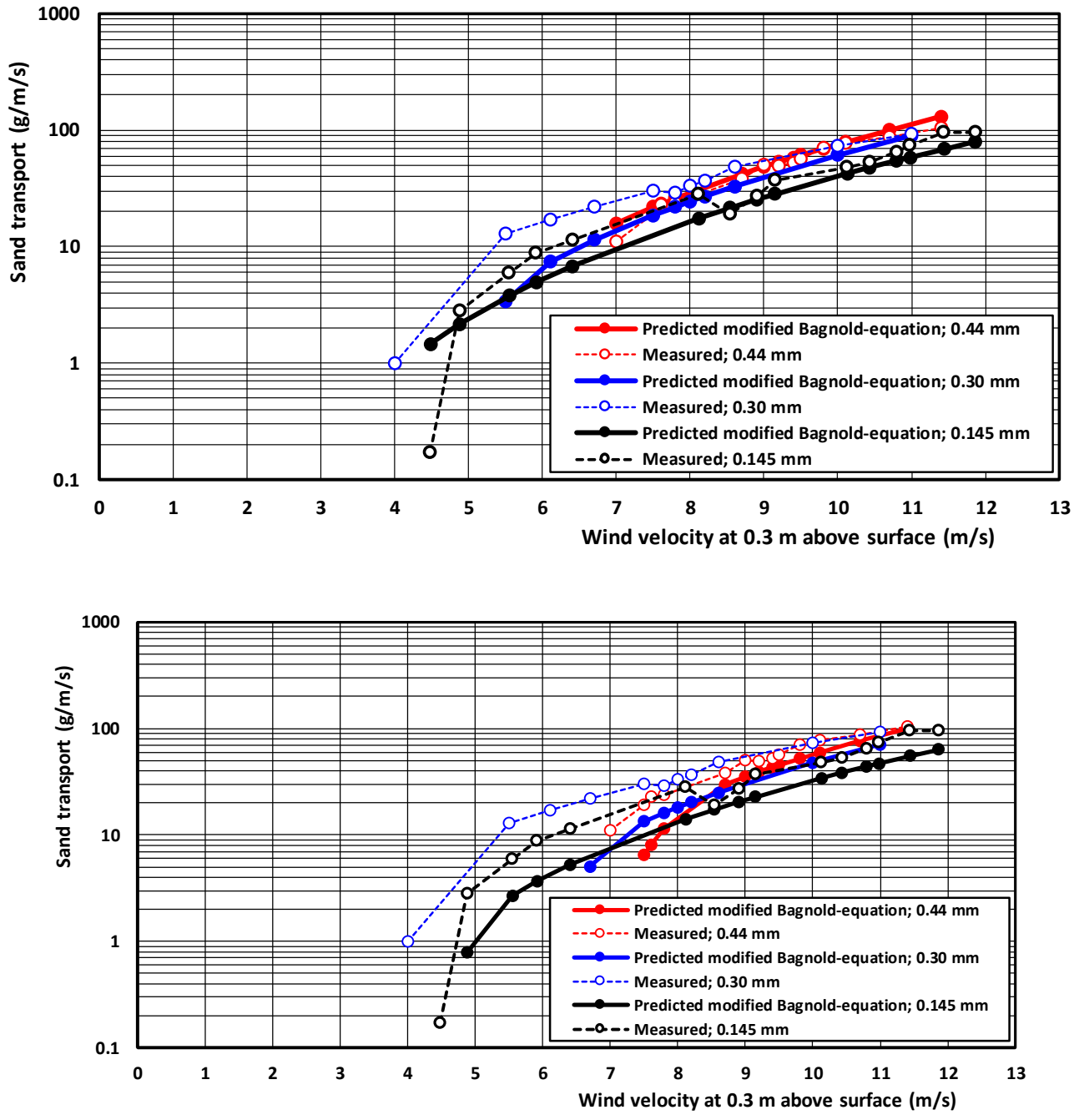

Figure 2.3.4 *Predicted and measured wind-blown sand transport; wind tunnel data of Belly (1964) and Modified Bagnold-equation (2.8) α_B=2 and α_{th}=0.08 (upper) and α_{th}=0.1 (lower)*

The predicted transport values increase for increasing particle diameter and for increasing wind velocity. The excess shear velocity to the power of 3 closely yields a curve which closely follows the measured values. Equation (2.8) can represented the measured transport of sand with d_{50}=0.145 and 0.3 mm very well, but the transport of sand with d_{50}=0.44 mm is substantially over-predicted. The effect of the particle diameter is somewhat too strong. The power of the particle diameter (β=0.5) is somewhat too high. The measured transport rates at low wind speeds are best represented by α_{th}=0.08 instead of 0.1, as found for the VR-equation.

In part 3, it is shown that the new VR-equation and the modified Bagnold-equation with the same model settings yield excellent results for field sites.

3. Description of laboratory and field instrumentation

3.1 General

Both laboratory and field experiments have been done to study wind blown sand transport and the effect of moisture and shells on the transport processes. New equipment has been designed and used. Descriptions are given in Sections 3.2 and 3.3.

3.2 Laboratory instrumentation

New laboratory experiments have been performed in two mini wind tunnels with a length of 100 cm (see **Figure 3.1**). The bottom and side walls of the tunnels consist of wood (multiplex 18 mm). The tunnel cover is made of transparent perspex material. The internal dimensions of the two tunnels are 50x50 mm² and 60x60 mm². The tunnel height can be reduced by inserting a short wooden ramp (length of 30 cm and height of 18 mm) in the tunnel to increase the wind velocity. At the downwind end of each tunnel, a small plywood tray filled with sand can be inserted. The top surface of the tray (and sand) is flush with the top surface of the wooden tunnel bottom. The length of the tray is 250 mm and the height of the tray is 18 mm. The horizontal end part of the ramp is always flush with the sand surface of the tray. The wind flow is generated by a standard hair fohn which can produce constant wind velocities up to 25 m/s. The fohn produces a very steady wind flow with only very minor fluctuations due to turbulence (smaller than 5% of the time-averaged velocity). Strong wind velocity gusts often up to 20% as observed in field conditions are fully absent. The wind velocity is maximum if the nose of the fohn is placed inside the tunnel. Lower wind velocities can be obtained by placing the fohn at some distance (10 to 30 cm) from the tunnel entrance.
The wind velocity was measured with a small-cup-type wind velocity meter (Kaindl-windmaster 2; Kwm2; Figure 3.1) at the downwind end of the tunnel at an elevation of 30 mm above the surface. The Kwm2 is manufactured by Kaindl (Germany) and has a rotor diameter of 22 mm and a cup height of 10 mm. The wind velocities measured by the Kwm2-meter have been compared to those of a larger windcup-meter (Eole, JDC-Switzerland, see Section 3.3). The wind speeds measured by the Kwm2-meter are systematically about 15% higher than the values of the Eole windmeter, see **Table 3.2.1**.
The measured wind velocities (at 30 mm above the surface) are in the range of 5 to 11 m/s. The wind velocity can be increased to 15 m/s by inserting a short ramp (length=300 mm; height=18 mm) and placing the tray on a wooden block to keep the sand surface flush with the horizontal surface of the ramp. The wind flow is turbulent as the Reynolds number involved is about $Re=u_w h/\upsilon=10x0.05/0.00001.5=3\ 10^4$.

Fohn speed	**Wind velocity (m/s) at distance of 7 from Fohn**		**Wind velocity (m/s) at distance of 20 cm from Fohn**	
	Kwm2	**Eole**	**Kwm2**	**Eole**
Low	8.7 (+13%)	7.6	4.1 (+15%)	3.5
High	14.5 (+15%)	12.3	6.8 (+13%)	5.9

Table 3.2.1 *Comparison of Kwm2 and Eole windmeters*

The sand mass of the tray is determined by weighing on a scale accurate to 10 mg. The length of the sand bed in the tray has a length of about 0.2 m, which is about 8 times the height of the flow boundary layer. The length of the sand bed is sufficient to establish equilibrium sand transport with rolling particles at low velocities just above

the threshold value, but the length of the tray is much too short for the development of equilibrium transport at higher velocities.
The tunnels have been used to study the transport of dry sand just above the threshold value and the effects of of moisture and shells on the threshold shear velocity and the sand transport. The effective transport width of the tunnels is about 60% of the total width due to side wall effects, based on visual observation of the scour marks on the sand surface in the tray.
Two methods have been used to derive the bed shear velocity from the measured wind velocity at the downwind end of the tunnel: (i) velocity profile method and (ii) the flow discharge method. The mini wind tunnels have a relatively small width-depth ratio (b/h). Hence, the effect of the side walls and the roof on the bed -shear velocity acting on the sand surface must be taken into account.
The measured wind velocity distribution follows a logarithmic profile (R^2=0.99), see **Figure 3.2.1**. The bed-shear velocity and effective roughness are u_*=0.67m/s and k_s=0.00085 m for the data of **Figure 3.3.1**.

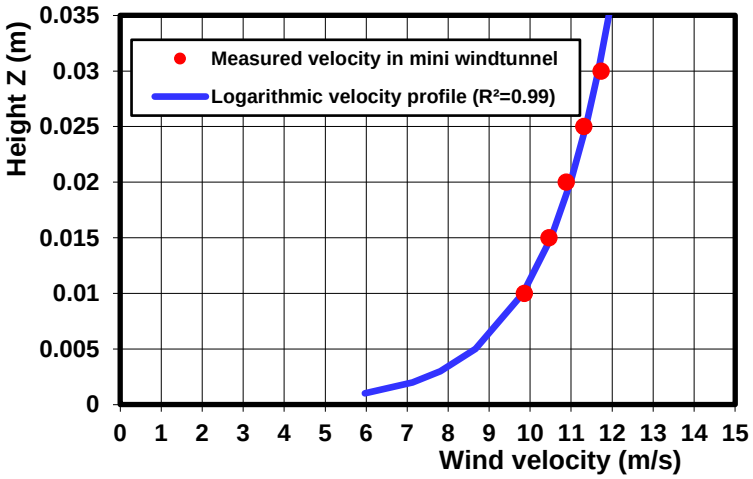

Figure 3.2.1 *Measured wind velocity profile in axis of mini wind tunnel (ST); u_*=0.67 m/s; k_s=0.00085 m*

The velocity profile method is based on the assumption that the velocity distribution in the tunnel is described by a logarithmic function, as follows:

$$u_w=(u_*/\kappa)\ln(30z_w/k_s) \quad (3.1a)$$

$$u_*=[\kappa u_{w,z}][\ln(30z_w/k_s)]^{-1} \quad (3.1b)$$

with: u_w= wind velocity measured at height z_w (=0.03 m) above sand surface in the tunnel axis; u_*= shear velocity; κ= coefficient Von Karman (=0.4); k_s= $2d_{50}$= effective sand roughness height of Nikuradse (Nikuradse 1933; Van Rijn 2011).

Using the wind velocity measured in the axis of the tunnel, the shear velocity in the axis is obtained.
To obtain the width-averaged shear velocity, it is proposed to use the width-averaged wind velocity: u_{ww}= α_{sw1} u_w with α_{sw}= coefficient $\cong$ 0.8-0.9 for small values of w/h$\cong$ 1 and $\alpha_{sw1} \rightarrow 1$ for w/h>>1.

The flow discharge method is is given by:

$$\tau_w=\rho(u_*)^2=\rho g\,[Q/(AC)^2 \quad (3.2a)$$

$$u_*=g^{0.5}\,[Q/(AC]=g^{0.5}[\,\overline{\overline{u}}\,/C] \quad (3.2b)$$

with:

τ_w= wall shear velocity;
Q= wind flow discharge, A= area of cross-section of wind tunnel;
$\overline{\overline{u}} = \alpha_{sw2}\, u_w$=cross-section-averaged wind velocity;
u_w= measured wind velocity at height z_w;
α_{sw2} =coefficient (≅0.8-0.9);
$C = 5.75 g^{0.5} \log(12R_e/k_{s,e})$= Chézy-coefficient;
R_e= effective hydraulic radius (≅$0.4h_{tunnel}$);
$k_{s,e}$= effective roughness height representing all tunnel walls (≅0.1 mm).

The C-values of the mini wind tunnels are estimated to be about 60 to 62 $m^{0.5}/s$ (wind tunnel height=0.05 and 0.06 m; A=0.0025 and 0.0036 m^2).
Both methods yield similar results, but the more straightforward velocity profile method is preferred (less uncertain coefficients).

Figure 3.1 *Mini wind tunnels*

Special calibration tests using uniform sand with known threshold shear velocities have been done to determine the bed-shear velocities generated in the mini wind tunnels. The tray was filled with fairly uniform sand and the wind velocity at threshold conditions (some grains moving) was measured, see column 3 of **Table 3.2.2**. Column 2 shows the average threshold shear velocity based on the Bagnold-Equation (2.9) and the instantaneous (related to gusts) threshold shear velocity. Based on observations, it is known that sand particles are set into motion by

the higher instantaneous velocities (gusts) of the wind velocity distribution. De Ruiter (1983) has found that the instantaneous shear velocities causing particle movement are about 15% to 20% higher than the average shear velocity determined from time-averaged velocity measurements. Herein, it assumed that the instantaneous values are 15% higher than the average values (see column 2 of Table 3.2.2). Column 4 shows the shear velocities determined from the measured velocities at the end of the wind tunnel, which can be interpreted as estimates of the instantaneous shear velocity as turbulence-related gusts are almost absent in the mini wind tunnel. The test results were used to calibrate the value of the α_{sw1}-coefficient resulting in: α_{sw1} =0.85. This coefficient is found to be almost constant for the present tests.

Type of sand	**Average threshold (Bagnold) and instantaneous threshold shear velocity (m/s)**	**Measured instantaneous wind velocity at z_w=0.03m above sand surface at threshold conditions (m/s)**	**Estimated instantaneous shear velocity based on velocity profile method $k_s=2d_{50}$ (α_{sw1}=0.85) (m/s**
Beach sand (Schokkerhaven) d_{10}=0.205 mm; d_{50}=0.38 mm; d_{90}=0.7 mm; d_{95}= 0.85 mm	0.29; 0.33	6.8 ± 5%	0.33 ± 15%
Uniform Sand (0.5-1 mm); d_{10}=0.57 mm; d_{50}=0.8 mm; d_{90}=0.95 mm; d_{95}= 1 mm	0.42; 0.48	9.2 ± 5%	0.49 ± 15%
Uniform Sand (0.4-0.8 mm) d_{10}=0.47 mm; d_{50}=0.6 mm; d_{90}=0.85 mm; d_{95}= 0.9 mm	0.36; 0.41	8.6 ± 5%	0.44 ± 15%
Uniform Sand (0.3-0.5 mm) d_{10}=0.27 mm; d_{50}=0.35 mm; d_{90}=0.46 mm; d_{95}= 0.5 mm	0.28; 0.32	7.1 ± 5%	0.34 ± 15%
Uniform Sand (0.1-0.3 mm) d_{10}=0.1 mm;d_{50}=0.17 mm; d_{90}=0.22 mm; d_{95}= 0.3 mm	0.19; 0.22	5.2 ± 5%	0.22 ± 15%

Table 3.2.2 *Measured wind velocities at threshold conditions (initiation of motion) of dry sand in mini tunnel*

3.3 Field instrumentation

At present, the simple mechanical trap-type samplers intercepting the moving particles of the saltation layer are the most reliable instruments to obtain field data for calibration of transport models. Sampling times should be sufficiently long (say 10 minutes) to integrate over fluctuations due to turbulence and wind gusts. Many samplings should be done at the "same" location to reduce variability due to small transverse and streamwise gradients.

Field experiments have been done using trap-type samplers. The equipment used for measuring aeolian sand transport in field conditions consists of a short stainless steel mast with three wind cup velocity meters (cup-type sensors) and four trap type tubes and a separate bed load trap (**Figure 3.3.1**) placed close to the mast location.

The wind velocity is measured by using three JDC-wind cup meters (type Eole) with averaging time interval of 1 minute. The Eole-meter is manufactured by JDC (Switzerland) and has a rotor diameter of 45 mm and cup height of 22 mm. The accuracy of the instrument specified by the manufacturer is ±3%. The three available instruments were compared to each other in a wind flow produced by a hair fohn placed at about 7 cm from the cup axis. Each instrument gave a value within the interval 14 ± 0.5 m/s (variation range of 4%). During field experiments at the PH-site on the island of Texel (March-April 2020; Van Rijn 2020), the Eole cup-meter was compared to the wind cup meter values of a KUL-windmast of the University of Leuven (Belgium). The wind was almost parallel to the beach and the Eole-meter was positioned at 1.2 m above the surface at a distance of 10 m sidewards between the mast and the water line. The results are shown in **Figure 3.3.3**. The wind velocities of the Eole-

meter are, on average, about 5% higher than those measured at the wind mast. This systematic difference is most likely related to the position of the wind cup-meters. The KUL-mast was more close to the dune front, and the Eole-meter was positioned at mid-beach where the wind velocities may have been slightly higher.
The sand transport was measured using a trap-type sampling instrument (LVR sampler; **Figure 3.3.1**) consisting of:

- rectangular bed load trap (internal width=93 mm; internal height= 71 mm) with a 70 μm-bag;
- circular tube-type traps (internal tube diameter= 36 mm; equivalent square diameter=32 mm) with 70 μm-bag attached to a mast of about 1.5 m;

The traps are placed in the wind direction (as indicated by a small vane attached to the mast).
The LVR-sampler is very similar to the Sherman streamer trap (SST; Sherman et al., 2014). The SST trap system consists of a vertical stack of thin stainless-steel rectangular frames enclosed with nylon mesh that maximizes flow through the trap and minimizes flow distortion. This cost-effective set of traps is easy to use, quick to deploy, easy to retrieve samples in the field and have excellent efficiency (Sherman et al., 2014), (Farrell and Swan, 2016). The total transport of sand can be determined by summation of the transport data of the bottom trap with vertical height of 71 mm and the circular tube -type traps placed at various near-bed elevations (range of 100 to 300 mm above the surface; almost no transport above 300 mm). Based on practical experience (see Table 6.3.3), the transport of sand in the layer 0 to 71 mm measured by the bottom trap is mostly about 70% of the total transport for high wind speeds to about 100% for low wind speeds. About 30% of the total transport takes place in the layers above the bottom trap and can be derived by exponential interpolation from the measured fluxes which are defined in the center points of the tube-type traps (Ellis et al., 2009). Small interpolation errors may occur to determine the transport of sand in the unmeasured layers between the tube-type traps. The overall error of the total transport is estimated to be less than 15%. To get a better understanding of the accuracy of the new LVRS-trap sampler, the measured data of the LVRS trap sampler are compared to those of other trap sampler which can measure the transport of sliding, rolling and saltating particles, see **Figure 3.3.2**. Fairly good agreement can be observed. No systematic sampling errors seem to be present.

Various other trap-type samplers are available (Poortinga et al., 2013). The original Wilson and Cooke trap consists of a bottle containing an inlet and outlet, whereby the trapped sediment is deposited in the bottle. In later studies, these bottles were mounted on a pole equipped with a sail to ensure that the inlet was always directed towards the wind. This extended setup is called the Modified Wilson and Cooke (MWAC) trap. The MWAC-traps showed good performance in a wind tunnel study (Poortinga et al. 2013). The MWAC- trap may be problematic to use at coastal beaches in strong winds with rain and salt sprays leading to blocking/clogging of the small intake openings (De Grande and De Moor, 2019). Bottles/traps close to beach surface may easily generate small scour holes and can therefore not be used close to the sand surface, where most of the sand is moving.

The number of sand particles moving along the sand surface can be detected by using a saltiphone. A saltiphone is a commercially available sampler which consists of a microphone installed in a stainless-steel tube mounted on a ball bearing. Sand particles that hit the microphone produce a high-frequency signal. Frequencies of about 8 Khz are amplified and used to determine saltation whereas other frequencies that are caused by rain and wind are reduced using a narrow band filter. Two output signals are provided: a digital pulse and an analogue voltage. The digital signal gives an output that is translated into number of counts. The analogue output signal also provides this information but has the additional option of measuring the intensity of particle impacts because it measures the energy of impact on the membrane. In this mode, the output signal represents the kinetic energy of the particles, and thus particle size and speed. Calibration is required to relate the output variables to sand transport rates. Calibration problems are the accuracy of input reference conditions (other trap-type sampler co-located beside the sensor), the saturation effects, the sensitivity of each microphone affecting the acoustic signal

and the cleanliness of the output signal (noise ratio). A similar type of sensor is the piezo-electric sensor which generates an electric pulse when a saltating particle hits the piezoelectric element. Laser-based systems use a laser beam and photo sensors to detect sediment particles crossing the laser beam.

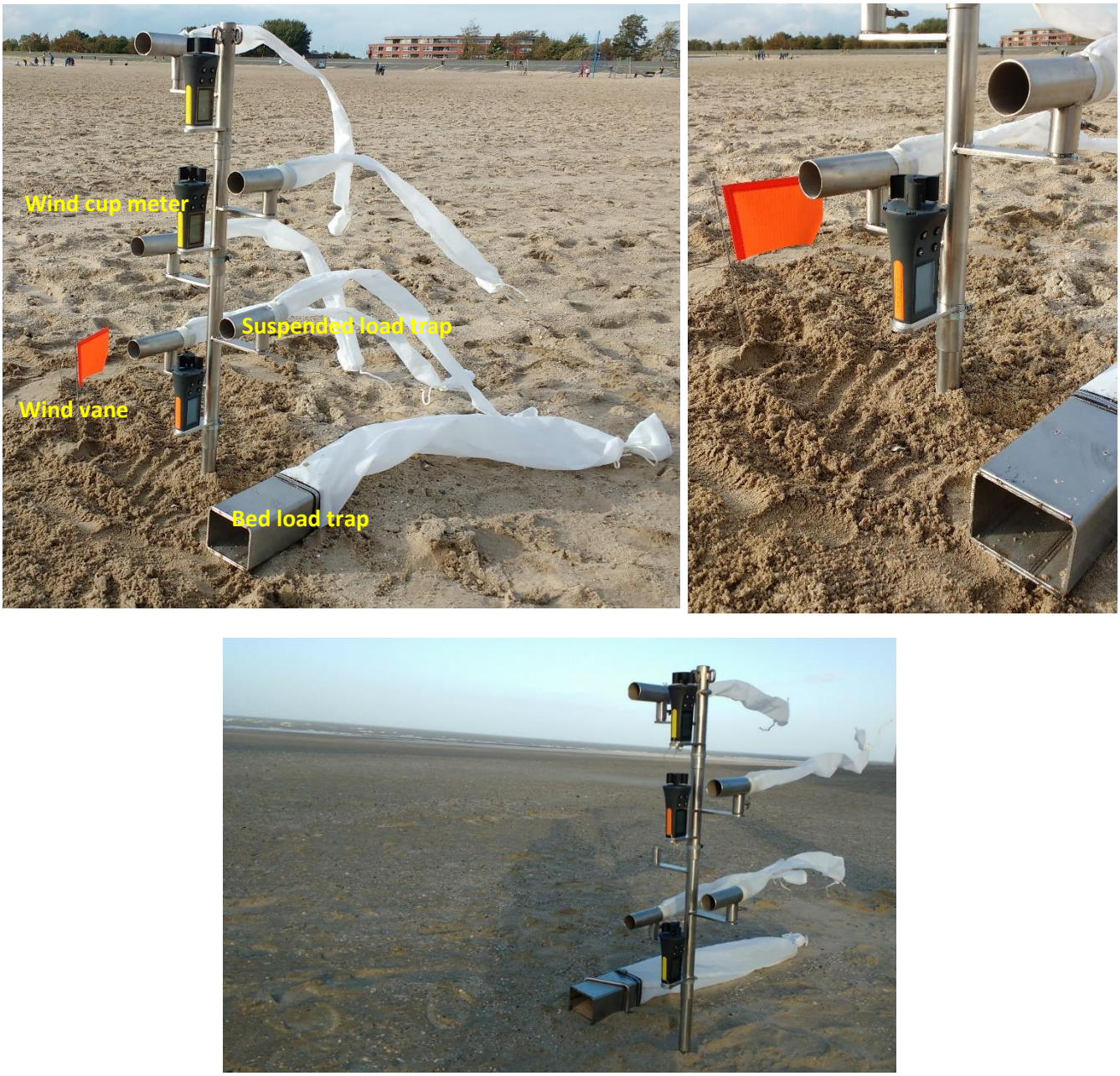

Figure 3.3.1 *LVR-sampler: mechanical trap instrument for sliding, rolling, saltating and suspended sand particles (upper: Lemmer beach Holland; lower: Zeebrugge beach, Belgium)*

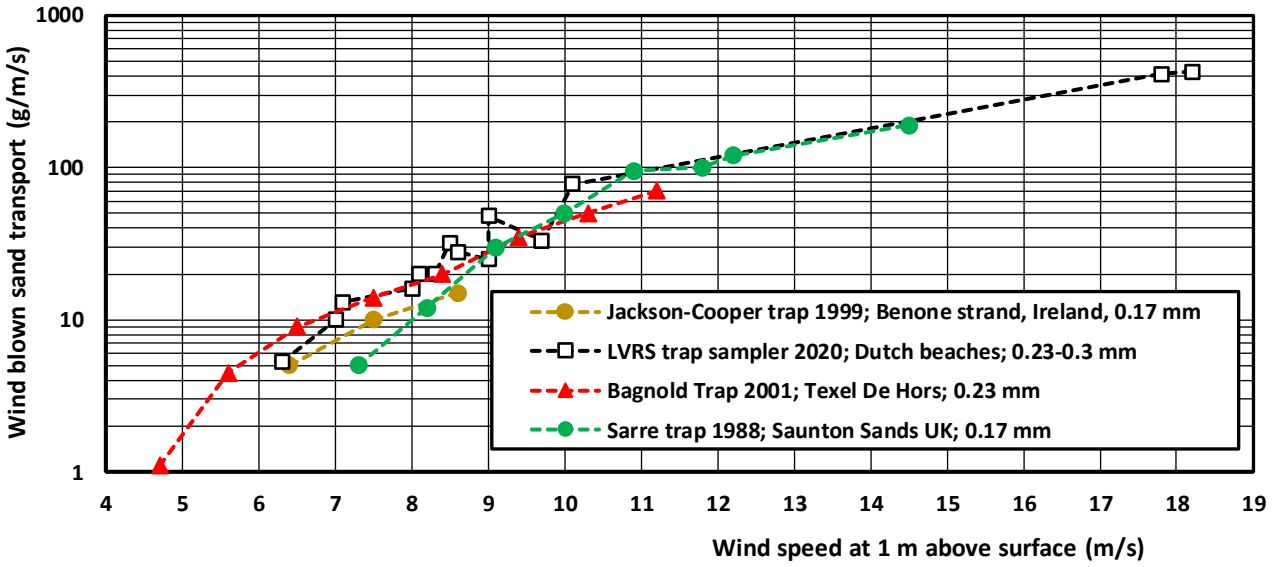

Figure 3.3.2 *Comparison of transport rates measured by LVRS-trap sampler and other trap samplers*

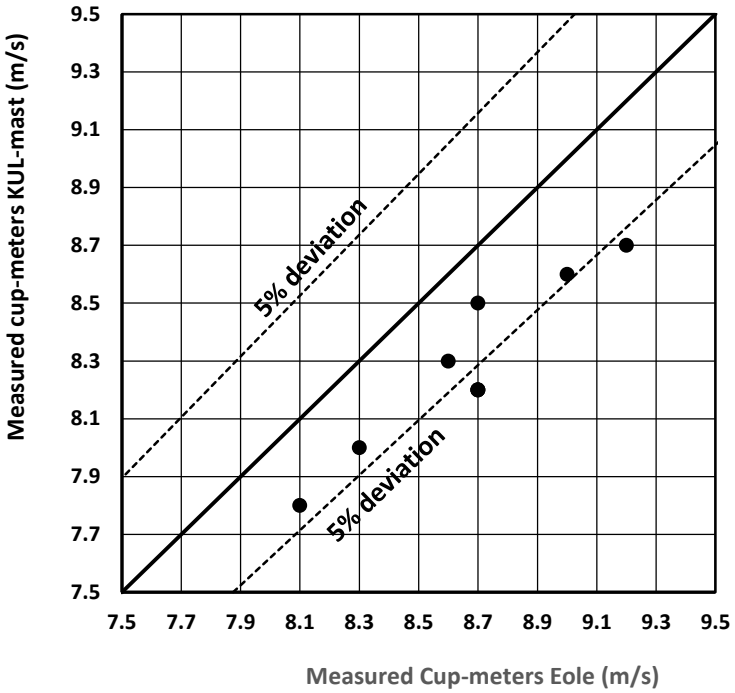

Figure 3.3.3 *Comparison of measured wind velocities of wind-cup meters at height of 1.2 m above surface, PH-site, Texel, The Netherlands (March-April 2020)*

4. Effect of moisture content on aeolian transport

4.1 Processes and definitions

Rainfall and related moisture content of the upper layer of sand has a strong effect on the mobility and transport of beach sand. Wind tunnel experiments with dry and moist sand (up to 8%) show that wind blown sand transport is strongly reduced with a factor of 2 to 10 for wind velocities in the range of 10 to 20 m/s (Hotta, 1984). Moisture contents up to 8% had much less effect (< factor 2) for high wind velocities in the range of 20 to 30 m/s.
The reduction of sand transport in moist sand conditions is related to cohesion and adhesion effects between particles resulting in an increase of the surface resistance against erosion (threshold shear velocity). Cohesion and adhesion effects may result from the presence of moisture, salt, algae, clay, organic matter and calcareous materials. Even low levels of moisture may effectively reduce the transport rate of dry sand. However, intensive rainfall may also increase the sand transport rate by splash effects promoting saltation processes. Moisture content (w) may be the direct result of precipitation, water spray, wave uprush near the water line or capillary action (adhesive forces; surface tension forces).

Moisture fraction is generally defined as: w= mass water of sample/mass dry sand of sample (moisture content is moisture fraction x 100%). Moisture content of a saturated sample can be computed by the expression $w_{saturated}=[\varepsilon/(1-\varepsilon)][\rho/\rho_s]x100\%$ with ε= porosity factor (0.35-0.45 for sand); ρ= water density ($\cong$1000 kg/m³); ρ_s= sand density ($\cong$2650 kg/m³), yielding $w_{saturated}$= 20%-30%. Generally, moisture contents are in the range of 0 to 10%, as the pores are not fully saturated with water.
Let us assume that a sand particle with diameter D is covered by a thin water film with thickness δ except at the particle contact points; any other pore water is absent.
The volume of the water film is: $V_{wf} = 1.33\pi\ [(0.5D+\delta)^3-(0.5D)^3]$ and the mass is: $M_{wf}=\rho V_{wf}$.
The volume of the sand particle is: $V_{sand}=1.33\pi(0.5D)^3$ and the mass is $M_{sand}=\rho_s V_{sand}$.
The mass ratio of water and dry sand defined as the moisture fraction is:
$w= M_{wf}/M_{sand}= \rho[(0.5D+\delta)^3-(0.5D)^3]/[\rho_s(0.5D)^3]$.
Using: D=200 μm for sand, δ=0.01D=2 μm, it follows that: $w \cong 0.025$ (2.5%).
Thus, a thin water film with thickness equal to 2 μm surrounding a sand particle of 200 μm yields a moisture content of about 2.5%. A water film of 1 μm yields a moisture content of 1%. Dry sand has a moisture content < 0.25% (Han et al., 2011). In conditions with a moisture content > 2.5%, the sand transport rate is strongly reduced to a very small value. In conditions with w=10% (near the water line), the surface is so saturated that aeolian transport reduces to almost zero even under very strong winds.

Moist beach surfaces can be differentiated based on the darkness of the surface. Dark surfaces have higher moisture contents, whereas brighter (lighter) surfaces have lower moisture contents. Using this approach, a quick estimate of the percentage moist and dry areas of a particular beach zone can be obtained. The precise moisture content can be simply determined by taking samples from the upper layer of the beach surface (drying and weighing). The sampling depth should be of the order of the dominant transport layer thickness. Visual observations from aeolian transport studies reveal that the thickness of the mobile transport layer is of the order of a few millimeters (Ho, 2012). Mechanical sampling of thin layers of sand is tedious and laborious, both in laboratory and field conditions. Furthermore, the moisture content after rainfall can be highly variable, spatially due to topographic variations (bed forms, cusps, runnels, depressions) and temporally due to solar radiation and wind evaporation. The mid and upper beach areas tend to be the driest areas. Moisture content is relatively high in areas with plant vegetation at the base of the foredune and in areas sheltered form direct solar radiation. To deal with spatial and temporal variability, the moisture content should be determined at many locations in a relatively short period of time. In practice, a method based on taking samples for analysis in the laboratory

(drying end weighing) is not very suitable to cover a wide grid of sampling points in the upwind area of the location where the aeolian transport is studied. A better solution is to use an electronic probe based on measuring conductivity of the sand between pins inserted in the upper sand layer (Atherton et al., 2001; Yang and Davidson-Arnott, 2005). Most probes consist of four stainless steel pins that are inserted into the sand. The difference in impedance/conductivity between the pins and the sand results in a reflection of this signal. The output is a moisture content value which is representative for the sand layer with a thickness equal to the pin length inserted in the sand bed. Accurate determination of the moisture content requires probe-calibration by using in-situ samples. Yang and Davidson-Arnott (2005) have found that a pin insertion length smaller than 20 mm including the calibration procedure taking thin sand samples, reduces the precision and accuracy of the probe substantially. Therefore, a pin length of 20 mm is proposed as the best compromise between accuracy and small layer thickness. However, it should be realized that the moisture content of the most upper mobile sand layer with thickness of a few millimeters is less than that of a layer of 20 mm. This practical field approach focusing on the moisture content of the upper 20 mm is still useful if the threshold shear velocity of the sand can be related to the moisture content of the upper 20 mm.

So far, various laboratory experiments have been done in which the threshold velocity is related to the moisture content of the upper 2 to 5 mm of the sands surface (Chepil, 1956; Belly 1965; Hotta et al., 1984; Saleh and Fryrear, 1995; Cornelis and Gabriels 2003; McKenna and Neuman, 2008; Han et al. 2011). McKenna and Neuman stuied the effect of humidity on wind-driven and transport in a laboratory flume. Relative humidity was varied between 15% and 80% and the critical shear velocity increased from 0.26 to 0.3 m/s for 0.125 mm sand and from 0.31 to 0.34 m/s for 0.21 mm sand.

The relationships between the threshold shear velocity and the moisture content of the upper 2 to 5 mm as found in wind tunnel studies cannot really be used for field conditions as it is problematic to measure the moisture content of the upper 2 to 5 mm at many locations within a short time period. Very few field studies on the (time dependent) effect of moisture on sand transport have done. Horikawa et al. (1982) found that sediment drying occurred much more slowly in the laboratory than in the field. Jackson and Nordstrom (1997) made an attempt to study the importance of time-dependent moisture effects in the field. Their results show that the mass flux is affected by temporal variations in moisture content. Wiggs et al. (2004) found that moisture contents in the range of 1% up to 3% have a minor effect on the mass flux of sand for wind speeds of about 9 m/s at 0.3 m above the surface. Van Dijk et al. (1996) have found that sand transport is reduced significantly immediately after the end of a rainfall event due to the higher resistance of the wet surface against entrainment of sand particles although the wind velocity is still the same. The saltation process of dry sand particles continues over the wet spots (Van Dijk et al., 1996; Davidson-Arnott et al. 2008). Davidson-Arnott et al. (2008) report an increase of the threshold wind speed and shear velocity of only 20% for 0.26 mm-sand in the case of an increase of the moisture content from 1 to 4% in field conditions. Udo et al. (2008) found an increase of a factor of 2 for 0.18 mm-sand in the case of an increase of the moisture content from 0 to 10%. The field results show a large discrepancy compared to those for wind tunnel conditions. Most likely, this is caused by the thickness of the top layer in which the moisture content is measured. The field data are valid for a top layer with a thickness of about 20 mm, whereas the laboratory data refer to the topmost layer of 1 to 5 mm. The moisture content of the thin top layer of 1 to 5 mm in field conditions will be much lower than the average value over a layer of 20 mm. The field experiments (Davidson-Arnott, 2008) also show that the moisture content at a certain location and thus the critical shear velocity can change rapidly over a period of minutes to hours due to drainage and/or drying by wind and sun. Large variations of the critical wind speeds were observed: $u_{w,min}$= 5 m/s (lowest wind speed with sediment transport) and $u_{w,max}$= 9 m/s (highest wind speed without sediment transport) mainly due to variations of the moisture content. Davidson-Arnott et al. (2008) have also found that the transport above a flat, hardpacked (damp) surface can be relatively high if there is a drier surface upwind of the damp surface. Based on this, the wind-driven sediment transport is highly variable in space and usually intermittent in time, depending on moisture conditions.

4.2 Moisture variations during drying of beach sand

4.2.1 Drying processes

Rainfall water penetrates into the beach sand and disappears through percolation and evaporation. The percolation rate of water in sand is about 0.01 to 0.1 mm/s or about 100 to 1000 mm/day. Most water disappears to deeper layers by percolation effects, because the percolation rate is much higher than the evaporation rate, which is about 1 mm/day in winter to about 8 mm/day in the summer for wind speeds between 3 and 15 m/s (see **Figure 4.2.1**) based on the formulae given by Lin (2001; see tool on www.lenntech.nl). The evaporation rate depends on the humidity, the temperature and the wind speed. The evaporation rate decreases for higher humidity values.

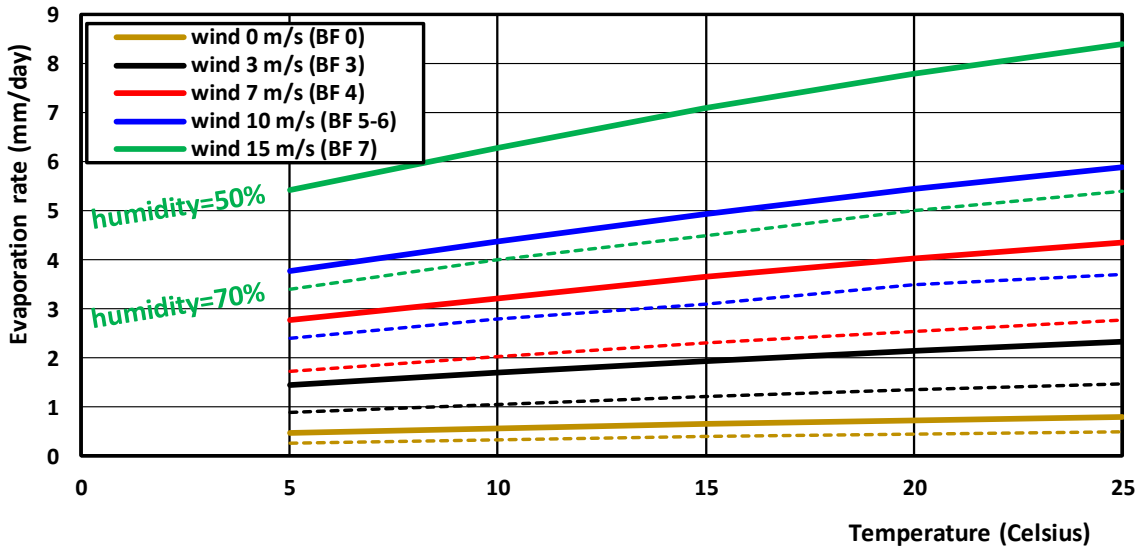

Figure 4.2.1 *Evaporation rate as function of temperature and wind velocity (solid= humidity=50%; dashed=70%)*

The beach sand layer above the ground water table consists of three sublayers: i) lower layer with capilar-type water, ii) middle layer with funicular-type water and iii) upper layer with pendular-type or hanging-type water ter due to adhesive effects. The moisture content in the upper layer with hanging water strongly depends on the rainfall intensity and the percolation rate of water in sandy soil. If the rainfall intensity is greater than the percolation rate, the upper sand layer will be become fully saturated with water. However, the rainfall intensity (0.0004 to 0.001 mm/s) at most beaches is much smaller than the percolation rate (0.01 to 0.1 mm/s) resulting in hanging-water conditions in the upper beach layer.

The maximum moisture content in the upper layer with hanging-water conditions is about 15%. This latter value can easily be determined by an experiment with a layer of beach sand (thickness= 20 mm; d_{50}= 0.38 mm) placed in a tray with perforated bottom plate and soaked with water. After a few minutes, the excess water is drained off through the perforated bottom plate and the moisture content be found by weighing and drying resulting in moisture values of about 15%. In practice, the moisture content in the upper layer of 20 mm during and immediately after rainfall is found to be much lower with values of about 8% during during normal rainfall intensity values based on field tests (**Table 4.2.1**). The amount of water in a layer of sand can be converted to an

equivalent layer thickness of water by the equation: δ_{water}= (w/100) [(1-ε)(ρ_s/ρ_w)]δ_{sand} with ε=porosity of sand, w= moisture content (%), ρ_s=density of sand, ρ_w =density of water, δ_{sand} =thickness of sand layer. Using: ε=0.4, w=8%, δ_{sand} =20 mm it follows that δ_{water}≅2.6 mm. To reduce the moisture content from 8% to 2%, an equivalent water layer of about 2 mm has to be removed. Given an evaporation rate of 1 mm/day in winter (**Figure 4.2.1**), it will take about 2 days (48 hours) to bring the moisture content below 2% in winter. In summertime with a light breeze the evaporation rate is about 4 mm/day (**Figure 4.2.1**) resulting in a drying time of about half a day (12 hours).

Field and laboratory experiments with moist sand layers have been done to determine the drying time of moist sand, which is herein defined as the time period after rainfall to get a moisture content below 2 %. Based on field observations, the sand surface of the beach is almost dry (moisture content below 0.5%) with loose particles if the moisture content of the upper 20 mm is below 2%.

4.2.2 Laboratory experiments

The new laboratory tests consisted of the wetting and drying of a tray (diameter of 150 mm) filled with beach sand (Schokkerhaven d_{50}= 0.35 mm, d_{90}=0.7 mm; thickness of 20 mm). The sand in the tray was wetted using a simple plant sprayer and the moist sand was mixed to get a uniform moisture content. The tray had a perforated bottom to allow water to drain vertically downwards onto a dry towel. The initial moisture content was about 8% to 9%. This range of moisture contents was mostly observed at field sites immediately after rainfall. The tray was weighed regularly to observe the drying process at temperatures in the range of 5 to 25 °C. During some tests, the drying process was speed up by placing a ventilator upwind of the tray simulating a light breeze (measured wind velocity of 2.7 to 4.5 at 2 cm above the tray; BF 3 to BF 4).

Figure 4.2.2A shows the decrease of the moisture content of the upper 5 and 20 mm as function of time for the laboratory experiments. **Figure 4.2.2B** shows the same results for a layer of 20 mm only.

If no wind is present, the drying process at room temperature proceeds rather slow. The drying of beach sand from w_{20mm}=16% to below 2% takes about 100 hours for a layer of 20 mm thick and a temperature of 15 to 17 °C. When the initial moisture content is 8%, the drying time to below 2% is about 30 hours in conditions without wind and a temperature of 20 to 25 °C, about 55 hours for a temperature of 15 to 17 °C and about 120 hours for a temperature of 5 to 10 °C. The drying during the night-hours is somewhat less than during the day-hours. When a light wind of BF 3 is present, the drying time reduces substantially to about 5 hours (temperature 20 to 25 °C), 10 hours (15 to 17 °C) and 45 hours (5 to 10 °C).
The moisture content of the upper 5 mm of this layer of 20 mm is about 30% to 50% lower. During the final phase of the drying process with moisture content values below 4% (layer of 20 mm), dry spots are become visible at the sand surface. Many dry spots are visible with moisture content values below 2%. A marked feature during the drying process is the presence of a thin crusty top layer (1 mm thick), which may be formed due to presence of calcareous materials (shell fragments) and very fine cohesive sediments. This crust layer remains present during most of the drying process and significantly reduces the mobility of the sand particles.

When the initial moisture content is 8%, the drying time to below 2% is about 55 hours in conditions without wind and a temperature of 15 to 17 °C. Based on **Figure 4.2.1**, the evaporation rate is about 0.7 mm/day (temperature=17 C, humidity of about 50%) for no wind conditions resulting in a drying time of 2 mm/(0.7 mm/day) ≅ 3 days (72 hours) which is about 25% higher than the observed value of 55 hours. Hence, the values of **Figure 4.2.1** may be somewhat conservative. During the drying process, various small and isolated spots with

a relatively low moisture content were visible (lighter yellow color) at the sand surface. The grains at these spots could easily be set in motion by blowing gently over the sand surface.

The drying time was much smaller in the presence of a slight wind (4.5 m/s at 2 m above surface; BF3) produced by a ventilator. The drying time to bring the moisture content from w_{20mm}= 8% to below 2% was about 10 hours for layer of 20 mm (temperature 15 to 17 °C). The drying time of the upper layer of 5 mm was about 10% to 30% lower in the initial phase of the drying process, and about 50% lower in the final phase of the drying process. The moisture content of the upper 5 mm was about 1% (almost dry with loose mobile particles), whereas that of the 20 mm layer was about 2% (see green curve with open circles; **Figure 4.2.2A**). Based on **Figure 4.2.1**, the evaporation rate is about 3 mm/day for a temperature of 17 C (humidity=50%) and a wind speed of 4.5 m/s resulting in a drying time of 2 mm/(3 mm/day)=2/3 day (16 hours), which is somewhat higher than the observed value of 10 hours.
The observed drying time of a 20 mm sand layer was much higher (about 37±8 hours) for a low temperature of 5 to 10 C (winter conditions) and light wind speed of 4.5 m/s. The evaporation rate based on **Figure 4.2.1** is about 1.5 mm/day (temperature= 7 °C, humidity=70%; wind 4.5 m/s) resulting in a drying time of 2 mm/(1.5 mm/day)= 1.33 days or 32 hours which is somewhat smaller (15%) than the observed value of 37 hours.

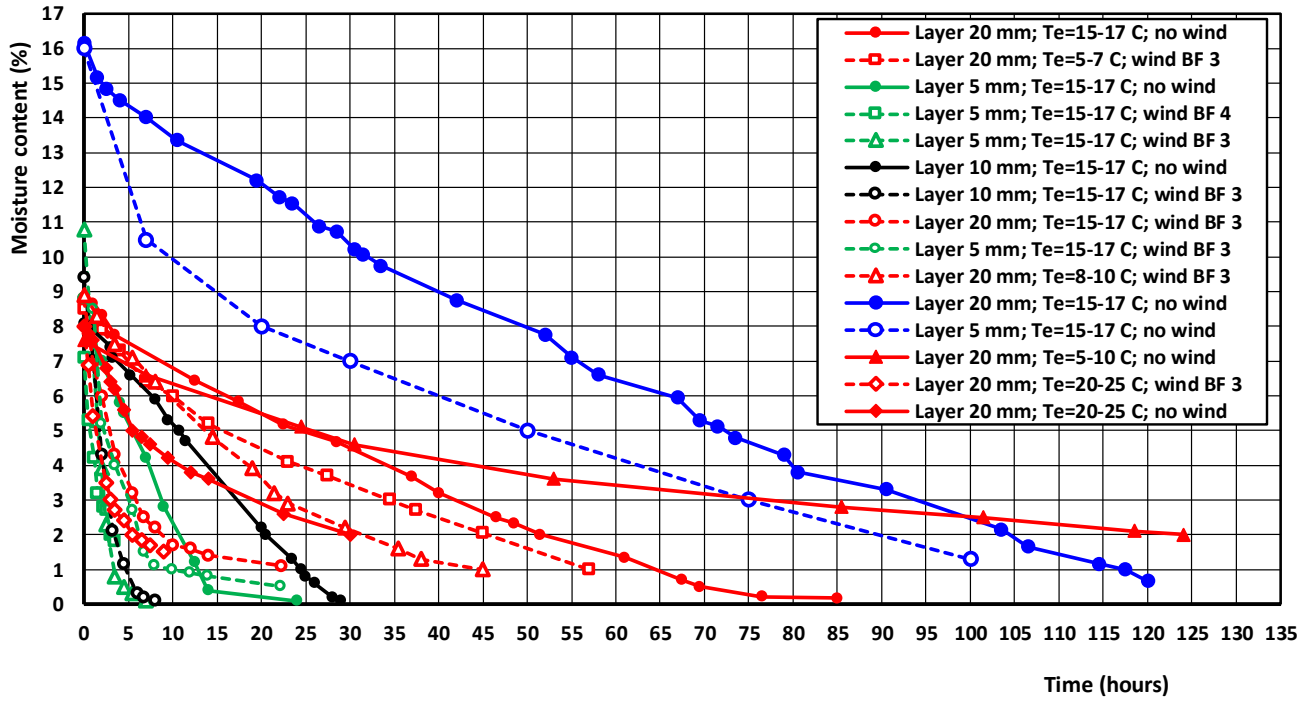

Figure 4.2.2A *Moisture content of drying beach sand (d_{50}=0.35 mm) as function of time in laboratory; initial moisture content of 8%-16%; layers 5 and 20 mm; no wind and light wind (4.5-7.2 m/s at 2 m)*

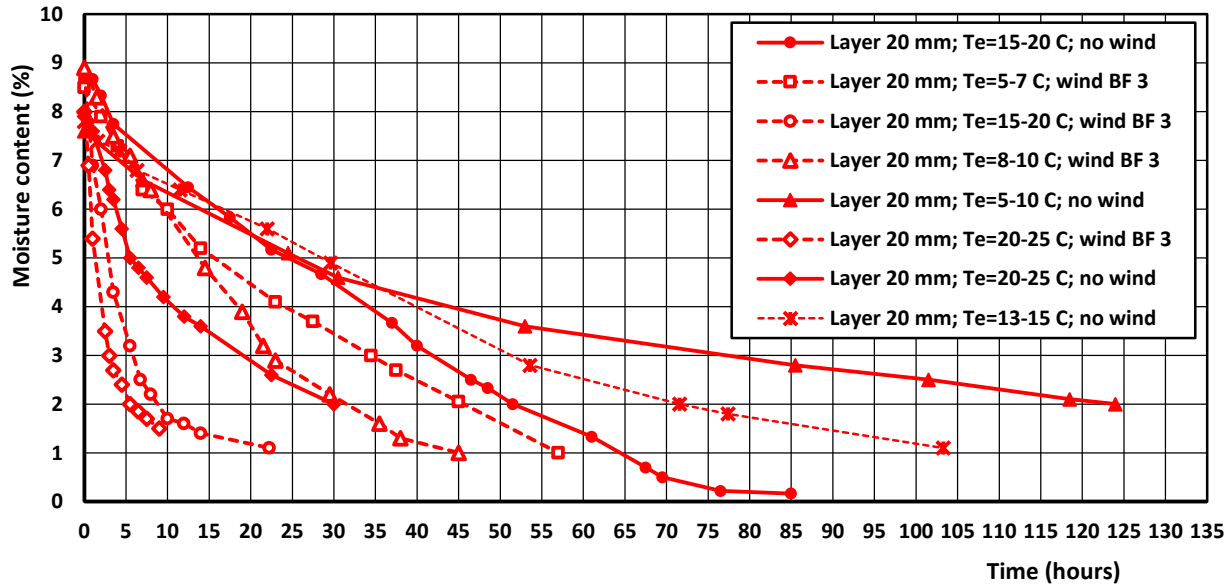

Figure 4.2.2B *Moisture content of drying beach sand (d_{50}=0.38 mm) as function of time in laboratory; initial moisture content of 8%; layer 20 mm; no wind and light wind (4.5-7.2 m/s at 2 m)*

4.2.3 Field observations

The field tests consisted of the sampling and drying of beach sand (from various beaches in The Netherlands and Belgium, see **Table 4.2.1**. Sand layers with a thickness of 5 mm and 20 mm were scraped from the sand surface at the end of a period with rainfall and at various times during the drying process. The moisture content of the samples was determined by drying (in an oven at temperature of 150 °C) and weighing of the dry samples.
Long-continued rainfall (4 hours of more) will lead a relatively thick layer of moist sand (20 to 50 mm), but short-duration rainfall of maximum 1 hour only yields a thin layer of moist sand (5 mm) on top of dry sand, as shown in **Figure 4.2.3**. A long period of dry weather (days) at the beach of Callantsoog (Netherlands) in February 2020 had resulted in a dry sand layer with thickness of about 10 to 15 mm. Immediately after rainfall (duration about 1 hour), the moist content of the top layer of 5 mm was about 9.5 %. The moisture content of the upper 20 mm was about 3.5% at about 50 m from the waterline and about 8% at 5 m from the waterline. No wind-induced sand transport was observed at wind velocity of about 6 m/s at z=1.1 m above the surface (Beaufort 4).

Figure 4.2.3 *Beach surface immediately after rainfall in winter; 8 Feb. 2020; Callantsoog, Netherlands*
Left: vertical cut with moist top layer of 5 mm and dry layer of 10 to 15 mm;
Right: moist layer is removed with spade showing dry sand surface beneath

Date	Location and weather	Sand d_{50}, d_{90} (mm)	Surface features (m)	Temperature (C) and Moisture content (%)	Percentage shell (%)	Wind velocity (m/s) at height z (m)	Shear velocity (m/s) and bed roughness (m)	Sand transport
19 Oct 2019	Lemmer beach (b=100 m); dry sunny	0.3; 0.9	0.01-0.05 (ir)	17; 5% in upper layer of 5 mm; 6% in upper layer of 20 mm (7 dayhours a.r.)	<3%	BF 2-3 z=0.3; u=3.6 z=0.64; u=3.9 z=0.86; u=4.4	u_*=0.28; k_s=0.052	none; loose surface particles
1 Feb. 2020	Lemmer beach (b=100 m); dry	0.3; 0.9	0.01-0.05 (ir)	9; 5.1 % in layer of 20 mm; 10 dayhours after rain	<3%	BF 5 z=0.2; u=4.8 z=0.5; u=5.6 z=1.0; u=6.6	u_*=0.45; ks=0.08	none; wet surface (crust)
26 Oct 2019	Schokkerhaven beach (b=15 m); dry	0.34; 0.7	5-50 mm	15; 1.5% in upper layer of 5 mm; 1.7% in layer of 20 mm (30 hrs a.r.)	<3%	BF 3-4 z=0.3; u=4.0 z=0.75; u=4.9 z=1.5; u=5.3	u_*=0.28; k_s=0.02	none; loose surface particles
3 Nov 2019	Schokkerhaven beach (b=15 m) rainy weather	0.34; 0.7	5-50 mm	15; 8.6% in upper layer of 5 mm and 7% in upper layer of 20 mm (during rainfall)	<3%	BF 3 n.m.	n.m	none
4 Nov. 2019	Schokkerhaven beach (b=15 m) at t=9 hrs; dry	0.34; 0.7	5-50 mm	10; 3% in upper layer of 5 mm; 4% in upper layer of 20 mm (10 night-hrs a.r.)	<3%	BF 3 n.m.	n.m	none
4 Nov. 2019	Schokkerhaven beach (b=15 m) at t=17 hrs; rainy	0.34; 0.7	5-50 mm	10; 7.8% in upper layer of 5 mm; 6.7% in upper layer of 20 mm (during rainfall)	<3%	BF 3 n.m.	n.m	none
5 Nov. 2019	Schokkerhaven beach (b=15 m) at t=17 hrs; dry	0.34; 0.7	5-50 mm	10; 4.4% in upper layer of 5 mm 5.2% in upper layer 20 mm (10 dayhrs a.r.)	<3%	BF 2 n.m.	n.m	none; surface layer very firm
7 Nov. 2019	Schokkerhaven beach (b=15 m) at t=17 hrs; rain	0.34; 0.7	5-50 mm	10; 8.1% in upper layer of 5 mm; 7.5% in upper layer 20 mm (during rainfall)	<3%	BF 4 n.m.	n.m	none; surface layer very firm
8 Nov. 2019	Schokkerhaven beach (b=15 m) at t=15 hrs; dry and sunny	0.34; 0.7	5-50 mm	10; 1.7% in upper layer of 5 mm; 3% in upper layer 20 mm (20 hrs a.r.; 13 night-hrs; 7 day-hrs)	<3%	BF 3 n.m.	n.m	none; loose surface particles
7 Dec 2019	Zeebrugge beach (b=100 m) at t=15 hrs; dry and sunny	0.2; 0.4	1-30 mm	10; 4.3% in upper layer of 5 mm; 4.7% in upper layer of 20 mm (6 hrs a.r.)	<5%	BF 6		

ir= irregular due to ripples and/or foot steps; BF=Beaufort scale; a.r.=after rainfall; ab=above bed surface, b= beach width; z=height above sand surface; u= wind velocity at height z above surface

Table 4.2.1A *Drying time of field samples*

Date	Location and weather	Sand d_{50}, d_{90} (mm)	Surface features (m)	Temperature (C) and Moisture content (%)	Percentage shell (%)	Wind velocity (m/s) at height z (m)	Shear velocity (m/s) and bed roughness (m)	Sand transport
11 Feb 2020	Callantsoog beach dry	0.23; 0.5		Te= 5 C layer 20 mm time=- 0,6,10,12 hrs mc=8%, 3.5%; 2.1%, 1.8%	<3%	BF 7-8		
15 July 2020	Callantsoog beach dry	0.23; 0.5		Te=20-22 C layer 20 mm time= 0, 1, 2, 3, 4, 5, 6 ,8 hrs mc=8.5%, 7%; 5.8%, 4.7%, 3.5%, 2.6%, 1.8%, 1.2 %	<3%	BF2		none
6 Aug 2020	Callantsoog beach dry	0.23; 0.5		Te=28-30 C layer 20 mm time= 0, 0.5, 1.0, 1.5, 2.25, 3.25, 4.25, 6.75 hrs mc=8%, 7.2%; 6.2%, 5.2%, 3.8%, 2.7%, 1.8%, 0.6 %	<3%	BF2		none

Table 4.2.1B *Drying time of field samples*

Field data results of the drying of beach sand are shown in **Figure 4.2.4** and can be described as follows:

- during and immediately after rainfall, the moisture content of the top layer of 5 mm is higher than that of a layer of 20 mm;
- after rainfall during the drying process, the moisture content of the upper layer of 5 mm is about 15% to 30% lower than that of the layer of 20 mm and
- the total drying time of the upper 20 mm to bring the moisture content below 2% is of the order of about 30 hours in field conditions with moderate winds (< 4 to 5 m/s) and temperature of 5 to 10 ^{o}C (autumn period).

The drying proceeds much faster in strong winds. At the beach of Callantsoog in February 2020 with temperature of 5^{o} C and a storm wind of BF7, the moisture content of the top layer of 20 mm reduced from about 8% to 3.5 % in about 6 hours. The sand at the dune top where the wind was stronger (BF8) was dry after 6 hours. The laboratory test with the same initial moisture content, but much lower wind conditions produced a much larger drying time of about 40 hours for a layer of 20 mm. Based on **Figure 4.2.1**, the evaporation rate is about 1 mm/day for a temperature of 7 ^{o}C, wind of 3 m/s and humidity of 70% giving a drying time of 2 mm/(1 mm/day)=2 days or 48 hours for a layer of 20 mm.
Field sites in early April 2020 with temperatures of 10 to 15 ^{o}C (beaches of Callantsoog; Schokkerhaven, Lemmer) had a completely dry top layer of about 30 mm after a period of 5 to 10 days without any rainfall. The subsoil below the top layer was still very moisty.
Hotta et al. (1984) report a drying time of 3 hours for the topmost layer of 3 mm after rainfall in the summer. Yang and Davidson-Arnott (2005) and Davidson-Arnott et al. (2008) measured the moisture content of beach sand (top layer of 20 mm; 0.26 mm sand) in the period mid-May to Mid-June 2002 at Greenwich Dunes, Prince Edward Island National Park, Canada using a Delta-T Theta probe. They found that the drying is greatest at the mid-beach area where the water table is more than 0.5 m below the sand surface; the reduction of moisture content from 5% to 2% was about 3.5 hours in summer conditions.

Wiggs et al. (2004) determined the moisture content of the upper 2 mm of the sand surface using a scraper and found a decrease from about 7% to about 5% over a period of 5 hours in conditions with a temperature of 15 °C and a gusty wind of BF4 in September 1998, which is in good agreement with the data of Callantsoog beach in The Netherlands (see **Figure 4.2.4**).

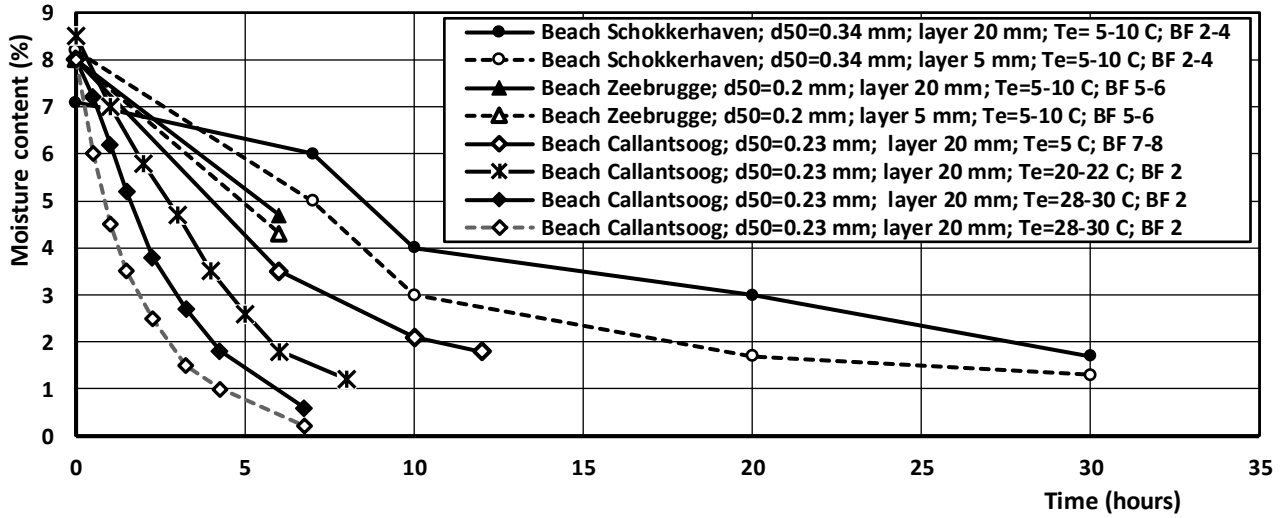

Figure 4.2.4 *Moisture content of drying beach sand as function of time in field conditions initial moisture content of 7% to 9% of upper 20 mm; light to hard winds (BF 2 to 6)*

4.2.4 Summary of results

Rapid measurement of the moisture content in field conditions requires the use of an electronic conductivity sensor focusing on a layer of at least 20 mm thick for reasons of accuracy (sensor pin length of 20 mm). The conductivity method is less accurate for thinner layers. Field data show that the moisture content of the top 20 mm-layer immediately after a rainfall event is about 8%. The moisture content gradually decreases during the drying process. The drying proceeds relatively rapid during windy conditions and high temperatures A remarkable feature of natural beaches is the simultaneous presence of moist and dry spots during the drying process in windy conditions. At the beach of Zeebrugge (Belgium), it was observed that about 60% of the surface was still wet (w_{20mm}=4.7%) and about 40% was already dry at about 6 hours after the last rainfall event. Dry mobile sand particles were observed to accumulate in local depressions of the beach surface. Measured sand transport was intense and close to the equilibrium values (Section 6). The percentage of dry spots will increase rapidly for increasing drying time. In the final phase of the drying process, the moisture content of the upper 20 mm is about 2% and the topmost 5 mm has a moisture content of about 1% giving a dry beach appearance with loose, mobile sand particles.

The drying process can be characterized by the time period ($T_{8\%-2\%}$) which is the required time to bring the moisture content of the topmost layer of 20 mm from 8% immediately after rain fall to below 2%. It is most practical to focus on the upper 20 mm, as the sampling of a layer of 20 mm at field sites is easy whereas the sampling/scraping of very thin layers (mm's) is problematic. Laboratory and field observations show that the beach surface is dry when the moisture content of the upper 20 mm is below 2%. **Figure 4.2.5** and **Table 4.2.2** show values of $T_{8\%-2\%}$ as function of the temperature and the wind velocity (defined at 1 m above the surface). Laboratory and field data are represented by the error bars. When wind is absent, the $T_{8\%-2\%}$-value is quite high: 120 hours for temperature in the range of 5-10 °C and 50 hours for 15 to 17 °C. When light winds are present (wind velocity=4 to 5 m/s), the $T_{8\%-2\%}$-value decreases to about 30 hours for a temperature of 5 to 10 °C (winter)

and to 10 hours for 15 to 17 °C (summer). The characteristic drying time during stronger winds (wind velocity > 5 m/s; BF 4) are assumed to be slightly less. The drying time was observed to be about 5 hours in conditions with BF 5 to 6 and temperature of about 17 °C (after 3 hours about 50% of the surface was dry).

Temperature/Wind force	**Drying time from moisture content of 8% to 4%; many dry spots are present for a moisture content of 4%; sand transport is slightly restricted**	**Drying time from moisture content of 8% to 2%; surface is almost dry; sand transport is not restricted for a moisture content of 2%**
Winter period 5-10 °C	50 hours (no wind) 10 hours (BF 2-3) 5 hours (BF 7-8)	120 hours (no wind) 30 hours (BF 2-3) 10 hours (BF 7-8)
Late Autumn period 10-15 °C	35 hours (no wind) 6 hours (BF 2-3)	75 hours (no wind) 20 hours (BF 2-3)
Late Spring period 15-20 °C	20 hours (no wind) 4 hours (BF 2-3)	60 hours (no wind) 10 hours (BF 2-3) 5 hours (BF 5-6)
Summer period 20-25 °C	12 hours (no wind) 3 hours (BF 2-3)	35 hours (no wind) 6 hours (BF 2-3)
Summer period 28-30 °C	6 hours (no wind) 2 hours (BF 2-3)	15 hours (no wind) 4 hours (BF 2-3)

Table 4.2.2 *Characteristic drying times for the top layer of 20 mm beach sand*

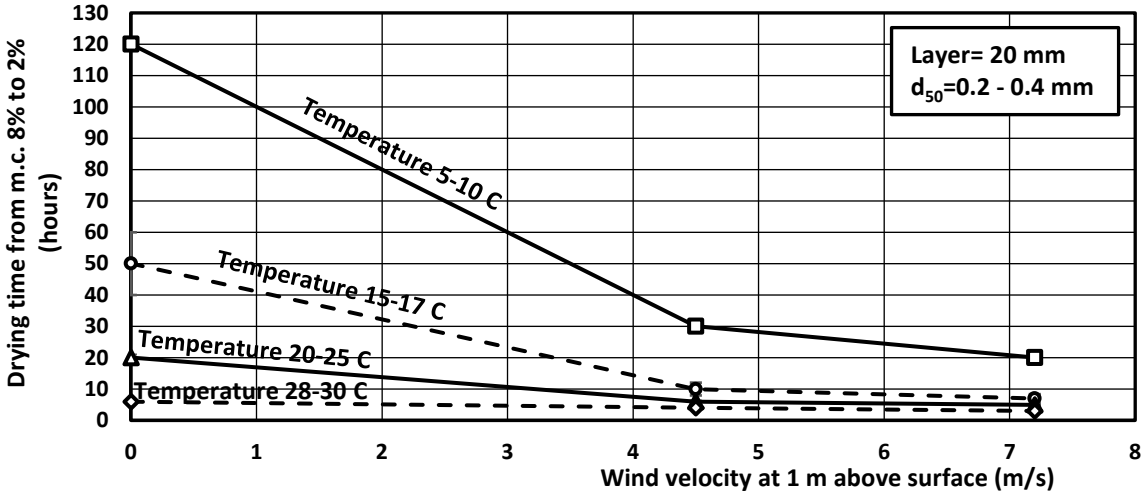

Figure 4.2.5 *Characteristic drying time of beach sand (layer 20 mm) with moisture content from 8% to 2%; Beach sand of 0.2 to 0.4 mm*

4.3 Effect of moisture content on threshold shear stress

4.3.1 Laboratory experiments

Various authors have studied the influence of moisture on the threshold shear velocity of sand particles by wind in wind tunnel conditions (Chepil, 1956; Belly, 1964; Hotta et al., 1984; Saleh and Fryrear, 1995; Cornelis and Gabriels, 2003 and Han et al., 2011) and in field conditions (Davidson-Arnott et al., 2005, 2008; Udo et al., 2008).

The effect of the moisture content on the threshold shear velocity is generally represented by: $u_{*,th,moist}=\alpha_w u_{*,th,B}$. The α_w-coefficient strongly depends on the moisture content and the layer thickness considered.

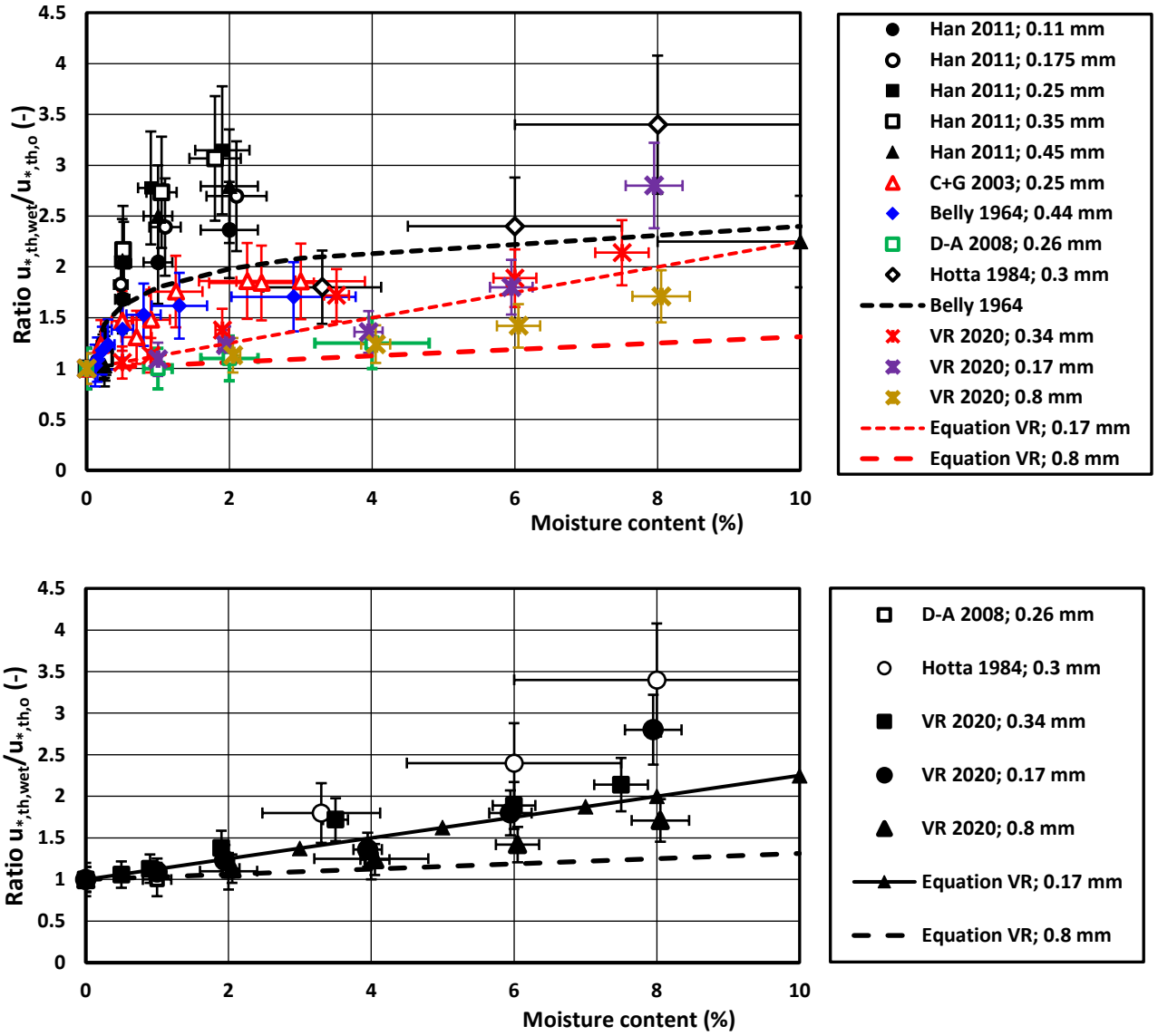

Figure 4.3.1 *Threshold shear velocity as function of particle diameter and moisture content; Old laboratory data (Han et al. 2011; Cornelis and Gabriels 2008; Belly 1964), New laboratory data of Van Rijn (this study) and field data (Davidson-Arnott et al. 2008; Hotta 1984)*

Available laboratory data of Belly (1964), Hotta et al. (1984), Cornelis and Gabriels (2003) and Han et al. (2011) are shown in **Figure 4.3.1**. The effect of moisture is negligibly small for moisture content < 0.25% (Han et al. 2011). The threshold shear velocity increases for increasing moisture content. The scatter and error ranges are relatively large, which is most likely caused by the different definitions and measuring method used by the various researchers. The wind tunnel data of Belly refer to the upper 1 mm of the surface, as he used a moist air flow. The wind tunnel data of Hotta et al. refer to a layer of 5 mm as samples with thickness of 5 mm were taken from the surface. The wind tunnel data of Cornelis and Gabriels and Han et al. refer to a layer of 1 to 3 mm. A basic problem is the rapid decrease of the moisture content due to the blowing wind, even for very short run

times (< 2 min, Cornelis and Gabriels, 2003). Belly proposed an expression relating the α_w-coefficient to the moisture content (of the upper 1 to 2 mm), see **Figure 4.3.1**. Other expressions are also proposed in the Literature. Most of these expressions are, however, not very practical as the moisture content of the upper few millimeters is required as input. Electronic sensors for rapid and detailed measurements over short spatial and temporal scales are available but accurate field measurements can only be done over a vertical distance of at least 20 mm, as shown by Davidson-Arnott et al. (2008). They report an increase of the threshold wind speed and shear velocity of only 20% for 0.26 mm-sand in the case of an increase of the moisture content from 1 to 4% (upper 20 mm) in field conditions, see **Figure 4.3.1**. Udo et al. (2008) found an increase of a factor of 2 for 0.18 mm-sand in the case of an increase of the moisture content from 0 to 10% (upper 20 mm).
The field results show a large discrepancy compared to those for wind tunnel conditions. Most likely, this is caused by the thickness of the top layer in which the moisture content is measured. The field data are valid for a top layer with a thickness of about 20 mm, whereas the laboratory data refer to the topmost layer of 1 to 5 mm. The moisture content of the thin top layer of 1 to 5 mm in field conditions will be much lower than the average value over a layer of 20 mm. The field experiments (Davidson-Arnott, 2008) also show that the moisture content at a certain location and thus the critical shear velocity can change rapidly over a period of minutes to hours due to drainage and/or drying by wind and sun. Large variations of the critical wind speeds were observed: $u_{w,min}$= 5 m/s (lowest wind speed with sediment transport) and $u_{w,max}$= 9 m/s (highest wind speed without sediment transport) mainly due to variations of the moisture content. Davidson-Arnott et al. (2008) have also found that the transport above a flat, hardpacked (damp) surface can be relatively high if there is a drier surface upwind of the damp surface. This was also found by Van Dijk et al. (1996). Thus, the wind-driven sediment transport is highly variable in space and usually intermittent in time, depending on moisture conditions. Delgado-Fernandez (2010, 2011) found that the moisture conditions of natural beaches can be crudely classified into three categories: a) dry with w_{20mm}<2% and a fully developed saltation system; b) medium with w_{20mm}=2 to 10% and restricted sand transport and c) wet with w_{20mm}>10% and sand transport is completely prevented.
De Vries et al. (2014) have found that the transition zone of about 30 m around the high tide line at a dutch beach (Sand Motor, South-Holland) in which the moisture content reduces from about 5% to 2% is an important source of sand for the gradual pickup (entrainment) of sand, as other supply-limiting factors (shells, vegetation) are absent in that zone.
Brakenhoff et al. (2019) have studied the moisture content in cross-shore direction from the low tide water line to the upper dry beach and developed a prediction model for the surface moisture content calibrated with data from a mesotidal beach in The Netherlands. The width of the intertidal beach was about 60 m. Their results show that the lower 30% of the intertidal beach is always saturated with water and w_{20mm}> 20%. Up to the high tide line, the moisture content reduces from 20% to 5% depending on the tidal stage; drying rates were found to be 50% in 2.5 hours. Above the high tide line, the moisture content decreased from about 5% at the high tide line to about 2% at about 30 m beyond the high tide line in conditions without rainfall. This latter zone is the transition zone to the dry beach, where the moisture content solely depends on precipitation (rainfall).

Additional laboratory experiments on the influence of moisture content on the threshold shear velocity have been done in a mini-wind tunnel (see Section 3), focussing on the moisture content of the upper 20 mm. Dry sand was mixed with tap water and a layer (20 mm) of wet sand was placed in the tray at the end of the mini wind tunnel. Three particle sizes (d_{50}=0.17, 0.34 and 0.8 mm) were used. The wind velocity was raised in steps until particle movement of grains was observed visually. Surface crust formation was observed in the tests with 0.17 mm-sand and 0.34 mm-sand. Individual sand particles and tiny sand balls of clustered particles (3 mm) were observed to be eroded from the crusted sand surface in these tests. Crust formation was not observed in the tests with 0.8 mm-sand; individual sand particles were observed to be rolling along the surface at threshold conditions. The measured data are given in **Table 4.3.1**. The shear velocities of Table 4.3.1 are based on Equation (3.1b) with α_{sw}=0.85. The ratio (α_w-coefficient) of the threshold value of moist sand and dry sand is shown in **Figure 4.3.1**. The α_w-values of 0.8 mm-sand are significantly smaller than those of 0.17 mm-sand. Crust formation

resulting in stronger adhesive/cohesive effects was clearly observed for 0.17 and 0.34 mm-sand but not for 0.8 mm-sand.
The data of the present wind tunnel tests and the field data of Davidson-Arnott (2008) can be reasonably well represented by the following expression:

$$\alpha_{w,20mm} = 1+0.1\,(d_{50,ref}/d_{50})\,w_{20mm} \qquad (4.1)$$

with: w_{20mm}= moisture content in upper 20 mm of surface, $d_{50,ref}$= median particle size of reference sand(0.25 mm), d_{50}=median particle size. Equation (4.1) yields higher values for finer sands as found in the present tunnel tests (crust formation effect). Equations (4.1) which is valid for the upper layer of 20 mm yields relatively small values compared to the laboratory data for thin layers (2 to 5 mm), see **Figure 4.3.1**. This can be partly understood by the vertical moisture variations. The moisture levels of the upper 2 to 5 mm are smaller than the moisture level of a layer of 20 mm, see **Figure 4.3.1**. The effect of the grain size on the $\alpha_{w,20mm}$-coefficient is a bit speculative, as not may data points are available. However, during field work on the wet intertidal beach of coarse sand on the island of Texel (Prins Hendrik sand beach) it was observed that the coarse sand grains were mobile during strong winds with BF7 in conditions with a moisture conte of about 7% to 11%.
Application of Equation (4.1) requires input data of the moisture content of the topmost 20 mm of the sand bed, either from measurements or from a prediction model for the moisture content.

Type of sand	**Moisture content in layer of 20 mm w_{20mm} (%)**	**Wind velocity at z_w=0.03m above sand surface at threshold conditions $u_{w,th,initiation}$ (m/s)**	**Bed-shear velocity at threshold conditions (α_{sw}=0.85; Eq. 3.1b) $u_{*,th,initiation}$ (m/s)**
Schokkerhaven beach; d_{50}=0.34 mm	7.5	14.5	0.68
	6.0	12.8	0.60
	3.5	11.5	0.55
	1.9	9.4	0.44
	0.9	7.7	0.36
	0.5	7.2	0.34
	0	6.8	0.32
Uniform sand (0.1-0.3 mm); d_{50}=0.17 mm	8	14.5	0.62
	6	9.4	0.40
	4	7.1	0.30
	2	6.2	0.27
	1	5.5	0.24
	0	5.2	0.22
Uniform sand (0.5-1 mm); d_{50}=0.8 mm	8	15.3	0.77
	6	12.8	0.64
	4	11.1	0.56
	2	10.2	0.51
	0	8.9	0.45

inaccuracy of moisture content= ±5%; inaccuracy of threshold wind velocity= ±10%;
inaccuracy of bed-shear velocity=±15%

Table 4.3.1 *Measured bed-shear velocity at threshold conditions (initiation of motion) in mini wind tunnel for dry and moist sand*

4.3.2 Field observations

During the field experiments at the beach of Callantsoog (NL), many observations of conditions with initiation of motion have been made. The basic data are given in **Section 6.3**. **Figure 4.3.2** shows a diagram which can be used to determine the wind speed at which sand transport is initiated for given moisture levels of the upper 20 mm of the beach surface. Initiation of movement of dry sand grains occurs at a critical wind speed (at 1 m above the sand surface) of about 5.7 to 6.3 m/s for grains of 0.2 to 0.3 mm. The critical wind speed increases significantly for increasing moisture levels. After a rainfall event the moisture content of the upper 20 mm is about 8% to 10%, which requires a wind speed of 12 m/s (BF7) to generate sand transport processes. The wind speed of the Beaufort scale is defined at a height of 10 m above the surface. The wind speed at 1 m above the surface is about 75% of that at a height at 10 m, assuming a logarithmic velocity distribution. Data of Svasek and Terwindt during a summer storm are shown. The data of Davidson-Arnott et al. (2008) represent the threshold range of sand transport with minimum and maximum wind speeds during which sand movement was observed by a saltiphone-sensor.
Equation (4.1) gives a very reasonable representation of the separation between transport and no transport. It should be realized that Equation (4.1) represents a hard transition between transport and no transport, whereas in reality a much more smooth transition will occur.

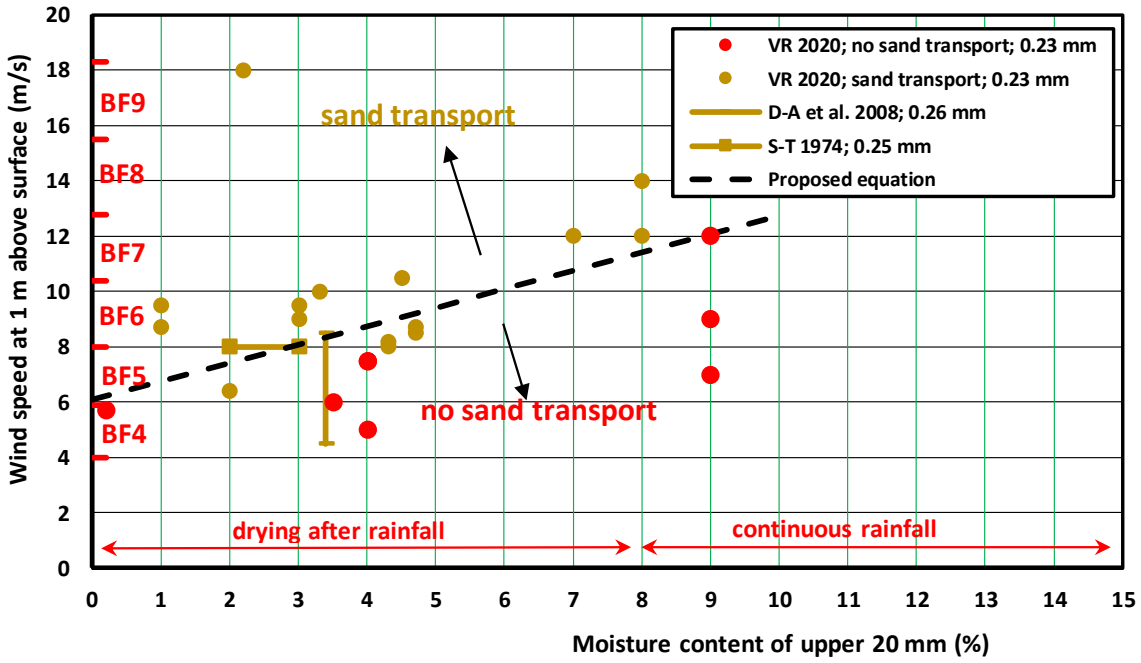

Figure 4.3.2 *Effect of moisture content and wind speed on initiation of sand transport*
VR=Van Rijn 2020 (this study); D-A=Davidson-Arnott et al. 2008; S-T= Svasek and Terwindt 1974
(BF is defined at height of 10 m above surface)

4.4 Effect of moisture content on sand transport

4.4.1 Field observations

Field experiments show that during rainfall events with strong winds the sand transport process is dominated by the sand blasting and splash-type processes. This latter mode of sand transport is reduced significantly immediately at the end of a rainfall event due to the higher resistance of the wet surface against entrainment of

sand particles although the wind velocity is still the same (Van Dijk et al., 1996). In the drying period after rainfall, both dry and wet spots are present at the beach surface. Particle entrainment is less at the wet spots than at the dry spots. However, the saltation process of dry sand particles continues over the wet spots (Van Dijk et al., 1996; Davidson-Arnott et al., 2008). This effect was also observed in the wind tunnel experiments of Van Dijk et al. (1996) consisting of wind flow of 9 m/s over trays (length=2.5 m, layer of 20 mm) filled with dry sand followed by trays (length=5 m) with wet sand. The different moisture values are in the range of 0 to 5%. Based on detailed measurements, various effects were observed:
a) entrainment of sand particles at moist surface by the dry incoming sand particles;
b) increase of saltation height over the hard, wet surface (higher particle jumps) and
c) strong decrease of the sand flux close to the hard surface due to reduced particle entrainment and
d) ongoing but slightly reduced sand transport over the hard surface (25% reduction of transport at end of hard section with mc-values > 4% compared to that at end of dry section).
The hard, wet sand surface functions as a transport plain for the saltating particles coming from the dry sand spots. Particle entrainment is reduced at the wet surface, but still significant. Splash-type transport is important during conditions with intensive rainfall (> 1 mm/hour), as shown by De Ploey (1980) for dune sand in Belgium. The annual dune changes were observed to occur mainly in a time period of 3 to 4 hours, particularly during rainy periods in autumn and winter with strong splash-type transport conditions.

Svasek and Terwindt (1974) measured sand transport by wind during 6 summer weeks on a Dutch beach Noordwijkerhout north of The Hague. The beach sand has d_{50} of about 0.25 mm. Wind velocities were measured in 9 points between 0.03 and 3 m above the sand surface. The effective roughness height (k_s) was found to be in the range of 0.3 and 1 mm based on the analysis of the measured velocity profiles. Sand transport was measured by using sand traps placed in the bed consisting of rectangular iron boxes (0.9x0.25x0.1 m) with the upper edge of the boxes being flush with the upwind sand surface. The minimum required fetch length was found be about 20 m. The moisture content was measured by scraping beach sand with a layer thickness of about 10 mm. The threshold shear velocity of dry sand was found to be in the range of 0.165 to 0.185 m/s. It was observed that that once sand movement was started at some place, other downwind areas with higher moisture contents also experienced initiation of motion due to the impact of incoming saltating particles (sand blasting effect). At high wind velocities, rain caused a decrease of sand transport due to the impact of the rain drops on the saltating particles reducing saltation heights. However, immediately after the rain, the sand movement increases again to almost the original level.

4.4.2 Laboratory experiments

Cornelis and Gabriels (2004) have studied splash-type sand transport by performing wind tunnel experiments with rain on 0.25 mm-sand. The maximum rain intensity in the tunnel is about 100 mm/hour. Splash-type transport rates were in the range of 0.5 to 2 g/m/s for wet sand at a wind shear velocity of 0.5 m/s, which is quite low compared to transport rates of 50 to 100 g/m/s for dry sand at the same shear velocity of 0.5 m/s. They concluded that when the sand surface is too wet for transport by wind forces, movement of sand can still occur due to splash-type saltation, which will stop when rain fall stops. At most exposed beach sites, the contribution of splash-type of sand transport to the annual transport is only minor.

New experiments have been done (by the author) in the mini wind tunnel to study the reduction of sand transport by various moisture levels. Moist beach sand from Schokkerhaven with d_{50}=0.34 mm was placed in the small tray at the end of the wind tunnel.

The sand transport tests consisted of:

- dry sand (200 g) was mixed with tap water (2 g for mc=1% to 16 fg for mc=8%) to get a uniform moisture content;
- moist sand was placed in the tray and slightly pressed to get a smooth surface; the top layer was placed quite loosely (see **Figure 4.4.4**);
- tray with moist sand was placed in the wind tunnel and the wind flow was started for a short period (1 to 15 minutes) to keep the moisture content as constant as possible;
- three tests with increasing wind velocity (between about 10 and 16 m/s) were done;
- tray was weighed, dried (in an oven at 150 °C) and weighed again;
- the sand transport rate was determined from the sand loss (gram) divided by the product of time period (s) and tray width of 0.05 m.

In some tests there was sand feed from the upwind tunnel entrance, but in most tests there was no sand feed. The data are given in **Table 4.4.1**. The volume of the smallest tray is about 120 ml and can contain about 200 gr of dry sand resulting in a bulk density (incl. pores) of about 1600 kg/m^3. The initial moisture content was varied in the range of 1% to 8%. The overall moisture content during each test was slightly smaller than the initial value due to evaporation (no more than 10%). A typical feature of moist sand is crust formation due to presence of minor calcareous (shell fragments) and silt/clay particles reacting with water. Crust formation was observed during all tests with 0.38 mm-sand and mc-values between 0.5% and 8%. The crust could easily be broken locally by slight ticking to the side wall of the tunnel to generate vibrations. This simulates to some extent the high-frequency oscillations due to gust-turbulence which are present in nature but absent in the mini-wind tunnel. High-frequency oscillations will help to break the surface crust.

Figure 4.4.1 shows the effect of moisture content on the measured sand transport rates as function of the measured wind velocity without upwind sand feed. The variation of the measured sand transport rates is about 20% to 30% based on repetitive tests. The variation of the measured wind velocity is not more than 5%. The sand transport rate of dry sand particles increases from about 10 g/m/s at a wind velocity of 10 m/s to about 100 g/m/s at a wind velocity of 16 m/s (factor 10 for velocity increase of factor 1.5) expressing a strong non-linearity effect. At a high velocity of 16 m/s at 0.03 m above the sand surface, the transport is very intensive with continuous movement at all places and the sand is removed from the tray within 30 sec. The measured sand transport rates without sand feed in the mini wind tunnels are much smaller than the equilibrium transport rates due to the limited length of the sand trays.
No particle movement and sand transport were observed for a moisture content of 7% to 8% for wind velocities up to 16 m/s (at 0.03 m above the sand surface). Similarly, no movement and transport were observed for an initial moisture content of 4% and wind velocities up to 14 m/s. Wind velocity alone over a moist sand surface can only generate minor entrainment of sand particles. During the tests with moist sand beds (mc between 1% and 8%), the entrainment of sand particles was slightly stimulated to break the surface crust by slight ticking against the side wall of the tunnel. The stability of particles in lower layers of the tray was not much affected by artificial stimulation as the transport slowed down after removal of the surface particles. Despite the artificial breaking of the crust, the sand transport rates were small to very small for moisture content in the range of 1% to 8%.
Overall, the sand transport was very minor during these tests with initial mc-values of 1% to 8% and a factor of 100 less than that for dry sand (see **Figure 4.4.1**).
The smallest mc-value used was mc=0.5% in tests S22 to S24. The effect of a very minor moisture content was still clearly manifest. The sand was slightly sticky reducing the sand transport at the end of the tray by a factor of 5 to 6 compared to the sand transport of dry sand. **Figure 4.4.5** shows the sand surface after the test; the sand surface is slightly irregular and small, moisty sand balls can be seen.

The test results of **Figure 4.4.1** show that the sand transport rate is significantly reduced by a wind flow over a moist bed. This changes markedly if dry sand is fed from the upwind tunnel entrance, which is illustrated in **Figure 4.4.2** for moist sand with initial percentage of 2%. The wind velocity is 12 m/s at 0.03 m above the sand surface. The sand transport rate is very small during the first 15 minutes and increases slightly to about 0.5 g/m/s in the period 15 to 60 minutes, mainly due to the crust formation. The sand transport process is highly intermittent due to the ongoing drying process. Layers of dry grains are intermittently removed, but no transport is generated at places where the crust is too strong. It is noted that the transport rate of dry sand for a wind velocity of about 12 m/s is much higher with a value of about 55 g/m/s (**Figure 4.4.3**). The sand transport ceases almost completely in the period 60 to 140 min due to the formation of local crusts. The sand surface is irregular with grooves and accumulations (small balls of sand). At time t=140 minutes, the sand feed of about 1 g/m/s was started resulting in very rapid crust breaking and erosion of the sand surface due to the sand blasting effect of the incoming sand particles. The sand transport rate during the last 6 minutes increased from 0 to about 5 g/m/s. The moisture content of the sand remaining in the tray was found to be 1.5%.

Figure 4.4.3 shows test results with sand feed of about 20 g/m/s and moist sand in the range of 1% to 8%. Test results without sand feed are also shown. In all tests, the same sand was used and the wind velocity was set to 12 m/s at (0.03 m above the sand surface). The sand transport rate measured at the end of the sand tray is almost none for moist sand of 1% to 8% in conditions without sand feed. The sand transport rates increase markedly (more than factor 10) when sand is feed is present (see **Figure 4.4.6**). This is mainly caused by the sand blasting effect of the incoming sand particles. At high wind speeds, the transport of sand is so intense that most of the entrainment of grains is caused by the impact of moving grains rather than the impact of the air flow. This proves that moist sand is mainly set into motion by the impacts of incoming saltating sand particles. Similar observations were done by Van Dijk et al. (1996) in a large wind tunnel.

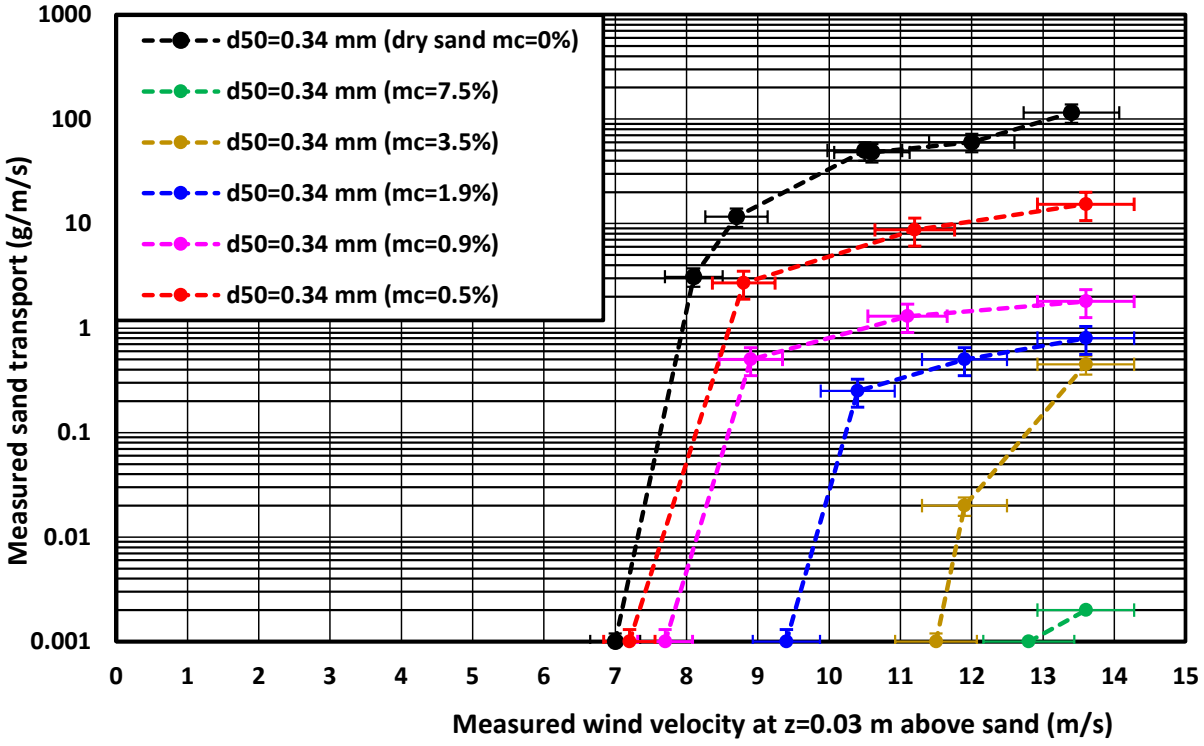

Figure 4.4.1 *Measured sand transport as function of wind velocity; effect of moisture content (no sand feed)*

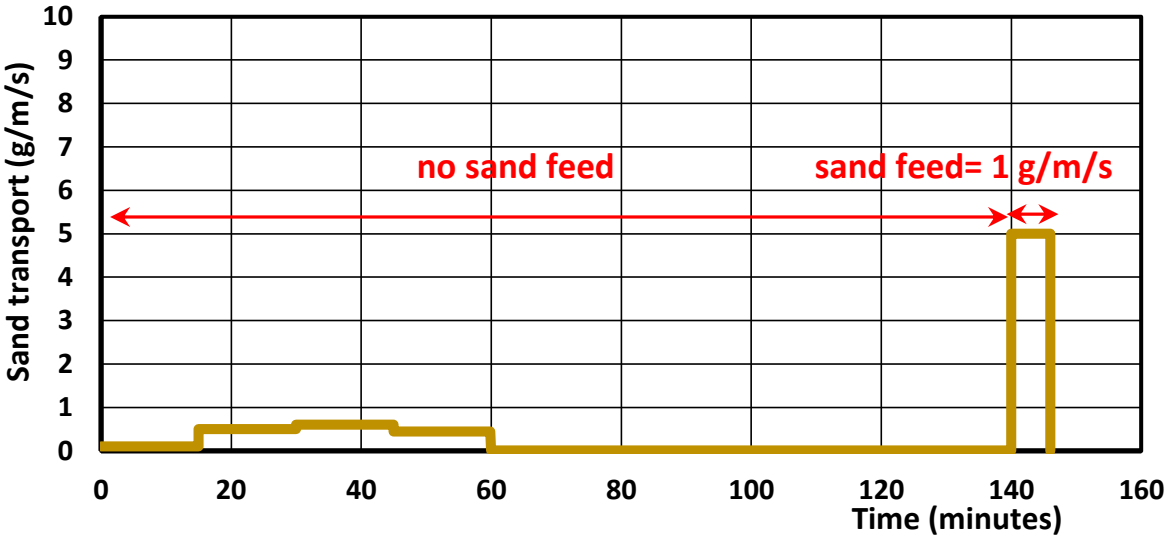

Figure 4.4.2 *Measured sand transport as function of time; wind velocity= 12 m/s at 0.03 m above surface (S28)*

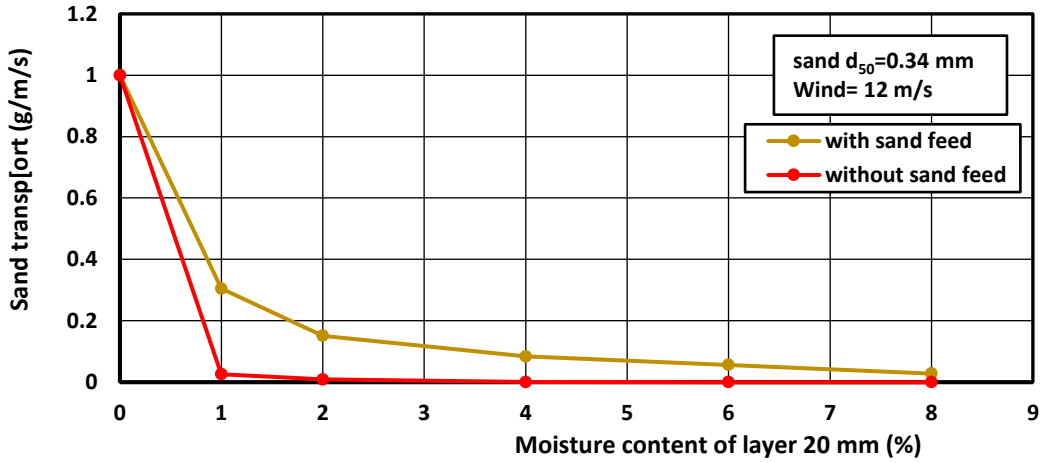

Figure 4.4.3 *Measured sand transport as function of moisture content with and without sand feed; wind velocity = 12 m/s at z=0.03 m above sand surface*

Figure 4.4.4 *Sand surface before test with initial moisture content of 8% (upper), 4% (middle) and 0.5% with slight additional irregularities (lower)*

Figure 4.4.5 *Sand surface at end of test (S23) with initial moisture content of 0.5%*

Figure 4.4.6 *Sand surface with initial moisture content of 2% after t=125 minutes, wind velocity=12 m/s (S28)*

Beach sand	Test duration (sec)	Sand diameters d_{50}; d_{90} (mm)	Moisture content (%)	Measured wind velocity at height z_w=0.03 (m/s)	Measured sand mass eroded from tray (g)	Sand feed and measured sand transport rate (g/m/s)
Schokkerhaven S1	(ST)	0.34; 0.7	0 (dry)	6.8	0	0; 0
Schokkerhaven S2	(WT)	0.34; 0.7	0 (dry)	6.8	0	0; 0
Schokkerhaven S3	60 (WT)	0.34; 0.7	0	8.7	36.2	0; 11.6
Schokkerhaven S4	60 (WT)	0.34; 0.7	0	10.6	149.5	0; 48.0
Schokkerhaven S5	110 (ST)	0.34; 0.7	0	8.1	14.3	0; 3.1
Schokkerhaven S6	60 (ST)	0.34; 0.7	0	10.5	126.6	0; 50
Schokkerhaven S7	60 (ST)	0.34; 0.7	0	11.9	140.3	0; 56
Schokkerhaven S8a	30 (ST)	0.34; 0.7	0	13.4	160.7	0; 128
Schokkerhaven S8b	35 (ST)	0.34; 0.7	0	13.4	157.0	0; 107
Schokkerhaven S9	60 (ST)	0.34; 0.7	8.	8.3	0	0; 0
Schokkerhaven S10	60 (ST)	0.34; 0.7	7.5	11.9	0	0; 0
Schokkerhaven S11	60 (ST)	0.34; 0.7	7	13.6	0	0; 0 (s.g.m.)
Schokkerhaven S12	60 (ST)	0.34; 0.7	4	8.3	0	0; 0
Schokkerhaven S13	60 (ST)	0.34; 0.7	3.5	14.9	0	0; <0.01 (s.g.m.)
Schokkerhaven S14	540 (ST)	0.34; 0.7	3	13.6	10	0; 0.45 (s.c.d)
Schokkerhaven S15	60 (ST)	0.34; 0.7	2	8.3	0	0; 0 (no movement)
Schokkerhaven S16	600 (ST)	0.34; 0.7	2	10.4	7	0; 0.25 (s.c.d.)
Schokkerhaven S17	900 (ST)	0.34; 0.7	2	11.9	18	0; 0.5 (s.c.d.)
Schokkerhaven S18	900 (ST)	0.34; 0.7	1.8	13.6	30	0; 0.8 (s.c.d.)
Schokkerhaven S19	600 (ST)	0.34; 0.7	1-0.9	8.9	12	0; 0.5 (s.c.d.)
Schokkerhaven S20	600 (ST)	0.34; 0.7	1-0.9	11.1	32	0; 1.3 (s.c.d.)
Schokkerhaven S21	780 (ST)	0.34; 0.7	1-0.9	13.6	60	0; 1.8 (s.c.d.)
Schokkerhaven S22	400 (ST)	0.34; 0.7	0.5	8.8	46	0; 2.7
Schokkerhaven S23	240 (ST)	0.34; 0.7	0.5	11.2	87	0; 8.7
Schokkerhaven S24	180 (ST)	0.34; 0.7	0.5	13.6	116	0; 15.3
Schokkerhaven S25	135 (ST)	0.34; 0.7	8	12	9	20; 1.6
Schokkerhaven S26	110 (ST)	0.34; 0.7	6	12	15	20; 3.2
Schokkerhaven S27	110 (ST)	0.34; 0.7	4	12	22	20; 4.8
Schokkerhaven S28	125 (ST)	0.34; 0.7	2	12	45	20; 8.6
Schokkerhaven S29	130 (ST)	0.34; 0.7	1	12	95	20; 17.4

ST=Smallest tunnel: width of tray=0.042 m; tunnel height=0.051 m; α_{sw}=0.85
WT=Wider tunnel: width of tray=0.052 m; tunnel height=0.061 m; α_{sw}=0.85
inaccuracy wind velocity= ±5%; inaccuracy shear velocity=±15%; inaccuracy sand transport= ±20%;
s.g.m.=some grains moving; s.c.d.= surface crust disturbed locally

Table 4.4.1 *Measured data of threshold shear velocity and sand transport in mini windtunnel*

5. Effect of coarse fraction (gravel and shells) on aeolian sand transport

5.1 Processes and definitions

Wind-induced sand transport is strongly reduced when the surface is covered with high quantities of shells, shell fragments and gravels.
Shells (calcium carbonate) and gravels can protect the beach surface against erosion of the sand particles. Large percentages of shell and gravels are mostly found on the upper part of natural beaches outside the wave action zone and on beaches with nourished sand. Literature on this topic is rather scarce and mostly qualitative. The two main effects of shells on the sand transport process are: i) shells cover a certain area of the bed which is not available for sand particle erosion and ii) sand particles in the direct vicinity of shells are less exposed to the wind forces (hiding effect). Observations in wind tunnels and field conditions show that shells of different sizes tend to interlock and form clusters (spatial organization; Mckenna et al., 2012; Strypsteen 2019). At the Dutch sand motor site with shell cover values up to 20%, sufficient sand particles were winnowed from the shelly bed to give appreciable erosion and deposition volumes of sand (De Vries and Hoonhout, 2017; Hoonhout and De Vries, 2017, 2019). Based on these observations, it is herein assumed that the effects of shells on the sand transport process can be best represented for engineering purposes by a simple reduction coefficient acting on the transport rate. This coefficient is derived from the experiments in wind tunnels (Van der Wal, 1999 and McKenna et al. 2012). It is realized that this approach only gives the supply-limiting effect.
Van der Wal (1998) studied the effect of shells on the wind-induced transport rate of beach sand. Beach sand samples were taken from 5 sites along the Dutch coast and tested in a wind tunnel. The d_{50} varied in the range of 0.21 to 0.35 mm. The percentage of coarse materials consisting of gravel, stones and shells (> 2 mm) varied in the range 1 to 30%. A tray with (length=1.22m; width=0.33 m; height=0.03m) was filled with weighed oven-dried sand and placed in the middle of the test section. The sample surface was smoothed and levelled to the tray edges. The wind speed was gradually increased over one minute to about 11 m/s and kept at this speed for another minute. Then, the wind speed was gradually returned to zero over one minute. After the experiment, the sand was reweighed. The percentage of sand blown off during the test was calculated for each of the experiments. The sand transport rate without shells was reduced by about 60% for a shell percentage of 7% and by about 80% to 85% for shell percentages of 18% to 32%. Shell pavements were formed during the wind tunnel experiments with shell-rich beach samples.
McKenna et al. (2012) conducted a wind tunnel study on the effect of shells on the erosion of a sand bed with a total area of about 10 m². Wind velocities were in the lower range of 8 to 12 m/s (BF<7). Three types of shells were used: crushed shells with cover percentages between 12% and 22% (heights 1.1 to 1.6 mm); small shells < 12.7 mm with cover percentages between 17% and 43% (height 2.6 to 5.7 mm) and large shells > 12.7 mm with cover percentages between 14% and 30% (heights 7 to 9.2 mm). The freestream velocity was gradually increased until the cumulative number of particle counts recorded by a piezoelectric impact sensing device began to increase continuously. A sediment trap at the downwind end was used to collect sand particles eroded from between the shells. The test was terminated when the transport rate dropped to a negligible value (<0.05 g/cm/s). It was observed that the shells were organized into chains and clusters with the long axis of many of the shells appearing to be aligned with the wind flow. The threshold wind velocity and shear velocity were found to increase by about 15% to 25% for a cover of 15% and about 35% to 45% for a cover of 43%. The amount of erosion after the test (in kg/m^2) was recorded showing almost no erosion for the largest cover values of 40% both for small and large shells. Erosion is reduced by a factor of 5 to 10 by increasing the cover of shell from about 15% to about 30%-40%. Crushed shells are less effective than small/large shells.
Information of the effect of gravel on sand transport can be obtained from a study of Tan et al. (2013). They studied the change in sand transport from a pure sand bed to a bed covered with gravel (20 to 55 mm) using a mobile wind tunnel operated in the Gobi Desert in China. The sand transport was reduced by about 20% for a gravel coverage of 10%, about 40% for a gravel coverage of 20%. The maximum reduction was about 50% for

gravel coverage of 30% up to 70%. The basic cause of the sand transport reduction is the decrease of the wind velocities in the lowest layer of 50 to 100 mm above the sand surface (measured by thin Pito-tubes) due to the presence of the large gravel particles. As a consequence of the reduced sand transport rates, deposition of sand was observed at the bed covered with gravel particles. Similar findings are given by Gillies et al. (2006). Wind-blown sand transport is substantially reduced if numerous roughness elements are present on a sand surface. Sand transport was measured between plastic buckets (4 different configurations) resting on a flat horizontal sand surface. Results of these tests indicate that sediment transport rates through patches of roughness are controlled by the roughness density depending on the dimensions (width, height) and number of elements. Sand transport reductions based on comparison with upwind trap results were as large as 90%.

Important parameters appear to be the fetch length and the uniformity of the shell cover. In wind tunnel experiments, the fetch length is relatively small (1 to 8 m in the studies discussed herein) and the initial shell cover is quite uniform in space. In field conditions, the fetch length is often larger than 50 m and the shells are not uniformly distributed over the beach surface. Shell clusters are pronounced features at natural beaches (Strypsteen 2019). McKenna et al. (2012) have observed in their wind tunnel experiments that the shells are not operating independently, but rather display some degree of spatial organization resulting in shell clusters of partly interlocking shells of different sizes. Shells are sometimes rolling coming to rest against others downwind resulting in clusters. Corridors of lower shell coverage are generated at the sand surface. This justifies the use of a simple supply-limiting coefficient for engineering practices. Herein, the reduction effects based on the tests of Van der Wal (1998) and Mckenna et al. (2012) are simply represented in Equation (2.6b) by a reduction factor acting on the transport rate (Van Rijn and Strypsteen 2020):

$$\alpha_{cf}=(1-2p_{cf}/100)^2 \qquad (5.1a)$$

with p_{cf}=percentage of coarse shells (<30%). The sand transport rate as affected by shells was not measured directly in the studies considered herein (van der Wal, 1999; Mckenna et al., 2012; Hoonhout and De Vries, 2017, 2019) and thus Equation (5.1a) could not be tested against measured transport rates. Equation (3.8), which is only valid for a shell cover < 30%, is herein used as a transport-limiting factor acting on the sand transport rate to obtain a quick engineering scan of the effect of shells in reducing sand transport on nourished shelly beaches. The gradual development of an armor layer of coarse shells in time cannot be represented in this way, as it requires a more detailed approach. Basically, the simulation of sand transport in conditions with a relatively wide grain size distribution (d_{90}/d_{10}> 10) and significant shell cover values (10% to 30%) requires an approach with multiple fractions including a book-keeping process for each grid cell and vertical sand layer. Hiding and exposure effects must be included as well as roughness variation effects (Raupach 1992; Van Rijn 2007). The present model can be extended to a fractional approach (Van Rijn 2007). Using such an approach, the changes in surface conditions can be simulated both in space and time. Hoonhout and De Vries (2017) used a fractional model to study the windblown sand transport at a large-scale mega-nourishment (sand motor in The Netherlands). They found that the intertidal zone and the transition zone with minimum shells were the dominant sources of sand for windblown sand transport. The dry beach plain with abundant shell cover (5% to 15%) developed a beach armor layer suppressing the pickup of sand particles to some degree. However, such an approach is far more complex with many coefficients and calibrations involved and may be a bridge too far for engineering purposes (see detailed discussion by McKenna et al., 2012). Van Rijn and Strypsteen (2020) have shown that Equation (5.1a) predicts meaningful results for the Dutch sand motor site which is a shelly beach plain/nourishment site. Model improvements based on detailed research in wind tunnels and at field sites focusing on the sand transport processes with wide grain size distributions including/excluding shells are highly recommended.

5.2 Effect of coarse fractions (gravel and shells) on sand transport based on laboratory experiments

The reduction of sand transport due to the presence of shells was studied by by tests in the mini wind tunnel (see Section 3.2). The wind velocities were in the range of 10 to 13 m/s. Uniform sand with d_{50}=0.35 mm (see **Table 3.2.2**) was used. The tray was filled with sand and shells were placed on the sand surface, see **Figure 5.2.1**. The percentage of shells covering the sand surface was varied in the range of 0% to 60%. The width of the shells was in the range of 8 to 25 mm; the length in the range of 10 to 20 mm. The shells were immobile at low wind velocities of 10 m/s. To prevent erosion of shells at high wind velocities of 12 to 13 m/s, the shells were glued to the sand surface. The loss of sand from the tray was measured by weighing before and after each test. Most tests were repeated to determine the variability. The sand transport rate (in g/m/s) at the end of the tray was determined as the loss of sand divided by the test time and the tray width. **Figure 5.2.2** shows the sand transport rate ($q_{s,o}$) in tests without coarse materials at the end of the tray as function of the measured wind velocity (at 30 mm above the surface).Similar tests with gravel (**Figure 5.2.1 right**) have been performed. The mass percentage of gravel with sizes in the range of 2 to 6 mm was varied in the 10% to 60%

Figure 5.2.3 shows the test results for shells and gravel. The measured sand transport rates at the end of the tray are made dimensionless by dividing by the measured transport rate ($q_{s,o}$) without shells or gravel. The gravel percentage is given in terms of the mass percentage, which is approximately equal (within ±10%) to the area percentge based on detailed analysis of photos of the tray with gravel surface. The effect of gravel particles is much stronger than that of the shells. The individual shells have a streamlined shape leading to increased velocities around the shells with more intensive erosion. The smaller gravel particles are much more widely spread and have a stronger hiding effect than individual shells.

The effect of shells can be crudely represented by: $q_s=(1-p_{shells}/100)^{1.5}\, q_{s,o}$ (5.1b)

with $q_{s,o}$=sand transport without shells and p_{shells}=percentage of shells. For example, p_{shells}=30% gives $q_s \cong 0.6\, q_{s,o}$ (reduction of 40%).

The effect of gravels can be crudely represented by: $q_s=(1-2p_{gravel})^3\, q_{s,o}$ (5.1c)

with $q_{s,o}$=sand transport without gravel and p_{gravel}=percentage of gravel (%). For example, p_{gravel}=30% gives $q_s \cong 0.06\, q_{s,o}$ (reduction of 94%).

Figure 5.2.1 *Laboratory setup with shells and gravel in tray of mini wind tunnel*

The results of Van der Wal (1998) and Tan et al. (2013) are also shown in **Figure 5.2.3**. Beach sand samples were taken from 5 sites along the Dutch coast and tested in a wind tunnel at wind velocity of 11 m/s by Van der Wal (1998). The d_{50} varied in the range of 0.21 to 0.35 mm. The percentage of coarse materials consisting of gravel, stones and shells (> 2 mm) varied in the range 7% to 32%. A tray with (length=1.22m; width=0.33 m; height=0.03m) was filled with weighed oven-dried sand and placed in the middle of the test section. After the experiment, the sand was reweighed. The results of Van der Wal (1998) for sand samples with a coarse fraction of gravel and shells are in very good agreement with the gravel results of the mini wind tunnel. This suggests that gravel is the dominant factor with respect to the reduction of sand transport. The result of Tan et al. (2013) for large gravel particles of 20 to 30 mm are more in agreement with the test results of shells. It seems that fewer larger gravel elements offer less hiding and shielding than many smaller gravel particles.

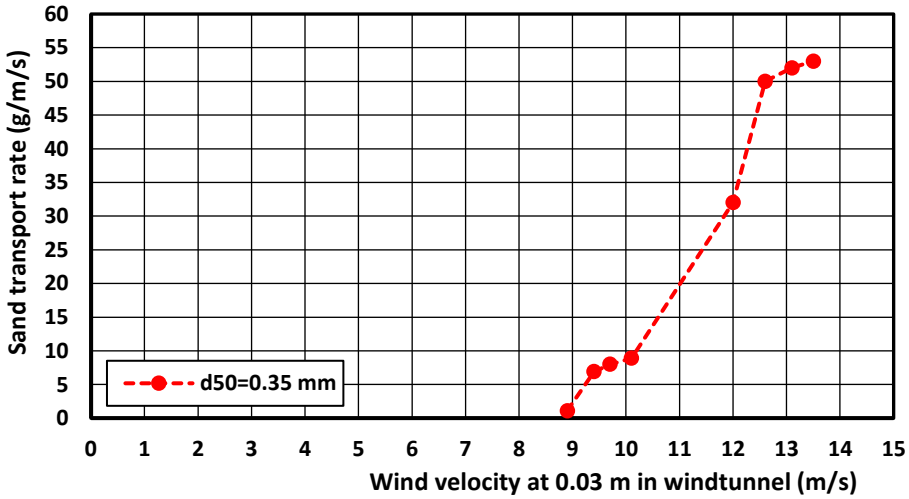

Figure 5.2.2 *Sand transport at end of tray in mini wind tunnel without shells and gravel; d_{50}=0.35 mm*

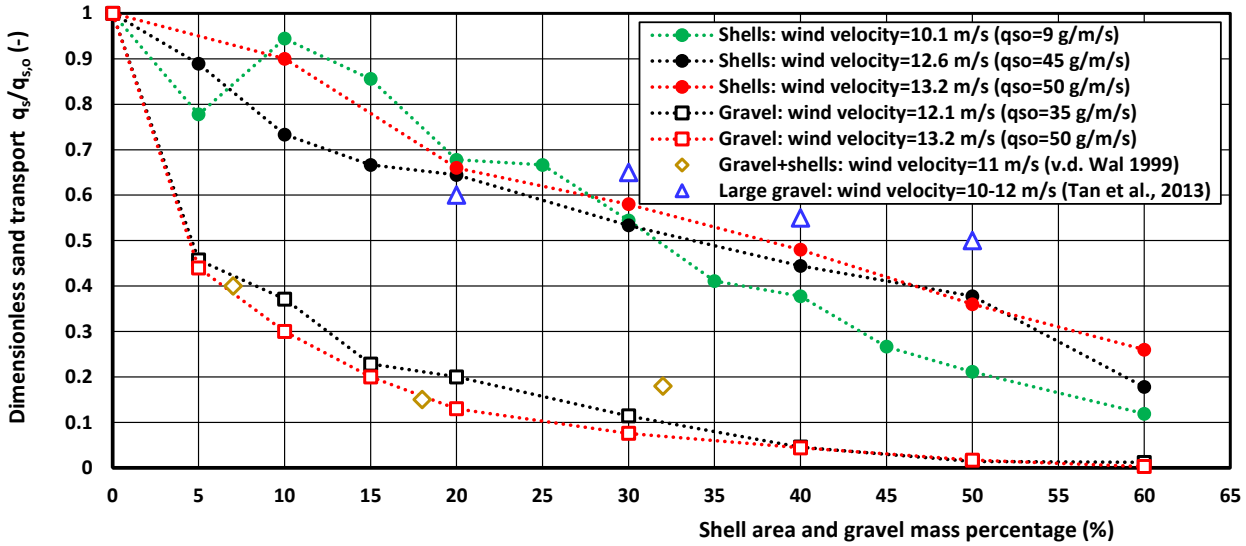

Figure 5.2.3 *Effect of shells and gravel on wind-induced sand transport; laboratory tests in mini windtunnel ($q_{s,o}$= sand transport without coarse materials)*

5.3 Effect of armour layer on sand transport at Prins Hendrik beach, Texel

Field measurements have been done at the man-made beach of the Prins Hendrik site on the island of Texel, The Netherlands in the period between 12 March and 21 April 2020 (Strypsteen et al., 2021). An oblique spit is situated along the north part of the beach enclosing a lagoon between the north beach and the spit. The core of the beaches is made of medium fine sand (0.2 to 0.3 mm) and is covered by a protection layer of coarse materials of gravel and shells to reduce the erosion of sand and thus to minimize the maintenance costs. The dredging and construction works of the beach and dune system using sand dredged from the North Sea bed was completed in December 2018.

The d_{50} and d_{90}-values of samples taken after completion of the construction works are, as follows:

- d_{50} between 0.5 and 1 mm at the south part of the dry beach between NIOZ-harbour and PH-station;
- d_{50} between 0.6 and 2 mm at the spit;
- d_{90} between 2 and 5 mm at both parts.

The largest gravel size is about 10 mm (flat ellipse type gravel). The percentage of sediment with grain sizes > 2 mm varies in the range of 15% to almost 50%.

Comparison of grain sizes of samples taken at the dry beach in early winter 2018 (post-construction) and in Spring 2020 show very similar values in the range of 0.5 to 2 mm for the d_{50} and in the range of 1 to 5 mm for the d_{90}, which means that most of the armouring process (removal of finer fractions by wind) took place during construction in the autumn period of 2018.

During the field measurements at the beach near the beginning of the spit in March 2020, a small pit was made at mid beach to study the vertical structure of the top layer of the dry beach. Samples were taken at several levels below the surface, see **Figure 5.3.1**. The coarse fraction of the top layer of the dry beach consists of sand (about 50%), very coarse gravel (about 40%) and shells (5% to 10%) in agreement with the post construction values. This upper layer effectively is an armour layer reducing windblown sediment transport. A similar pit was made in the middle of the spit. The coarse top layer had a thickness of about 5 to 10 mm. The sediment beneath the coarse armour layer over a depth of 0.3 m was sand with d_{50} of about 0.3 mm with very minor gravel and shell (<3%).

Analysis of samples taken at other locations during the field survey shows that the surface of the dry beach is very coarse with a percentage p_{cf}> 2mm of 30% to 50% similar to the post-construction values; the d_{50}-values of the sand fraction (< 2 mm) are in the range of 0.3 to 0.5 mm. The surface samples from the wet beach near the water line are less coarse with p_{cf}-values smaller than 20% and d_{50} of the sand fraction of about 0.4 to 0.5 mm. The surface samples at the dune front and crest consist of sandy materials with d_{50}-values in the range of 0.3 to 0.35 mm (no coarse fraction).

Wind-blown sediment transport was measured at various locations inside and outside the measurement area:

- Measurement area (MA): 12 March 2020;
  at the mid dry beach at about 40 m from the water line;
  at the lower dry beach at about 20 m from water line (see **Figure 5.3.2**);
  at armour top layer of coarse gravel and shells; finer gravel moved during strong wind gusts; horizontally-lying and vertically-sitting shells remained immobile; sand was eroded from between coarse materials and from upwind locations (dune foot with finer sands); trapped sediment consisted mainly of sand (no coarse gravel; no shells); measured sand transport rate was about 7 g/m/s at wind speed of 8 m/s at 1.25 m above surface;
- Measurement area (MA): 12 March 2020;
  at lower dry beach at about 20 m from water line; similar armour layer structure as mid beach location; measured sand transport rate was 1 g/m/s at wind speed of 10 m/s at 1.25 m above surface;
- Measurement area (MA): 12 March and 27 March 2020;
  at wet intertidal beach at about 5 to 10 m from the water line with moisture levels of 7.5% to 12.5% during BF 5 to 6 from SW (parallel to beach) on 12 march 2020 and during BF 6 to 7 from NNE (parallel to beach)

on 27 March 2020; sand transport was relatively large at the wet beach where no armour layer was present; coarse sand particles of the wet upper layer were observed to move during strong wind gusts; sand was also eroded at dry spots near the uprush line (about70% wet spots and 30% dry spots); sand transport rates were in the range of 25 to 65 g/m/s at wind speeds of 9.5 to 10.5 m/s at about 1.2 m above the surface;

- Outside measurement area: 29 March 2020;
  at south dry beach near NIOZ harbour during BF 6 to 7 from NNE (parallel to dune); beach surface was fairly flat with irregularities up to 50 mm; upper layer of 5 mm was fairly dry with moisture level < 1%; moisture level of upper 20 mm was 2.5%; a clear armour layer was not present, although minor shells, coarse sand and gravel were widely present at this location; sand transport was intense with value of 48 g/m/s at wind speed of 9.5 m/s at 1.25 m above surface.

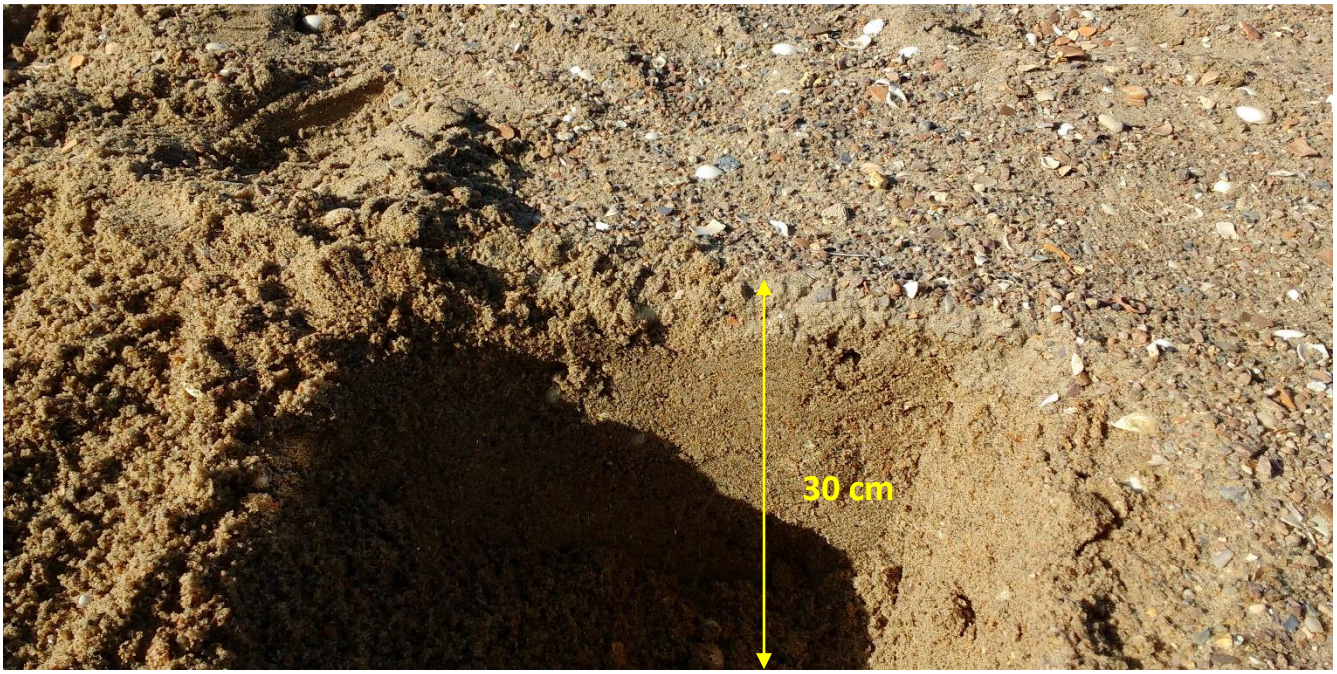

Figure 5.3.1 *Vertical structure and composition of top layer with armour layer and deeper coarse sand layer, sand spit Prins Hendrik site, Texel, 12 March 2020*

Based on the available data in conditions with BF7 (12 March 2020), the windblown sand transport at the wet beach without armour layer was in the range of 25 to 65 g/m/s (**Figure 5.3.3**), whereas the sand transport at the dry beach with armour layer was in the range of 4 (± 50%) g/m/s, which is a factor of 10 smaller due to the effect of the armour layer.
The sediment trapped in the bags of the traps consisted of sand particles smaller than 2 mm; gravel material and shells were not trapped.
Visually, it was observed that shells and gravel were almost immobile during the wind strength of BF7 on 12 March 2020. Based on the threshold wind speeds for initiation of motion of sediment, it is found that gravel material > 1 mm can only be moved in conditions with wind speeds of about 11 m/s at 1 m above the surface (BF7; 10 days per year). The highest wind speed measured on 12 March 2020 at the dry armoured beach was about 10.5 m/s at 1.2 m above the surface, which means that gravel > 1 mm is mostly immobile. During strong wind gusts, gravel of 1 mm can be moved, but gravel of 2 mm remains immobile. Wind strengths of BF8 and higher (2 days per year) are required to set gravel of 2 mm in motion.

Figure 5.3.2 *Measuring setup of windblow sediment transport with bag-type traps and wind cupmeters, Prins Hendrik beach, Texel; 12 March 2020*

Sediment transport predictions have been made using the single and multi fraction methods of Van Rijn and the field data of the Prins Hendrik site on Texel (Equation (2.6b) and (2.12a) of Section 2.1).
Three zones across the beach and dune profile are considered:

- lower intertidal (wet) beach with d_{50}=0.5 mm and d_{90}=1 mm (no shell; no gravel); moisture content of 7%
- upper beach with armour layer with gravel and shells; represented by 7 fractions (see **Table 5.3.1**); moisture content of 2%; percentage shells=5%; percentage of moist spots=50%;
- dune front and dune crest.

Fraction size (mm)	**Percentage (%)**	**d_{50} of mixture (mm)**	**d_{90} of mixture (mm)**
0.1-0.3	5	0.77	5
0.3-0.5	10		
0.5-0.7	15		
0.7-1.0	25		
1-2	20		
2-4	15		
4-10	5		
shells	5		
	Total=100		

Table 5.3.1 *Sediment composition of upper beach material with armour layer, Prins Hendrik site, Texel*

The sediment of the upper beach with armour layer of coarse materials is represented by 7 fractions, see **Table 5.3.1**. The d_{50} and d_{90} of this armoured surface layer are 0.77 and 5 mm. The percentage of coarse materials including shells > 2 mm is 25%. These latter values (d_{50} = 0.77 mm; d_{90} = 5 mm; p_{cf} = 20%; p_{shell} = 5%) are used in the single fraction method. Moisture effects are neglected as the upper layer of the beach sand was fairly dry (< 1%) in most cases. The predicted transport rates of the single fraction method represent equilibrium (saturated) values for dry conditions as moisture effects are small (α_w = 1) and fetch-limiting effects are neglected (α_{ad} = 1; very long fetch).
All measured sand transport rates and the predicted results of the single and multi fraction methods are shown in **Figure 5.3.3**. The exponent (n) of the hiding-exposure factor (Equation 2.13) is set to n=0.5.

The single fraction method for sand without a significant coarse fraction yields values which are quite good for the intertidal beach and somewhat too small (maximum underprediction of factor of 2) for the open dune spots with narrowly graded sand (no coarse fraction). Measured transport rates at other locations are significantly below the predicted values due to supply-limiting effects (short fetch, armour layer).

The transport rates measured at the armoured beach surface are significantly overpredicted (factor of 10) if the coarse fraction is not taken into account. The overprediction of the single fraction method reduces for higher wind speeds further away from the threshold speeds. The effect of the coarse fraction in the single fraction method can be simply represented by a reduction factor acting on the transport rate: $\alpha_{cf} = (1\text{-}2p_{cf}/100)^{\beta}$ with p_{cf} = percentage of coarse materials (%) and β = coefficient ($\cong$ 2 to 3). Using p_{cf} = 20% and β = 2 to 3 in the single fraction method yields significantly lower transport rates.

The predicted value of the multi fraction method is remarkably close to the measured value for a wind velocity of 10 m/s. **Table 5.3.2** shows that only the fine fractions are transported at lower wind speeds and the coarser fractions are set in motion at higher wind speeds. The predicted transport rates of the multi fraction method will be smaller for n=1 (exponent of hiding-exposure factor), as the threshold value of the finer fractions will be higher for n=1.

Wind speed at z=1.3 m (m/s)	**Single fraction method (g/m/s)**	**Multi fraction method (g/m/s)**							
		0.2 mm	**0.4 mm**	**0.6 mm**	**0.85 mm**	**1.5 mm**	**3 mm**	**7 mm**	**Total**
9.5	8.8	0.05	0.1	0.16	0	0	0	0	0.3
10	17.0	0.12	0.25	0.57	0.95	0	0	0	1.9
10.5	26.6	0.2	0.7	1.9	3.2	0	0	0	6.0
11	36.1	0.3	1.6	3.3	5.7	0	0	0	10.9
11.5	45.3	0.4	2.6	4.9	8.6	2.0	0	0	18.5
12	55.8	0.9	3.8	6.8	11.6	4.2	0	0	27.4
13	80.7	2.1	6.2	10.3	17.5	9.2	0	0	45.3
14	111.7	3.6	8.8	14.4	24.7	15.4	0	0	66.9
15	149.5	4.9	11.9	19.4	33.5	23.1	3.9	0	99.6

Table 5.3.2 *Predicted sediment transport of single and multi fraction methods for Prins Hendrik site, Texel*

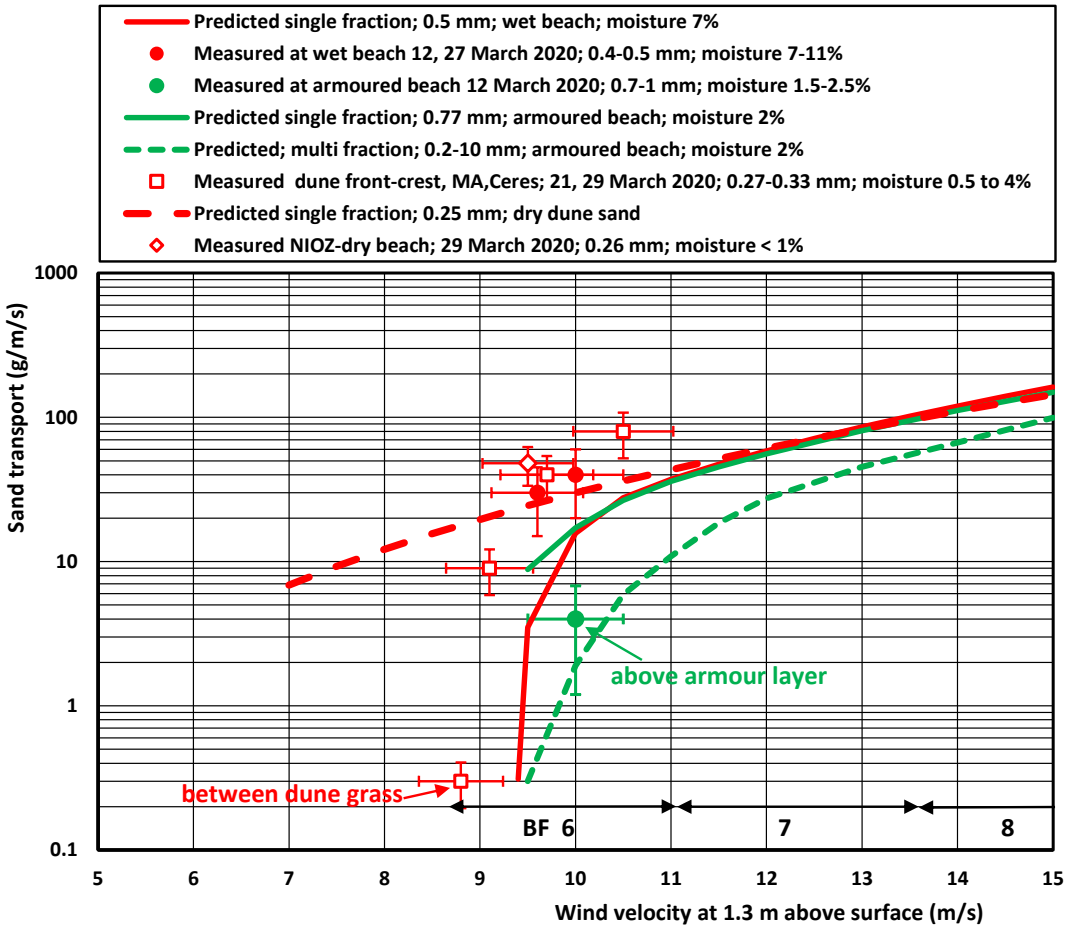

Figure 5.3.3 *Measured and predicted sediment transport values, Prins Hendrik site, Texel*

6. Field measurements at beaches in Belgium and The Netherlands

6.1 General

Many new field measurements of sand transport have been done at various beaches (see **Table 6.1.1**) in Belgium and The Netherlands in the period December 2019 to April 2021 using the LVRS-trap sampler (Section 3). Beach conditions were dry, moist and combinations of dry and moist spots. Wind conditions were up to Beaufort 9 (20 m/s). The measurement period of the trap sampler was in the range of 5 minutes at high wind speeds to 30 minutes at low speeds. During this period, many 1 minute-averaged wind speeds were measured at 3 height above the surface at a location within 0.5 m from the mouth of the trap. Sand samples of the upper 20 mm of the surface were taken for determination of sand composition (d_{50}, d_{90}), percentage of coarse materials (> 2 mm) and moisture content (w_{20}). Photographs were taken for determination of bed irregularities. At most dates in late spring and summer the beach surface was dry. At most dates in winter and autumn, the beach surface was moist. Sometimes, the beach surface showed combinations of dry (lighter colors) and moist spots (darker colors). The percentage of dry and wet spots upwind of the trap sample was visually estimated. The elapsed time since the last rainfall period was also estimated. In all, 55 new high-quality field data sets are available for analysis and verification of transport equations (see Section 2).
The field data at the beach of Callantsoog in February 2020 are discussed in more detail as the weather was quite stormy in this month. The storms Ciara (9 February) and Dennis (15 February) hit the coast with peak velocities up to 20 m/s at 1.5 m above the beach surface. Most of the time, the wind was almost parallel to the coast (from southwest). The wind strength distribution over 20 days between 9 and 29 February was approximately: 50% BF6; 15% BF7, 5% BF8 and 2% B9. On 9 February, a record sand transport measurement of 425 g/m/s at a wind speed of 18 m/s at 1 m above the surface was made. About 20 rainfall events were measured in the period between 9 and 29 February 2020. The maximum rain intensity was about 5 mm/hour. The total duration of the rainfall in February 2020 was about 90 hours (about 13% of the time; twice the normal value). The duration of the rainfall events was in the range of 0.5 hour to 16 hours with an average duration of about 4.5 hours. The periods with dry weather (dry time) after rainfall varied between 1 hour and maximum 36 hours for the period between 9 and 29 February.
Many beach samples were taken and mostly the moisture content at the upper beach was higher than about 2%. Most of the time between 9 and 29 February the sand surface of the beach was moist. Nevertheless, sand transport was intense in this period as long the wind speed was higher than BF6.

Location	**Grain size**			
	d_{10} (μm)	d_{50} (μm)	d_{90} (μm)	coarse > 2 mm (%)
Lemmer (NL); inland, recreational beach	150	300	900	<5
Schokkerhaven (NL); inland, recreational beach	205	340	700	<3
Callantsoog (NL); coastal, tidal beach	160	230	400	<3
Groote Keeten (NL); coastal, tidal beach	150	240	450	<1
Zandvoort (NL); coastal, tidal beach	150	250	400	<1
Texel-Den Hoorn; coastal, tidal beach	180	270	450	<1
Texel- Prins Hendrik; Wadden Sea, dry tidal beach	140	260	500	<3
Texel- Prins Hendrik; Wadden Sea, wet intertidal beach	200	400	1000	<5
Zeebrugge (BE); coastal, tidal beach	140	200	400	<3
Koksijde (BE); coastal, tidal beach	150	230	400	<5
Oostende (BE); coastal, tidal beach	180	300	500	<5
Mariakerke (BE); coastal, tidal beach	170	310	600	<3

Table 6.1.1 *Sand characteristics of beaches in Belgium and The Netherlands*

6.2 Field measurements at various beaches in Belgium

6.2.1 Zeebrugge beach

Location: Zeebrugge beach, Belgium (8 December 2019 and 11 February 2020).
Fairly flat upper beach with some irregularities (1-30 mm) and shells (5% to 10%), see **Figure 6.2.2**.
Dry sand was accumulated in the depressions of irregularities, from where it could easily be eroded during strong wind gusts, see **Figures 6.2.1** and **6.2.2**. Detailed data are given in **Tables 6.1.1** and **6.2.1**.

Figure 6.2.1 *Zeebrugge beach (Belgium) with darker moisty areas and lighter dry areas; BF6; December 2019*

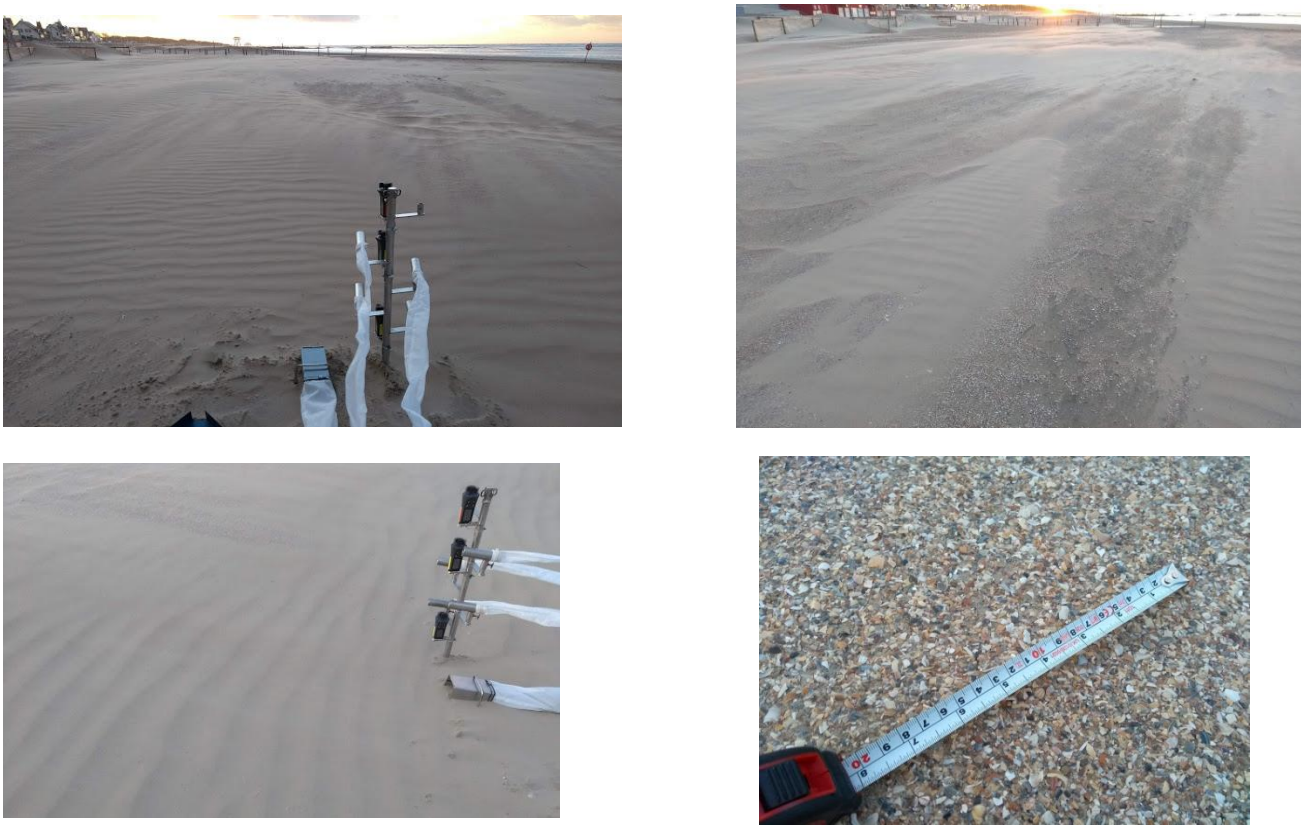

Figure 6.2.2 *Zeebrugge beach (Belgium) with darker moisty areas and lighter dry areas; many spots with shell fragments; small-ripples at many places; BF7; February 2019*

6.2.2 Koksijde beach

Location: Koksijde beach, Belgium (10, 12 and 15 February 2020)
Fairly flat upper beach with some irregularities and minor shell fragments < 5%; flat intertidal beach.
Sand transported at intertidal beach is eroded at drier spots of upper beach.
Detailed data are given in **Tables 6.1.1** and **6.2.1**.
Beach conditions are shown in **Figures 6.2.3** to **6.2.6**.

6.2.3 Oostende beach

Location: Oostende beach, Belgium (17 February 2020)
Fairly flat intertidal beach with some irregularities and minor shell fragments < 5%.
Sand transported at intertidal beach is eroded at drier spots of upper beach.
Detailed data are given in **Tables 6.1.1** and **6.2.1**.
Beach conditions are shown in **Figures 6.2.7**.

Figure 6.2.3 *Koksijde K1 upper beach (Belgium) with darker moisty areas (80%) and lighter dry areas (20%); some spots with minor shell fragments; small-ripples at many places; BF6; 10 February 2020*

Figure 6.2.4 *Koksijde K2 upper beach (Belgium) with darker moisty areas (10%) and lighter dry areas (90%); some spots with minor shell fragments; small-ripples at many places; BF7; 12 February 2020*

Figure 6.2.5 *Koksijde K3 lower beach (Belgium) with moist surface in intertidal zone; shell fragments at many locations; BF6; 12 February 2020*

Figure 6.2.6 *Koksijde K4 upper beach landward of intertidal zone; small-scale ripples; increasing wind towards end of measurement period BF6/7, 15 February 2020*


Figure 6.2.7 *Oostende lower intertidal beach; very moisty surface; small-scale ripples at some spots; BF6/7; 17 February 2020*

Location Date Duration	Beach		Moisture (%)			Wind conditions		Wind transport (g/m/s) in layers (mm) and test duration (s)
	d_{50} (mm) d_{90} (mm) p_{shell} (%)	Description	upper 5mm	upper 20mm	p_m (%)	height (m) and velocity (m/s)	direction and fetch length (m)	
Z1 Zeebrugge 8 December 2019; dry Te=10 °C	0.2; 0.4 <3%	fairly flat middle beach with irregu-larities 1-30 mm;	4.3% 6 hrs alr	4.7% 6 hrs alr	60%	z=0.35; u=6.5 ±0.5 z=0.71; u=7.7 ±0.5 z=0.92; u=8.0 ±0.5 u_*=0.60 m/s (R^2=0.95) k_s=135 mm	almost parallel FL>500 (no SL)	layer 0-71: 9 layer 71-300: 1 Total: 10 g/m/s (mt=840 s)
Z2 Zeebrugge 8 Dec 2019; Te=10 °C dry	0.2; 0.4 <3%	fairly flat upper beach with irregularitie s 1-30 mm;	4.3% 6 hrs alr	4.7% 6 hrs alr	60%	z=0.31; u=6.9 ±0.5 z=0.68; u=8.0 ±0.5 z=0.895; u=8.3 ±0.5 u_*=0.54 m/s (R^2=0.95) k_s=55 mm	almost parallel FL> 500 (no SL)	layer 0-71: 13 layer 71-300: 1 Total: 14 g/m/s (mt=600 s.)
Z3: Zeebrugge 11 Feb 2020 Te=8 °C dry	0.3 0.5 10%	Middle, flat beach with irregul arities 1- 30 mm		3.7% 24 hrs alr	80%	z = 0.26; u= 8.3 ± 0.1 z = 0.63; u= 9.5 ± 0.3 z = 0.84; u= 11.3 ± 0.3 u_* = 0.91 m/s k_s = 22 mm	Parallel FL > 500 (no SL)	layer 0-71: 34 layer>71: 3 total: 37 g/m/s (mt = 3600 s)
K1: Koksijde 10/02/2020 (light rain)	0.2 0.4 5%	Middle, flat beach with irregulari ties 1 – 20 mm		4.5% 9 hrs alr (some light rain)	80%	z = 0.46; u = 8 ± 0.4 z = 0.83; u = 8.4 ± 0.4 z = 1.04; u = 9.6 ± 0.4 u_* = 0.72 m/s k_s = 17 mm	Almost parallel FL ≈ 100	layer 0-71: 14 layer>71: 2 total: 16 g/m/s (mt = 1680 s)
K2: Koksijde 12/02/2020	0.25 0.45 10%	Middle, flat beach with irregul arities 1- 30 mm		3.6% 48 hrs alr	10%	z = 0.32; u= 7.3 ± 0,8 z = 0.69; u= 9.0 ± 0,7 z = 0.9; u= 10.1 ± 1,7 u_* = 1.04 m/s k_s = 590 mm	Parallel FL > 500 (no SL)	layer 0-71: 21.4 layer 71-290: 2.6 layer 290-320: 0.01 total: 23 g/m/s (mt = 2700 s)
K3: Koksijde 12/02/2020	0.27 0.46 < 5%	Intertidal, flat beach with no irregul arities		12.1% 48 hrs alr	90%	z = 0.34; u= 5.7 ± 1,1 z = 0.71; u= 7.5 ± 1,2 z = 0.92; u= 7.8 ± 1 (variable wind; minor wind sometimes) u_* = 0,87 m/s	Parallel FL > 500 (no SL)	layer 0-71: 1.89 layer 71-300: 0.11 layer 300-330: 0.01 total: 2 g/m/s (mt = 1800 s)

						k_s = 736 mm		
K4: Koksijde 15/02/2020	0.2 0.35 < 5%	Middle, flat beach with small irregularities 1-20 mm		8.9 %	90%	z = 0.17; u= 6.6 ± 1.7 z = 0.54; u= 8.2 ± 1.2 z = 0.75; u= 8.7 ± 1.6 (increasing wind) u_* = 0.56 m/s k_s = 47 mm	Onshore FL≈ 50m	layer 0-71: 7.3 layer >71: 0.7 total: 8 g/m/s (mt = 2160 s)
O1: Oostende 17/02/2020 (rainy)	0.3 0.46 < 5%	Lower intertidal beach with irregularities 1-20 mm		5.5 % 1 hr alr	90%	z = 0.17; u= 3.5 ± 0.8 z = 0.54; u= 5.9 ± 0.9 z = 0.75; u= 8 ± 1.5 increasing wind 9 to 12 m/s; u_* = 0,95 m/s k_s=120 mm	Parallel FL > 500 (no SL)	layer 0-71: 7.3 layer>71: 0.7 total: 8 g/m/s (mt = 2700 s)
O2: Oostende 17/02/2020 (rainy)	0.34 0.47 < 5%	Lower intertidal beach with irregularities 1-20 mm		16.8 % 2hr alr	90%	z = 0.18; u= 6.5 ± 1.9 z = 0.55; u= 7.9 ± 1.6 z = 0.76; u= 8.4 ± 2.6 intermittent strong gusts; u_* = 0.52 m/s k_s = 37 mm	Parallel FL > 500 (no SL)	layer 0-71: 27 layer 71-150: 2.6 layer 150-180: 0.4 layer >180: 0.1 total: 30 g/m/s (mt = 1020 s)

BF=Beaufort wind scale; p_{shell}= percentage shells at beach surface; alr=after last rainfall;
FL= fetch length; SL= supply limitation; TL= transport limitation; hp= hard moist patches; dp=relatively dry patches
p_m= percentage of beach surface with moist appearance at measurement location; z= height above bed; u= wind velocity at height z; mt=measuring time sand transport; mc= moisture content

Table 6.2.1 *Wind transport data at beaches in Belgium 2019, 2020*

6.3 Field measurements Callantsoog beach, The Netherlands

6.3.1 Storm month February 2020

The beach of Callantsoog is situated near the naval base town of Den Helder in the north of the province of North -Holland. The beach width is about 50 to 80 m and consists of medium fine sand (d_{10}=0.17 mm; d_{50}= 0.23 mm; d_{90}=0.4 mm; percentage coarse materials > 1 mm=1%). Based on Rijkswaterstat 1984, the mean grain size along the coast of North-Holland is d_{50}=0.25 ± 0.03 mm over a distance of 50 km. Many beach restaurants (at spacing of 300 to 500 m) on wooden piles are situated at the upper dry beach close to the dune foot. During conditions with wind flow parallel to the beach, the wind flow along the beach is severely disturbed (macro-scale turbulence) resulting in relatively large shear velocities and roughness values (> 100 mm).
The beach of Callantsoog was attacked by storm winds with Beaufort 6 to 9 in the period Sunday 9 February to Monday 29 February 2020, see **Figure 6.3.1**. The wind rose for February 20-20 is given in **Figure 6.3.2**. The wind data are from the inland weather station De Kooy, which is about 5 km from the beach. The dominant wind direction is from South-West.
The storms Ciara (9 February) and Dennis (15 February) hit the coast with peak velocities up to 20 m/s at 1.5 m above the beach surface. Most of the time, the wind was almost parallel to the coast (from South-West). The wind strength distribution over 20 days between 9 and 29 February was approximately: 50% BF6; 15% BF7, 5% BF8 and 2% B9.
About 20 rainfall events were measured in the period between 9 and 29 February 2020 (see **Figure 6.3.1**). The maximum rain intensity was about 5 mm/hour. The total duration of the rainfall in February 2020 was about 90 hours (about 13% of the time; twice the normal value). The duration of the rainfall events was in the range of 0.5 hour to 16 hours with an average duration of about 4.5 hours. The periods with dry weather (dry time) after rainfall varied between 1 hour and maximum 36 hours for the period between 9 and 29 February. Most of the dry time was in the range of 10 to 20 hours (Figure 6.3.2 lower right), which is less than the required dry time of 30 hours (see **Figure 4.2.5**) to obtain a sand surface of dry, loos sand particles in the winter time. During the

measurement days on the beach (grey lines on Figure 6.31), many samples were taken and mostly the moisture content at the upper beach was higher than about 2%. The periods between rainfall events were not long enough to ensure sufficient drying of the sand surface. Hence, most of the time between 9 and 29 February the sand surface of the upper beach was moist. Nevertheless, sand transport was intense in this period as long the wind speed was higher than BF6.

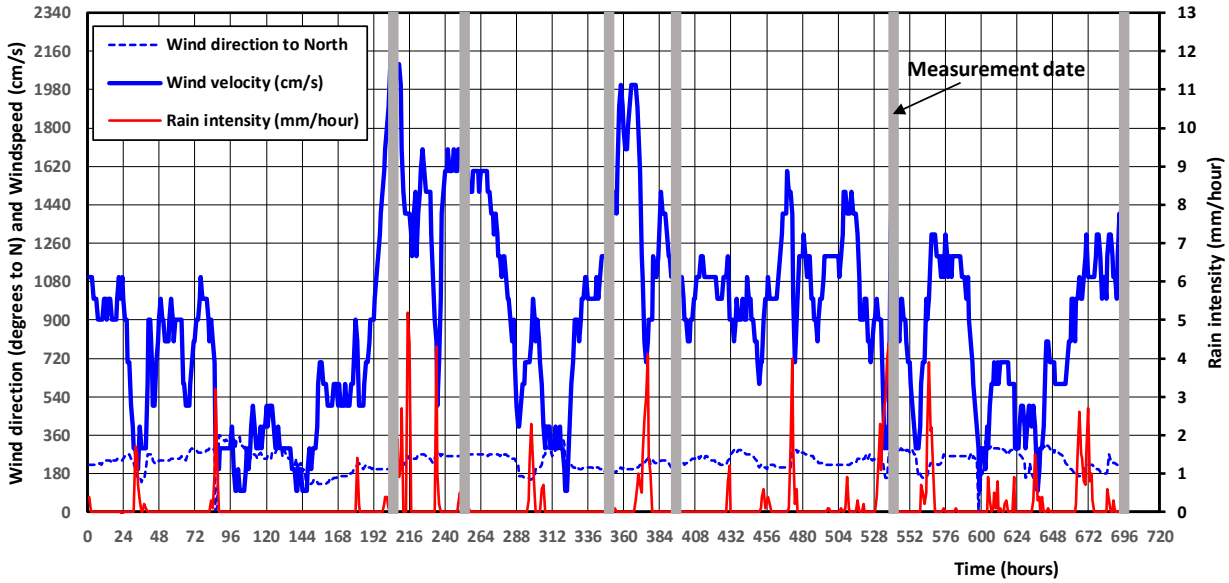

BF6: 1080-1380 cm/s; BF7: 1390-1710 cm/s; BF8: 1720-2070 cm/s; BF9: 2080-2440 cm/s

Figure 6.3.1 *Wind speed, wind direction (at height of 10 m) and rainfall intensity during the month February 2020; weather station De Kooy, The Netherlands*

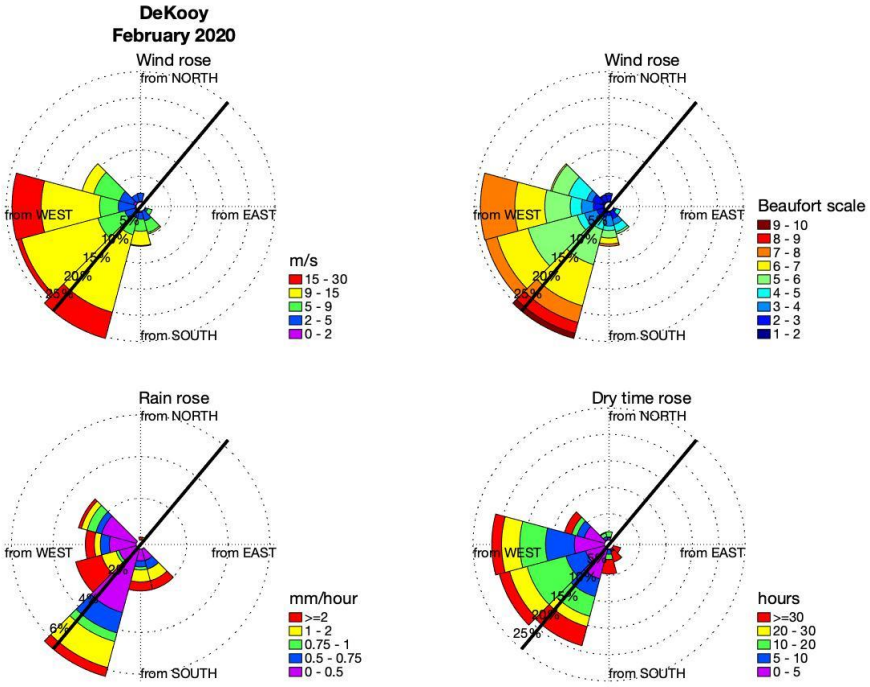

Figure 6.3.2 *Upper: Wind (m/s and beaufort scale),*
Lower: Rain rose (mm/hour) and dry time with no rain (hours)
February 2020; weather station De Kooy near Callantsoog, The Netherlands

De Kooy February 2020						
wind class->	0-2 m/s	2-5 m/s	5-9 m/s	9-15 m/s	>15 m/s	total
hours wind						
0-30	5.00	-	-	-	-	5.00
30-60	-	-	-	-	-	-
60-90	-	-	-	-	-	-
90-120	5.00	-	-	-	-	5.00
120-150	9.00	5.00	8.00	-	-	22.00
150-180	9.00	18.00	17.00	10.00	-	54.00
180-210	7.00	5.00	24.00	59.00	28.00	123.00
210-240	10.00	11.00	45.00	106.00	5.00	177.00
240-270	17.00	20.00	47.00	81.00	28.00	193.00
270-300	14.00	10.00	52.00	20.00	-	96.00
300-330	12.00	5.00	5.00	-	-	22.00
330-360	12.00	5.00	-	-	-	17.00
total	**100.00**	**79.00**	**198.00**	**276.00**	**61.00**	**714.00**
hours rain						
0-30	1.50	-	-	-	-	1.50
30-60	-	-	-	-	-	-
60-90	-	-	-	-	-	-
90-120	-	-	-	-	-	-
120-150	0.60	-	2.00	-	-	2.60
150-180	5.00	3.20	4.80	5.90	-	18.90
180-210	1.90	-	2.00	8.10	7.70	19.70
210-240	-	0.70	7.20	15.80	1.40	25.10
240-270	0.90	1.10	4.40	3.50	1.30	11.20
270-300	1.40	1.20	4.10	2.40	-	9.10
300-330	0.50	-	0.50	-	-	1.00
330-360	-	-	-	-	-	-
total	**11.80**	**6.20**	**25.00**	**35.70**	**10.40**	**89.10**
mm rain						
0-30	4.50	-	-	-	-	4.50
30-60	-	-	-	-	-	-
60-90	-	-	-	-	-	-
90-120	-	-	-	-	-	-
120-150	0.20	-	3.60	-	-	3.80
150-180	10.20	5.00	4.20	8.90	-	28.30
180-210	1.80	-	1.00	10.20	7.80	20.80
210-240	-	0.20	13.00	19.50	3.40	36.10
240-270	0.30	1.70	9.30	11.50	0.70	23.50
270-300	0.80	4.70	8.80	6.00	-	20.30
300-330	0.90	-	1.00	-	-	1.90
330-360	-	-	-	-	-	-
total	**18.70**	**11.60**	**40.90**	**56.10**	**11.90**	**139.20**
Dry > 30 hours						
0-30	-	-	-	-	-	-
30-60	-	-	-	-	-	-
60-90	-	-	-	-	-	-
90-120	1.00	-	-	-	-	1.00
120-150	6.00	4.00	6.00	-	-	16.00
150-180	1.00	10.00	10.00	-	-	21.00
180-210	3.00	-	3.00	17.00	-	23.00
210-240	5.00	2.00	-	3.00	-	10.00
240-270	6.00	7.00	1.00	-	-	14.00
270-300	5.00	2.00	5.00	3.00	-	15.00
300-330	-	-	-	-	-	-
330-360	-	-	-	-	-	-
total	**27.00**	**25.00**	**25.00**	**23.00**	**-**	**100.00**
Dry > 5 hours						
0-30	1.00	-	-	-	-	1.00
30-60	-	-	-	-	-	-
60-90	-	-	-	-	-	-
90-120	1.00	-	-	-	-	1.00
120-150	6.00	4.00	6.00	-	-	16.00
150-180	4.00	14.00	11.00	4.00	-	33.00
180-210	5.00	-	17.00	39.00	9.00	70.00
210-240	10.00	8.00	32.00	38.00	-	88.00
240-270	15.00	16.00	33.00	51.00	16.00	131.00
270-300	8.00	6.00	17.00	4.00	-	35.00
300-330	9.00	-	-	-	-	9.00
330-360	8.00	3.00	-	-	-	11.00
total	**67.00**	**51.00**	**116.00**	**136.00**	**25.00**	**395.00**

Table 6.3.1 *Data of wind speed, wind direction, rain intensity; duration of rain and dry periods; February 2020; weather station De Kooy near Callantsoog, The Netherlands*

9 February 2020

The winter storm Ciara attacked the Dutch coast on 9 February 2020. The wind strength was as follows:

- BF 7 to 8 between 6.00 to 10.00 hrs;
- BF 9 between 10.00 to 16.00 hrs;
- BF 9 to 8 between 16.00 to 20.00 hrs;
- BF 8 to 7 between 20 and 24 hrs.

Figure 6.3.3 *Wind transport at the beach of Callantsoog; storm Ciara; BF 9 to 10; 9 February 2020*

Wind transport measurements were done on 9 February 2020 between 11.00 and 14.00 hrs during the peak of the storm (see grey line, Figure 6.3.2). The wind direction was almost parallel to the beach (no supply-limitation). The total beach width was about 70 m. The beach slope was about 1 to 25. The beach sand was d_{50}= 0.23 mm and d_{90}= 0.45 mm. The measurements were done at about 30 to 40 m from the waterline where the moisture content of the upper 20 mm was measured to be 2.2%. As the sand surface was flat, no dry sand could accumulate in local depressions.
The detailed conditions are given in **Table 6.3.3A,B,C**. One minute-averaged wind velocities were in the range of 17 to 20 m/s (repeated three times). The wind velocity was always measured within 1 m of the trap location. Dry sand was transported close to the moist surface in a transport layer of about 30 cm high and was particularly intensive during high-velocity wind gusts, see **Figure 6.3.3**.
Sand transport was measured by using two bag-type traps, see **Figure 6.3.3**. The rectangular big trap was lying on the sand surface and was filled in about 3 minutes (about 3 kg). The smaller tube-type traps was at about 20 cm above the sand surface. Detailed values are given in **Table 6.3.3A,B,C.** The wind transport was about 0.4 kg/m/s during the peak of the storm which lasted for about 6 hours. Using a beach width of 70 m and storm duration of 6 hours, the total sand transport passing over the beach is about 0.4x70x6x3600≅600,000 kg or 380 m³.

11 February 2020

A second storm attacked the coast of Callantsoog at 11 February 2020. During this event, the wind attacked the beach under an angle of 20°. The beach width was only 10 to 20 m due to high tide (tidal range ≅1.5 m) and storm setup ≅1 m). The beach was wet due to rainfall, which ended at about 11.00 hrs. The weather was dry up to about 18.00 hrs with moisture levels of 4% to 5%. Despite a wind force of BF 7 to 8 with wind velocities in the range of 10 to 12 m/s at about 1.5 m above the sand surface, there was no sand transport in the period with dry weather due supply-limited and transport-limited conditions. After 5 hours, the sand at the dune top (about 10 m above the beach with a wind velocity as high as 16.5 m/s) was dry again resulting in wind-included transport at the dune top. The sand at the beach with lower wind speed was still wet. One sand transport measurement was done at the dune foot which is at 3 m above the lower beach, see **Figure 6.3.4**. The measured sand transport over 22 minutes was extremely low (1 g/m/s; **Table 6.3.3A,B,C**). The wind velocity was about 8 m/s at 1.15 m above surface at the dune foot location. The wind velocity close to the top of the dune was measured to be about 16.5 m/s. The wind velocities at the dune foot location are much smaller (factor 2) due to pressure buildup necessary to divert the streamlines away from the dune foot location over the dune crest

Figure 6.3.4. *Wind transport at the dune foot of Callantsoog, storm BF 7 to 8; 11 February 2020*

16 February 2020

A third storm (Dennis) occurred on 15 and 16 February 2020 with wind speeds up to 14 m/s (BF6 to 8). The wind was almost parallel to the beach and the water setup was about 1 m resulting in a beach width of about 50 m during low tide and 20 m during high tide. The middle and upper beach was wet on 15 February at most places due to the high water levels at previous days. Hard moist patches with a dark grey color (70% of the beach surface) and relatively dry patches with a light grey color (30% of beach surface) were present, see **Figure 6.3.5**. The moisture content of the hard patches was about 10%; the moisture content of the relatively dry patches was only 1%. Sand transport measurements were done on 15 February (BF6) during dry weather and one-minute-averaged wind velocities up to 9 m/s (maximum wind speed= 13 m/s). Sand transport was intense during wind gusts over a hard, moist beach surface (**Table 6.3.3A,B,C**). Most sand was moving is a transport layer of about 10 cm high. The sand trapped in the bags had a moisture content of 0.5 to 1%.

On 16 February at 11.00 hrs the wind strength was about BF8 and mostly parallel to the beach. Sand transport was intense over the hard, flat and wet beach surface. Sand transport continued during intense rainfall (many showers). When sand is moving during conditions with strong winds (> BF7) parallel to the beach, the transport process continues during intense rainfall. The wind strength dropped in the afternoon at 15 hrs to about BF5/6. The beach was very wet with mc=24% near the HW line to about 10% at the dune foot (at 40 m from the HW line) due to previous inundation and rainfall processes. Sand transport was absent during these conditions, see **Figure 6.3.6**. When the beach is very wet with mc-values above 10%, sand transport cannot be initiated, not even by very strong winds of BF8. Most likely, the process is initiated after a few hours of drying processes by strong parallel winds attacking the dune foot and dune front where the mc-levels are relatively low (5% to 10%). Supply-limitation processes seem to be are absent during conditions with strong parallel winds (>BF7).

Figure 6.3.5 *Wind transport at beach Callantsoog; storm BF 6 to 7; 15 February 2020; sand transport during wind gusts (upper); measuring setup (lower)*

Figure 6.3.6 *Wind transport at beach Callantsoog; post-storm BF 5; 16 February 2020; very wet beach; no sand transport*

22 February 2020

A minor fourth storm hit the beach of Callantsoog on 22 and 23 February 2020. The wind strength was about BF7 to 8 under an angle of about 45° to the beach. The beach width was about 45 m at low water. The lower beach (width of about 15 m) was almost flat and very wet (mc=8 to 15%). The upper beach (width of about 30 m) was very irregular with ripple type features due to erosion holes behind debris and plant rests (see **Figure 6.3.7**). Lighter and darker colors can be observed. The lighter colors indicate patches of sand with relatively low moisture levels (about 3%) deposited in the lee of the irregularities. As the incoming wind was oblique to the beach, the fetch length of the upper beach was about 50 m. No sand transport was observed at the wet lower beach. During stronger wind gusts with increasing wind speeds from about 8 to 12 m/s (at about 1.5 above the surface), sand was eroded from the lee areas behind the ripple type features on the upper beach and transported towards the dune foot area. Sand transport was maximum during a rain shower with wind gusts up to 14 m/s (**Figure 6.3.8**). The sand transport process was not slowed down over the wet surface. The wind speed dropped significantly to BF 5/6 after the end of the rain shower event. No sand transport was measured as the wind speed of BF 5 to 6 was not able to produce sand particle movement (no rolling, sliding, saltation). Detailed data are given in **Table 6.3.3A,B,C**.

Figure 6.3.7 *Sand transport measurement at the upper beach near the dune foot of Callantsoog; BF7 to 8; 22 February 2020*

Figure 6.3.8 *Sand transport measurement at the upper beach near the dune foot of Callantsoog; BF 8; 22 February 2020*

29 February 2020

A minor fifth storm hit the beach of Callantsoog on 29 February 2020. The wind strength was about BF7 almost parallel to the beach. The beach width was about 45 m at low water. The lower beach (width of about 15 m) was almost flat and very wet (mc=8 to 15%). The upper beach (width of about 30 to 40 m) was flat with alternating dark (wetter) and light (drier) spots. Sand is eroded at the upper beach during strong wind gusts and spread out by large-scale vortices (turbulence) over the full width of the beach down to the water line. Sand transport continued during light rain when the sand surface was wet. The measuring setup (during light rain) is shown in **Figure 6.3.9**. Erosion patterns around shells were present at some places of the upper beach, see **Figure 6.3.10**. Sand transport was occurring at the drier upper beach with moisture levels of 1% to 3%, but also along the hard, wet lower beach. Detailed data are given in **Table 6.3.3A,B,C**.

Figure 6.3.9 *Measuring setup on 29 February, Callantsoog, The Netherlands*

Figure 6.3.10 *Erosion around shells, Callantsoog, 28 February 2020*

Location Date Duration	Beach		Moisture (%)			Wind conditions		Wind transport (g/m/s) in layers (mm) and test duration (s)
	d_{50};d_{90} (mm) p_{shell}	Description	upper 5mm	upper 20mm	p_m (%)	height (m) and velocity (m/s)	direction and fetch length (m)	
Callantsoog 9 February 2020; dry Te= 8° C BF9	0.23; 0.4 <3%	flat middle beach; no irregularities	2% 10 hrs alr	2% 10 hrs alr	80%	z=0.55; u= 16.0±1.5 z=0.84; u= 17.0±1.5 z=1.43; u= 18.7±1.5 u_*=1.14 m/s (R^2>0.9) k_s=60 mm	almost parallel FL> 500 (no SL; no TL)	layer 0-71: 260/285 layer 71-215: 100 layer 215-246: 40 total: 410/425 (mt=240s)
Callantsoog 9 February 2020; dry Te= 8° C BF9	0.23; 0.4 <3%	flat middle beach; no irregularities	2% 10 hrs alr	2% 10 hrs alr	80%	z=0.55; u= 16.0±1.5 z=0.84; u= 17.5±1.5 z=1.43; u= 19.0±1.5 u_*=1.12 m/s (R^2>0.9) k_s=50 mm	almost parallel FL> 500 (no SL; no TL)	layer 0-71: 295 layer 71-215: 100 layer 215-246: 40 total: 435 (mt=150 s)
Callantsoog 11 February 2020; dry Te= 5° C BF7 to 8	0.23; 0.4 <3%	dune foot; flat surface upwind	4.0% 5 hrs alr	4.0% 5 hrs alr	100 %	z=0.25; u=6.5 ±0.5 z=0.55; u=7.2 ±0.5 z=1.15; u=7.7 ±0.5 u_*=0.32 m/s (R^2>0.9) k_s=2 mm	angle=20° to shore normal; FL= 10 (SL; TL)	layer 0-71: 1 g/m/s (mt=1320 s)
Callantsoog 15 February 2020 Te=12° C dry BF6 to 7	0.23; 0.4 <3%	flat middle beach; ripples (0-30 mm) at some hard patches	same	17% at hp 1% at dp; 10 hrs alr	70% (hp)	z=0.25; u=7.5 ±0.5 z=0.55; u=8.1 ±0.5 z=1.13; u=9.5 ±0.5 u_*=0.52 m/s (R^2>0.9) k_s=28 mm	almost parallel FL> 500 (no SL; no TL)	layer 0-71: 35 layer 71-104: 7 layer 104-136: 3 total: 45 (mt=600 s) (mc= 0.5-1%)
Callantsoog 15 F 2020 Te=12° C dry BF6 to 7	0.23; 0.4 <3%	flat middle beach ripples (0-20 mm) at some hard patches	same	17% at hp 1% at dp; 10 hrs alr	70% (hp)	z=0.25; u=8 ±0.7 z=0.55; u=9 ±0.7 z=1.13; u=10.5 ±0.7 u_*=0.66 m/s (R^2>0.9) k_s=62 mm	almost parallel FL> 500 (no SL; no TL)	layer 0-71: 48 layer 71-104: 9 layer 104-136: 3 total: 60 (mt=600 s) (mc=0.5-1%)
Callantsoog 16 F 2020; 11.00 hrs; Te=10° dry/rainy BF8	0.23; 0.4 <3%	flat upper beach; hard, wet surface	same	15%; HW line 8% dune foot	90% (hp)	BF 8; velocities not measured	almost parallel FL> 500 (no SL)	continuous sand transport (nm); also during intense rainfall showers (transport not measured)
Callantsoog 16 F 2020; at 15.00 hrs Te=10° C very rainy BF5 to 6	0.23; 0.4 <3%	flat upper beach; hard moist surface (width 40 m at 2 hours after HW); setup= 1 m	same	24%; HWline 23%; 8m HW 19%; 16m HW 12%; 24m HW 11%; 32m HW 9%; 40 m HW (4 hours of intense rain)	100 % (hp)	z=1.48; u=7 ±0.5 z=0.85; u=6.3 ±0.5 z=0.35; u=5.5 ±0.5 u_*=0.41 m/s (R^2>0.9) k_s= 50 mm	almost parallel; angle=70° to normal FL> 500 (no SL)	no sand transport due high moisture content (4 hours rain)

BF=Beaufort wind scale; p_{shell}= percentage shells at beach surface; alr=after last rainfall;
FL= fetch length; SL= supply limitation; TL= transport limitation; hp= hard moist patches; dp=relatively dry patches
p_m= percentage of beach surface with moist appearance at measurement location; z= height above bed; u= wind velocity at height z; mt=measuring time sand transport; mc= moisture content; nm=not measured

Table 6.3.3A *Wind transport data at beaches of Callantsoog and Lemmer, The Netherlands, February 2020*

Location Date Duration	Beach		Moisture (%)			Wind conditions		Wind transport (g/m/s) in layers (mm) and test duration (s)
	d_{50};d_{90} (mm) p_{shell} (%)	Description	upper 5mm	upper 20mm	p_m (%)	height (m) and velocity (m/s)	direction and fetch length (m)	
Callantsoog 20 February dry; 10° C BF7 to 8	0.23; 0.4 <3%	flat middle beach	nm	nm 1 hour after last rainfall	50%	nm	almost parallel FL> 500 (no SL; TL)	intense sand transport (nm)
Callantsoog 21 February dry; 10° C BF 5 to 7	0.23; 0.4 <3%	flat middle beach	nm	nm 12 hours after last rainfall	25%	nm	oblique under 45° FL> 50 (SL; TL)	BF5: transport only at dunefoot BF 6 to 7: limited sand transport from waterline to dunes under angle of 45° (nm)
Callantsoog 22 February dry; 10° C BF 7/8	0.23; 0.4 <3%	upper beach near dune toe; veru irregular surface 0.01-0.2	nm	3.3% 4 hours after last rainfall	50%	z=1.48; u=11 ±1 z=0.85; u=9.5 ±1 z=0.55; u=9 ±1 u_*=0.82 m/s(R^2>0.9) k_s= 230 mm	oblique under angle 45° FL=50 (SL)	layer 0-71: 47 layer 71-105: 9 layer 105-136: 4 total: 60 g/m/s (mt=300 s) (mc<1%)
Callantsoog 22 February dry; 10° C BF 7/8	0.23; 0.4 <3%	upper beach near dune toe; very irregular surface 0.01-0.2	nm	3% 4 hours after last rainfall	50%	z=1.48; u=10 ±1 z=0.85; u=8.9 ±1 z=0.55; u=8.0 ±1 u_*=0.76 m/s (R^2>0.9) k_s= 225 mm	oblique under angle 45° FL=50 (SL)	layer 0-71: 27 layer 71-105: 6 layer 105-136: 2 total: 35 g/m/s (mt=480 s) (mc<1%)
Callantsoog 22 February rainy; 10° C BF 8	0.23; 0.4 <3%	upper beach near dune toe; very irregular surface 0.01-0.2	8%	5% during rainfall	100 %	z=1.48; u=13 ±1 z=0.85; u=11.9 ±1 z=0.55; u=10.7 ±1 u_*=0.92 m/s (R^2>0.9) k_s= 150 mm	oblique under angle 45° FL=50 (SL)	layer 0-71: 93 layer 71-105: 10 layer 105-136: 7 total: 110 g/m/s (mt=360 s) (mc<1%)
Callantsoog 22 February dry; 10° C BF 5/6	0.23; 0.4 <3%	upper beach near dune toe; very irregular surface 0.01-0.2	9%	5.5% 30 min after rainfall	100 %	z=1.48; u=6 ±0.5 z=0.85; u=5.3 ±0.5 z=0.55; u=5.0 ±0.5 u_*=0.41 m/s (R^2>0.95) k_s= 135 mm	oblique under angle 45° FL=50 (SL; TL)	layer 0-71: <1 g/m/s (almost no sand transport)
Callantsoog 24 February rain; 10° C BF 7	0.23; 0.4 <3%	upper beach	10-12%	9-12% during continuous rainfall over 6 hours (2 to 3 mm/hour)	100 %	nm	parallel	no transport (nm)
Callantsoog 26 February dry; 10° C BF 4	0.23; 0.4 <3%	upper beach	nm	4%; 2 hours after last rainfall	20%	nm	cross	no transport (nm)

BF=Beaufort wind scale; p_{shell}= percentage shells at beach surface; alr=after last rainfall;
FL= fetch length; SL= supply limitation; TL= transport limitation; hp= hard moist patches; dp=relatively dry patches
p_m= percentage of beach surface with moist appearance at measurement location; z= height above bed; u= wind velocity at height z; mt=measuring time sand transport; mc= moisture content; nm=not measured

Table 6.3.3B *Wind transport data at beaches of Callantsoog and Lemmer, The Netherlands; February 2020*

Location Date Duration	Beach		Moisture (%)			Wind conditions		Wind transport (g/m/s) in layers (mm) and test duration (s)
	d_{50};d_{90} (mm) p_{shell} (%)	Description	upper 5mm	upper 20mm	p_m (%)	height (m) and velocity (m/s)	direction and fetch length (m)	
Callantsoog 26 February dry; 10° C BF 4	0.23; 0.4 <3%	upper beach	nm	4%; 3 hours after last rainfall	50%	nm	cross	no transport (nm)
Callantsoog 28 February dry; 10° C BF 6	0.23; 0.4 <3%	upper beach	nm	4%; 3 hours after last rainfall	70%	nm	parallel	minor transport (nm)
Callantsoog 29 February 11.00 hrs dry; 10° C BF 5	0.23; 0.4 <3%	upper flat beach at 15 m from waterline	nm	1.5% at dark spots to 2.2 at white spots; 5 hours after last rainfall	50%	z=1.28; u=6.6 ±0.5 z=0.65; u=6.1 ±0.5 z=0.35; u=5.4 ±0.5 u_*=0.4 m/s (R^2>0.9) k_s= 45 mm	parallel FL=100	layer 0-71: 6 g/m/s (20 min)
Callantsoog 29 February 12.00 hrs dry; 10° C BF 5	0.23; 0.4 <3%	upper flat beach at 15 m from waterline	nm	1% to 2%; 6 hours after last rainfall (loose mobile sand at white spots)	30%	z=1.28; u=6.5 ±0.5 z=0.65; u=6.0 ±0.5 z=0.35; u=5.2 ±0.5 u_*=0.4 m/s (R^2>0.9) k_s= 50 mm	parallel FL>500	layer 0-71: 5.1 g/m/s (17 min)
Callantsoog 29 February 12.30 hrs dry; 10° C BF 5	0.23; 0.4 <3%	lower flat, hard beach at 15 m from waterline	nm	1% to 2% at upper beach; 10% at lower beach; 6 hours after last rainfall	30%	z=1.28; u=6.5 ±0.5 z=0.65; u=6.0 ±0.5 z=0.35; u=5.2 ±0.5 u_*=0.4 m/s (R^2>0.9) k_s= 50 mm	parallel FL>500	layer 0-71: 5.9 g/m/s (15 min)
Callantsoog 29 February 13.00 hrs rainy; 10° C BF 6/7	0.23; 0.4 <3%	upper flat beach	nm	4.7% at upper beach during light rain	100 0%	z=1.28; u=8.9 ±0.5 z=0.65; u=8.6 ±0.5 z=0.35; u=7.5 ±0.5 u_*=0.43 m/s (R^2>0.9) k_s= 8 mm	parallel FL>500	layer 0-71: 27 g/m/s (15 min)
Callantsoog 29 February 14.00 hrs rainy; 10° C BF 7	0.23; 0.4 <3%	upper flat beach; 20 m from water line	nm	4.5% at upper beach during light rain	100 0%	z=1.28; u=11.3 ±0.5 z=0.65; u=10.2 ±0.5 z=0.35; u=9.0 ±0.5 u_*=0.71 m/s (R^2>0.9) k_s= 63 mm	parallel FL>500	layer 0-71: 98 g/m/s layer 71-142: 13 total: 101 g/m/s (5 and 10 min)

BF=Beaufort wind scale; p_{shell}= percentage shells at beach surface; alr=after last rainfall;
FL= fetch length; SL= supply limitation; TL= transport limitation; hp= hard moist patches; dp=relatively dry patches
p_m= percentage of beach surface with moist appearance at measurement location; z= height above bed; u= wind velocity at height z; mt=measuring time sand transport; mc= moisture content; nm=not measured

Table 6.3.3C *Wind transport data at beaches of Callantsoog, The Netherlands; February 2020*

6.3.2 Months of April 2020 to April 2021

13 April 2020

The beach of Callantsoog is situated near the naval base town of Den Helder in the north of the province of North -Holland. The beach width is about 50 to 80 m and consists of medium fine sand (d_{10}=0.17 mm; d_{50}=0.23 mm; d_{90}=0.4 mm; p_{coarse}<3%). Many beach restaurants (at spacing of 300 to 500 m) on wooden piles are situated at the upper dry beach close to the dune foot. The surface of the upper beach is rather irregular due to depositional features in the lee of the structures, shell clusters and debris. During conditions with wind flow parallel to the beach, the wind flow along the beach is severely disturbed (macro-scale turbulence) resulting in relatively large shear velocities and roughness values (> 100 mm).

A strong wind from North with BF5 to 6 almost parallel to the beach was blowing on Monday 13 April 2020 during falling tide. The total beach width was about 40 to 50 m. Transport measurements were done on the dry upper beach at about 5 to 15 m from the water line and on the wet intertidal beach at about 5 to 10 m from the water line. The surface of the dry upper beach was covered with small-scale ripples with height of about 20 mm and length of about 200 mm, see **Figure 6.3.11**. The top layer of the upper beach was dry and loose over a depth of about 30 mm; the subsoil beyond this layer was moist. The time period since the last rainfall was at least 10 days. Sand transport was initiated at a wind velocity of about 6 m/s. Sand eroded from the upper dry beach was carried to the wet intertidal beach by turbulent vortices (cross-shore exchange processes) resulting in intense transport of dry sand over the flat, hard surface. The sand transport rate at the intertidal beach was about 25% to 50% higher than at the dry upper beach where the sand flow was retarded somewhat by the friction over the ripples, which was also observed by Davidson-Arnott et al. (2008). Details are given in **Table 6.3.3D**.

Figure 6.3.11 *Measuring setup on 13 April, Callantsoog, The Netherlands*

Location Date Duration	Beach		Moisture (%)			Wind conditions		Wind transport (g/m/s) in layers (mm) and test duration (s)
	d_{50};d_{90} (mm) p_{shell} (%)	Description	upper 5mm	upper 20mm	p_m (%)	height (m) and velocity (m/s)	direction and fetch length (m)	
Callantsoog 13 April 10.10 hrs; dry; 8° C BF 5 to 6	0.23; 0.4 <1%	upper dry beach 7 m waterline	<0.5%	<0.5%; 10 days after last rainfall	0%	z=1.25; u=8.0 ±0.5 z=0.60; u=6.2 ±0.5 z=0.30; u=5.0 ±0.5 u_*=0.79 m/s; k_s= 700 mm (R^2>0.95)	parallel FL>500	layer 0-71: 12 layer 71-100: 3 layer 100-135: 1 Total: 16 g/m/s (mt=900 s)
Callantsoog 13 April 10.28 hrs; dry; 8° C BF 5 to 6	0.23; 0.4 <1%	upper dry beach 8 m waterline	<0.5%	<0.5%; 10 days after last rainfall	0%	z=1.25; u=9.0 ±0.5 z=0.60; u=7.3 ±0.5 z=0.30; u=5.9 ±0.5 u_*=0.87 m/s; k_s= 600 mm (R^2>0.95)	parallel FL>500	layer 0-71: 21 layer 71-100: 3 layer 100-135: 1 Total: 25 g/m/s (mt=900 s)
Callantsoog 13 April 10.45 hrs; dry; 8° C BF 5 to 6	0.23; 0.4 <1%	upper dry beach 10 m waterline	<0.5%	<0.5%; 10 days after last rainfall	0%	z=1.27; u=8.3 ±0.5 z=0.62; u=7.0 ±0.5 z=0.32; u=6.0 ±0.5 u_*=0.67 m/s; k_s= 270 mm (R^2>0.95)	parallel FL>500	layer 0-71: 16 layer 71-100: 3 layer 100-135: 1 Total: 20 g/m/s (mt=900 s)
Callantsoog 13 April 11.03 hrs; dry; 8° C BF 5 to 6	0.23; 0.4 <1%	upper dry beach 10 m waterline	<0.5%	<0.5%; 10 days after last rainfall	0%	z=1.18; u=7.0 ±0.5 z=0.53; u=5.5 ±0.5 z=0.23; u=4.5 ±0.5 u_*=0.61 m/s; k_s= 400 mm (R^2>0.95)	parallel FL>500	layer 0-71: 8 layer 71-100: 1.5 layer 100-135: 0.5 Total: 10 g/m/s (mt=900 s)
Callantsoog 13 April 11.20 hrs; dry; 8° C BF 5 to 6	0.23; 0.4 <1%	lower wet intertidal beach 5 m waterline	5-8%	8-10%;	100 %	z=1.25; u=8.5 ±0.5 z=0.6; u=6.8 ±0.5 z=0.3; u=5.3 ±0.5 u_*=0.9 m/s; k_s= 840 mm (R^2>0.95)	parallel FL>500	layer 0-71: 28 layer 71-100: 3 layer 100-135: 1 Total: 32 g/m/s (mt=900 s)
Callantsoog 13 April 11.45 hrs; dry; 8° C BF 5 to 6	0.23; 0.4 <1%	upper dry beach 12 m waterline	<0.5%	<0.5%; 10 days after last rainfall	0%	z=1.22; u=8.1 ±0.5 z=0.57; u=7.5 ±0.5 z=0.27; u=5.5 ±0.5 u_*=0.69 m/s; k_s= 300 mm (R^2>0.95)	parallel FL>500	layer 0-71: 16 layer 71-100: 3 layer 100-135: 1 Total: 20 g/m/s (my=900 s)
Callantsoog 13 April 12.05 hrs; dry; 8° C BF 5 to 6	0.23; 0.4 <1%	lower wet intertidal beach 5 m waterline	5-8%	8-10%;	100 %	z=1.22; u=8.6 ±1.0 z=0.57; u=7.0 ±0.7 z=0.27; u=5.5 ±0.5 u_*=0.82 m/s; k_s= 550 mm (R^2>0.95);	parallel FL>500	layer 0-71: 24 layer 71-100: 3 layer 100-135: 1 Total: 28 g/m/s (mt=900 s)
Callantsoog 13 April 12.25 hrs; dry; 8° C BF 5 to 6	0.23; 0.4 <1%	upper dry beach 12 m waterline	<0.5%	<0.5%; 10 days after last rainfall	0%	z=1.22; u=7.1 ±0.8 z=0.57; u=5.7 ±0.6 z=0.27; u=4.5 ±0.5 u_*=0.69 m/s; k_s= 600 mm (R^2>0.95)	parallel FL>500	layer 0-71: 11 layer 71-100: 1.5 layer 100-135: 0.5 Total: 13 g/m/s (mt=900 s)

BF=Beaufort wind scale; p_{shell}= percentage shells at beach surface; alr=after last rainfall;
FL= fetch length; SL= supply limitation; TL= transport limitation; hp= hard moist patches; dp=relatively dry patches
p_m= percentage of beach surface with moist appearance at measurement location; z= height above bed; u= wind velocity at height z; mt=measuring time sand transport; mc= moisture content; nm=not measured

Table 6.3.3D *Wind transport data at beach of Callantsoog, The Netherlands; 13 April 2020*

24 October 2020

The wind strength was mild (BF5 to 6) from southwest and almost parallel to the beach (d_{10}=0.17 mm; d_{50}=0.23 mm; d_{90}=0.4 mm; p_{coarse}<2%). The measurements were done between 14.00 and 16.30 hours during dry weather (temperature of 14 to 15 °C) at the upper beach about 30 m from the dune foot line and about 40 m from the waterline, see **Figures 6.3.12** and **6.3.13**. The time period since the last rainfall was about 5 hours before the start of the measurements. The fetch length was > 500 m (wind parallel to beach). The beach width was about 70 m. The beach surface was almost flat with about 60% dry spots (moist percentage<1%) and 40% moist spots (moist percentage 3% to 5%), see **Figure 6.3.12**. At low wind velocities of 6.5 to 7 m/s at 1.25 m above the surface, only rolling sand transport was observed. The threshold wind velocity was observed to be about 6 m/s at 1.25 m above the surface. The thickness of the transport layer was smaller than 70 mm. The data are given in **Table 6.3.3E**.

Figure 6.3.12 *Measurement setup, upper beach Callantsoog, 24 October 2020 (dry spots are lighter; moist spots are darker)*

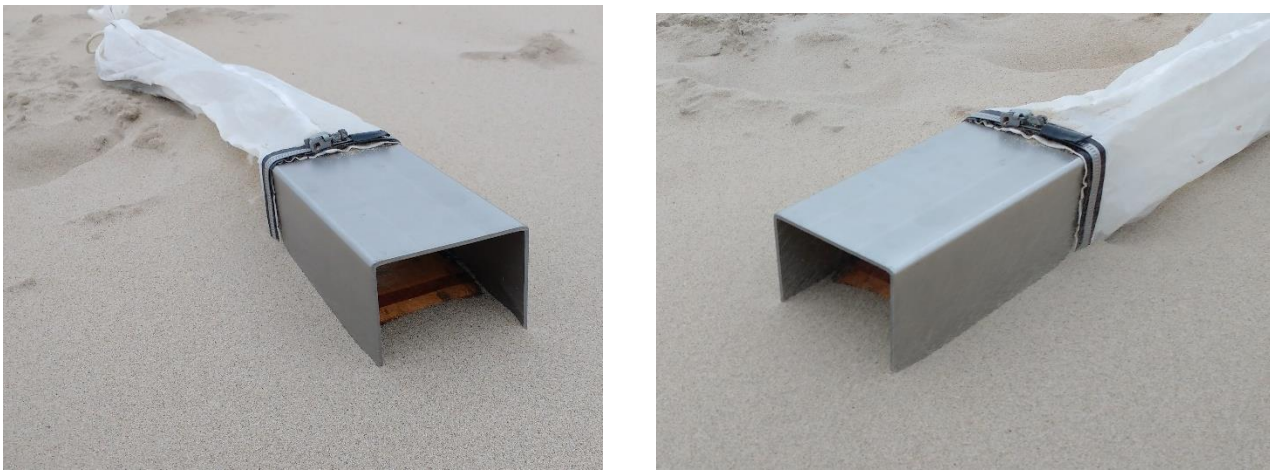

Figure 6.3.13 *Details of sampler mouth, Callantsoog 24 October 2020 (no scour at wind strength BF6)*

Location Date Duration	Beach		Moisture (%)			Wind conditions		Wind transport (g/m/s) in layers (mm) and test duration (s)
	d_{50};d_{90} (mm) p_{shell} (%)	Description	upper 5mm	upper 20mm	p_m (%)	height (m) and velocity (m/s)	direction and fetch length (m)	
Callantsoog 24 Oct 14.15 hrs; dry; 15° C BF 6	0.23; 0.4 <1%	upper dry beach 40 m to waterline	<5%	<5%; 5 hours after last rainfall	50%	z=1.25; u=8.9 ±0.5 z=0.60; u=7.6 ±0.5 z=0.30; u=6.8 ±0.5 u_*=0.59 m/s; k_s= 90 mm (R^2>0.95)	parallel FL>500	layer 0-71: 20 (mt=600 s)
Callantsoog 24 Oct 14.3 hrs; dry; 15° C BF 6	0.23; 0.4 <1%	upper dry beach 40 m to waterline	<5%	<5%; 5 hours after last rainfall	50%	z=1.25; u=9.1 ±0.5 z=0.60; u=8.1 ±0.5 z=0.30; u=7.1 ±0.5 u_*=0.56 m/s; k_s= 55 mm (R^2>0.95)	parallel FL>500	layer 0-71: 25 (mt=600 s)
Callantsoog 24 Oct 14.40 hrs; dry; 15° C BF 6	0.23; 0.4 <1%	upper dry beach 40 m to waterline	<5%	<5%; 5 hours after last rainfall	50%	z=1.25; u=8.1 ±0.5 z=0.60; u=7.5 ±0.5 z=0.30; u=6.1 ±0.5 u_*=0.56 m/s; k_s= 90 mm (R^2>0.95)	parallel FL>500	layer 0-71: 22 (mt=300 s)
Callantsoog 24 Oct 14.45 hrs; dry; 15° C BF 6	0.23; 0.4 <1%	upper dry beach 40 m to waterline	<5%	<5%; 5 hours after last rainfall	50%	z=1.25; u=8.2 ±0.5 z=0.60; u=7.3 ±0.5 z=0.30; u=6.1 ±0.5 u_*=0.59 m/s; k_s=135 mm (R^2>0.95)	parallel FL>500	layer 0-71: 24 (mt=600 s)
Callantsoog 24 Oct 14.55 hrs; dry; 15° C BF 6	0.23; 0.4 <1%	upper dry beach 40 m to waterline	<5%	<5%; 5 hours after last rainfall	50%	z=1.25; u=8.1 ±0.5 z=0.60; u=7.2 ±0.5 z=0.30; u=6.1 ±0.5 u_*=0.56 m/s; k_s= 115 mm (R^2>0.95)	parallel FL>500	layer 0-71: 23 (mt=600 s)
Callantsoog 24 Oct 15.10 hrs; dry; 15° C BF 6	0.23; 0.4 <1%	upper dry beach 40 m to waterline	<5%	<5%; 6 hours after last rainfall	50%	z=1.25; u=8.3 ±0.5 z=0.60; u=7.4 ±0.5 z=0.30; u=6.5 ±0.5 u_*=0.51 m/s; k_s= 52 mm (R^2>0.95)	parallel FL>500	layer 0-71: 27 (mt=600 s)
Callantsoog 24 Oct 15.20 hrs; dry; 15° C BF 6	0.23; 0.4 <1%	upper dry beach 40 m to waterline	<5%	<5%; 6 hours after last rainfall	50%	z=1.25; u=8.2 ±0.5 z=0.60; u=7.3 ±0.5 z=0.30; u=6.3 ±0.5 u_*=0.53 m/s; k_s= 80 mm (R^2>0.95)	parallel FL>500	layer 0-71: 25 (mt=600 s)
Callantsoog 24 Oct 15.35 hrs; dry; 15° C BF 5	0.23; 0.4 <1%	upper dry beach 40 m to waterline	<5%	<5%; 6 hours after last rainfall	50%	z=1.25; u=7.0 ±0.3 z=0.60; u=6.0 ±0.3 z=0.30; u=5.3 ±0.3 u_*=0.48 m/s; k_s= 110 mm (R^2>0.95)	parallel FL>500	layer 0-71: 7.4 (mt=360 s) only rolling transport
Callantsoog 24 Oct 15.40 hrs; dry; 15° C BF 5	0.23; 0.4 <1%	upper dry beach 40 m to waterline	<5%	<5%; 6 hours after last rainfall	50%	z=1.25; u=6.9 ±0.3 z=0.60; u=5.9 ±0.3 z=0.30; u=5.2 ±0.3 u_*=0.48 m/s; k_s= 120 mm (R^2>0.95)	parallel FL>500	layer 0-71: 6.4 (mt=600 s) only rolling transport
Callantsoog 24 Oct 15.55 hrs; dry; 15° C BF 5	0.23; 0.4 <1%	upper dry beach 40 m to waterline	<5%	<5%; 6 hours after last rainfall	50%	z=1.25; u=6.8 ±0.3 z=0.60; u=5.8 ±0.3 z=0.30; u=5.1 ±0.3 u_*=0.48 m/s; k_s= 135 mm (R^2>0.95)	parallel FL>500	layer 0-71: 5.6 (mt=720 s) only rolling transport

Callantsoog 24 Oct 16.15 hrs; dry; 15° C BF 5 to 6	0.23; 0.4 <1%	upper dry beach 40 m to waterline	<5%	<5%; 7 hours after last rainfall	50%	z=1.25; u=7.5 ±0.4 z=0.60; u=6.6 ±0.4 z=0.30; u=5.8 ±0.4 u_*=0.48 m/s; k_s= 75 mm (R^2>0.95)	parallel FL>500	layer 0-71: 12 (mt=600 s)

BF=Beaufort wind scale; p_{shell}= percentage shells at beach surface; alr=after last rainfall;
FL= fetch length; SL= supply limitation; TL= transport limitation; hp= hard moist patches; dp=relatively dry patches
p_m= percentage of beach surface with moist appearance at measurement location; z= height above bed; u= wind velocity at height z; mt=measuring time sand transport; mc= moisture content; nm=not measured

Table 6.3.3E *Wind transport data at beach of Callantsoog, The Netherlands; 24 October 2020*

11 March 2021

The wind strength was severe (BF8) from southwest and almost parallel to the beach (d_{10}=0.17 mm; d_{50}=0.23 mm; d_{90}=0.4 mm; p_{coarse}<2%). The measurements were done between 9.30 and 10.3 hours during dry weather (temperature of 8 °C) at the upper beach about 20 m from the dune foot line and about 50 m from the waterline, see **Figure 6.3.14**. The beach was very moist with minor dry spots (10%). The time period since the last rainfall was about 1 to 2 hours before the start of the measurements. It rained again during the last measurement (about 1 hour after the start). The fetch length was > 500 m (wind parallel to beach). The beach width was about 70 m. The beach surface was partly flat and partly covered feature shell-related scour marks (3 cm high deep scour holes around immobile shells). The bed surface consisted of about 10% reasonably dry spots (moist percentage <2%) and 90% moist spots (moist percentage 4% to 8%), see **Figure 6.3.14**. The data are given in **Table 6.3.3F**.

Figure 6.3.14 *Measurement setup, upper beach Callantsoog, 11 March 2021 (Beaufort 8)*

Location Date Duration	Beach		Moisture (%)			Wind conditions		Wind transport (g/m/s) in layers (mm) and test duration (s)
	d_{50};d_{90} (mm) p_{shell} (%)	Description	upper 5mm	upper 20mm	p_m (%)	height (m) and velocity (m/s)	direction and fetch length (m)	
Callantsoog 11 March 21; 9.30 hrs; dry; 8° C; BF 8	0.23; 0.4 <1%	upper beach 50 m to waterline	≅6%	≅4%; 1 hour after last rainfall	90%	z=1.20; u=12.3 ±0.5 z=0.55; u=10.0 ±0.5 z=0.25; u=9.1 ±0.5 u_*=0.84 m/s; k_s= 100 mm (R^2>0.95)	parallel FL>500	layer 0-71: 105 layer 71-150: 20 total: 125 (mt=240 s)
Callantsoog 11 March 21; 9.35 hrs; dry; 8° C; BF 8	0.23; 0.4 <1%	upper beach 50 m to waterline	≅6%	≅4%; 1 hour after last rainfall	90%	z=1.20; u=13 ±0.5 z=0.55; u=10.5 ±0.5 z=0.25; u=9.3 ±0.5 u_*=0.94 m/s; k_s= 160 mm (R^2>0.95)	parallel FL>500	layer 0-71: 110 layer 71-150: 25 total: 135 (mt=300 s)
Callantsoog 11 March 21; 9.40 hrs; dry; 8° C; BF 8	0.23; 0.4 <1%	upper beach 50 m to waterline	≅6%	≅4%; 1 hour after last rainfall	90%	z=1.20; u=12.2 ±0.5 z=0.55; u=10 ±0.5 z=0.25; u=9.1 ±0.5 u_*=0.76 m/s; k_s= 76 mm (R^2>0.95)	parallel FL>500	layer 0-71: 100 layer 71-150: 20 total: 120 (mt=300 s)
Callantsoog 11 March 21; 9.45 hrs; dry; 8° C; BF 8	0.23; 0.4 <1%	upper beach 50 m to waterline	≅6%	≅4%; 1 hour after last rainfall	90%	z=1.20; u=12.5 ±0.5 z=0.55; u=9.8 ±0.5 z=0.25; u=8.5 ±0.5 u_*=1.01 m/s; k_s= 288 mm (R^2>0.95)	parallel FL>500	layer 0-71: 110 layer 71-150: 20 total: 130 (mt=300 s)
Callantsoog 11 March 21; 9.50 hrs; dry; 8° C; BF 8	0.23; 0.4 <1%	upper beach 50 m to waterline	≅6%	≅4%; 1 hour after last rainfall	90%	z=1.20; u=13.3 ±0.5 z=0.55; u=10.3 ±0.5 z=0.25; u=9.0 ±0.5 u_*=1.1 m/s; k_s= 313 mm (R^2>0.95)	parallel FL>500	layer 0-71: 120 layer 71-150: 30 total: 150 (mt=300 s)
Callantsoog 11 March 21; 10.0 hrs; dry; 8° C; BF 8	0.23; 0.4 <1%	upper beach 50 m to waterline	≅6%	≅4%; 1 hour after last rainfall	90%	z=1.20; u=14.2 ±0.7 z=0.55; u=10.8 ±0.7 z=0.25; u= 9.0 ±0.7 u_*=1.32 m/s; k_s= 540 mm (R^2>0.95)	parallel FL>500	layer 0-71: 150 layer 71-150: 35 total: 185 (mt=300 s)
Callantsoog 11 March 21; 10.10 hrs; dry; 8° C; BF 8	0.23; 0.4 <1%	upper beach 50 m to waterline	≅6%	≅4%; 1 hour after last rainfall	90%	z=1.20; u=14.3 ±0.7 z=0.55; u=11.0 ±0.7 z=0.25; u= 9.3 ±0.7 u_*=1.27 m/s; k_s= 440 mm (R^2>0.95)	parallel FL>500	layer 0-71: 135 layer 71-150: 30 total: 165 (mt=300 s)
Callantsoog 11 March 21; 10.15 hrs; dry; 8° C; BF 8	0.23; 0.4 <1%	upper beach 50 m to waterline	≅6%	≅4%; 1 hour after last rainfall	90%	z=1.20; u=15.0 ±0.7 z=0.55; u=11.5 ±0.7 z=0.25; u= 9.3 ±0.7 u_*=1.45 m/s; k_s= 615 mm (R^2>0.95)	parallel FL>500	layer 0-71: 160 layer 71-150: 35 total: 195 (mt=240 s)
Callantsoog 11 March 21; 10.27 hrs; dry; 8° C; BF 8	0.23; 0.4 <1%	upper beach 50 m to waterline	≅6%	≅4%; 1 hour after last rainfall	90%	z=1.20; u=15.0 ±0.7 z=0.55; u=11.5 ±0.7 z=0.25; u= 9.0 ±0.7 u_*=1.53 m/s; k_s= 750 mm (R^2>0.95)	parallel FL>500	layer 0-71: 165 layer 71-150: 35 total: 200 (mt=240 s)
Callantsoog 11 March 21; 10.30 hrs; dry; 8° C; BF 8	0.23; 0.4 <1%	upper beach 50 m to waterline	≅6%	≅4%; moderate rain	100 %	z=1.20; u=14.2 ±0.7 z=0.55; u=11.3 ±0.7 z=0.25; u= 8.9 ±0.7 u_*=1.38 m/s; k_s= 575 mm (R^2>0.95)	parallel FL>500	layer 0-71: 120 layer 71-150: 25 total: 145 (mt=240 s)

BF=Beaufort wind scale; p_{shell}= percentage shells at beach surface; alr=after last rainfall;
FL= fetch length; SL= supply limitation; TL= transport limitation; hp= hard moist patches; dp=relatively dry patches

p_m= percentage of beach surface with moist appearance at measurement location; z= height above bed; u= wind velocity at height z; mt=measuring time sand transport; mc= moisture content; nm=not measured

Table 6.3.3F *Wind transport data at beach of Callantsoog, The Netherlands; 11 March 2021*

6.4 Field measurements at various other beaches in the Netherlands

6.4.1 Lemmer beach

This beach is a small recreational, inland beach with a bay-type shape (d_{10}=0.15 mm, d_{50}=0.3 mm; d_{90}=0.9 mm; $p_{shell+gravel} \cong$8%). The beach width is about 70 m. The beach surface consisted of small ripple-type features (lengths of 10 to 30 cm and heights between 10 and 50 mm), which may have been created by the many beach walkers. Due to the presence of substantial coarse fraction (**Figures 6.4.1A,B**), a minor armour layer of coarse materials has developed over time which reduces the sand transport somewhat.
Wind speed and sand transport measurements were done on 9 February 2020 when the local meteorological wind speed (at 10 above the ground) was BF6 to 7 (Storm Ciara). It was dry weather with a temperature of 8° C and about 10 hours after the last rainfall. On 9 February 2020, the sand surface consisted of dry and moist patches (50% moist; 50% dry); the moisture content at moist patches was 4% in top layer of 20 mm.
Dry sand was accumulating in the ripple troughs from where it was eroded during strong wind gusts. The main transport layer was relatively thin (< 10 cm). The ripple crests consisted of moist sand. Sand transport was measured in conditions with wind speeds up to 12 m/s at 1.5 m above the local beach surface, see **Figure 6.4.1**. The upwind fetch length was about 150 m (supply-limited). Two traps were used close together: the big rectangular trap and the smaller tube-type trap. The wind velocity was always measured within 1 m of the trap location. Detailed results are given in **Table 6.4.1**. The sand transport in the lowest layer of 32 mm based on the small trap is 14 g/m/s, while the sand transport in the lowest layer of 71 mm based on the big trap is 26 g/m/s.

On 23 May 2020, sand transport measurements were done in dry weather conditions with wind BF5. The sand surface was dry. The fetch length was about 100 m. The wind velocity at 1.27 m above the surface were in the range of 7 to 9 m/s. The threshold wind velocity at 1.3 m above the surface with rolling transport was about 8 m/s. Surface irregularities were about 0.03 m.

Figure 6.4.1A *Wind transport at the inland recreational beach of Lemmer; storm BF 7; 9 February 2020*

Figure 6.4.1B *Wind transport at the inland recreational beach of Lemmer; BF 5; 23 May 2020*

6.4.2 Texel beach Den Hoorn

The beach surface was wet after rainfall and fairly flat on 12 March 2020. The wind was almost normal to the beach. No sand transport was observed at the beach surface, not even at the slightly drier than the beach. The transport details are given in **Table 6.4.1**.
This sandy beach is situated at the south-western side of the island of Texel and is facing the North Sea with tidal range of 1.5 to 2 m. The beach material is sand with d_{50}=0.27 mm and d_{90}=0.35 mm; p_{shell}<1%%). The beach width is about 50 m. The tidal range is a bout 1.5 to 2m. Sand transport measurements have been done on 12 March 2020. The beach conditions are described in Table 6.4.1. On 12 March 2020, the beach conditions were: fairly flat beach surface with moisture level of about 5% just after a rainfall event; shore-normal wind of 7 m/s at 1 m above the surface; short fetch distance of about 20 m to mid beach. Sand transport was absent, except close to the dune foot and at the dune top where the moisture levels were lower (visually, lighter colour). Sand transport was observed at the side of the passage path over the dune crest. The local fetch was fairly short (about 20 m).

The beach was very narrow and wet on 21 January 2021, Therefore, sand transport measurements were only done in the dune toe area with an irregular surface of small-scale ripples (1 to 3 cm high), see **Figure 6.4.1C**. The wind at BF 7 from southwest was almost parallel to the beach. Intermittent sand sport was measured due to strong wind gusts. The transport details are given in **Table 6.4.1**.

Figure 6.4.1C *Wind transport at dune toe of Den Hoorn beach, Texel; BF 7; 21 January 2021*

Location Date Duration	Beach		Moisture (%)			Wind conditions		Wind transport (g/m/s) in layers (mm) and test duration (s)
	$d_{50};d_{90}$ (mm) p_{coarse}	Description	upper 5mm	upper 20mm	p_m (%)	height (m) and velocity (m/s)	direction and fetch length (m)	
Lemmer 9 February 2020; Te=8° C BF6 to 7	0.3; 0.9 10%	upper beach; rippled surface	3%	4.0% alr=5 hrs	50%	z=0.55; u=9 ±0.5 z=0.84; u=10 ±0.5 z=1.43; u=11.0 ±0.5 u_*=0.82 m/s (R^2>0.9) k_s=210 mm	FL≅ 150 (SL; TL)	Big trap layer 0-71: 26 g/m/s small trap layer 0-32: 14 g/m/s (mt=660 s)
Lemmer 23 May 2020; Te=16° C BF 5	0.3; 0.9 10%	upper beach; rippled surface (0.03 m)	0%	0%	0%	z=0.32; u=6.3±0.6 z=0.62; u=7.2 ±0.8 z=1.27; u=8.0 ±1.0 u_*=0.49 m/s (R^2>0.95) k_s=55 mm	FL≅ 100 (SL)	Big trap layer 0-71: 4 g/m/s (mt=3600 s)
Texel (Den Burg) 8 July 2013; 20°C, BF5	0.25; 0.5 <1%	rippled surface	0%	0%	0%	z=10; u=10.0 z=1; u=7.7	FL≅ 100	10 g/m/s based on filling of small pit
Texel (Den Hoorn) 12 March 2020; 9°C, BF6	0.27; 0.35 <1%	flat surface at dune top (almost dry sand)	1.5% after light rain	1.5% alr=0.5 hrs	70%	z=0.45; u=9.0 ± 1.0 z=0.75; u=9.5 ± 1.0 z=1.38; u=10.0 ±1.0 u_*=0.54 m/s (R^2>0.9) k_s=20 mm	FL≅ 20 (SL; TL) normal to dune	Big trap layer 0-71: 33 g/m/s during increasing wind speeds
Texel (Den Hoorn) 12 March 2020; 9°C, BF6	0.27; 0.35 <1%	flat surface at beach (width=30 m); 10 m from HW line		5% alr=0.5 hrs	100%	z=0.55; u=6.3 ± 0.5 z=0.85; u=7.0 ± 0.5 z=1.48; u=7.5 ± 0.5 u_*=0.48 m/s (R^2>0.9) k_s=80 mm	FL≅ 10 (SL; TL) wind normal to beach	no transport
Texel (Den Hoorn) 21 January 2021; 6°C, BF7	0.27; 0.4 <1%	irregular surface at dune toe; 20 m from HW line	4%-6%	4%-6% alr=1 hrs	80%	z=0.3; u=9.1 ± 0.5 z=0.6; u=10.3 ± 0.7 z=1.25; u=12.5 ± 1 u_*=0.96 m/s (R^2>0.95) k_s=215 mm	FL≅ 100	Big trap layer 0-71: 45 g/m/s layer >0.71: 5 g/m/s Total 45 g/m/s (mt=780 s)

BF=Beaufort wind scale; p_{shell}= percentage shells at beach surface; alr=after last rainfall;

FL= fetch length; SL= supply limitation; TL= transport limitation; hp= hard moist patches; dp=relatively dry patches
p_m= percentage of beach surface with moist appearance at measurement location; z= height above bed; u= wind velocity at height z; mt=measuring time sand transport; mc= moisture content; nm=not measured

Table 6.4.1 *Wind transport data at beaches of Lemmer and Texel, The Netherlands*

6.4.3 Groote Keeten beach, The Netherlands

The upper beach surface was dry and flat (no ripples), but somewhat irregular due to the presence of ridge and runnels, see **Figure 6.4.2**. No shells were present. The sand was completely dry and loose. The wind was blowing at BF 6 from the North and was almost parallel to the beach and dunes. The beach material is sand with d_{50}=0.24 mm and d_{90}=0.5 mm; p_{shell} <1% (no shells). The beach width between the dune foot and LW-line is about 90 m. The tidal range is about 1.5 m. Sand transport measurements have been done on 10 May 2020. The beach conditions are described in **Table 6.4.2**.

Figure 6.4.2 *Sand transport measurements at dry beach Groote Keeten 10 May 2020, The Netherlands*

Location Date Duration	Beach		Moisture (%)			Wind conditions		Wind transport (g/m/s) in layers (mm) and test duration (s)
	d_{50};d_{90} (mm) p_{shell}	Description	upper 5mm	upper 20mm	p_m (%)	height (m) and velocity (m/s)	direction and fetch length (m)	
Groote Keeten 10 May 2020; 12 °C BF6 from North	0.24; 0.4 <1%	flat dry surface; 60 m from waterline; 30 m from dune foot	0	0	0	z=0.28; u=6.4 ± 0.6 z=0.58; u=7.2 ± 0.7 z=1.23; u=8.7 ± 0.9 u_*=0.62 m/s (R^2>0.95) k_s=150 mm	FL>500 // to beach	Layer 0-70 mm: 19 g/m/s Layer70-135 mm: 3.5 g/m/s Layer 135-165 mm: 1.5 g.m/s total: 24 g/m/s (mt=600 s)
Groote Keeten 10 May 2020; 12 °C BF6 from North	0.24; 0.4 <1%	flat dry surface; 60 m from waterline; 30 m from dune foot	0	0	0	z=0.28; u=6.6 ± 1.0 z=0.58; u=7.5 ± 1.0 z=1.23; u=9.1 ± 1.2 u_*=0.68 m/s (R^2>0.95) k_s=190 mm	FL>500 // to beach	Layer 0-70 mm: 33 g/m/s Layer70-135 mm: 4 g/m/s Layer 135-165 mm: 2 g.m/s total: 39 g/m/s (mt=600 s)
Groote Keeten 10 May 2020; 12 °C BF6 from North	0.24; 0.4 <1%	flat dry surface; 60 m from waterline; 30 m from dune foot	0	0	0	z=0.28; u=7.1 ± 0.9 z=0.58; u=8.0 ± 1.0 z=1.23; u=9.7 ± 1.1 u_*=0.7 m/s (R^2>0.95) k_s=160 mm	FL>500 // to beach	Layer 0-70 mm: 37 g/m/s Layer70-135 mm: 4 g/m/s Layer 135-165 mm: 2 g/m/s total: 43 g/m/s (mt=600 s)
Groote Keeten 10 May 2020; 12 °C BF6 from North	0.24; 0.4 <1%	flat dry surface; 60 m from waterline; 30 m from dune foot	0	0	0	z=0.28; u=7.0 ± 0.8 z=0.58; u=7.9 ± 0.8 z=1.23; u=9.1 ± 1.0 u_*=0.73 m/s (R^2>0.95) k_s=200 mm	FL>500 // to beach	Layer 0-70 mm: 25 g/m/s Layer70-135 mm: 3.5 g/m/s Layer 135-165 mm: 1.5 g.m/s total: 30 g/m/s (mt=600 s)
Groote Keeten 10 May 2020; 12 °C BF6 from North	0.24; 0.4 <1%	flat dry surface; 60 m from waterline; 30 m from dune foot	0	0	0	z=0.28; u=6.6 ± 1.0 z=0.58; u=7.4 ± 1.0 z=1.23; u=9.0 ± 1.2 u_*=0.65 m/s (R^2>0.95) k_s=155 mm	FL>500 // to beach	Layer 0-70 mm: 26 g/m/s Layer70-135 mm: 3.5 g/m/s Layer 135-165 mm: 1.5 g.m/s total: 31 g/m/s (mt=600 s)
Groote Keeten 10 May 2020; 12 °C BF6 from North	0.24; 0.4 <1%	flat dry surface; 60 m from waterline; 30 m from dune foot	0	0	0	z=0.28; u=6.6 ± 1.0 z=0.58; u=7.4 ± 1.0 z=1.23; u=9.1 ± 1.2 u_*=0.68 m/s (R^2>0.95) k_s=185 mm	FL>500 // to beach	Layer 0-70 mm: 33 g/m/s Layer70-135 mm: 4 g/m/s Layer 135-165 mm: 2 g.m/s total: 39 g/m/s (mt=600 s)

BF=Beaufort wind scale; p_{shell}= percentage shells at beach surface; alr=after last rainfall;
FL= fetch length; SL= supply limitation; TL= transport limitation; hp= hard moist patches; dp=relatively dry patches
p_m= percentage of beach surface with moist appearance at measurement location; z= height above bed; u= wind velocity at height z; mt=measuring time sand transport; mc= moisture content; nm=not measured

Table 6.4.2 *Wind transport data at dry beach of Groote Keeten, 10 May 2020, The Netherlands*

6.4.4 Zandvoort beach, The Netherlands

The upper beach surface was dry and flat (no ripples) with very minor irregularities, see **Figure 6.4.3**. No shells were present. The sand was completely dry and loose. The wind was blowing at BF 6 to 7 from the south-south-west and was almost parallel to the beach and dunes. The fetch was long (> 200 m). The beach material is sand with d_{50}=0.23 mm and d_{90}=0.5 mm; p_{shell} <1% (no shells). The beach width between the dune foot and LW-line is about 100 m. The tidal range is about 1.5 m. Sand transport measurements have been done on 29 June 2020 at

about 30 m from the dune foot and about 20 m from the HW line of hard, wet interidal beach zone. The beach conditions are described in **Table 6.4.3**.

Location Date Duration	Beach		Moisture (%)			Wind conditions		Wind transport (g/m/s) in layers (mm) and test duration (s)
	$d_{50};d_{90}$ (mm) p_{shell}	Description	upper 5mm	upper 20mm	p_m (%)	height (m) and velocity (m/s)	direction and fetch length (m)	
Zandvoort 13.18-13.28 29 june 20 21°C; BF6 from SSW	0.25; 0.4 <1%	flat dry surface; 30 m from dune foot	0	0	0	z=0.3; u=6.9 ± 0.5 z=0.6; u=8.3 ± 0.7 z=1.25; u=10.0 ± 0.7 u_*=0.87 m/s (R^2>0.98) k_s=400 mm	FL≧200 angle of 70° to beach	Layer 0-70 mm: 18.5 g/m/s Layer70-165 mm: 4.5 g/m/s total: 23 g/m/s (mt=600 s)
Zandvoort 13.33-13.43 29 june 20 21°C; BF6 from SSW	0.25; 0.4 <1%	flat dry surface; 30 m from dune foot	0	0	0	z=0.3; u=6.8 ± 0.5 z=0.6; u=8.4 ± 0.7 z=1.25; u=9.9 ± 0.7 u_*=0.87 m/s (R^2>0.98) k_s=380 mm	FL≧200 angle of 70° to beach	Layer 0-70 mm: 24.3 g/m/s Layer70-165 mm: 5.7 g/m/s total: 30 g/m/s (mt=600 s)
Zandvoort 13.47-13.57 29 june 20 21°C; BF6 from SSW	0.25; 0.4 <1%	flat dry surface; 30 m from dune foot	0	0	0	z=0.3; u=6.3 ± 0.5 z=0.6; u=7.7 ± 0.6 z=1.25; u=9.0 ± 0.7 u_*=0.77 m/s (R^2>0.98) k_s=315 mm	FL≧200 angle of 70° to beach	Layer 0-70 mm: 16.1 g/m/s Layer70-165 mm: 3.9 g/m/s total: 20 g/m/s (mt=600 s)
Zandvoort 14.00-14.10 29 june 20 21°C; BF7 from SSW	0.25; 0.4 <1%	flat dry surface; 30 m from dune foot	0	0	0	z=0.3; u=7.0 ± 0.5 z=0.6; u=8.7 ± 0.6 z=1.25; u=10.5 ± 0.7 u_*=0.98 m/s (R^2>0.99) k_s=515 mm	FL≧200 angle of 70° to beach	Layer 0-70 mm: 27 g/m/s Layer70-165 mm: 6 g/m/s total: 33 g/m/s (mt=600 s)
Zandvoort 14.13-14.23 29 june 20 21°C; BF7 from SSW	0.25; 0.4 <1%	flat dry surface; 30 m from dune foot	0	0	0	z=0.3; u=7.5 ± 0.5 z=0.6; u=9.2 ± 0.6 z=1.25; u=11.0 ± 0.7 u_*=0.98 m/s (R^2>0.99) k_s=420 mm	FL≧200 angle of 70° to beach	Layer 0-70 mm: 30 g/m/s Layer70-165 mm: 6 g/m/s total: 36 g/m/s (mt=600 s)
Zandvoort 14.26-14.36 29 june 20 21°C; BF6 from SSW	0.25; 0.4 <1%	flat dry surface; 30 m from dune foot	0	0	0	z=0.3; u=6.4 ± 0.8 z=0.6; u=8.3 ± 0.9 z=1.25; u=9.3 ± 1 u_*=0.81 m/s (R^2>0.95) k_s=350 mm	FL≧200 angle of 70° to beach	Layer 0-70 mm: 20.7 g/m/s Layer70-165 mm: 4.3 g/m/s total: 25 g/m/s (mt=600 s)
Zandvoort 14.40-14.50 29 june 20 21°C; BF7 from SSW	0.25; 0.4 <1%	flat dry surface; 30 m from dune foot	0	0	0	z=0.3; u=8.1 ± 0.7 z=0.6; u=10.2 ± 0.9 z=1.25; u=11.2 ± 1 u_*=0.864 m/s (R^2>0.95) k_s=200 mm	FL≧200 angle of 70° to beach	Layer 0-70 mm: 32.6 g/m/s Layer70-165 mm: 6.4 g/m/s total: 39 g/m/s (mt=600 s)
Zandvoort 14.53-15.03 29 june 20 21°C; BF7 from SSW	0.25; 0.4 <1%	flat dry surface; 30 m from dune foot	0	0	0	z=0.3; u=7.3 ± 0.5 z=0.6; u=9.3 ± 0.5 z=1.25; u=11.0 ± 0.7 u_*=1.03 m/s (R^2>0.95) k_s=520 mm	FL≧200 angle of 70° to beach	Layer 0-70 mm: 31.6 g/m/s Layer70-165 mm: 5.4 g/m/s total: 37 g/m/s (mt=600 s)
Zandvoort 15.06-15.16 29 june 20 21°C; BF7 from SSW	0.25; 0.4 <1%	flat dry surface; 30 m from dune foot	0	0	0	z=0.3; u=6.7 ± 0.6 z=0.6; u=9.1 ± 0.7 z=1.25; u=10.5 ± 0.7 u_*=1.06 m/s (R^2>0.97) k_s=660 mm	FL≧200 angle of 70° to beach	Layer 0-70 mm: 32.4 g/m/s Layer70-165 mm: 5.6 g/m/s total: 38 g/m/s (mt=600 s)
Zandvoort 13.18-13.28	0.25; 0.4 <1%	flat dry surface; 30 m from dune foot	0	0	0	z=0.3; u=7.4 ± 0.8 z=0.6; u=10.1 ± 0.9 z=1.25; u=11.4 ± 1 u_*=1.11 m/s (R^2>0.95)	FL≧200 angle of 70° to beach	Layer 0-70 mm: 36.8 g/m/s Layer70-165 mm: 7.2 g/m/s total: 44 g/m/s (mt=600 s)

29 june 20 21°C; BF7 from SSW						k_s=575 mm		

BF=Beaufort wind scale; p_{shell}= percentage shells at beach surface; alr=after last rainfall;
FL= fetch length; SL= supply limitation; TL= transport limitation; hp= hard moist patches; dp=relatively dry patches
p_m= percentage of beach surface with moist appearance at measurement location; z= height above bed; u= wind velocity at height z; mt=measuring time sand transport; mc= moisture content; nm=not measured

Table 6.4.3 *Wind transport data at dry beach of Zandvoort, 29 June 2020, The Netherlands*

Figure 6.4.3 *Sand transport measurements at dry beach Zandvoort 29 June 2020, The Netherlands*

6.5 Analysis of field transport measurements

The available field data have been used to reveal some specific features of sand transport related to the effects of fetch, moisture and coarse materials.
Many measurements of sand transport rates have been made at the beaches of Zeebrugge (Belgium), Callantsoog and Texel (The Netherlands). The median particle diameter (d_{50}) is in the range of 0.2 to 0.35 mm. The moisture content of the upper 20 mm is in the range of 1% to 5%. The highest wind speed at about 1 m above the sand surface at Callantsoog was about 19 m/s on 9 February 2020 resulting in a sand transport rate of about 425 g/m/s, which is a factor 50 higher than the lowest measured sand transport of about 6 g/m/s at a wind speed of 6.5 m/s at 1 m above the sand surface. Fully saturated equilibrium sand transport was present in conditions with winds parallel to the beach, even in conditions with rainy weather. Entrainment of sand mostly occurs in the drier areas of the upper beach, dune foot and dune front, but also from underneath the beach houses with open pile foundation structures.
Most of the data sets (75% for dry sand and 85% for moist sand) have wind velocities $u > 1.5\ u_{th,initiation}$ with $u_{th,initation}$=threshold wind velocity at 1 m above surface for ititiation of motion (see Table 1), which means continuous transport conditions (Stout and Zobeck, 1997). In 15% to 25% of the cases, the transport conditions are intermittent ($u_{th,cessation} < u < u_{th,\ initiation}$).

Figure 6.5.1 shows the effect of fetch distance and moisture on sand transport. For clearness, only the experimental range of the many sand transport rates measured in dry beach conditions are shown. Most of the new Dutch data refer to conditions with a very long fetch as the wind was almost parallel to the beach. At some dates in February 2020, the wind was oblique to normal from the sea and the distance between the edge of the hard, wet intertidal beach and the measurement location was in the range of 5 to 50 m resulting in non-saturated (non-equilibrium) sand transport rates. The effect is minor (factor 1.5) for relatively high wind speeds> 10 m/s, but major (factor 5 to 10) for relatively low wind speeds < 9 m/s, see open circles in **Figure 6.5.1**.

The effect of moisture is also shown in **Figure 6.5.1**. For clearness, only the experimental range of the many sand transport rates measured in dry beach conditions are shown. Most of the measured sand transport values in moist conditions are within the experimental range of the dry transport values, particularly for the higher wind speeds > 10 m/s. For low wind speeds < 9 m/s, the sand transport rates is slightly reduced in moist conditions. The field data at Saunton Sands are taken form the plots of Sarre (1988) and refer to moist conditions up to 14%. His data are in excellent agreement with the moist data of Callantsoog open triangles), which contributes to confidence in the new equipment of the author. The intense transport of sand at higher wind speeds in moist conditions can be explained by the entrainment of sand from the drier spots which are always there (between vegetation at the dune front, near obstacles and from beneath the beach houses on piles). The presence of dry spots with lighter color was a very prominent feature during measurements in moist conditions (a few hours after the last rainfall) at the beach of Callantsoog and other beaches. Finally, the effect of coarse materials is discussed. **Figure 6.5.1** shows 2 data points (solid squares) from a beach with a coarse armor layer, where sand transport was very low at a wind speed of about 10 m/s (factor 10 lower than the values of the experimental range). Equation (5.1c) yields a reduction of 95% for a gravel percentage of 30% in agreement with the field data.

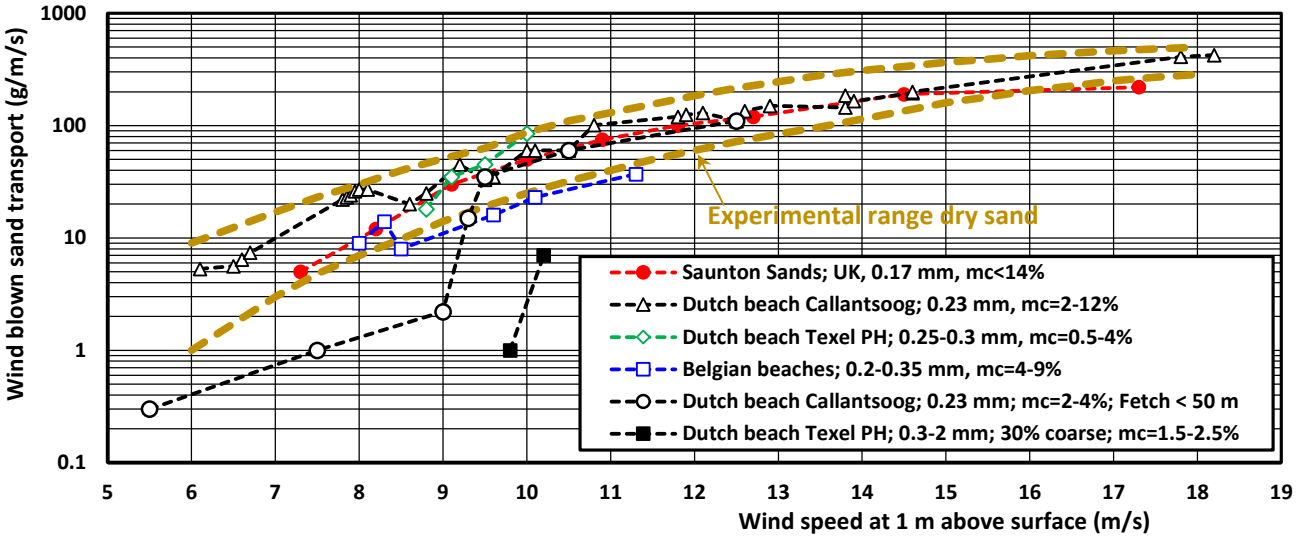

Figure 6.5.1 *Effect of fetch distance, moisture and coarse materials on aeolian transport*

Supply-limited conditions due to rainfall were only observed during various events.
On 16 February 2020 with wind conditions of about BF7, the wind dropped suddenly from BF7 to BF5 (parallel to the beach), no sand transport was measured for a wind speed of about 7 m/s at 1 m above the sand surface and moisture levels of 9% to 12% at the upper beach (about 4 hours after the last rainfall).

On 24 February 2020, the wind speed suddenly increased to BF7 (parallel to the beach) after a rainfall event; no sand transport was visually observed at the moist upper beach (5 hours after last rainfall). On other dates with BF7, the sand transport continued during rainfall. Thus, the chronology of wind speed and rainfall also is important. An increasing strong wind up to BF7 over a wet surface leads to supply-limited conditions, but sand transport due a strong steady wind (BF7) is not reduced (limited) by rainfall creating a wet surface.

The moisture levels of the field data are all in the range of 1% to 8%. Most of the measurements were made in the winter period of December 2019 to March 2020 when a moist sand surface was present at the beach of Zeebrugge and Callantsoog. Some measurements were made in conditions with rainy weather.
The effects of moisture (rainfall) on sand transport in winter months can be summarized, as follows:

- when strong winds (> BF>6) are blowing for a relatively period (5 to 10 days), the beach will become relatively narrow due to storm setup and mostly consists of a hard, wet lower beach with moisture levels of 8% to 15% and a narrow upper beach with moisture levels of 1% to 8%.
- when the beach is wet due to rainfall and the wind strength is mild (BF<6), sand transport is minor as the wind speed is not able to generate significant particle motion. It will take about 5 to 10 hours in winter to dry the beach surface and generate sand transport processes.
- when the beach is wet due to rainfall and a strong wind starts blowing parallel to beach, sand transport will rapidly be intense as the upwind fetch is very long and sand can be easily eroded from the drier areas (dune foot, dune front and from underneath beach houses which are often built on open pile structures); dry sand accumulates in depressions on the beach (in the lee of ripples etc.) from where it is eroded during strong wind gusts (BF7 to 8); sand transport quickly develops to the saturation rate over a fetch length of about 100 m; Sarre (1988) measured sand transport rates comparable to that of dry sand during conditions with moisture levels up to 14%.
- when the wind is strong (>BF 6) and parallel to the beach, sand transport is initiated at the upper beach and spread out over the full width of the beach; the sand transport at the drier upper beach and at the wetter lower beach is of the same order of magnitude.
- when the wind is strong (>BF6) and parallel to the beach, sand transport continues during rain showers; moving sand will become wet; the saltation height and length may be reduced somewhat but the fast moving particles can still erode sand from the wet surface (sand blasting effect); sand transport may be moderately reduced in the case of very intense rainfall; splash-type of transport will be generated during strong showers due to raindrop impacts at the sand surface; however, splash-type transport is only 10% of dry sand transport at the same wind velocity; sand transport stops during rainfall and light winds (BF3 to BF5).
- when the wind is normal or under an oblique angle to the beach, sand transport does not occur at the wet lower beach in conditions; sand transport at the upper beach will be very restricted as the fetch length is only about 30 to 50 m (supply-limited conditions, except at very wide beaches).
- when the beach is wet with high moisture levels due to regular inundation by macro-tides and/or a relatively long period with rain, the saturation distance along the wet beach may increase significantly (factor 2 to 3) based on the data of Sarre (1988). This severely limits sand transport for conditions with wind normal to the beach, but it is not of importance for conditions with parallel winds as the upwind fetch is very long.

7 Verification of proposed aeolian transport equations for dry and moist sand

7.1 General

Various old data sets from the Literature and new data sets of Dutch beaches for moist sand conditions with moisture contents > 2% have been used for calibration of the proposed methods (Van Rijn-equation and modified Bagnold-equation, see Section 2). In all, 81 n ew data points of beaches in Belgium and the Netherlands have been used.
The field data from the Literature and the new data are briefly described hereafter.

7.2 Data sets used for verification of sand transport equations

Field experiments at beaches in Ireland, Portugal and Brazil (Sherman et al., 2013)
Data were obtained from field experiments conducted at three sites (Inch Spit, Ireland, Esposende, Portugal and Jericoacoara, Brazil). The Inch site (April 1994) is part of a morphodynamically dissipative beach system in Dingle Bay, on the south-western coast of Ireland. The field site at Esposende, along the northern coast of Portugal, was near the downwind end of a parabolic dune trough (May and June 2006). The upwind surface was flat and unobstructed and almost horizontal near the sand traps. During the experiments the sand surface was dry, and winds blew parallel to the trough with a fetch of approximately 80 m. Blowing sand was trapped using vertical arrays of hose-type traps. Samples for grain size analyses were obtained from sand caught in the traps.
Located on the north-eastern coast of Brazil, the Jericoacoara site was also near the downwind end of a parabolic dune trough, but at a location approximately 500 m from the shoreline. The upwind surface was flat and unobstructed, with a fetch of approximately 100 m, and the surface was almost horizontal near the traps. During the experiments, the wind blew parallel to the trough and the surface sediments were dry. Sand transport rates were measured with vertical hose-type trap arrays and grain size samples were obtained from the trapped sands. In order to estimate shear velocity using the cup anemometer data, wind speeds were averaged over time intervals coincident with those for sand trap data. The number of data was reduced to 32 data sets (5 for Inch Spit; 12 for Esposende and 15 for Jericoacoara) by selecting: i) only those wind profiles with a best-fit line R^2 exceeding 98%, ii) only those data for which the sand moisture content was less than 2% and iii) data sets with sand transport rates larger than about 0.3 g/m/s (1 kg/m/hour). Many of the data points of each site have wind speeds close together (within ±0.2 m/s) and are herein clustered resulting in 2 data points for Inch Spit in Ireland, 6 for Esponsende in Portugal and 5 for Jericoacoara in Brazil, see **Table 7.2.1**.

Inch spit, Ireland and Esponsende dune, Portugal					**Jericoacoara dune, Brazil**				
ID	d_{50} (mm)	u_* (m/s)	u_1 (m/s)	q_s (g/m/s)	ID	d_{50} (mm)	u_* (m/s)	u_1 (m/s)	q_s (g/m/s)
I2,3,4,5	0.17	0.39	7.4	2.5	J12	0.27	0.54	7.9	20
I1	0.17	0.4	8.2	6.8	J9, 11	0.27	0.52	8.5	20.7
					J6,7,8,10	0.29	0.55	8.9	18.1
E3,4,8,10,12	0.3	0.38	7.7	2.9	J2,4	0.23	0.67	9.7	22
E7,9	0.34	0.4	8.1	8.9	J1,3,5,13	0.28	0.63	9.7	28
E1,2,5,6	0.31	0.5	8.6	8.5	J14,15	0.43	0.57	10	22

u_*= shear velocity; u_1= wind speed at 1 m above surface; q_s= sand transport rate
Table 7.2.1 *Transport data (dry sand) at field sites in Ireland, Portugal and Brazil (Sherman et al., 2013)*

Field experiments at Saunton Sands beach in UK (Sarre 1988)

Sarre (1988) measured wind transport at a British intertidal site using a vertical sand trap, together with simultaneous monitoring of wind speed and moisture levels up 18% in the top 1-2 mm surface layers of sand (beach sand of 0.17 mm). Measured transport rates were in the range of 0.1 to 220 kg/m/s. The beach site was Saunton Sands bordering the Bristol Channel, located within Barnstaple Bay, SW England. The beach is a wide, low-angle intertidal plain backed by dunes. The beach width is about 700 m in the North and about 1500 m in the South during spring tides with tidal range of 7 m (beach slope of 7/1500≅ 1 to 200). The trap is a 1 m long pvc tube (39 mm in diameter) with two slits cut down opposite sides over 750 mm of the tube length. The front slit is 10 mm wide and the rear slit is 25 mm wide and covered with 100 μm nylon mesh. The traps are placed by simply dropping the bottom 250 mm into a precut hole in the beach. The trap was exposed for periods ranging from 1 to 180 minutes depending on the sand transport rates. Moisture levels were measured by scraping sand the top 1 to 2 millimeters of sand into moisture tins, the samples were dried and weighed. Samples were collected over a large area of the intertidal zone, together with specific sites upwind of the measurement location. The wind speed was measured at 2 m above the sand surface and the shear velocity was determined by using a bed roughness of k_s=3 mm. Rarely any bed forms were visible at the damp intertidal zone. A selection of measured sand transport rates with an inaccuracy of about ± 50% is given in **Table 7.2.2** (derived from Figure 3 of Sarre, 1988). The data of Sarre were smoothed to obtain a trend line from which the transport data were taken. The data of Sarre show that moisture levels < 14% in the surface layers have little effect on the transport rates, whereas higher levels 14-18% and > 18% have an increasingly pronounced effect. The fetch length over moist sand upwind of the measurement location was always in the range of 150 to 500 m. On few occasions sand was in motion when the mean wind velocity was below the impact threshold velocity, which was caused by large-scale turbulence (wind gusts). The threshold shear velocity (with very low transport rates) was found to be in the range of 0.14 to 0.2 m/s for 0.17 mm sand. Sarry notes that there are large variations in moisture levels over this large beach plain, which are often poorly represented by the average value. Most likely, the data set of Sarre (1988) represent conditions with transport of sand supplied from drier upwind sources and transported over a wide beach plain which is regularly inundated due to tidal variations in dry weather (no rainfall).

Predicted values using the original Bagnold equation were somewhat lower than the measured values for the higher wind velocities (> 10 m/s), but this equation overpredicted for the lower wind speeds (< 10 m/s). Sarre concluded that the best predictions were obtained by using equations based on the cube of the shear velocity with inclusion of a threshold term. Moisture levels up to 14% were neglected without effect on the predicted sand transport rates suggesting that moisture levels up to 14% have little effect on sand transport process and that, once movement has been initiated at some point on the beach, transport rates are similar to those over dry sand beaches. The predictability was found be less for low wind velocities approaching threshold conditions, when the moisture levels and wind gust contributions become increasingly important.

Saunton Sands, UK						
ID	d_{50} (mm)	mc (%)	u_* (m/s)	u_2 (m/s)	u_1 (m/s)	q_s (g/m/s)
1	0.17	<14	not available	8	7.3	5 ±50%
2	0.17	<14	not available	9	8.2	12 ±50%
3	0.17	<14	not available	10	9.1	30 ±50%
4	0.17	<14	not available	11	10	50 ±50%
5	0.17	<14	not available	12	10.9	75 ±50%
6	0.17	<14	not available	13	11.8	100 ±50%
7	0.17	<14	not available	14	12.7	120 ±50%
8	0.17	<14	not available	15	14.5	190 ±50%
9	0.17	<14	not available	16	17.3	220 ±50%

u_*= shear velocity; u_1= wind speed at 1 m above surface; q_s= sand transport rate; mc= moisture content

Table 7.2.2 *Transport data at field site Saunton Sands along Bristol Channel, UK (Sarre 1988)*

Field experiments at Wildwood beach, New Yersey, USA (Jackson and Nordstrom, 1997)

Jackson and Nordstrom (1997) studied (8 to 19 March 1994) the influence of changes in surface moisture content on sand entrainment and transport on the beach of Wildwood, New Yersey, USA.

The field site is located near the north end of a 10 km long barrier island. The mean tidal range is 1.25; mean spring range is 1.5 m. Beach sediments are very well-sorted, fine sand. Sand transport weas measured using 4 Leatherman traps placed vertically in the bed. The tube-type traps have an opening on the front side and on the rear side. The bottom of the front opening is flush with the beach surface, but scour problems may occur. The trap was removed every 10 minutes to determine the trapped sand mass. Three data points were taken from the plots. Data derived form plots are given in **Table 7.2.3**.

ID	d_{50} (mm)	mc (%)	u_* (m/s)	u_1 (m/s)	q_s (g/m/s)
1	0.165	3	0.22	5.5	2 ±50%
2	0.165	3	0.27	6	4 ±50%
3	0.165	3	0.33	7	6 ±50%

u_*= shear velocity; u_1= wind speed at 1 m above surface; q_s= sand transport rate; mc= moisture content

Table 7.2.3 *Transport data at field site Wildwood beach, New Yersey., USA (Jackson and Nordstrom 1997)*

Field experiments at beach site in Ireland (Jackson and Cooper 1999)

Jackson and Cooper (1999) conducted an experiment to examine the influence of fetch distance on aeolian sediment transport on a natural sand beach at Benone Strand, County Londonderry, Northern Ireland. The site consisted of a wide dissipative beach (150 m wide at low tide and 80 m wide during high tide). An abundant dry sediment supply (d_{50}=0.17 mm) was available during the experiment. Wind velocity measured at 0.6 m above the sand surface ranged from 2 to 8 m/s. The fetch was in the range of 10 to 60 m. A circular trap (diameter 0.25 m; effective square diameter=0.22 m) coplanar with the sand surface was used to measure the sand transport rate. A fetch of about 15 to 20 m was required to get equilibrium sand transport for wind velocities up to 8 m/s. Their field data show sand transport rates of about 5, 10, 15 g/m/s for wind velocities of 6.4, 7.5 and 8.6 m/s at 1 m above surface (their rates are given in g/s for the circular trap which are converted herein to transport rates per unit width in g/m/s by dividing through an effective trap width of 0.22 m).

Field experiments at beach De Hors on Texel, The Netherlands (Hijma and Lodder 2001)

Hijma and Lodder (2001) measured the transport of dry sand by wind on the beach De Hors (very flat and wide beach plain) on the island of Texel, The Netherlands. The beach plain is a flat sand plain with d_{50}=0.23 mm between the sea and the fore dune. This plain is about 2 km wide and 4 km long. Small, barchan-like dunes of about 20 cm high and several meters long are migrating along the beach surface. At very high tide the beach plain is completely under water, but most of the time it is dry. Various sand traps were used. The sand trap of Bagnold (1973) and that of Sarre (1988) were found to give the most accurate results.

The Bagnold-trap is a wooden horizontal sand trap of 60 cm wide and 120 cm long which is placed in a pit made in the bed. Six bags are placed in the trap. Sand particles with a saltation length smaller than 120 cm are trapped. The trap efficiency is over 100% because the trap is open on every side and the sand can therefore fall in the bags from every side due to variation of the wind direction.

The trap of Sarre (1988) is a modification of the Leatherman-trap and consists of a tube with a length of 100 cm and a diameter of 39 mm, which is placed vertically in the sand bed. On opposite sides of the tube, two openings with length of 75 cm are present. The width of the front opening is 10 mm and the width of the rear opening is 25 mm. The rear opening is covered with nylon mesh of 50 μm to trap the sand particles, which fall to the bottom

of the trap. The front opening has to be placed in the wind direction with the bottom of the front opening flush with the sand surface. The trap is removed from the sand bed after each measurement.
In total, 63 measurements with the Bagnold-trap and 41 measurements with the Sarre-trap were done. During the measurements wind velocity profiles were measured with cup-meters and sediment samples were taken in order to determine the mean grain size and the critical shear velocity. The mean grain size was 0.23 mm. The critical shear velocity was 0.19 m/s. Measured shear velocities ranged from 0.19 to 0.83 m/s. The data used herein were taken from the table given by Strypsteen et al. (2021), see Table 2.4.2. The wind velocity at 1.3 m above the sand surface was computed by using a logarithmic velocity profile $u=u_*/\kappa \ln(30z/k_s)$ with u_*= shear velocity (m/s), κ= constant of Van Karmann, k_s= roughness height (m). The k_s-values was assumed to be in the range of 0.01 to 0.03 m. The basic data are given in **Table 7.2.4**.

ID	d_{50} (mm)	u_* (m/s)	$u_{1.3}$ (m/s)	q_s (g/m/s)
1	0.23	0.22	5	1.2
2	0.23	0.28	5.6	3.8
3	0.23	0.38	6.5	8
4	0.23	0.42	7.3	21
5	0.23	0.48	7.9	25
6	0.23	0.5	8.6	43
7	0.23	0.42	8.7	22
8	0.23	0.48	9.6	25
9	0.23	0.6	9.8	55
10	0.23	0.62	12.2	127
11	0.23	0.66	13.1	145

u_*= shear velocity; u_1= wind speed at 1 m above surface; q_s= sand transport rate
Table 7.2.4 *Transport data (dry sand) at beach De Hors, Texel, The Netherlands (Strypsteen et al., 2021)*

Field experiments at beach Prins Hendrik on Texel, The Netherlands (Strypsteen et al., 2021)
Van Rijn (2020) has executed field measurements at the Prins Hendrik beach site on the island of Texel (The Netherlands) in spring 2020. The field measurements are extensively described by Van Rijn (2020) and Strypsteen et al. (2021).

Field experiments at Aberffraw beach in Wales (Wiggs et al., 2004)
Wiggs et al. (2004) studied the influence of changes in surface moisture content on sand entrainment and transport on the meso-tidal Aberffraw beach with d_{50}=0.2 mm in Anglesey, North Wales. High frequency (1 Hz) wind velocities measured with hot-wire anemometers were combined with grain impact data from a Sensit monitor and mass flux measurements from a standard sand trap. Surface and near-surface moisture contents were assessed gravimetrically from surface sand scrapes and also directly by using a Theta-Probe. The results indicate a time-dependent change in dominant control of the sand transport system from moisture to wind speed, dependent upon the moisture content of the surface sediment. A moisture content of nearly 2% (where moisture was adhered to transported sediment) appeared to have little or no impact on the rate of sand flux.
Data derived form plots are given In **Table 7.2.5**.

ID	d_{50} (mm)	mc (%)	u_* (m/s)	u_1 (m/s)	q_s (g/m/s)
1	0.2	1	na	11.5	90 ±50%
2	0.2	2.5	na	11.0	30 ±50%
3	0.2	3	na	10.5	50 ±50%

u_*= shear velocity; u_1= wind speed at 1 m above surface; q_s= sand transport rate; mc= moisture content
na= not available

Table 7.2.5 *Transport data at field site Aberffraw beach, Anglesey, Wales (Wiggs et al. 2004)*

Field experiments at two beaches in Belgium by Strypsteen (2019) and Campos (2018)

Strypsteen (2019) and Campos (2018) conducted field experiments at the beaches of Mariakerke and Koksijde in Belgium. The beach of Mariakerke (d_{50}=0.31 mm) is fairly flat and contains some shell fragments due to regular nourishments. The measurements were performed in the dry upper beach zone without much shells. The bed roughness (k_s) is smaller than 10 mm. The beach of Koksijde consists of sand (d_{50}=0.21 mm) with small-scale bed irregularities (ripples) and many shell fragments (5%) with height of the order of 30 mm. The bed roughness (k_s) is in the range between 10 and 50 mm. Wind-induced sand transport was measured by using MWAC-sand traps. Campos (2018) measured sand transport due to wind at the upper beach of Koksijde (Belgium) on 24 November 2014 during dry weather conditions using the bag-type streamer traps of Sherman et al. (2014). This trap consists of 6 sub-traps in a stack; each trap height=50 mm; the trap width=100 mm. The d_{50}-value of the beach sand was d_{50}=0.22 mm. The moisture content of the upper 20 mm is estimated to be < 2%. The data set of Campos (2018) is very detailed and highly accurate.

Many of the original data points of each site have wind speeds close together (within ±0.2 m/s) and are herein clustered resulting in 8 data points for Mariakerke beach and 8 for Koksijde beach in Belgium, see **Table 7.2.6**.

Mariakerke beach, Belgium				**Koksijde beach, Belgium**			
ID	d_{50} (mm)	u_1 (m/s)	q_s (g/m/s)	ID	d_{50} (mm)	u_1 (m/s)	q_s (g/m/s)
MS1	0.31	6.0	2.0	KS1	0.22	8.8	8.6
MS2	0.31	6.5	3.3	KS2	0.22	9.5	17.3
MS3	0.31	7.5	3.7	KS3	0.22	10.5	26.1
MS4	0.31	8.1	8.2	KS4	0.22	11.8	37.3
MS5	0.31	8.2	9.3	KC1	0.22	8.6	13
MS6	0.31	9.0	16	KC2	0.22	9.8	22
MS7	0.31	9.5	26.5	KC3	0.22	10.1	22
MS8	0.31	10.0	27	KC4	0.22	10.7	28

u_*= shear velocity; u_1= wind speed at 1 m above surface; q_s= sand transport rate; KC= Koksijde beach measured by Campos (2018); KS= Koksijde beach measured by Strypsteen (2019)

Table 7.2.6 *Transport data (dry sand) at field sites in Belgium (Strypsteen, 2019)*

Field experiments at three beaches in Belgium by Lietaer 2020)

Lietaer (2020) has used to the LVRS-trap sampler to measure aeolian sand transport at the beaches of Koksijde, Zeebrugge and Oostende in Belgium. Many of the data were taken at the wet intertidal beach; most of the transported sand originates from drier spots at the upper beach close to the dune foot. The intertidal beach was completely wet. The clustered data (7 data points) are given in **Table 7.2.7C**.

All verification data

Tables 7.2.7A,B,C summarize all data used (129 data points) in the verification computations.

Data	d_{50} (mm)	d_{90} (mm)	Coarse material p_{cf} (%)	Percentage moist spots p_m (%)	Moisture content w_{20mm} (%)	Wind velocity u_w (m/s)	height of wind velocity z_w (m)	Measurd shear velocity u_* (m/s)	$q_{s,measured}$ (g/m/s)
1. Koksijde BE (Strypsteen 2019)	0.22	0.4	1	0	0	8.6	1	0.32	13
2. Koksijde BE	0.22	0.4	1	0	0	9.8	1	0.54	22
3. Koksijde BE	0.22	0.4	1	0	0	10.1	1	0.55	22
4. Koksijde BE	0.22	0.4	1	0	0	10.7	1	0.5	28
5. Koksijde BE	0.22	0.4	1	0	0	8.8	1	0.4	8.6
6. Koksijde BE	0.22	0.4	1	0	0	9.5	1	0.52	17.3
7. Koksijde BE	0.22	0.4	1	0	0	10.5	1	0.58	26.1
8. Koksijde BE	0.22	0.4	1	0	0	11.8	1	0.7	37.3
1. Mariakerke BE (strypsteen 2019)	0.31	0.6	5	0	0	6	1	0.3	2
2. Mariakerke BE	0.31	0.6	5	0	0	6.5	1	0.32	3.3
3. Mariakerke BE	0.31	0.6	5	0	0	7.5	1	0.42	3.7
4. Mariakerke BE	0.31	0.6	5	0	0	8.1	1	0.45	8.4
5. Mariakerke BE	0.31	0.6	5	0	0	8.2	1	0.45	9.3
6. Mariakerke BE	0.31	0.6	5	0	0	9	1	0.42	16
7. Mariakerke BE	0.31	0.6	5	0	0	9.5	1	0.47	26.5
8. Mariakerke BE	0.31	0.6	5	0	0	10	1	0.52	27
1. Callantsoog NL	0.23	0.4	3	0	0	6.3	1.28	0.48	5.3
2. Callantsoog NL	0.23	0.4	3	0	0	7	1.18	0.61	10
3. Callantsoog NL	0.23	0.4	3	0	0	7.1	1.22	0.69	13
4. Callantsoog NL	0.23	0.4	3	0	0	8	1.25	0.79	16
5. Callantsoog NL	0.23	0.4	3	0	0	8.1	1.22	0.67	20
6. Callantsoog NL	0.23	0.4	3	0	0	8.3	1.27	0.59	20
7. Callantsoog NL	0.23	0.4	3	0	0	8.5	1.25	0.9	32
8. Callantsoog NL	0.23	0.4	3	0	0	8.6	1.22	0.82	28
9. Callantsoog NL	0.23	0.4	3	0	0	9	1.25	0.87	25
10. Callantsoog NL	0.23	0.4	3	0	0	18.5	1.43	1.12	410
11. Callantsoog NL	0.23	0.4	3	0	0	19	1.43	1.14	425
1. Texel Den Hoorn	0.27	0.4	1	0	0	10	1.38	0.54	33
1. Texel Prins Hendrik NL	0.27	0.5	3	0	0	9.5	1.25	0.64	48
2. Texel Prins Hendrik NL	0.26	0.5	1	0	0	10.7	1.27	0.8	78
1. Texel De Hors NL (Hijma and Lodder 2001)	0.23	0.5	3	0	0	5	1.3	0.22	1.2
2. Texel De Hors NL	0.23	0.5	3	0	0	5.6	1.3	0.28	3.8
3. Texel De Hors NL	0.23	0.5	3	0	0	6.5	1.3	0.32	8
4. Texel De Hors NL	0.23	0.5	3	0	0	7.3	1.3	0.38	21
5. Texel De Hors NL	0.23	0.5	3	0	0	7.9	1.3	0.43	25
6. Texel De Hors NL	0.23	0.5	3	0	0	8.6	1.3	0.48	43
7. Texel De Hors NL	0.23	0.5	3	0	0	8.7	1.3	0.52	22
8. Texel De Hors NL	0.23	0.5	3	0	0	9.6	1.3	0.58	25
9. Texel De Hors NL	0.23	0.5	3	0	0	9.8	1.3	0.62	55
10. Texel De Hors NL	0.23	0.5	3	0	0	12.2	1.3	0.72	127

11. Texel De Hors NL	0.23	0.5	3	0	0	13.1	1.3	0.85	145

Table 7.2.7A *Verification data (41) of aeolian sand transport; dry beach sand*

Data	d_{50} (mm)	d_{90} (mm)	Coarse material p_{cf} (%)	Percentage moist spots p_m (%)	Moisture content w_{20mm} (%)	Wind velocity u_w (m/s)	Height of wind velocity z_w (m)	Measured shear velocity u_* (m/s)	$q_{s,measured}$ (g/m/s)
1. Groote Keeten NL	0.24	0.5	1	0	0	8.5	1.23	0.62	24
2. Groote Keeten NL	0.24	0.5	1	0	0	8.9	1.23	0.68	39
3. Groote Keeten NL	0.24	0.5	1	0	0	9.5	1.23	0.7	43
4. Groote Keeten NL	0.24	0.5	1	0	0	8.9	1.23	0.73	30
5. Groote Keeten NL	0.24	0.5	1	0	0	8.8	1.23	0.65	31
6. Groote Keeten NL	0.24	0.5	1	0	0	8.9	1.23	0.68	39
1. Zandvoort NL	0.25	0.4	1	0	0	9.7	1.25	0.87	23
2. Zandvoort NL	0.25	0.4	1	0	0	9.6	1.25	0.87	30
3. Zandvoort NL	0.25	0.4	1	0	0	8.7	1.25	0.77	20
4. Zandvoort NL	0.25	0.4	1	0	0	10.2	1.25	0.98	33
5. Zandvoort NL	0.25	0.4	1	0	0	10.7	1.25	0.98	36
6. Zandvoort NL	0.25	0.4	1	0	0	9.	1.25	0.81	25
7. Zandvoort NL	0.25	0.4	1	0	0	10.9	1.25	0.86	39
8. Zandvoort NL	0.25	0.4	1	0	0	10.7	1.25	1.03	37
9. Zandvoort NL	0.25	0.4	1	0	0	10.2	1.25	1.06	38
10. Zandvoort NL	0.25	0.4	1	0	0	11.1	1.25	1.11	44
1. Benone IR (Jackson and Cooper 1999)	0.17	0.35	0	0	0	6	0.6	na	5
2. Benone IR	0.17	0.35	0	0	0	7	0.6	na	10
3. Benone IR	0.17	0.35	0	0	0	8	0.6	na	15
1. Inch Spit IR (Sherman et al., 2013)	0.17	0.4	0	0	0	7.4	1	0.39	2.5
2. Inch Spit IR	0.17	0.4	0	0	0	8.2	1	0.4	6.8
1. Esponsende PT (Sherman et al., 2013)	0.3	0.6	0	0	0	7.7	1	0.38	2.9
2. Esponsende PT	0.34	0.7	0	0	0	8.1	1	0.4	8.9
3. Esponsende PT	0.31	0.7	0	0	0	8.6	1	0.5	8.5
1. Jericoacoara BR (Sherman et al., 2013)	0.27	0.6	0	0	0	7.9	1	0.54	20
2. Jericoacoara BR	0.27	0.6	0	0	0	8.5	1	0.52	20.7
3. Jericoacoara BR	0.29	0.6	0	0	0	8.9	1	0.55	18.1
4. Jericoacoara BR	0.23	0.5	0	0	0	9.7	1	0.67	22
5. Jericoacoara BR	0.28	0.6	0	0	0	9.7	1	0.63	28
6. Jericoacoara BR	0.43	0.9	0	0	0	9.9	1	0.57	22

na= not available

Table 7.2.7B *Verification data (30) of aeolian sand transport; dry beach sand*

Data	d_{50} (mm)	d_{90} (mm)	Coarse material p_{cf} (%)	Percentage moist spots p_m (%)	Moisture content w_{20mm} (%)	Wind velocity u_w (m/s)	Height of wind velocity z_w (m)	Measured shear velocity u_* (m/s)	$q_{s,measured}$ (g/m/s)
1. Zeebrugge BE	0.2	0.4	3	30	4.7	8	0.9	0.6	10
2. Zeebrugge BE	0.2	0.4	3	30	4.7	8.3	0.9	0.54	14
3. Zeebrugge BE	0.2	0.4	10	80	3.7	11.3	0.84	0.91	37
1. Koksijde BE	0.2	0.4	3	80	4.5	9.6	1.04	0.72	16
2. Koksijde BE	0.25	0.45	10	10	3.6	10.1	0.9	1.04	23
3. Koksijde BE	0.35	0.35	3	90	8.9	8.7	0.75	0.56	8
1. Oostende BE	0.3	0.5	5	90	5.5	8	0.75	0.95	8
1. Lemmer NL	0.3	0.9	5	30	4	11	1.43	0.82	26
1. Texel Prins Hendrik NL	0.4	1	5	70	11	10.5	1.21	0.6	65
2. Texel Prins Hendrik NL	0.4	1	5	70	8	9.5	1.23	0.48	27
3. Texel Prins Hendrik NL	0.4	1	5	70	12	9.6	1.25	0.62	35
4. Texel Prins Hendrik NL	0.4	1	5	70	12	9.6	1.25	0.62	25
5. Texel Prins Hendrik NL	0.26	1	5	50	4	9.5	1.2	0.64	25
1 Texel Den Hoorn	0.27	0.4	1	80	5	12.5	1.25	0.96	45
1. Callantsoog NL	0.23	0.4	3	100	4.7	8.9	1.28	0.43	27
2. Callantsoog NL	0.23	0.4	3	70	8	9.5	1.13	0.52	45
3. Callantsoog NL	0.23	0.4	3	50	3	10	1.48	0.76	35
4. Callantsoog NL	0.23	0.4	3	70	8	10.5	1.13	0.66	60
5. Callantsoog NL	0.23	0.4	3	50	3.3	11	1.48	0.82	60
6. Callantsoog NL	0.23	0.4	3	100	4.5	11.3	1.28	0.71	101
7. Callantsoog NL	0.23	0.4	3	100	5	13	1.48	0.92	110
8. Callantsoog NL	0.23	0.4	3	80	2	19	1.43	1.14	435
9. Callantsoog NL	0.23	0.4	1	60	4	6.8	1.25	0.48	5.6
10. Callantsoog NL	0.23	0.4	1	60	4	6.9	1.25	0.48	6.4
11. Callantsoog NL	0.23	0.4	1	60	4	7.0	1.25	0.48	7.6
12. Callantsoog NL	0.23	0.4	1	60	4	7.5	1.25	0.48	12
13. Callantsoog NL	0.23	0.4	1	60	4	8.1	1.25	0.56	23
14. Callantsoog NL	0.23	0.4	1	60	4	8.1	1.25	0.56	22
15. Callantsoog NL	0.23	0.4	1	60	4	8.2	1.25	0.59	24
16. Callantsoog NL	0.23	0.4	1	60	4	8.2	1.25	0.53	26
17. Callantsoog NL	0.23	0.4	1	60	4	8.3	1.25	0.51	27
18. Callantsoog NL	0.23	0.4	1	60	4	8.9	1.25	0.59	20
19. Callantsoog NL	0.23	0.4	1	60	4	9.1	1.25	0.56	25
20. Callantsoog NL	0.23	0.4	1	90	6	12.3	1.2	0.84	125
21. Callantsoog NL	0.23	0.4	1	90	6	13	1.2	0.94	135
22. Callantsoog NL	0.23	0.4	1	90	6	12.2	1.2	0.76	120
23. Callantsoog NL	0.23	0.4	1	90	6	12.5	1.2	1.01	130
24. Callantsoog NL	0.23	0.4	1	90	6	13.3	1.2	1.1	150
25. Callantsoog NL	0.23	0.4	1	90	6	14.2	1.2	1.32	185
26. Callantsoog NL	0.23	0.4	1	90	6	14.3	1.2	1.27	165
27. Callantsoog NL	0.23	0.4	1	90	6	15	1.2	1.45	195
28. Callantsoog NL	0.23	0.4	1	90	6	15	1.2	1.53	200
29. Callantsoog NL	0.23	0.4	1	90	6	14.2	1.2	1.38	145
1. Saunton Sands UK (Sarre 1988)	0.17	0.55	0	70 (ea)	(ea)	8	2	na	7

2. Saunton Sands UK	0.17	0.55	0	70	8	9	2	na	12
3. Saunton Sands UK	0.17	0.55	0	70	8	10	2	na	30
4. Saunton Sands UK	0.17	0.55	0	70	8	11	2	na	50
5. Saunton Sands UK	0.17	0.55	0	70	8	12	2	na	75
6. Saunton Sands UK	0.17	0.55	0	70	8	13	2	na	100
7. Saunton Sands UK	0.17	0.55	0	70	8	14	2	na	120
8. Saunton Sands UK	0.17	0.55	0	70	8	16	2	na	190
9. Saunton Sands UK	0.17	0.55	0	70	8	19	2	na	220
1. Aberffraw UK (Wiggs et al., 2004)	0.2	0.5	0	50 (ea)	1	11.5	1	na	90
2. Aberffraw UK	0.2	0.5	0	50	2.5	11	1	na	30
3. Aberffraw UK	0.2	0.5	0	50	2	10.5	1	na	50
1. Wildwood USA (Jackson+Nordstrom 1997)	0.165	0.4	0	50 (ea)	3	5.5	1	0.22	2
2. Wildwood USA	0.165	0.4	0	50	3	6	1	0.27	4
3. Wifldwood USA	0.165	0.4	0	50	3	7	1	0.33	6

ea= estimated by author Van Rijn; na= not available

Table 7.2.7C *Verification data (58) of aeolian sand transport; moist beach sand*

7.3 Comparison of measured and predicted transport rates for dry and moist sand

Most of the commonly-accepted sand transport equations are based on the shear velocity at a power in the range of 2 to 3. Inaccuracies of the shear velocity are magnified due to the non-linear relationship between sand transport and shear velocity (Sherman, 2020). The shear velocity is derived from the measured velocities above the sand surface assuming a logarithmic velocity distribution. The shear velocity derived from the velocity profile expresses the effects of both the skin friction forces between the static and moving grains and the form drag forces of the roughness elements upwind of the measurement location such as bed relief, bed forms, debris and other obstacles present on the sand surface. Van Rijn and Strypsteen (2020) assume that the near-bed aeolian sand transport is driven by the grain-related shear velocity rather than the total shear velocity. The grain-related shear velocity (based on Equation 2.14) is smaller than the total shear velocity, as shown in Figure 7.3.1 for data measured at the beach of Callantsoog (The Netherlands). The predicted values are smaller than the measured values, except for extreme conditions when the surface irregularities are flattened by high wind velocities resulting in grain shear velocity values approaching to the overall shear velocity.

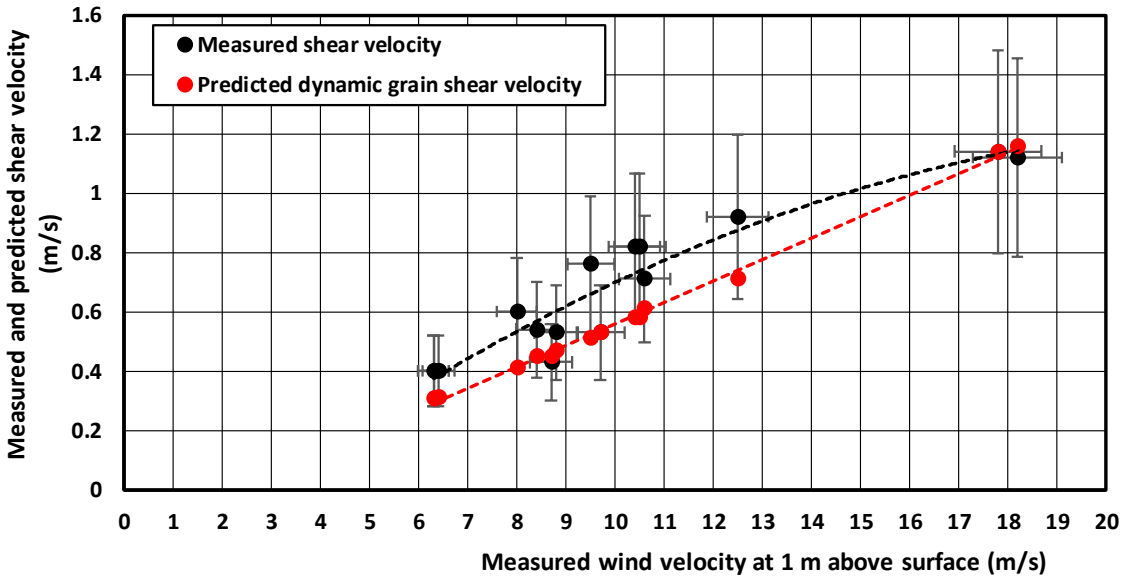

Figure 7.3.1 *Measured and predicted shear velocity; Beach Callantsoog, 2020*

To demonstrate that the grain-related shear velocity is a better parameter for representing aeolian sand transport, the measured transport rates of dry sand (68 data points; Tables 7.2.7A,B) are plotted as function of the grain-related shear velocity (based on Equation 2.14) and the total shear velocity, see **Figure 7.3.2**. As the grain-related shear velocity is smaller than the total shear velocity, the group of open symbols lies to the right of the group of solid symbols. Both groups can be represented by power functions showing a power of 3.1 for the open symbol group with R^2=0.71 and a power of 2.2 with R^2=0.6 for the solid symbol group. Thus, the correlation between sand transport and grain-related shear velocity is significantly better (less scatter).

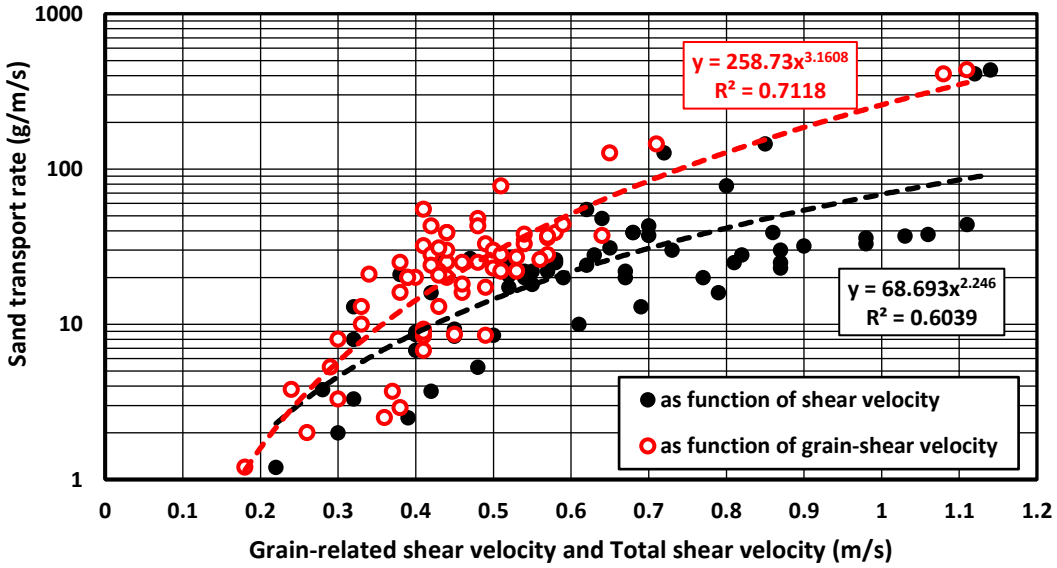

Figure 7.3.2 *Measured sand transport as function of grain-related shear velocity and total shear velocity*

The predictive equations of modified-Bagnold (Equations (2.8), (2.9)) and van Rijn (Equations (2.6b), (2.9), (2.10), (2.14)) have been verified using old and new field data sets, see **Tables 7.2.7A,B**.
The input data are: the measured wind velocity and height at which the wind velocity is measured, the d_{50} and d_{90}-values and percentage of coarse materials; the percentage of dry (p_d) and moist (p_m) spots upwind of the sampling location and the moisture content of the upper 20 mm of the moist spots (w_{20mm})**.**
The transport rates for moist sand conditions are based on: $q_s=(1-p_m/100)q_{s,d} + p_m/100\ q_{s,m}$
with: $q_{s,d}$= sand transport at dry spots; $q_{s,m}$=sand transport at moist spots; p_d= percentage of dry spots; p_m=percentage of dry spots at the beach upwind of the measurement location ($p_m+p_d=100\%$). The p_m and p_d values are not known for the literature data, but estimated as good as possible based on the available information.

The computation procedure of the predictive model of Van Rijn for dry sand is, as follows:
1) specify input data;
2) compute threshold shear velocity;
3) compute T-parameter (transport stage parameter);
4) compute grain-related roughness (k_s);
5) compute grain-related shear velocity ($u_{*,gr}$);
6) compute sand transport.

Other parameters are: $\kappa=0.4$; $\rho_{air}=1.2$ kg/m³; $\rho_{sand}=2650$ kg/m³; $\alpha_B=2$, $d_{50,ref,\ Bagnold}=0.00025$ m; $\alpha_{VR}=1.8$, $\beta=0.1$, $\alpha_{th}=0.08$.

The measured transport rates of dry sand are plotted as function of the wind speed at 1 m above the surface in **Figure 7.3.3**. The data of the Dutch beaches (Callantsoog, Texel), Benone Strand and Koksijde beach C are in fairly good agreement, which is most likely related to the use of bottom traps at all these sites. The field data of Mariakerke beach show relatively small values, which is most likely related to the use of the MWAC-bottles with the lowest opening at 0.05 m above the sand surface (less reliable as the sand transport below 0.05 m is not measured).
The measured data can be reasonably well represented by the new VR-transport equation based on the dynamic grain shear velocity. The power 3 relationship between the sand transport rate and the excess shear velocity squared is found to be valid for low and high wind conditions.

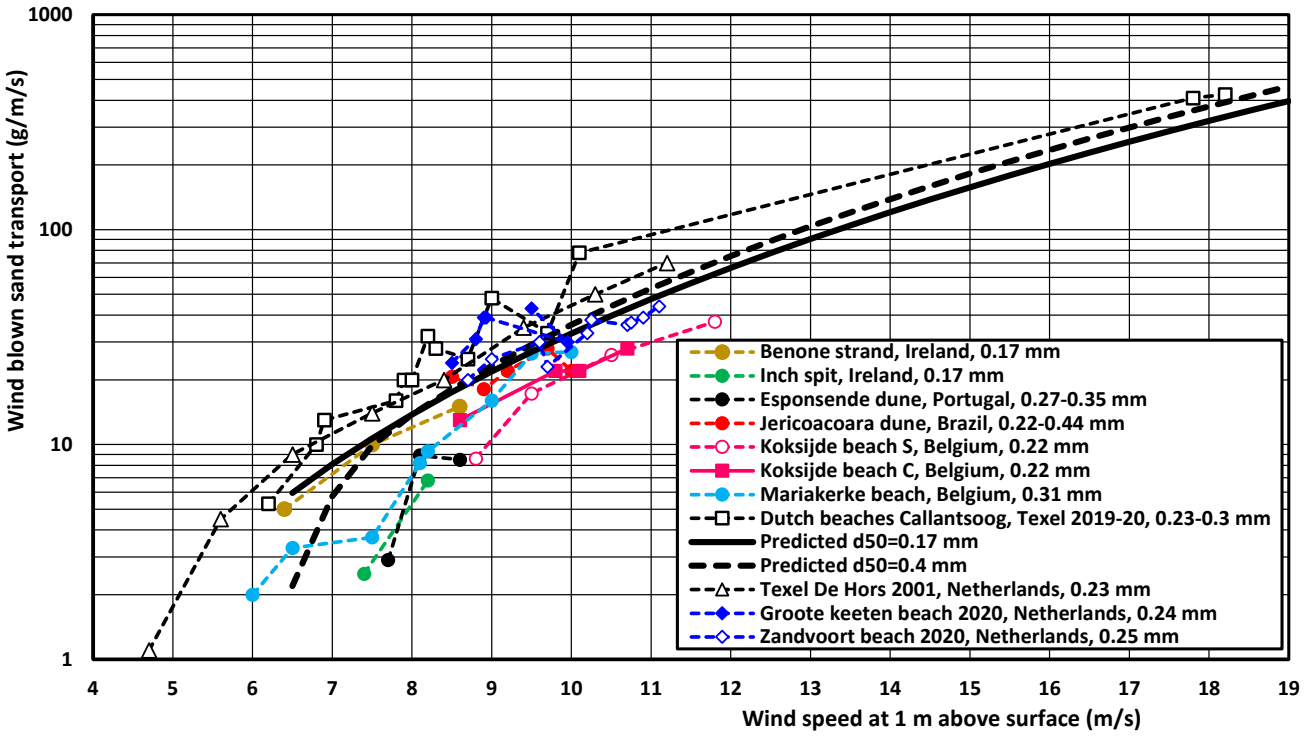

Figure 7.3.3 *Measured sand transport as function of wind speed at 1 m above the surface; dry sand data (Koksijde S refers to the data of Strypsteen 2019; Koksijde C refers to the data of Campos 2018)*

Figure 7.3.4left shows the plot of measured and predicted transport rates of the for dry sand conditions for the VR-transport equations. About 87% of the predicted data (71 data points) are within a factor of 2 of the measured values. The measured transport rates are slightly overpredicted for stronger wind conditions. The modified Bagnold-equations produces a score of 79%.

Figure 7.3.4right shows a similar plot for moist sand conditions. Now 91% of the predicted data (58 data points) of the VR-method are within a factor of 2 of the measured values. The Modified Bagnold-equations produces a score of 67%. The high scores of the VR-method are obtained for α_{VR}=1.8, β=0.1 (power of grain size) and α_{th}=0.08 (threshold coefficient), which also gave the best results for the wind tunnel data of Belly (1964), see Section 2.2. Thus, the field data seem to confirm that the influence of the grain size in the range of 0.15 to 0.4 mm is minor and is better represented by a power of 0.1 than 0.5. Three very high transport rates were measured on 9 February 2020 during a storm with high wind velocities around 19 m/s (BF 9). The bag of the bed load sampler was full in 4 minutes. These record transport rates with values in the range of 400 to 450 g/m/s reveal that the transport rate depends on a power 3 relationship up to wind velocities of 19 m/s. However, this conclusion is not very solid as only a few data points are available in the high wind velocity range of 13 to 20 m/s (BF 7 to 9). This emphasizes the need for more data in this range. The VR-method seems to underpredict for wind velocities > 10 m/s, which is most likely caused by the wind gustiness effect. The field transport measurements are strongly influenced by short-duration (30 s) wind gusts within the measuring period of say 10 minutes, whereas the predicted transport is based on a time-averaged wind velocity neglecting the gust effect. A method to solve this may be the introduction of a gust coefficient in the range 1.05 to 1.1 acting on the time-averaged wind velocity.

Exploratory computations have been made with a gust coefficient acting on the wind velocity: $\alpha_{gust}=1+0.1\tanh(u_w-u_{w,th}/u_w)$ with $u_{w,th}$= threshold wind speed (6 to 7 m/s) resulting $\alpha_{gust}\cong 1$ for low wind speeds increasing to 1.05 for high wind speeds (u_w=20 m/s). This approach yields slightly better agreement for higher wind velocities. More research is required to define an appropriate gust coefficient.

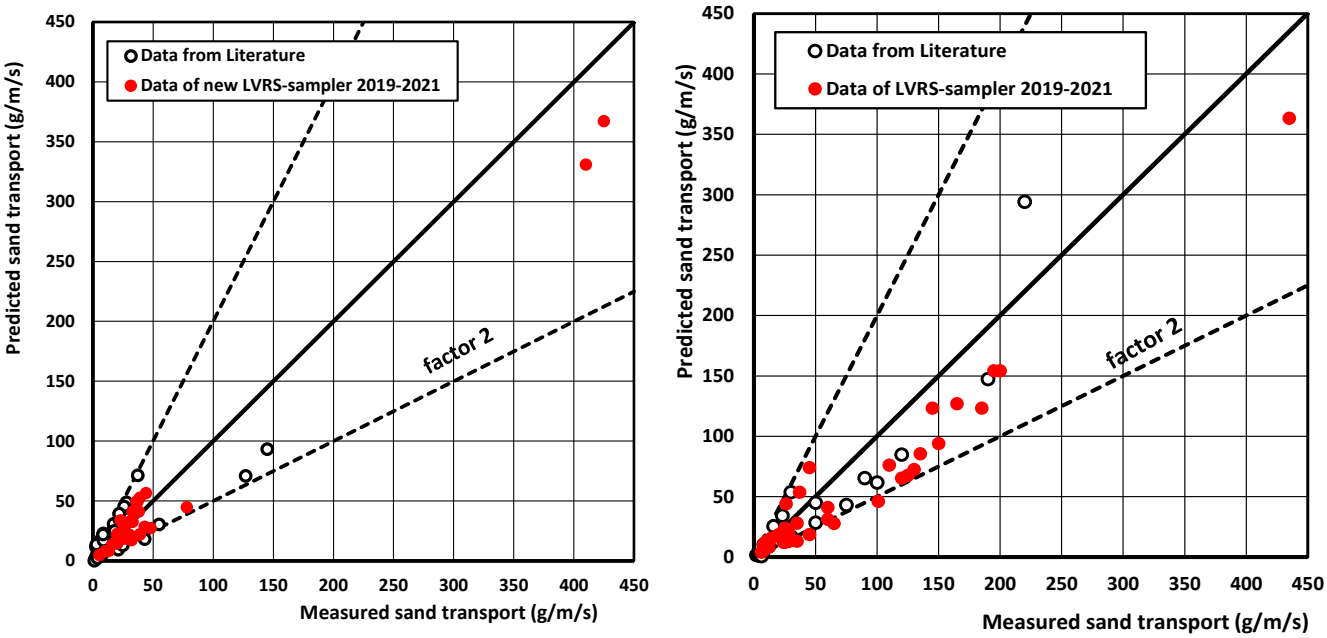

Figure 7.3.4 *Comparison of measured and predicted sand transport; VR-transport equations*
Left: dry beach surface (71 data points); Right: moist beach surface (58 data points)

Figure 7.3.5 shows the ratio of measured and predicted sand transport as function of the wind speed for the new VR-transport equation. It can easily be counted that 10 (11%) of the 128 data points are outside the range of a factor of 2 and thus 89% are within a factor of 2. As regards the dry sand data points, about 50% of the data points are above and under the ratio of 1 (no bias). As regards the moist sand data points, most values are above the ratio of 1 indicating underprediction. Most likely, the effect of moist sand on the predicted sand transport is somewhat too strong. The new VR-sand transport equation seems to work well for low very wind speeds (5 to 7 m/s) and very high wind speeds (15 to 20 m/s).

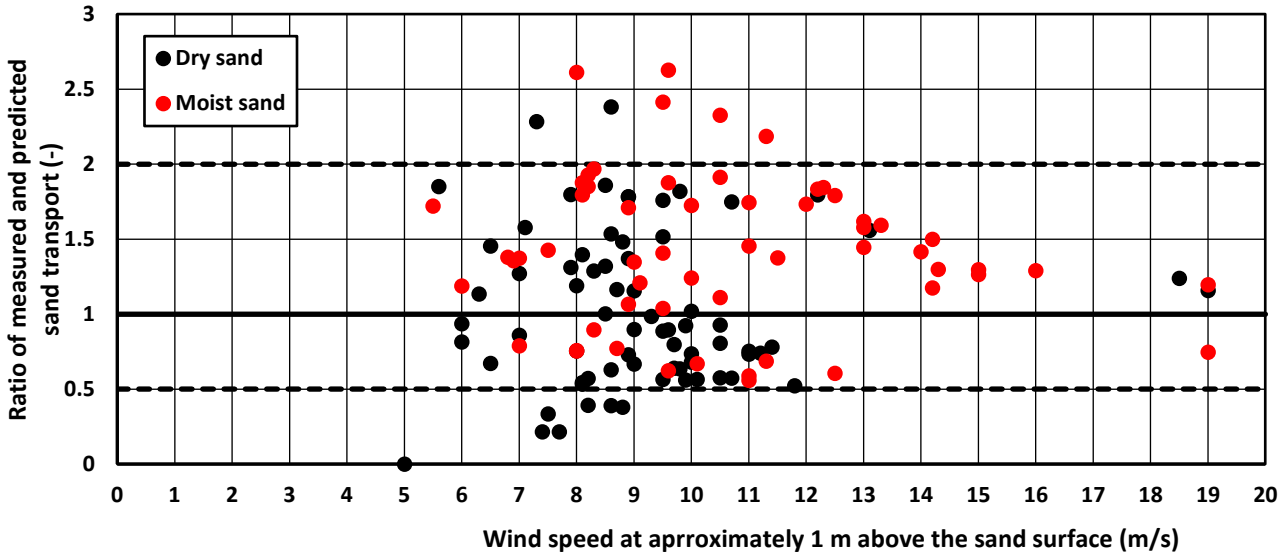

Figure 7.3.5 *Ratio of measured and predicted sand transport for new VR-transport equation*

7.4 Comparison of measured and predicted transport rates for dry sand at low velocities

Special attention is given to the transport of dry sand just beyond the threshold value based measurements at the beach of Callantsoog (The Netherlands) and in the mini wind tunnel (see Section 3) and in the field.
Very small transport rates at low velocities are of less practical importance, but it is interesting to determine the type of relationship between transport and shear stress around the threshold conditions and to determine the predicting ability of available deterministic transport equations for low shear stresses and intermittent transport conditions.
The field tests were done at the beach of Callantsoog in The Netherlands (29 February, 13 April and 24 October 2020) in conditions with fairly dry sand during wind velocities of 5 to 8 m/s. (BF 4 to 6). The median particle size (d_{50}) at the beach of Callantsoog is in the range of 0.2 to 0.26 mm (0.23±0.03 mm). In addition, a series of tests have been done in a mini wind tunnel (length=1 m ; width=0.06 m, see Section 3) to measure the sand transport rate of dry particles at low wind velocities just above the threshold conditions. The wind flow with a constant velocity (without gusts) is generated by a commercial hair fohn. The wind velocity can be increased gradually by placing the fohn closer to the tunnel entrance. The sand transport rate was determined from the mass difference of the tray (length of 0.2 m) with sand before and after the test. The effective transport width at the sand surface of the tray is 0.03 m based on visual observations of the scour marks. The test duration was in the range of 40 to 100 s. The tray was filled with sand with a smooth surface flush with the edges of the tray and weighed (mass of about 320 g). Some tests were done with a flat sand surface, but most tests were done with an irregular sand surface consisting of small (artificial) ripple type irregularities with height of 5 mm at the sand surface. Four types of uniform dry sand with diameters 0.17 mm, 0.35, 0.6 and 0.8 mm were used. In addition, two sand samples (C1, C2) from the beach of Callantsoog (The Netherlands) were used. The median particle size (d_{50}) at the beach of Callantsoog is in the range of 0.2 to 0.26 mm (0.23±0.03 mm). Sample C1 is the original beach sand with $d_{50}\cong$0.23 mm excluding coarse fraction of gravels and shell fragments (removed using a sieve of 1 mm), see **Figure 7.4.1**. Sample C2 is taken from trapped sand of the bed load sampler (Section 3.3) and consists of slightly finer sand with $d_{50}\cong$0.2 m without coarse materials. The sand characteristics are also given in **Table 7.4.1**.

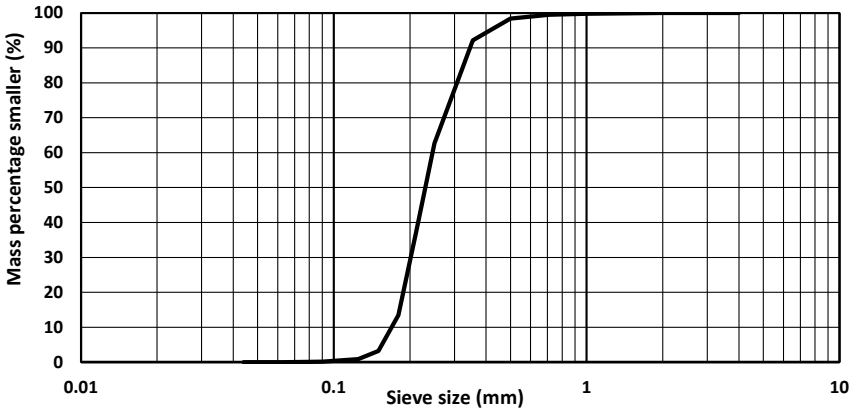

Figure 7.4.1 *Particle size distribution of sample C1; beach sand Callantsoog, The Netherlands*

The wind velocity ($u_{0.03}$) was measured in the axis of the tunnel at 0.03 m above the sand surface at the end of the tray using a miniature wind velocity meter (Kaindl windmaster2; Kwm2; miniature cup-rotor of 25 mm wide and 10 mm high). It is noted that the wind velocity in the tunnel is a constant wind velocity without gusts as present in nature (prototype). To compare the wind tunnel data to field data, the wind $u_{0.03}$ has been converted to a virtual wind velocity u_1 at 1 m above the surface using the equation $u_1=\alpha_{log}u_{0.03}$ with α_{log}= coefficient related to logarithmic velocity profile ($\cong$1.5 for a bed roughness of about 0.5 mm; velocity at 1 m is about 50 % higher than that at 0.03 m)

First, the instantaneous threshold wind velocities of the sand samples used in the mini wind tunnel are discussed. The values are shown in **Table 7.4.1** and **Figure 7.4.2**. The measured threshold velocities are higher (15% to 20%) than the predicted values based on the Bagnold-equation with $\alpha_{th,\ initiation}$=0.1. The time-averaged (over 10 minutes) threshold wind velocity measured at the beach of Callantsoog with d_{50}=0.23 mm is about 6 m/s (at z=1 m above surface). The same sand in the mini tunnel requires a velocity of 7.7 m/s for initiation of motion. The measured threshold velocity at the beach of Callantsoog is close to the predicted value of the Bagnold-equation with coefficient=0.1. The threshold wind velocity measured at the beach of Callantsoog (6 m/s) represents the time-averaged velocity including wind gusts. The peak velocities in field conditions over a short period of say 10 minutes can be represented by $u_{peak}=u_{mean}+\sigma_U$ with σ_U =0.15-0.2u_{mean} (Stout and Zobeck, 1997). Thus, the peak velocities (instantaneous velocity) causing initiation of particle motion at the beach are about 15% to 20% higher resulting in values in the range of 7.1 to 7.5 m/s which is fairly close to the value of 7.7 m/s measured in the tunnel. The wind velocities measured in the tunnel are almost constant with very minor turbulent fluctuations (<3%) and can therefore be seen as instantaneous velocities. The instantaneous threshold velocity can be represented by the Bagnold-equation with a coefficient α_{th}=0.12. The threshold velocity for cessation of motion is much smaller, see **Figure 7.4.2**.
The results of the sand transport experiments at low velocities at the beach of Callantsoog on 29 February, 13 April and 24 October 2020 using the bed load sampler (see Section 3.3) are shown in **Figure 7.4.3**. The basic data are taken from **Tables 6.3.3C,D,E**. The transport rates of sand with d_{50}=0.23 mm were measured in the velocity range of 6 to 8 m/s (time-averaged values over 10 minutes). Predicted transport rates are shown for different values of the cessation threshold coefficient ($\alpha_{th,cessation}$=0.07 and 0.08). The predicted values for $\alpha_{th,cessation}$=0.07 are quite good for velocities in the range of 6 to 7.5 m/s, but somewhat too small for the velocity range of 7.5 to 8 m/s. The predicted transport rates are somewhat too small for $\alpha_{th,cessation}$=0.08. Two effects are important in the low velocity regime: i) sand transport ceases at a much lower velocity than that for initiation of erosion and ii) the finer sand particles (< 0.15 mm) are more easily winnowed from the sand surface resulting in higher transport rates. The sand trapped in the bed load sampler at the beach of Callantsoog was finer ($d_{50} \cong$ 0.2 mm)

than the original bed material (d_{50}≅0.23 mm). The representation of these processes by a deterministic transport equation requires a relatively small threshold value ($\alpha_{th,cessation}$=0.07).

Sand	Instantaneous threshold wind velocity at z=0.03 m above bed for initiation of motion in mini wind tunnel $u_{0.03}$ (m/s)	Instantaneous threshold wind velocity at 1 m above bed u_1 for initiation of motion (m/s)
Uniform: d_{50}=0.17 mm (0.1-0.3 mm)	4.3	6.5
Uniform: d_{50}=0.35 mm (0.3-0.5 mm)	6.7	8.7
Uniform: d_{50}=0.6 mm (0.4-0.8 mm)	7.1	10.7
Uniform: d_{50}=0.8 mm (0.5-1 mm)	8.4	12.6
C1 Callantsoog beach d_{50}=0.23 mm; without coarse materials	5.1	7.7
C2 Callantsoog beach d_{50}=0.2 mm; no coarse materials	4.8	7.2

Table 7.4.1 *Threshold wind velocities of various types of sand in mini wind tunnel*

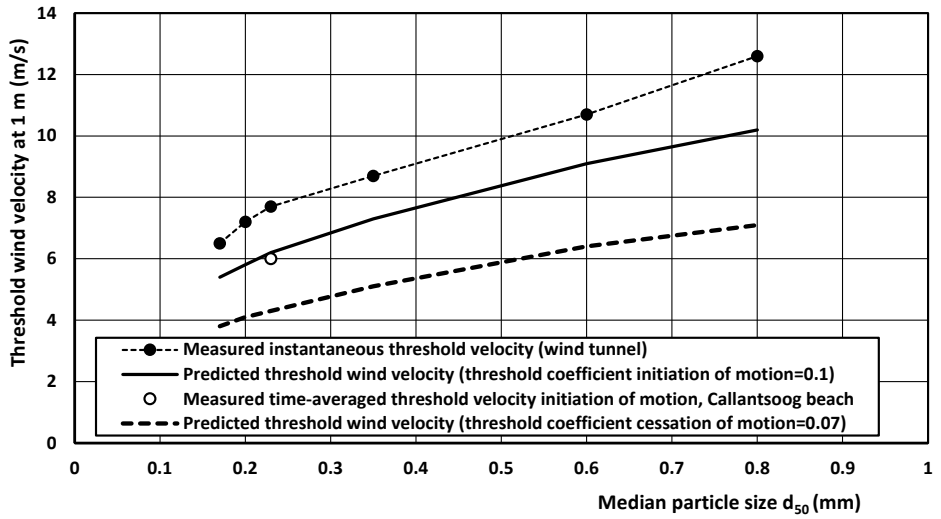

Figure 7.4.2 *Threshold wind velocity of sand bed*

Figure 7.4.3 also shows predicted values of the Multi-Fraction (MF) method using the VR-transport equation. The MF-method (Section 2.1.2) has been used with 7 fractions: 5% of 0.06-0.1 mm; 10% of 0.1-0.15 mm; 20% of 0.15-0.2 mm; 25% of 0.2-0.25 mm; 20% of 0.25-3 mm; 15% of 0.3-0.35 mm and 5% of 0.35-0.4 mm (d_{50}=0.23 mm) and hiding-exposure coefficient equal to 1. The results of the MF-method are almost the same as those of the Single-Fraction (SF) method. The MF-method is most suitable for widely graded sediments with a substantial coarse fraction, but has no added value for fine almost uniform sediments.
The strong increase of the measured transport rates in the velocity range of 7.5 to 8 m/s (**Figure 7.4.3**) may be caused by wind gust effects.

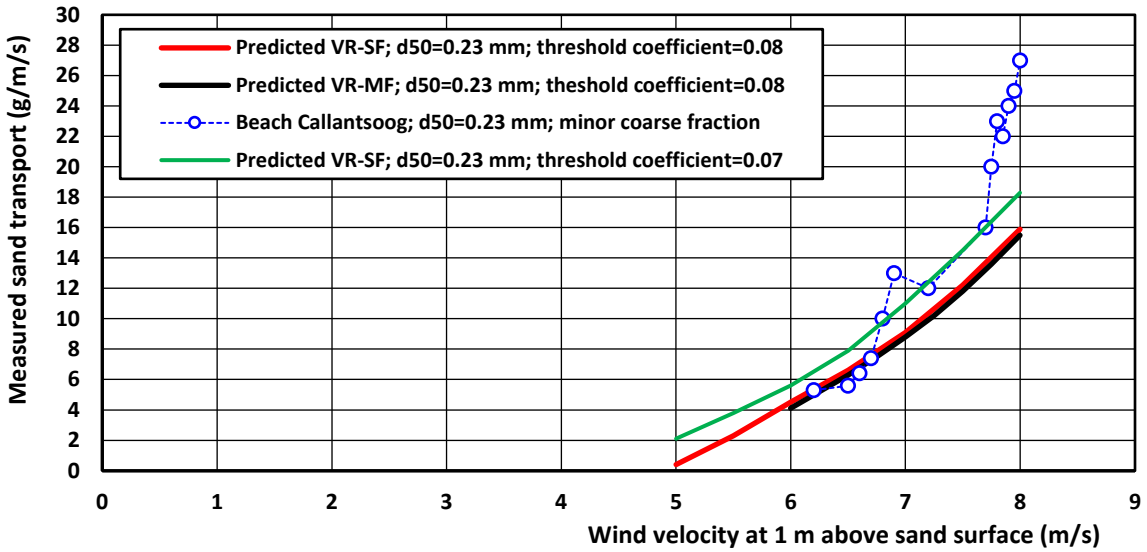

Figure 7.4.3 *Sand transport at low velocities at beach of Callantsoog, The Netherlands*
VR-SF= Van Rijn equation based on Single Fraction method; MF= Multi-Fraction method

The results of the sand transport experiments with dry sand in the mini wind tunnel at low velocities are given in **Table 7.4.2** and in **Figure 7.4.4**. The error range of the measured transport rates is about ±30% based on the variation of repetitive tests. It can be observed that the measured sand transport rates at low velocities are strongly related to the particle size and the associated threshold wind velocity. Larger particles have a higher threshold velocity and thus a lower transport rate at the same velocity.

Figure 7.4.5 shows the results of both the tunnel tests and the field experiments. The results are plotted as function of an excess shear stress parameter u_{1m}^2-$u_{th,cessation}^2$, with $u_{th,cessation}$= threshold velocity at cessation of transport (transport=0). Sand transport is assumed to be intermittent for $u_{1m} < 1.3\ u_{th,cessation}$. Sand transport is clearly higher for sand of 0,.17 mm than for 0.23 mm, but the results of particles in the range of 0.35 to 0.8 mm are somewhat scattered without a clear trend. The measured sand transport data suggests a nonlinear relationship between transport and shear stress, particularly the field data at the transition from intermittent to continuous transport at velocities > 7.5 m/s (excess parameter > 40). The measured field data of Callantsoog beach can be reasonably well represented by the VR-sand transport equation using $\alpha_{th,cessation}$=0.07, which is based on a nonlinear relationship (power 1.5) between transport and shear stress . Using $\alpha_{th,initiation}$=0.10, the predicted sand transport values are much too small. Based on this, it is concluded that the threshold value can be best represented by the cessation threshold value.
It is noted that these measurements in the mini wind tunnel should be seen as exploring as it is questionable whether the measured transport rates in the mini tunnel represent equilibrium conditions given the short length (0.2 m) of the sand tray. The adjustment length for establishing equilibrium sand transport with only rolling particles is most likely fairly small, but its proper value is unknown. More research is required to better determine the effect of particle diameter on the transport rates at low velocities.

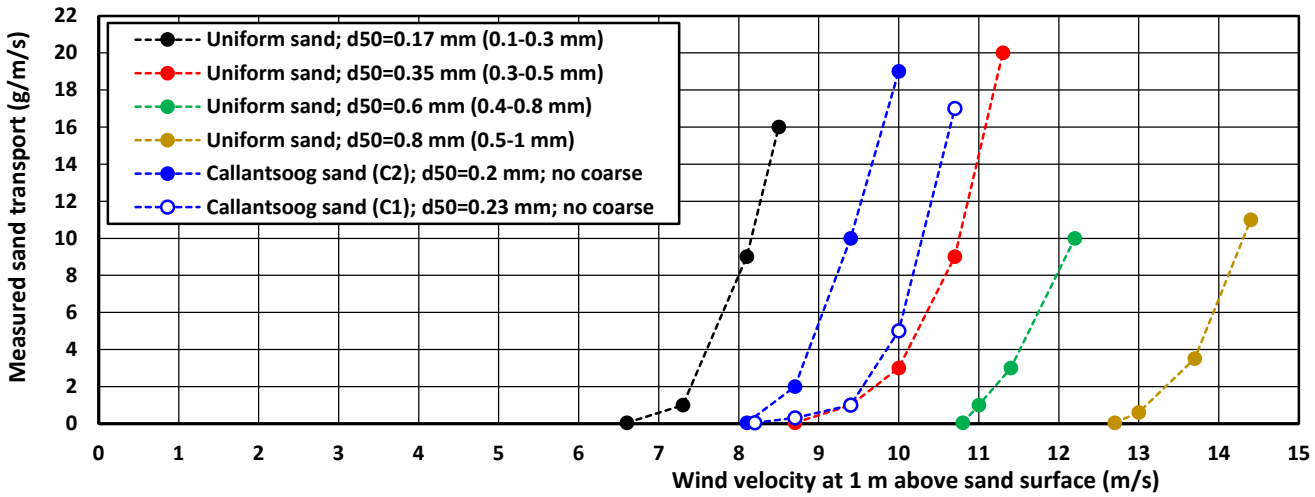

Figure 7.4.4 *Sand transport at low velocities in mini wind tunnel*

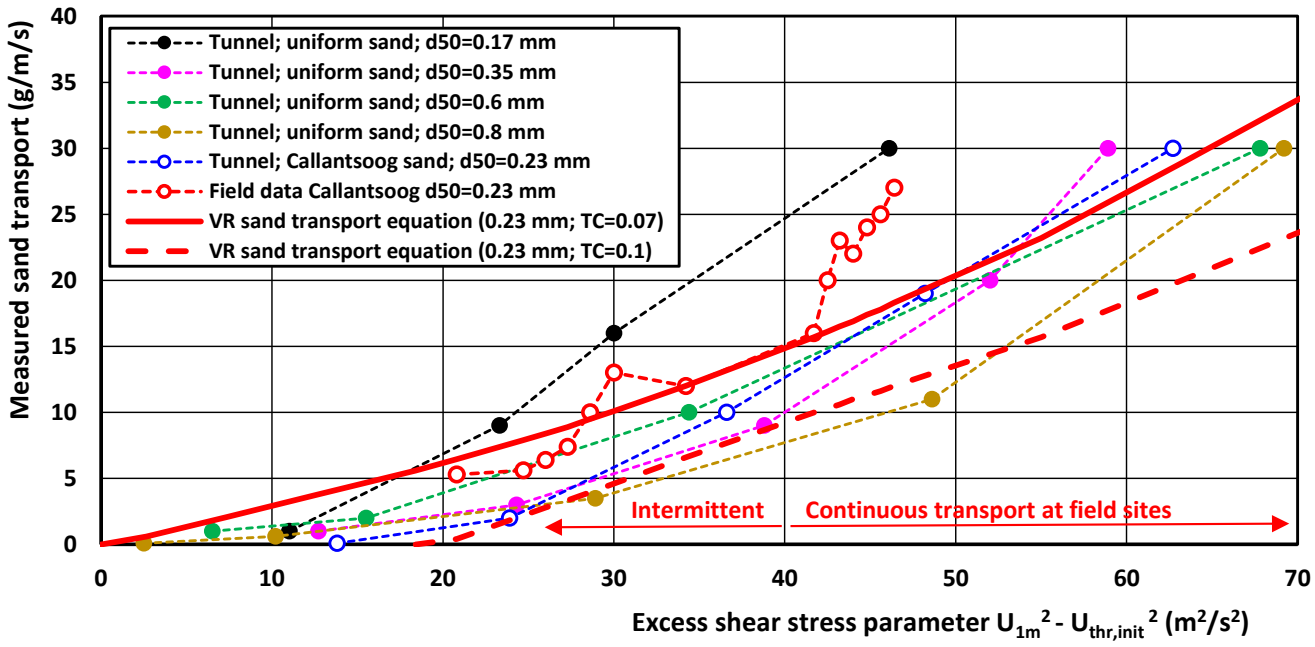

Figure 7.4.5 *Sand transport at low velocities as function of excess shear stress parameter*

Sand (mm)	Measured wind velocity at 0.03 m above sand surface in tunnel (m/s)	Computed wind velocity at 1 m above sand surface in nature (m/s)	Measured sand transport rate (g/m/s)	
			irregular surface	flat surface
Tunnel: 0.17	4.9	7.3	1	0.8
	5.4	8.1	9	6
	5.7	8.5	16	9
	6.3	9.4	30	26
Tunnel: 0.35	6.3	9.4	1	
	6.7	10	3	
	7.1	10.7	9	
	7.5	11.3	20	
	7.7	11.6	30	
Tunnel: 0.6	7.3	11	1	
	7.6	11.4	2	
	8.1	12.2	10	
	9	13.5	30	
Tunnel: 0.8	8.5	12.7		<0.1
	8.7	13		0.6
	9.1	13.7		3.5
	9.6	14.4	13	11
	10.1	15.1		30
Tunnel: Callantsoog beach sand (C1) d_{50}=0.23 mm excluding coarse fraction > 1 mm	5.5	8.2	<0.1	
	5.8	8.7	0.3	
	6.3	9.4	1	
	6.7	10	5	
	7.1	10.7	17	
	7.5	11.3	28	
Tunnel: Callantsoog beach (C2) d_{50}=0.2 mm; no coarse fraction	5.4	8.1	<0.1	
	5.8	8.7	2	
	6.3	9.4	10	
	6.7	10	19	
	7.1	10.7	30	
Field measurements: Callantsoog beach sand1) 29 February 2020 13 April 2020 24 October 2020 d_{50}=0.23 mm minor coarse (< 2%)		6.2	5.3	
		6.5	5.6	
		6.6	6.4	
		6.7	7.4	
		6.8	10	
		6.9	13	
		7.2	12	
		7.7	16	
		7.8	20	
		7.8	23	
		7.8	22	
		7.9	24	
		7.9	25	
		8	27	

Table 7.4.2 *Transport of dry sand at low wind velocities in mini wind tunnel*

8. Sand transport predictions for coastal sites

8.1 General

Long term estimates of the aeolian sand transport at the Dutch coast can be obtained from the long term development of the foredunes or from long term sand transport predictions. The Dutch dune system consists of large rows of parabolic dunes with most fore dune heights in the range of 10 to 20 m and extending over a maximum width of 4.5 km in the center part (south of Zandvoort). This system was formed in the period between 800 and 1600 AD (Jelgerma et al., 1970). Pool and Van der Valk (1988) have shown that the development of this younger dune system can be explained by a long term annual onshore wind transport of about 50 m^3/m/year.
Nowadays, the annual wind transport rates are much lower, as the maximum annual migration of the dune foot is of the order of 1 m/year for beaches having a width of about 100 to 150 m (Mulder and Tonnon, 2011). Given an average dune height of 15 m and a maximum dune migration velocity of 1 m/year, the maximum annual wind transport is of the order of 15 x 1=15 m^3/m/year, which is much smaller than the annual onshore wind transport capacity of dry sand of about 50 to 100 m^3/m/year for the Dutch wind climate. Various limiting transport factors can be identified: rainfall, shells, vegetation, salt crusts and wind velocity reduction in front of high dunes (obstacle effect).
The proposed equations (modified Bagnold method and VR-method; Section 2) have been used to predict the long term annual wind transport at the sandy beach of Callantsoog in the north-west part of The Netherlands. The wind and rain data are taken from the inland weather station De Kooy, which is about 5 km inland of the beach of Callantsoog. The wind velocity and direction at the beach of Callantsoog seaward of the dune system are not the same at that measured at the open space of the inland weather station. Ideally, long term wind data should be measured directly on the beach. In practice, this is not feasible at low costs. Therefore, it is only possible to use the available wind data from nearby weather stations.
Two effects are studied in more detail: the effect of a large-scale obstacle (foredune) on the wind velocities and the inclusion and representation (schematization) of the rain data. This latter can to some extent be avoided by using the annual time series of rainfall data (rain intensity and rain duration).

8.2 Effect of wind modification on sand transport predictions

8.2.1 General

Long term wind transport predictions at beaches are most often based on wind velocities measured at regional weather or airport stations. The wind velocity at these stations is measured at an openly exposed location for all directions. The wind velocity and direction measured at these stations are not the same as those on the beaches. When the weather station is situated at an inland location, the wind velocities at the beach will most likely be somewhat higher than those at the inland location (inland-beach effect).
When the beach considered is backed by high foredunes (> 10 m), the wind velocity in the lower boundary layer at the beach may be reduced due to the obstacle effect created by the foredunes, particularly for shore-normal wind conditions. Due to pressure buildup in front of the foredune, the wind streamlines near the beach surface are gradually pushed upwards resulting in lower wind velocities (Wiggs et al., 1996; Hesp et al., 2005; Bauer et al., 2012). This effect will be stronger for higher and steeper foredunes (obstacle-effect).
Summarizing, the wind velocity at the beach can be related to the wind velocity at a nearby regional location (weather station) by: $u_{w,beach}=f_r\, f_o\, u_{w,regional}$ with: f_r= conversion factor from regional (inland) wind at height of 10 m to beach wind at height of 10 m (assumed to constant for all directions; range of 1 to 1.2), f_o= obstacle factor related to the wind direction, the height at which the beach wind is measured, the height and the steepness of the obstacle (foredune). The f_o-factor will be smallest for small measurements heights above the beach surface.

8.2.2 Obstacle effect due to presence of foredunes

De Winter et al. (2020) have observed that local 10-minute averaged wind speed and direction on the beach in front of a high foredune (obstacle) can differ from the regional wind conditions at an open site (here measured 15 km away from the study site). Large objects such as high dunes cause a buildup of pressure on their upwind side which leads to a smooth transition of streamlines around the object and reduced wind velocities in the high-pressure area. This means that at the dune foot and at the beach local wind speeds should be lower compared to a regionally representative wind speed due to the buildup of pressure in front of the foredune. This effect increases for higher and steeper foredunes and less oblique winds.
All field experiments (two field campaigns of 6 weeks; autumn 2015 and 2017) were conducted approximately 3 kilometers south of the beach town Egmond aan Zee, The Netherlands. The median grain size (d_{50}) of the quartz sands on the beach is about 0.25 mm. The tidal range is between 1.2 and 1.8 m. The beach has a width varying between 30 and 100 m and is backed by high dunes (up to 22 m). Depending on the tidal water level, and thus varying beach width, between 3 and 6 ultrasonic anemometers were deployed in a cross-shore array from the waterline to the dune foot with a spacing of about 10 m. One of the ultrasonic anemometers had a fixed location at the dune foot (3 m above mean sea level) and was used here as a local reference station. The sampling frequency was 10 Hz and the measuring height was 0.9 m.
Regional wind conditions were measured at a meteorological station of the Dutch national weather service in IJmuiden-harbour, which is about 15 km south of the beach site. This weather station on top of a short tower on the end of the southern harbour breakwater is openly exposed to winds from all sea directions ($f_r \cong 1$). Regional wind velocities (up to 18 m/s at height of 10 m) were converted to a velocity at 0.9 m above the surface (assumed roughness k_s=0.03 m; yielding: $u_{reg,0.9m}$=0,.74 $u_{reg,10m}$).
Regional wind speeds at IJmuiden transformed to 0.9 m height ranged between 0.4 and 18.2 m/s, and were compared to the local wind speeds measured at 0.9 m at the beach in Egmond aan Zee with speeds ranging from 1.0 to 14.3 m/s. During conditions with dune-normal winds, the maximum windspeeds at the beach were 6 to 8 m/s, where the regional wind speeds were 12 to 14 m/s. The results show that the local wind velocities are smaller than the regional wind velocities except for velocities smaller than 3.0 to 4.0 m/s. The ratio of local over regional wind speed at the beach site (not close to the dune foot) is about 0.4 when the wind direction is dune-normal. The wind speeds at the dune foot were found to be about 50% smaller than those at the beach for dune-normal conditions and about 20% smaller for almost dune-parallel winds. This ratio increases with increasing obliquity towards almost 1 for alongshore winds. The wind direction of local winds at the intertidal and dry beach are almost the same as those of the regional winds. Deviation of the wind velocity (wind steering) only occurs at the dune foot and is the largest (about 13˚ larger than the incoming wind angle) with oblique approaching winds of 40˚ from the dune normal. Perpendicular and nearly alongshore winds do not show any steering near the dune foot. The use of local rather than regional wind conditions in a potential transport equation reduced the predicted annual aeolian transport substantially (factor 2 to 3).
The measured results of De Winter et al. (2020) are herein described by a simple linear function, as follows:

$$u_{w,midbeach} = f_r\, f_o\, u_{w,regional} \qquad (8.1.a)$$

$$f_o = f_{o,m}\,[1-abs(\theta)/90] + abs(\theta)/90 \qquad (8.1b)$$

with: θ= wind incidence angle to the shore-normal (degrees); f_r= conversion factor for wind velocity from inland to coast (1.0 to 1.1); $f_{o,m}$= minimum value of f_o-coefficient (input value depending on obstacle height; range of 0.5 to 1).
Equation (8.1) yields values between $f_{o,m}$ and 1 depending on the wind incidence angle; $f_o = f_{m,o}$ for shore normal wind and f_o=1 for shore-parallel wind.

8.3 Representation of rainfall and surface moisture in sand transport predictions

Field observations show that the sand transport is restricted by moisture (rainfall) effects.
The transport conditions on dry and moist beaches can most generally be described, as follows:

- moist sand is eroded and transported over a moist beach surface; mostly in conditions with major storm events and high wind speeds (BF>7);
- dry sand is eroded from dry spots (also from relatively dry bed form crests) and from dry upwind sources (sheltered areas, under beach houses/buildings on piles); mostly during minor storm events (BF> 6);
- dry sand is eroded and transported over a dry beach surface; mostly during dry summer conditions with daily winds (BF>4).

Table 8.6.1 summarizes the sand transport restrictions for various (strength) combinations of wind and rain fall in a fairly wet and windy climate as present along the beaches in North-Western Europe based on experiences of the author during many field trips/visits. The percentage of occurrence of each condition (each cell) is an estimated value based on available knowledge and common sense. Sand transport is restricted in about 30% of the time in conditions with no rainfall (supply-limited conditions). During rainfall with strong to stormy winds parallel to the beach, sand transport continues as rainfall has not much effect. Splash-type transport may be dominant in strong rains and mild winds. Strongly restricted transport occurs in about 20% of the time during light rainfall and immediately after rain fall with light winds.
Moisture effects are almost not of importance for wind conditions parallel to the beach because the fetch is then almost infinite and dry sand is always available at some spots from the erosion process is initiated. Moisture effects are very important for wind conditions with very oblique or normal winds from offshore. The fetch over the wet lower intertidal zone and the moist upper beach is generally too short for the development of equilibrium sand transport conditions resulting in underloading conditions.

Rain	**No rain**			**Light rain < 1 mm/hour**	**Medium rain 1-5 mm/hour**	**Strong rain > 10 mm/hour**
Wind	**m.c. <2%**	**2-8%**	**8-15%**	**m.c.=4-8%**	**8-10%**	**10-15%**
Light wind 5-8 m/s (< BF4)	unrestricted wind transport 50% of time	slightly restricted 5-10%	restricted transport 5-10% of time	restricted transport 5-10% of time	very restricted; minor splash-type transport may occur 3-5% of time	very restricted; minor splash-type transport may occur <1% of time
Strong wind 8-15 m/s BF5 to 7	unrestricted wind transport 10% of time	wind ⊥: restricted wind//: unrestricted 5-10%	wind ⊥: restricted wind//: slightly restricted 3-5% of time	wind ⊥: restricted wind//: unrestricted 3-5% of time	wind ⊥: restricted some splash-type tr. wind//: unrestricted tr. and splash-type tr. <1% of time	wind ⊥: very restricted; splash-type transport wind//: slightly restricted; splash-type transport <1% of time
Storm wind > 15 m/s BF8 to 10	unrestricted wind transport 1% of time	wind ⊥: restricted wind//: unrestricted 1% of time	wind ⊥: restricted wind//: slightly restricted 1% of time	wind ⊥: restricted wind//: unrestricted 1% of time	wind ⊥: slightly restricted only splash-type tr. wind//: unrestricted tr. and splash-type tr. <1% of time	wind ⊥: slightly restricted only splash-type transport wind//: unrestricted and splash-type tr. <1% of time

m.c.= moisture content; wind ⊥ = wind normal to beach (often supply-limited as beach width usually< 100 m); wind//= wind parallel to beach (no supply-limitation as upwind sources are abundant; fetch length > 1000 m)

Table 8.3.1 *Effect of rainfall and wind on type of sand transport at exposed beach sites*

Based on field observations during and after rainfall events, three types of transport periods are herein distinguished (see also **Figure 8.3.1**):

- rainfall period with almost wet sand surface and moisture levels of about 8% in the upper 20 mm of the sand bed; no sand transport for low wind velocities < 10 m/s;
- drying period with wet and dry spots on the beach surface; moisture levels gradually reduce from 8% to 2% and;
- almost dry period when moisture levels of the upper 20 mm are below 2% (mc-levels of upper 1-5 mm are below 1%).

The duration of the drying period strongly depends on the wind strength and the air temperature (see **Section 4.2**). The drying period can be schematized in a series of blocks (histograms) with decreasing values of the moisture percentage and the percentage of wet spots. For example, six hours after the last rainfall event at the beach of Zeebrugge (Belgium), the percentage of wet spots at the upper beach surface was still about 50% with moisture level of 4% and only slightly reduced sand transport rates.

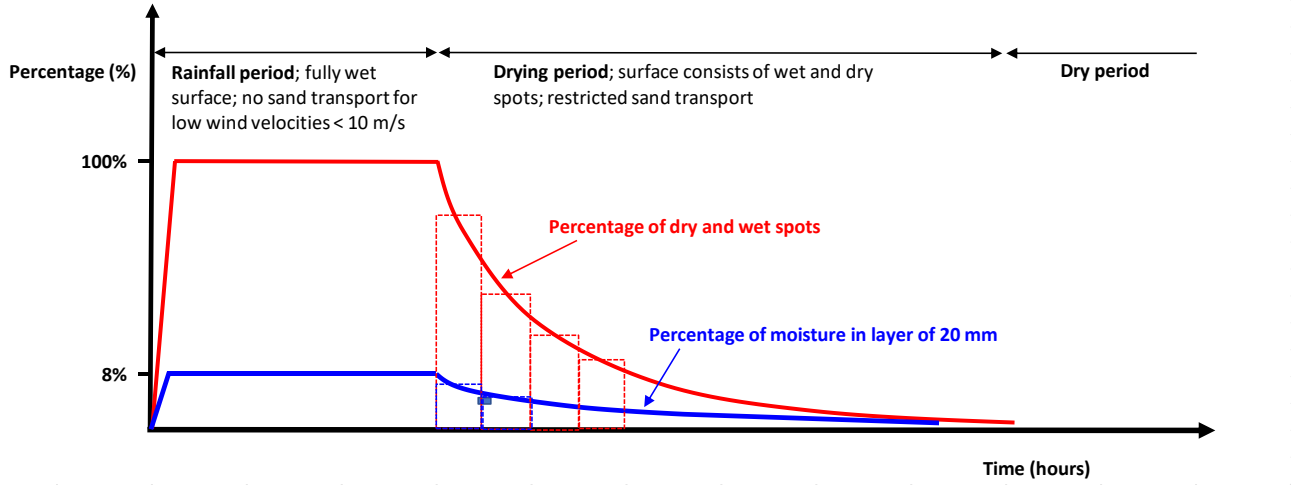

Figure 8.3.1 *Beach surface conditions during and after rainfall event*

To be able to predict the sand transport rate in conditions with dry and wet spots on the beach surface, it proposed to consider the transport in each period separately and then make a summation over all wet and dry conditions. This can be formulated as follows:

$$q_{s,total} = \sum^{N} [(\alpha_r q_{s,m,i}) t_{r,i} + \{(1-p_{m,i}/100)\, q_{s,d,i} + (p_{m,i}/100)\, q_{s,m,i}\}(T_{8\%-2\%,i}) + (q_{s,d,i}) t_{d,i}]/\rho_{d,sand} \quad (8.2)$$

with:

$q_{s,total}$= total sand transport over a series of events (m^3/m/events); $q_{s,d,i}$ = transport of sand (kg/m/s) over dry surface in event i; $q_{s,m,i}$ = transport of sand over moist surface (spot) in event i; α_r = reduction coefficient = 1 for wind velocities (at 1 m above surface) > 10 m/s and ; α_r = 0 for low wind velocities < 10 m/s; $t_{w,i}$ = duration of event i with a constant wind velocity $u_{w,i}$ and angle of of incidence θ_i; $t_{r,i}$ = duration of rainfall period in event i; $T_{8\%-2\%,i}$= duration of drying period after rainfall in event i based on results of Section 4.2 ($T_{8\%-2\%,i}$= $t_{w,i}$-$t_{r,i}$ if $t_{w,i}$-$t_{r,i}$<$T_{8\%-2\%,i}$); $t_{d,i}$=$t_{w,i}$ – $t_{r,i}$ – $T_{8\%-2\%,i}$= duration of dry period with dry surface in event i; p_d=percentage of dry spots, p_m= percentage of moist spots in the drying period (p_m+p_d=100%), N= total number of events.

Equation (8.2) consists of three terms. The first term represents the sand transport during periods with rainfall including splash-type transport (latter component is neglected in this study). Sand transport during rainfall is absent (α_r=0) for low wind velocities (at 1 m above surface) < 10 m/s and continues (α_r=1) for wind velocities > 10 m/s. The middle term represents the combined (restricted) transport over dry and wet spots during the drying period. The last term represents the transport of sand in dry beach conditions. The parameters to be specified as input data are: $t_{w,i}$, $t_{r,i}$, $T_{8\%-2\%,i}$, $p_{m,i}$, $w_{20mm,i}$. The effect of rainfall on sand transport is zero by setting $t_{r,i}$=$T_{8\%-2\%,i}$=$p_{wet,i}$= 0.

8.4 Sand transport predictions for Callantsoog beach, The Netherlands

8.4.1 General

The VR-transport equation (Section 2) has been used to compute the total sand transport at the beach of Callantsoog (The Netherlands) in 4 typical months representing the 4 seasons of spring (May), summer (August), autumn (December) and winter (February). Each month is assumed to be representative for 3 months to determine the annual sand transport.
The shore normal at Callantsoog makes a positive angle of about 100° to North. The beach is backed by high foredunes (height up to 15 m). The beach sand consists of sand with d_{50}=0.23 mm. The wind and rain conditions have been taken from a weather station at 5 km inland (De Kooy near Den Helder) from the beach. The adjustment coefficient (α_{ad}) due to limited fetch length is represented by α_{ad} =$[0.5b/(0.1+\cos\alpha)L_{ad}]^{0.6}$ with b= dry beach width= 70 m; α=wind incidence angle to shore normal; L_{ad}= maximum adjustment distance (=100 m) and $\alpha_{ad,maximum}$=1. This results in a variation of between α_{ad} =0.5 (shore normal) and α_{ad} =1 (shore parallel).

8.4.2 Rainfall at Callantsoog beach

The long term annual rainfall in The Netherlands is about 750 to 800 mm over a total period of 550 to 600 hours. The annual-average rainfall based on averaging the data of 10 years (2009-2019) at weather station De Kooy near the beach of Callantsoog is about 763 mm in about 585 hours (about 7% of the time), see **Table 8.4.2**. Thus, the annual-average rainfall intensity is 763/585=1.3 mm/hour. There are about 200 rainfall events per year with average duration of 585/200≅3 hours. **Figure 8.4.1** shows the annual wind and rain roses based on the data from **Table 8.4.2**.
The roses of dry periods with duration longer than 5 and 30 hours are also shown. These periods of dry weather yield a decreasing moisture content (upper layer of 20 mm) of about 2% in summer and in winter (**Tables 4.2.1, 4.2.2**).
Each annual season is represented by a characteristic month, as follows: February for the cold and dry winter season, May for spring season, August for summer season and December for the windy autumn season, see **Table 8.4.1**. Detailed data of these four characteristic months are given in **Annex A** and **B**.
The rainfall is lowest in February and highest in August. The duration of the rainfall is lowest (5% of the time) in May, and highest (10% of the time) in December. In the winter month February, the periods with dry weather larger than 30 hours (required to reduce the moisture content of the upper beach layer of 20 mm to 2%, see Figure 6) occur during about 35% of the time. Thus, reasonably dry beach sand available for wind transport occurs during 35% of the time in February.
In the summer month August, the periods with dry weather larger than 5 hours (required to reduce the moisture content of the upper beach layer of 20 mm to 2%) occur during about 75% of the time. Thus, reasonably dry beach sand available for wind transport occurs during 75% of the time in August

There are about 200 rainfall events (per year) with duration of about 3 hours; each rainfall event is followed by a drying period of 5 to 10 hours in summer and spring and 20 to 30 hours in autumn and winter resulting in a total period with restricted sand transport of 100 (3+7.5) + 100 (3+25)=3850 hours (with moisture levels in the range of 2% to 8%). Thus, the percentage of time with restricted sand transport is about 3850/(365x24) x 100%≅45%. This means that the effect of rainfall on wind transport is meaningful, but not dominant. Most of the time (55%), the beach is sufficiently dry for unrestricted or slightly restricted sand transport.

Month	Duration of wind in 4 classes				Rainfall data			
	0-5 m/s	5-9 m/s	9-15 m/s	> 15 m/s	total mm	duration hours	dry time > 5 hrs	dry time > 30 hrs
February (673 hrs)	310 hrs 46%	270 hrs 40%	85 hrs 13%	4.7 hr 0.7%	44 mm	57 hrs 8%	480 hrs 70%	245 hrs 35%
May (736 hrs)	450 60%	255 35%	35 5%	0 0%	59	34 5%	575 80%	360 50%
August (735 hrs)	465 63%	230 30%	35 5%	0.6 <1%	92	45 6%	540 75%	300 40%
December 740 hrs)	310 42%	275 37%	150 20%	6.1 0.8%	73	70 10%	455 60%	190 25%

Table 8.4.1 *Wind and rain data of 4 characteristic months (February, May, August and December); Station De Kooy (2009-2019)*

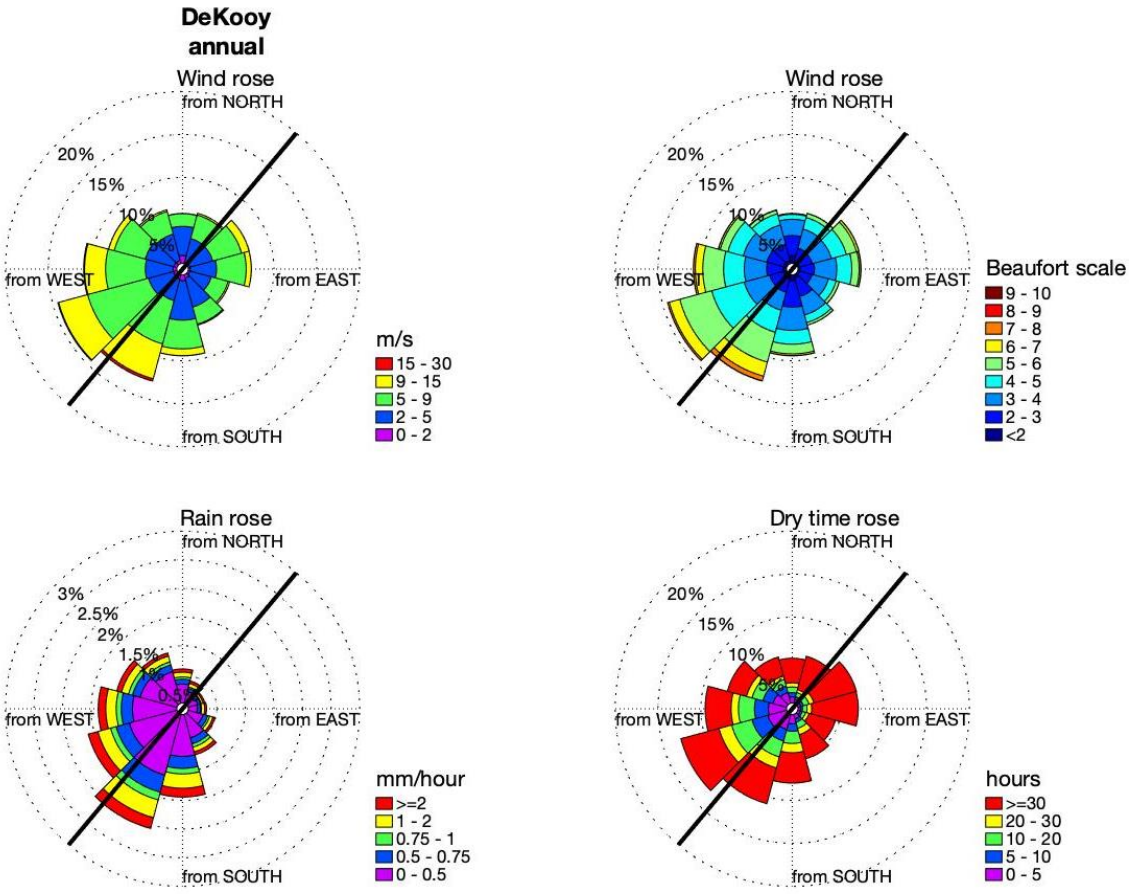

Figure 8.4.1 *Annual wind, rain and dry time; Station De Kooy (2009-2019)*

De Kooy Annual						
wind class->	0-2 m/s	2-5 m/s	5-9 m/s	9-15 m/s	>15 m/s	total
hours wind						
0-30	192.70	174.50	101.60	1.50	-	470.30
30-60	156.10	227.40	238.20	36.50	-	658.20
60-90	167.40	220.00	248.60	42.80	0.50	679.30
90-120	139.40	185.50	140.70	5.70	-	471.30
120-150	207.90	172.50	74.30	2.40	-	457.10
150-180	299.90	250.50	202.50	24.40	0.50	777.80
180-210	237.10	167.70	302.30	177.90	9.70	894.70
210-240	172.40	272.60	666.90	249.20	4.70	1 365.80
240-270	201.90	229.30	430.40	163.40	5.90	1 030.90
270-300	199.00	235.20	270.90	61.30	1.60	768.00
300-330	202.60	234.90	185.70	17.70	0.50	641.40
330-360	219.80	165.10	70.80	1.00	-	456.70
total	**2 396.20**	**2 535.20**	**2 932.90**	**783.80**	**23.40**	**8 671.50**
hours rain						
0-30	7.84	5.92	8.69	0.88	-	23.33
30-60	4.55	4.49	7.99	3.95	-	20.98
60-90	4.90	5.40	9.16	1.90	-	21.36
90-120	3.78	9.26	9.56	1.01	-	23.61
120-150	9.13	11.89	12.15	1.78	-	34.95
150-180	12.15	21.12	33.44	8.16	0.20	75.07
180-210	10.45	14.76	39.98	38.00	3.08	106.27
210-240	7.52	16.37	42.29	29.34	0.66	96.18
240-270	8.12	11.43	28.52	15.88	0.76	64.71
270-300	9.14	10.38	20.58	7.95	0.26	48.31
300-330	8.76	12.40	15.01	2.76	0.10	39.03
330-360	11.17	10.34	8.71	0.31	-	30.53
total	**97.51**	**133.76**	**236.08**	**111.92**	**5.06**	**584.33**
mm rain						
0-30	13.11	9.76	10.41	1.17	-	34.45
30-60	5.63	5.06	7.88	3.52	-	22.09
60-90	7.44	7.70	10.37	0.89	-	26.40
90-120	4.09	8.11	6.25	1.36	-	19.81
120-150	12.06	13.57	11.89	2.17	-	39.69
150-180	17.24	21.46	33.57	8.07	0.41	80.75
180-210	16.87	19.85	53.79	41.32	2.80	134.63
210-240	8.23	18.19	64.67	38.37	0.86	130.32
240-270	12.36	16.88	45.16	25.41	1.22	101.03
270-300	14.37	16.17	28.95	13.45	0.39	73.33
300-330	9.90	18.46	24.99	4.71	0.30	58.36
330-360	13.84	14.40	12.62	0.44	-	41.30
total	**135.14**	**169.61**	**310.55**	**140.88**	**5.98**	**762.16**
Dry > 30 hours						
0-30	108.20	114.80	63.70	0.10	-	286.80
30-60	97.70	167.60	165.90	16.50	-	447.70
60-90	113.80	166.30	180.40	32.40	0.10	493.00
90-120	92.50	129.50	93.80	3.50	-	319.30
120-150	119.60	86.40	32.40	0.10	-	238.50
150-180	141.10	98.30	51.10	3.40	-	293.90
180-210	117.90	66.80	85.90	31.60	0.10	302.30
210-240	79.50	113.00	215.10	43.50	-	451.10
240-270	97.20	87.10	92.00	10.20	-	286.50
270-300	84.50	74.20	37.70	3.80	-	200.20
300-330	92.50	80.60	32.50	0.70	-	206.30
330-360	104.50	62.80	17.40	-	-	184.70
total	**1 249.00**	**1 247.40**	**1 067.90**	**145.80**	**0.20**	**3 710.30**
Dry > 5 hours						
0-30	158.70	147.30	76.90	0.10	-	383.00
30-60	137.70	205.80	213.60	25.40	-	582.50
60-90	151.30	205.10	224.50	38.80	0.10	619.80
90-120	126.40	162.80	117.60	4.00	-	410.80
120-150	179.10	133.20	50.30	0.10	-	362.70
150-180	251.20	184.70	119.10	10.60	-	565.60
180-210	198.90	120.30	187.00	85.30	2.50	594.00
210-240	140.50	209.10	475.60	138.70	0.90	964.80
240-270	164.90	172.60	270.20	75.80	1.60	685.10
270-300	151.40	166.70	134.30	23.60	0.50	476.50
300-330	156.50	159.90	81.70	5.00	-	403.10
330-360	169.20	107.30	34.50	-	-	311.00
total	**1 985.80**	**1 974.80**	**1 985.30**	**407.40**	**5.60**	**6 358.90**

Table 8.4.2 *Annual wind speed, direction, rain periods, rain intensity and dry periods; Station De Kooy (2009-2019, The Netherlands*

8.4.3 Effect of rainfall and wind modification on annual sand transport at Callantsoog beach

Effect of rainfall, moisture and beach drying

Sand transport predictions based on the VR-equation (Section 2) have been made for 4 characteristic months: spring (May), summer (August), autumn (December) and winter (February).

The wind and rain climate of each of the 4 months are schematized in 24 events with constant wind velocity, direction and rainfall based on available data. The measured wind and rainfall values (averages over 10 years) conditions are given in **Table 8.4.3** based on **Table 8.4.2**. The rainfall intensity is not used, as it is assumed that the splash-type sand transport during rainfall is negligibly small.
Unknown parameters are the duration of the drying period ($T_{8\%-2\%}$), the percentage of dry (p_d) and moist (p_m) spots at the beach in the drying period, and the moisture content (w_{20mm}) of the moist spots. The effect of these parameters was studied by defining various scenarios, see **Tables 8.4.4** and 8**.4.5**. Annual-integrated values are obtained by assuming that each month is representative for a season of 4 months, see **Table 8.4.5**.

The effect of rainfall on the total sand transport over one month is given in **Table 8.4.4** for various cases (schematizations for the drying period; percentage of wet spots on the beach and moisture levels).

The base Case (0) is defined by assuming that the sand transport over a dry and wet surface is the same (no effect of rainfall).

Case 1 assumes that there is no transport during rainfall and no restricted sand transport in the drying period resulting in a transport reduction of about 5% in May to 15% in December/February.

Case 3 is an extremely conservative case with a relatively long drying period, a high percentage of wet spots (>50%) and high moisture levels (>4%) during the drying period resulting in restricted transport with a reduction of about 30% in summer and 35% in winter. The drying period is represented by one condition (one histogram) for reasons of simplicity, but multiple histograms can be used as well.

The transport reductions are somewhat smaller in the drier months of May and August, see **Table 8.4.4**.
Annual-integrated values are obtained by assuming that each month is representative for 4 months, see **Table 8.4.5**.
Case 0: the net annual dune-ward transport is about 36 m^3/year (neglecting rainfall effects).
Case 2 and 3: the duneward sand transport is reduced to about 25 m^3/year (30% smaller).
Measured annual deposition values at the dune front due to onshore-directed wind transport in some years at the beach of Callantsoog (erosion and deposition are fluctuating over the years) are in the range of 10 to 15 m^3/year.
Thus, the predicted value of about 25 m^3/m/year is somewhat too high (over-predicted). Overprediction may occur as the wind data have been taken from an inland station neglecting the obstacle effects (height of the foredunes; about 10 to 15 m). De winter et al. (2019) have shown that the onshore winds at a beach backed by high foredunes are substantially reduced (maximum 50%).
The net annual alongshore transport to the North is about 52 m^3/year for the base case (neglecting rainfall effects) and 35 to 45 m^3/year (maximum 30% smaller) for the other cases with different rainfall and drying schematizations. The net alongshore transport is significantly higher than the dune-ward transport of sand, which is caused by the dominant winds from the south-west direction.
Summarizing, the effect of rain fall (moisture) on annual sand transport is maximum 30%.

Wind conditions		February		May		August		December	
Wind velocity at 10 m of event i (m/s)	Wind incidence angle i (°)	Duration of wind event i (hours)	Duration of rainfall in event i (hours)	Duration of wind event i (hours)	Duration of rainfall in event i (hours)	Duration of wind event i (hours)	Duration of rainfall in event i (hours)	Duration of wind event i (hours)	Duration of rainfall in event i (hours)
7	195; 15	18.0	1.33	10.0	1.1	10.8	2.0	27.3	3.0
7	225; 45	32.0	1.84	34.4	1.5	54.0	2.3	40.8	2.6
7	255; 75	18.3	1.62	19.2	1.2	34.5	1.5	31.6	2.12
7	285; 105	11.8	1.12	11.2	0.6	17.2	1.2	20.0	2.0
7	315; 135	6.8	0.77	15.0	0.5	5.8	1.0	13.0	1.1
7	345; 165	2.7	0.59	9.8	1.0	3.3	0.94	3.0	0.63
9	195; 15	9.1	0.66	5.0	0.54	5.4	0.91	13.6	1.55
9	225; 45	16.0	0.93	17	0.72	27.0	1.21	22.0	1.32
9	255; 75	9.1	0.81	9.5	0.61	17.0	0.71	15.3	1.1
9	285; 105	6.0	0.55	6.6	0.3	8.5	0.63	10.1	0.96
9	315; 135	3.3	0.38	7.4	0.23	2.9	0.46	6.5	0.61
9	345; 165	1.3	0.30	4.2	0.38	1.6	0.42	1.5	0.32
12	195; 15	27.5	6.09	5.9	0.84	2.1	0.52	50.0	8.92
12	225; 45	30.6	3.64	17.6	0.85	19.9	0.60	35.5	4.97
12	255; 75	11.9	1.82	3.9	0.47	8.1	0.35	34.1	2.27
12	285; 105	1.1	0.15	0.7	0.48	1.9	0.29	12.4	1.28
12	315; 135	0.5	0.41	0	0	0.5	0.09	3.9	0.47
12	345; 165	0	0	0	0	0.5	0.07	0.5	0.2
16	195; 15	3.2	0.64	0	0	0	0	3.3	1.29
16	225; 45	0.5	0.14	0	0	0.6	0	0.6	0.13
16	255; 75	0.5	0.15	0	0	0	0	1.0	0.03
16	285; 105	0	0	0	0	0	0	0.7	0.06
16	315; 135	0	0	0	0	0	0	0	0
16	345; 165	0	0	0	0	0	0	0	0
Total		210.2 hours	23.9 hours	177.4 hours	11.3 hours	221.6 hours	15.2 hours	346.7 hours	36.9 hours

Wind incidence angle (to North) from where the wind is coming and going to (180° difference)

Table 8.4.3 *Wind and rain conditions in February, May, August and December (2009-2019), Station De Kooy near beach Callantsoog, North-Holland, The Netherlands*

Cases	Duration of rainfall period (hours)	Duration drying period ($T_{8\%-2\%,i}$) (hours)	Percentage of wet spots at beach ($p_{m,i}$) (%)	Moisture content of wet spots (layer of 20 mm) (%)	Predicted sand transport during 1 month in onshore and alongshore direction (m^3/m)	Reduction of transport with respect to fully dry surface (%)
Feb0	0	0	0	0	2.8; 5.2	0; 0
Feb1	variable (Table 8.4.1 and 8.4.3)	0	0	0	2.5; 4.4	10%; 15%
Feb2	variable (Table 8.4.1 and 8.4.3)	15	50	4	2.0; 3.6	30%; 30%
Feb3	variable (Table 8.4.1 and 8.4.3)	15	75	5	1.7; 3.2	40%; 40%
Feb4	variable (Table 8.4.1 and 8.4.3)	30	50	4	2.0; 3.6	30%; 30%
Feb5	variable (Table 8.4.1 and 8.4.3)	30	30	3	2.1; 3.9	25%; 25%
May0	0	0	0	0	2.0; 2.2	0; 0
May1	variable (Table 8.4.1 and 8.4.3)	0	0	0	1.9; 2.1	5%; 5%
May2	variable (Table 8.4.1 and 8.4.3)	10	30	3	1.6; 1.8	20%; 20%
May3	variable (Table 8.4.1 and 8.4.3)	10	50	4	1.2; 1.4	40%; 40%
May4	variable (Table 8.4.1 and 8.4.3)	20	30	3	1.6; 1.7	20%; 20%
May5	variable (Table 8.4.1 and 8.4.3)	20	20	2	1.6; 1.8	20%; 20%
AUG0	0	0	0	0	2.5; 2.4	0; 0
AUG1	variable (Table 8.4.1 and 8.4.3)	0	0	0	2.4; 2.3	4%; 4%
AUG2	variable (Table 8.4.1 and 8.4.3)	5	30	3	2.0; 1.9	20%; 20%
AUG3	variable (Table 8.4.1 and 8.4.3)	5	50	4	1.8; 1.7	30%; 30%
AUG4	variable (Table 8.4.1 and 8.4.3)	10	30	3	2.0; 1.9	20%; 20%
AUG5	variable (Table 8.4.1 and 8.4.3)	10	20	2	2.1; 2.0	15%; 15%
DEC0	0	0	0	0	4.7; 7.6	0; 0
DEC1	variable (Table 8.4.1 and 8.4.3)	0	0	0	4.3; 6.3	10%; 15%
DEC2	variable (Table 8.4.1 and 8.4.3)	15	50	5	3.1; 4.9	35%; 35%
DEC3	variable (Table 8.4.1 and 8.4.3)	15	75	5	3.0; 4.8	35%; 35%
DEC4	variable (Table 8.4.1 and 8.4.3)	30	50	4	3.3; 5.1	30%; 30%
DEC5	variable (Table 8.4.1 and 8.4.3)	30	30	4	3.4; 5.3	30%; 30%

December= windiest month; August = wettest month; February= driest month

Table 8.4.4 *Predicted sand transport for various rainfall, drying periods and moisture levels in February, May, August and December (2009-2019)*

Cases		Predicted annual sand transport in duneward direction (m^3/year)	Predicted net annual sand transport in alongshore direction (m^3/year)
0	no effect of rainfall and moisture (no restrictions t_r=0; $T_{8\%-2\%}$=0, w_{20mm}=0)	36	52
1	restricted transport during rainfall (for light winds only) and no restricted sand transport in the drying period (w_{20mm}= 0)	33	45
2	restricted transport during rain; restricted transport in drying period with relatively short drying period; low percentage of moist spots (p_m>50%); low moisture levels (w_{20mm} >4%)	26	37
3	restricted transport during rain; restricted transport in drying period with relatively long drying period; high percentage of wet spots (p_m >50%); high moisture levels (w_{20mm} >4%)	23	33
4	restricted transport during rain; restricted transport in drying period with relatively long drying period; medium percentage of wet spots (p_m >50%); medium moisture levels (w_{20mm} >4%)	27	37
5	restricted transport during rain; restricted transport in drying period with relatively long drying period; medium percentage of wet spots (p_m >50%); low moisture levels (w_{20mm} >4%)	28	39

Table 8.4.5 *Effect of rain and beach drying on predicted annual sand transport at beach Callantsoog*

Wind modification effect

The VR-transport equation has been used to compute the total annual sand transport including the wind modification effects and the rainfall (moisture) effect at the beach of Callantsoog (The Netherlands).
The shore normal at Callantsoog makes a positive angle of 100° to North. The beach is backed by high foredunes (height up to 15 m). The beach sand consists of sand with d_{50}=0.23 mm and d_{90}=0.4 mm.
The wind and rain conditions are given in **Table 8.4.3**. The wind climate of each month is schematized in 24 events with constant wind velocity, direction and rainfall based on available data. The wind velocities at the beach are assumed to the somewhat higher than those at the inland station De Kooy (f_r=1.1). Equation (8.1) is used to represent the effect of the foredunes on the wind velocity at the beach. The results are given in **Table 4.8.6**.
Case 0A: inclusion of the inland-beach effect (f_r=1.1) leads to an increase of about 50% for the annual sand transport.
Case 0D: inclusion of the inland-beach effect (f_r=1.1) and a strong obstacle effect ($f_{o,m}$=0.7) leads to a decrease of 25% for the annual duneward sand transport. The annual longshore to the north shows an increase of 15% because the obstacle effect is weak for longshore directions.

Case 0E: inclusion of the obstacle effect only (no inland-beach effect on wind; no rain effect) leads to a reduction of 60% for the annual duneward sand transport.
Case 3C: inclusion of the obstacle effect (no inland-beach effect on wind) and inclusion of the rain effect leads to a reduction of 70% for the annual duneward sand transport. Comparing case 3C and Case 0A, the reduction is about 80%; duneward transport is factor 5 smaller.

The obstacle effect is stronger (60%) than the moisture effect (30%).

The relatively strong effect of the wind modification (inland-beach effect and the obstacle) using wind data from an inland wind station emphasizes the importance of long term wind measurements at the beach for accurate estimations of the annual wind transport.

Case	Effect of foredune (obstacle)	Total annual duneward sand transport for Case 1 (m^3/year)	Total net annual alongshore sand transport for Case 1 (m^3/year)
0	Excluding all effects (no rain effect; no wind modification effects; wind is taken from inland weather station)	36	52
0A	Including land-beach wind effect (fr=1.1); excluding obstacle effect; no rain effect	53 (+50%)	77 (+50%)
0B	Including land-beach effect (f_r=1.1) and including obstacle effect $f_{o,m}$=0.9; no rain effect	42 (+15%)	69 (+30%)
0C	Including land-beach effect (f_r=1.1) and including obstacle effect $f_{o,m}$=0.8; no rain effect	33 (-10%)	64 (+25%)
0D	Including land-beach effect (f_r=1.1) and including obstacle effect $f_{o,m}$=0.7; no rain effect	26 (-30%)	58 (+10%)
0E	Excluding land-beach effect (f_r=1) and including obstacle effect $f_{o,m}$=0.7; no rain effect	14 (-60%)	29 (-45%)
1B	Including land-beach effect (f_r=1.1); incl. obstacle effect $f_{o,m}$=0.7; incl. rain effect (Case 1)	24 (-35%)	49 (-5%)
3B	Including land-beach effect (f_r=1.1); incl. obstacle effect $f_{o,m}$=0.7; incl. rain effect (Case 3)	17 (-50%)	39 (-25%)
3C	Excluding land-beach effect (f_r=1); incl. obstacle effect $f_{o,m}$=0.7; incl. rain effect (Case 3)	11 (-70%)	25 (-50%)

Table 8.4.6 *Effect of wind modification and rainfall on wind transport at Callantsoog beach*

8.4.4 Effect of rainfall and wind modification on sand transport at Callantsoog beach in February 2020

Sand transport predictions based on the VR-method have been made for the storm month February 2020.
The wind and rain climate of this month is schematized in 28 events with constant wind velocity, direction and rainfall based on available data, see **Table 8.4.7**.

Wind conditions		**February 2020**	
Wind velocity at 10 m of event i (m/s)	**Wind incidence angle i (°)**	**Duration of wind event i (hours)**	**Duration of rainfall in event i (hours)**
7	195; 15	16	1
7	225; 45	30	5
7	255; 75	32	2.4
7	285; 105	35	2.1
7	315; 135	3	0.3
7	345; 165	0	0
9	195; 15	8	1
9	225; 45	15	2
9	255; 75	15	2
9	285; 105	17	2
9	315; 135	2	0.2
9	345; 165	0	0
13	195; 15	59	8.1
13	225; 45	106	15.8
13	255; 75	81	3.5
13	285; 105	20	2.4
13	315; 135	0	0
13	345; 165	0	0
17	195; 15	28	7.7
17	225; 45	5	1.4
17	255; 75	28	1.3
17	285; 105	0	0
17	315; 135	0	0
17	345; 165	0	0
19	195; 15	5	1
19	225; 45	5	1
19	255; 75	2	1
19	285; 105	2	1
Total		210.2 hours	23.9 hours

Wind incidence angle (to North) from where the wind is coming and going to (180° difference)

Table 8.4.7 *Wind and rain conditions in February 2020,*
Weather station De Kooy near beach Callantsoog, North-Holland, The Netherlands

The effect of rainfall and wind modification on the total sand transport over the month February 2020 is given in **Table 8.4.8**.

The base Case 0 is defined by assuming that the sand transport over a dry and wet surface is the same (no effect of rainfall and obstacle) resulting in a duneward sand transport of 17 m^3/m/month.
Case 1: including the effects of rainfall and wind modification, the wind transport reduces to about 9 m^3/m/month (reduction of 50%).
Case 2: the duneward sand transport reduces further to about 5 m^3/m/month (reduction of 70%) by including the wind modification effects.
Thus, the duneward sand transport in the storm month February 2020 is about 5 to 10 m^3/m/month (including all effects), which is much higher (factor 5) than the sand transport value of about 1 to 2 m^3/m/month (**Table 8.4.4**) in a normal month of February.
During the field measurements in February 2020 at the beach of Callantsoog, the author has observed deposition values at the dune toe in the range of 3 to 5 m^3/m over 3 weeks, which are of the same order of magnitude as the predicted dune ward sand transport.
The net longshore transport is much less affected (maximum 30%).

Case	Effect of rainfall and wind modification	Total net duneward wind transport in February 2020 (m^3/m/year)		Total net annual alongshore wind transport in February 2020 (m^3/m/year)	
		excluding rain	including rain	excluding rain	including rain
0	Rain: restricted transport during rain; restricted transport in drying period ($T_{8\%-2\%}$=30 hours; P_m=50%; w_{20mm}=4%) Wind modification: excluding land-beach effect (f_r=1); excluding obstacle ($f_{m,o}$=1);	17	13	26	20
1	Rain: restricted transport during rain; restricted transport in drying period ($T_{8\%-2\%}$=30 hours; P_m=50%; w_{20mm}=4%) Wind modification: including land-beach effect (fr=1.1); including obstacle ($f_{m,o}$=0.7 to 1)	11	9	29	21
2	Rain: restricted transport during rain; restricted transport in drying period ($T_{8\%-2\%}$=30 hours; P_m=50%; w_{20mm}=4%) Wind modification: including land-beach effect (fr=1.1); including obstacle ($f_{m,o}$=0.5 to 1)	7	5	25	18

Rain effect: drying period=30 hours; percentage wet spots= 50% and moisture level=4%
No rain: t_r=0, $T_{8\%-2\%=}$0, w_{20mm}=0

Table 8.4.8 *Effect of rain and wind modifications on wind transport at Callantsoog beach in February 2020*

8.5 Annual sand transport at Egmond beach including rainfall and wind modification

Similar predictions have been made for the beach of Egmond (d_{50}=0.25 mm; d_{90}=0.5 mm) based on the wind climate from weather station IJmuiden (15 km south of Egmond. This weather station at 15 km south of Egmond is situated on top of a short tower on the end of the southern harbour breakwater of IJmuiden and is openly exposed to winds from all sea directions ($f_r \cong 1$). The long term wind rose (winds at 10 m above surface) of IJmuiden is given in **Figure 8.5.1**.

The wind velocities at Egmond beach are assumed to the same as those at the station IJmuiden (f_r=1). The wind table used for Egmond beach based on the wind rose of IJmuiden is given in **Table 8.5.1**. The dominant wind direction is from south-west. About 43% of the time, the wind velocities are higher than 5 m/s and onshore-directed (from the sector west). About 4% of the time there is rain when the wind velocities are higher than 5 m/s and onshore-directed. The shore normal at Egmond makes a positive angle of 99° to North.
Equation (8.1) is used to represent the effect of the foredunes on the wind velocity at the beach. Equation (8.2) is used to represent the rainfall effect. The results are given in **Table 8.5.2**. It is clear that the obstacle effect has a very strong effect on the predicted sand transport. The sand transport is a factor of 3 smaller if the wind velocities at the beach are reduced by maximum 50% during shore-normal conditions ($f_{o,m}$=0.5). The duneward wind transport is reduced to 18 m³/m/year if the effects of rainfall and wind modifications both are included. This is a reduction of 80% with respect to Case 0 neglecting both effects (83 m³/m/year). Annual dune profile changes are of the order of 10 to 15 m³/m/year at Egmond beach (De Winter et al. 2020).

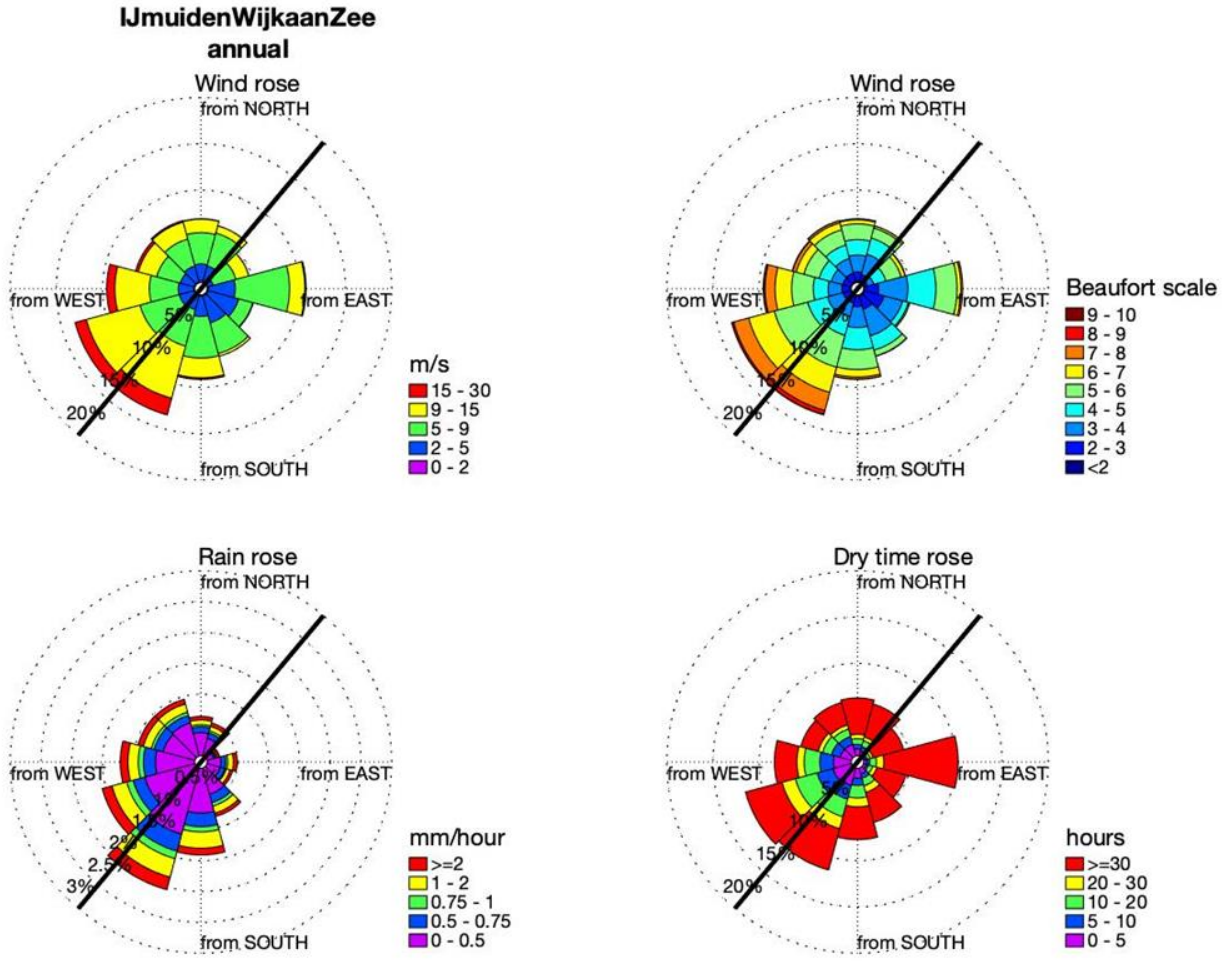

Figure 8.5.1 *Long term wind rose (at 10 m; 2009-2019) of coastal weather station IJmuiden, Netherlands*

Wind conditions		Year representative for 2007-2017	
Wind velocity at height of 10 m of event i (m/s)	**Wind incidence angle i (°)**	**Duration of wind event i (hours)**	**Duration of rainfall in event i (hours)**
7.5	195; 15	352	29
7.5	225; 45	449	25
7.5	255; 75	317	17
7.5	285; 105	240	16
7.5	315; 135	225	14
7.5	345; 165	286	14
13	195; 15	345	54
13	225; 45	532	50
13	255; 75	338	29
13	285; 105	163	21
13	315; 135	133	18
13	345; 165	96	12
17	195; 15	68	17
17	225; 45	99	15
17	255; 75	48	6.5
17	285; 105	30	8
17	315; 135	11	3.5
17	345; 165	4	1
19	195; 15	4	1
19	225; 45	4	1
19	255; 75	2	1
Total		3746 hours (43%)	353 hours (4%)

Wind incidence angle (to North) from where the wind is coming and going to (180° difference)

Table 8.5.1 *Wind and rain conditions in year, beach Egmond, North-Holland, The Netherlands*

Case	Effect of obstacle and rainfall	Total annual duneward wind transport (m^3/m/year)		Total net annual alongshore wind transport (m^3/m/year)	
		excluding rain	including rain	excluding rain	including rain
0	Rain: no restricted transport during rain; no restricted transport in drying period (t_r=0; w_{20mm}=0%) Wind modification: excluding land-beach effect (f_r=1); excluding obstacle ($f_{m,o}$=1);	83	65	106	81
1	Rain: restricted transport during rain; restricted transport in drying period ($T_{8\%-2\%}$=30 hours; P_m=30%; w_{20mm}=4%) Wind modification: encluding land-beach effect (fr=1); including obstacle ($f_{m,o}$=0.7 to 1)	41	32	79	59
2	Rain: restricted transport during rain; restricted transport in drying period ($T_{8\%-2\%}$=30 hours; P_m=30%; w_{20mm}=4%) Wind modification: encluding land-beach effect (fr=1); including obstacle ($f_{m,o}$=0.5 to 1)	26	18	66	49

Rain effect: drying period=30 hours; percentage wet spots= 30% and moisture level=4%

Table 8.5.2 *Effect of rain and wind modification on annual wind transport at Egmond beach*

9. References

Atherton, R.J., Baird, A.J. and Wiggs, G.F.S., 2001. Inter-tidal dynamics of surface moisture content on a meso-tidal beach. Journal of Coastal Research, Vol. 17, 482-489

Bagnold, RA., 1936. The Movement of Desert Sand. Proc. Royal Soc. London, Series A 157, 594-620.

Bagnold, R.A., 1937. The transport of sand by wind. Geographical J. Vol. 89, 409–38

Bagnold, R.A. 1941, 1954, 1973. The physics of blown sand and desert dunes. Methuen, New York.

Barchyn, T.E, Martin, R.L., Kok, J.F. and Hugenholtz, C.H., 2014. Fundamental mismatches between measurements and models in aeolian sediment transport prediction: the role of small-scale variability. Aeolian Research, Vol. 15, 245-251

Bauer, B.O., Davidson-Arnott, R.G.D., Hesp, P.A., Namikas, S.L., Ollerhead, J. and Walker, I.J., 2009. Aeolian sediment transport on a beach: surface moisture, wind fetch and mean transport. Geomorphology, Vol. 105, 106-116

Bauer, B.O., Davidson-Arnott, R.G.D., Walker, I.J., Hesp, P.A., Ollerhead, J., 2012, Wind direction and complex sedi-ment transport response across a beach-dune system. Earth Surface Processes and Landforms, 37, 1661–1677. https://doi.org/10.1002/esp.3306

Belly, P.Y., 1964. Sand Movement by Wind. U.S. Army Corps of Engineers, Technical Memorandum No 1, CERC, Washington, DC.

Brakenhoff, L.B., Smit, Y., Donker, J.J.A. and Ruessink, G., 2019. Tide-indiced variability in beach surface moisture: observations and modelling. Earth Surface Processes and Landforms, Vol. 44, 317-330

Campos, L.A.D., 2018. Quantification methods for aeolian sand transport on beaches. Doctoral Thesis, University of Twente, The Netherlands. Doi: 10.3990/1.9789036546676

Chepil, W.S., 1956. Influence of moisture on erodibility of soil by wind. Proc. Soil Sci. Soc. Am., 20, 288–292.

Comola, F., Kok, J.F., Chamecki, M. and Martin, R.L., 2019. The intermittency of wind-driven sand transport. Geophysical Research Letters, Vol. 46, 13, 13,430-13,440. Doi: 10.1029/2019GL085739

Cornelis, W.M., Gabriels, D., 2003. The effect of surface moisture on the entrainment of dune sand wind: an evaluation of selected models. Sedimentology Vol. 50, 771–790.

Cornelis, W.M., Gabriels, D., 2004. The effect of wind-driven rain on transport of sand by splash-saltation. Tropical Resource Management Papers, No. 50, ISBN 90-6754-843X

Davidson-Arnott, R.G.D., Bauer, B.O., Ollerhead, J., Hesp, P.A., Namikas, S. and Walker, I.J., 2005. Moisture and fetch effects on aeolian sediment transport rates during a fall storm, Greenwich dunes, Prince Edward Island. Canadian Coastal Conference.

Davidson-Arnott, R.G.D., Yang, Y., Ollerhead, J., Hesp., P.A. and Walker, I.J., 2008. The effects of surface moisture on aeolian sediment transport threshold and mass flux on a beach. Earth Surface Processes and Landforms, Vol. 33, 55-74. Doi:10.1002/esp.1527

De Grande, E. and De Moor, T., 2019. Influence of meteorological and environmental effects on aeolian transport (in Dutch). MSc. Thesis, KU Leuven, Belgium

Delgado-Fernandez, I., 2010. A review of the application of the fetch effect to modelling sand supply to coastal foredunes. Aeolian Research Vol. 2 (2-3), 61-70

Delgado-Fernandez, I., 2011. Meso-scale modelling of aelian sediment input to coastal dunes. Geomorphology Vol.130, 230-243

De Ploey, J., 1980. Some field measurements and experimental data on wind blown sands. In: Assessment of Erosion, edited by M. de Boodt and D. Gabriels, John Wiley & Sons, Chichester, 143-151.

De Ruiter, J.C.C., 1983. Incipient motion and pick-up of sediment as function of local variables. Report R657-XI, Delft Hydraulics, Delft, The Netherlands.

De Vries, S., Arens, S.M., De Schipper, M.A., and Ranasinghe, R., 2014. Aeolian sediment transport on a beach with a varying sediment supply. Aeolian Research Vol. 15, 235-244

De Vries, S. and Hoonhout, B., 2017. Field measurements on spatial variations in aeolian sediment availability at the sand motor mega nourishment. Aeolian Research Vo. 24, 93-104
De Winter, W., Donker, J., Sterk, G., Van Beem, J. and Ruessink, G., 2019. Regional versus local wind speed and direction at a narrow beach with a high and steep foredune. PlosOne (15(1) e-0226983; doi.org/10.1371/journal.pone.0226983
Dey, S., 2003. Threshold of sediment motion on combined transverse and longitudinal sloping beds. Journal of Hydraulic Research, Vol. 41, No. 4, 405-415.
Dong, Z., Liu, X. and Wang, X., 2002. Aerodynamic roughness of gravel surfaces. Geomorphology Vol 4, 17-31
Durán, O., Claudin, P. and Andreotti, B. 2011. On aeolian transport: grain-scale interactions, dynamical mechanisms and scaling laws. Aeolian Research. Vol. 3, 243–70
Einstein, H.A., 1950. The bed-load function for sediment transportation in open channel flow. Technical Bulletin No. 1026, U.S Department of Agriculture, Washington D.C., USA
Ellis, J.T., Li, B., Farrell, E.J. and Sherman, D.J., 2009. Protocols for characterizing aeolian mass-flux profiles. Aeolian Research 1, 19-26
Farrell, E.J. and Swann, C. 2016. Geomorphological Techniques. Chapter 3.1.4. British society for Geomorphology
Field, J.P. and Pelletier, J.D., 2018. Controlls on the aerodynamic roughness length and the grain size dependence of aeolian sediment transport. Earth Surface Processes and Landforms Vol. 43, 2616-2626. Doi: 10.1002/esp.4420
Gillies, J.A., Nickling, W.G. and King, J., 2006. Aeolian sediment transport through large patches of roughess in the atmospheric inertial layer. Journal of Geophysical Research Vol. 111, F02006. Doi: 10.1029/2005JF000434
Grass, A.J., 1973. Initial instability of fine sand bed. Journal of the Hydraulic Division, ASCE, Vol. 96, No. HY3
Guo, Z., Zobeck, T.M., Stout, J.E. and Zhang, K. 2012. The effect of wind averaging time on wind erosivity estimation, Earth Surf. Processes Landforms, 37(7), 797–802, doi:10.1002/esp.3222.
Han, Q., Qu, J., Liao, K., Zhu, S., Zhang, K., Zu, R. and Niu, Q., 2011. A wind tunnel study of aeolian sand transport on a wetted surface using sands from tropical humid coastal southern China. Environmental Earth Sciences, Vol. 64, 1375-1385; DOI 10.1007/s12665-011-0962-7
Hesp, P.A., Davidson-Arnott, R.G.D., Walker, I. Ollerhead, J., 2005. Flow dynamics over a foredune at Prince Edward Island, Canada. Geomorphology, 65, 71–84. https://doi.org/10.1016/j.geomorph.2004. 08.001
Ho, T., 2012. Experimental study of saltating particles in a turbulent boundary layer. Doctoral Thesis, University of Rennes, France
Hoonhout, B. and De Vries, S., 2017. Aeolian sediment supply at a mega nourishment. Coastal Engineering Vol. 123, 11-20
Hoonhout, B. and De Vries, S., 2019. Simulating spatiotemporal aeolian sediment supply at a mega nourishment. Coastal Engineering Vol. 145, 21-35
Horikawa, K., Hotta, S. and Kubota, S., 1982. Experimental study of blown sand on a wetted sand surface, Coastal Engineering in Japan, Vol. 25, 177-195,
Hotta, S., Kubota, S., Katori, S., Horikawa, K., 1984. Sand transport by wind on a wet sand surface. Proceedings 19th Coastal Engineering Conference. ASCE, New York, 1265–1281.
Jackson, N.L. and Nordstrom, K.F., 1997. Effects of time-dependent moisture content of surface sediments on aeolian transport rates across a beach Wildwood, New Yersey, USA. Earth Surface Processes and Landforms, Vol. 22, 611-621
Jackson, D. and Cooper, J., 1999. Beach fetch distance and aeolian sediment transport. Sedimentology, 517–522.
Jelgersma. S, De Jong, J, Zagwijn, W.H. and Van Regteren Altena, J.F., 1970. The coastal dunes of the western Netherlands; Geology, Vegetational history and Archaeology. Rijks Geologische Dienst RGD, Mededelingen Nieuwe Serie Vol. 21, 93-167
Kalinske, A.A., 1947. Movement of sediment as bed load in rivers. Trans. American Geophysical Union, Vol. 128, No. 4, USA

Kawamura, R., 1951. Study of sand movement by wind. Rep. Inst. Sci. Technol. Vol. 5, 95–112.
Kok, J.F., Parteli, E.J.R., Michaels, T.I. and Karam, D.B.., 2012. The physics of wind-blown sand and dust. Rep. Prog. Phys. Vol. 75, Doi:10.1088/0034-4885/75/10/106901
Lietaer, T., 2020. Validation of calculation model for aeolian sand transport (in Dutch). MSc. Thesis. University KU Leuven, Belgium
Lin, S.D., 2001. Water and Wastewater Calculations Manual, 2001, McGraw-Hill, New York.
Martin, R.L., Barchyn, T.E., Hugenholtz, C.H. and Jerolmack, D.J., 2013. Timescale dependence of aeolian sand flux observations under atmospheric turbulence. Journal of Geophysical Research: Atmospheres, Vol. 118, 9078-9092. Doi:10.1002/jgrd.50687
Martin, R.L. and Kok, J.F., 2017. Wind-invariant saltation heights imply linear scaling of aeolian saltation flux with shear stress. Science Advances Vol. 3 (6). Doi: 10.1126/sciadv.1602569
Martin, R.L. and Kok, J.F., 2018. Distinct thresholds for the initiation and cessation of aeolian saltation from field measurements. Journal of Geophysical Research: Earth Surface, Vol. 123, 1546-1564. Doi: 10.1029/2017JF004416
Martin, R.L., Kok, J.F., Barchyn, T.E., and Chamecki, M. 2018. High-frequency measurements of aeolian saltation flux: field-based methodology and applications. Aeolian Research. Doi: 10.1016/j.aeolia.2017.12.003
McKenna Neuman, C. and Sanderson, S., 2008. Humidity control of particle emissions in aeolian systems. Journal of Geophysical Research, Vol. 143, D02S14. Doi:10.1029/2007JF000780
McKenna Neuman, C., Li, B. and Nash, D., 2012. Micro-topographic analysis of shell pavements formed by aeolian transport in a wind tunnel simulation. Journal of Geophysical Research Vol. 117, F04003. Doi: 10.1029/2012JF002381
Meyer-Peter, E. and Mueller, R., 1948. Formulas for bed-load transport. Sec. Int. IAHR Congress, Stockholm, Sweden
Mulder, J. and Tonnon, P.K. 2011. Sand engine: background and design of a mega-nourishment pilot in The Netherlands. www.researchgate.net/publication/49115511
Nickling, W.G. and Ecclestone, M., 1981. The effects of soluble salts on the threshold shear velocity of fine sand. Sedimentology 28, 505-510
Nikuradse, J., 1933. Stromungsgesetz in rauhren rohren, Forschungsheft Arb. Ing. Wesen 361, Germany (English translation: Laws of flow in rough pipes; Tech. Rep. NACA Technical Memorandum, 1292).
Owen, P.R., 1964. Saltation of uniform grains in air. Journal of Fluid Mechanics, Vol. 20, 225-242
Paintal, A.S., 1971. Concept of critical shear stress in loose boundary open channels. Journal of Hydraulic Research, Vol. 9, No. 1
Pelletier, J.D. and Field, J.P., 2016 Predicting the roughness length of turbulent flows over landscapes with multi-scale microtopography. Earth Surface Dynamics Vol. 4, 391-404. Doi: 10.5194/esurf-4-391-2016
Pähtz, T. and Durán, O., 2018. The cessation threshold of nonsuspended sediment transport across aeolian and fluvial environments. Journal of Geophysical Research: Earth Surface, Vol. 123, 1638–1666. Doi.org/10.1029/2017JF004580
Pähtz, T. and Durán, O., 2020. Unification of aeolian and fluvial sediment transport rate from granular physics. Physical Review Letters. Doi: 10.1103/PhysRevLett.124.168001
Pähtz, T., Liu, Y., Xia, Y., Hu, P., He, Z. and Tholen, K., 2021. Unified model of sediment transport threshold and rate across weak and intense subaqueous bedload, windblown sand, and windblown snow. Journal of Geophysical Research: Earth Surface, Vol. 126. Doi. org/10.1029/2020JF005859
Pool, M.A. and Van der Valk, L., 1988. Volume computation of the Holland and Sealand young dunes (in Dutch). Kustgenese, Taskgroup 1000, Report BP10705, RGD, Haarlem, The Netherlands
Poortinga, A, Van Minnen, J., Keijsers, J., Riksen, M., Goossens, D. and Seeger, M., 2013. Measuring fast-temporal sediment fluxes with an analogue acoustic sensor: a wind tunnel study. Plos One, Volume 8, Issue 9, www.plosone.org

Raupach, M.R., 1992. Drag and drag partition on rough surfaces. Boundary Layer Meteorology Vol. 60, 375–395.
Saleh, A. and Fryrear, D.W., 1995. Threshold wind velocities of wet soils as affected by wind-blown sand. Soil Sci., 160, 304–309.
Sarre, R.D., 1988. Evaluation of aeolian sand transport equations using intertidal zone measurements, Saunton Sands, England, Sedimentology, Vol. 35, 671-679
Sherman, D.J., 1992. An equilibrium relationship for shear velocity and apparent roughness length in aeolian saltation. Geomorphology, Vol. 5, 419–431.
Sherman, D.J., 2020. Understanding wind-blown sand: six vexations. Geomorphology 366. Doi: 10.106/j.geomorph.2020.107193
Sherman, D.J. and Farrell, E.J. 2008. Aerodynamic roughness lengths over movable beds: comparison of wind tunnel and field data. Journal of Geophysical Research: Earth Surface Vol. 113; doi.org/ 10.1029/2007JF000784.
Sherman, D. J., Jackson, D. W. T., Namikas, S. L., and Wang, J., 1998. Wind-blown sand on beaches: An evaluation of models. Geomorphology, Vol. 22(2), 113–133. Doi: 10.1016/S0169-555X(97)00062-7
Sherman, D., Ellis, J.T., Li, B., Farrell, E.J., Maia, P. and Granja, H.M., 2013. Recalibrating aeolian sand transport models. Earth Surface and Landforms, Vol. 38, 169-178. Doi: 10.1002/esp.3310
Sherman, D.J., Swann, C. and Barron, J.D., 2014. A low-cost aeolian sand trap. Aeolian Research, Vol. 13, 31-34.
Stout, J. E., and Zobeck, T. M., 1997. Intermittent saltation. Sedimentology, Vol. 44 (5), 959–970
Strypsteen, G., 2019. Monitoring and modelling aeolian sand transport at the Belgian coast. Doctoral Thesis, KU Leuven, Belgium.
Strypsteen, G., Van Rijn, L.C. and Rauwoens, P., 2021. Comparison of equilibrium sand transport rate model predictions with an extended dataset of field experiments at dry beaches with long fetch distance. Journal of Aeolian Research
Strypsteen, G., Van Rijn, L.C., Hijma, M.P. and Lodder, Q., 2021. Reducing aeolian sand transport and beach erosion by using armour layer of coarse materials. Coastal Engineering, Vol. 166.
Svasek, J.N. and Terwindt, J.H.J., 1974. Measurements of sand transport by wind on a natural beach. Sedimentology, Vol. 21, 311-322
Tan, L., Zhang, W., Qu, J., Zhang, K., An, Z. and Wang, X., 2013. Aeolian sand transport over Gobi with different gravel coverages under limited sand supply: a mobile wind tunnel investigation. Aeolian Research 11, 67-74
Udo, K., Kuriyama, Y. and Jackson, D.W.T., 2008. Observations of wind-blown sand under various meteorological conditions at a beach. Journal of Geophysical Research Vol. 113, F04008. Doi: 10.1029/2007JF00936
Ungar, J.E. and Haff, P.K., 1987. Steady state saltation in air. Sedimentology, Vol. 34, 289-299
Van Dijk, P.M., Stroosnijder, L. and De Lima, J.L.M.P., 1996. The influence of rainfall on transport of beach sand by wind. Earth Surface Processes and Landforms, Vol. 21, 341-352
Valance, A., Rasmussen, K.R., Moctar, A.O.E and Dupont, P., 2015. The physics of aeolian sand transport. Comptes Rendus Physique, Elsevier Masson, Vol. 16 (1), 1-13. Doi: 10.1016/j.crhy.2015.01.006
Van der Wal, D., 1998. The impact of the grain-size distribution of nourishment sand on aeolian sand transport. Journal of Coastal Research, 14, 620-631
Van Rijn, L.C., 1982. Equivalent roughness of alluvial bed. Journal of Hydraulics Division, ASCE, Vol. 108, Hy 10, 1215-1218.
Van Rijn, L.C., 1984. Sediment Transport, Part III: Bed Forms and Alluvial Roughness. Journal of Hydraulic Engineering, ASCE, Vol. 110, No. 12.
Van Rijn, L.C., 1987. Mathematical modelling of morphological processes in the case of suspended sediment transport. Doctoral Thesis, Civil Engineering Department, Delft University of Technology, Delft, The Netherlands
Van Rijn, L.C., 1993. Principles of sediment transport in rivers, estuaries and coastal seas. AquaPublications, The Netherlands (www.aquapublications.nl)
Van Rijn, L.C., 2006/2012. Principles of sediment transport in rivers, estuaries and coastal seas, Part II. AquaPublications, The Netherlands (www.aquapublications.nl)

Van Rijn, L.C., 2007. Unified view of sediment transport by currents and waves, I: Initiation of motion, bed roughness, and bed-load transport. Journal of Hydraulic Engineering, 133(6), 649-667.
Van Rijn, L.C., 2007. Unified view of sediment transport by currents and waves, II: Suspended transport. Journal of Hydraulic Engineering, 133(6), 668-389.
Van Rijn, L.C., 2007. Unified view of sediment transport by currents and waves, III: Graded beds. Journal of Hydraulic Engineering, 133(7), 761-775.
Van Rijn, L.C., 2011. Principles of fluid flow and surface waves in rivers, estuaries and coastal seas. AquaPublications, The Netherlands (www.aquapublications.nl)
Van Rijn, L. C., 2019. Aeolian sand transpoprt processes, Part 1. Retrieved from https://www.leovanrijn-sediment.com/papers/Aeoliansandtransport2018.pdf
Van Rijn, L. C., 2020. Aeolian transport and erosion at the Prins Hendrik site, Texel. www.leovanrijn-sediment.com
Van Rijn, L.C. and Strypsteen, G., 2020. A fully predictive model for aeolian sand transport. Coastal Engineering, Vol. 156
Wiggs, G.F.S., Livingstone, I., Warren A., 1996. The role of streamline curvature in sand dune dynamics: evidence from field and wind tunnel measurements. Geomorphology,17,29–46. https://doi.org/10.1016/ 0169-555X(95)00093-K
Wiggs, G.F.S., Baird, A.J. and Atherton, R.J., 2004. Thy dynamic effects of moisture on the entrainment and transport of sand by wind. Geomorphology 59, 13-30
Yalin, M.S., 1972. Mechanics of sediment transport. Pergamon Press
Yang, Y. and Davidson-Arnott, R.G.D., 2005. Rapid measurements of surface moisture content on a beach. Journal of Coastal Research, Vol. 21, No. 3, 447-452
Yang, Y, Liu, L., Shi, P., Zhang, G., Xiong, Y., Lyu, Y., Guo, L., Liang, B., Zhao, M., Dai, J., Zuo, X, and Han, X., 2019. Aerodynamic grain-size distribution of blown sand. Sedimentology, Vol. 66, 590-603
Zhang, C.L., Zou, X.Y., Gong, J.R., Liu, J.R. and Liu, Y.Z., 2004. Aerodynamic roughness of cultivated soil and its influences on soil erosion by wind in a wind tunnel. Soil and Tillage Research Vol. 75, 53-59

Annex A: *Roses of wind speed, direction, rain periods, rain intensity and dry periods; Station De Kooy (2009-2019)*

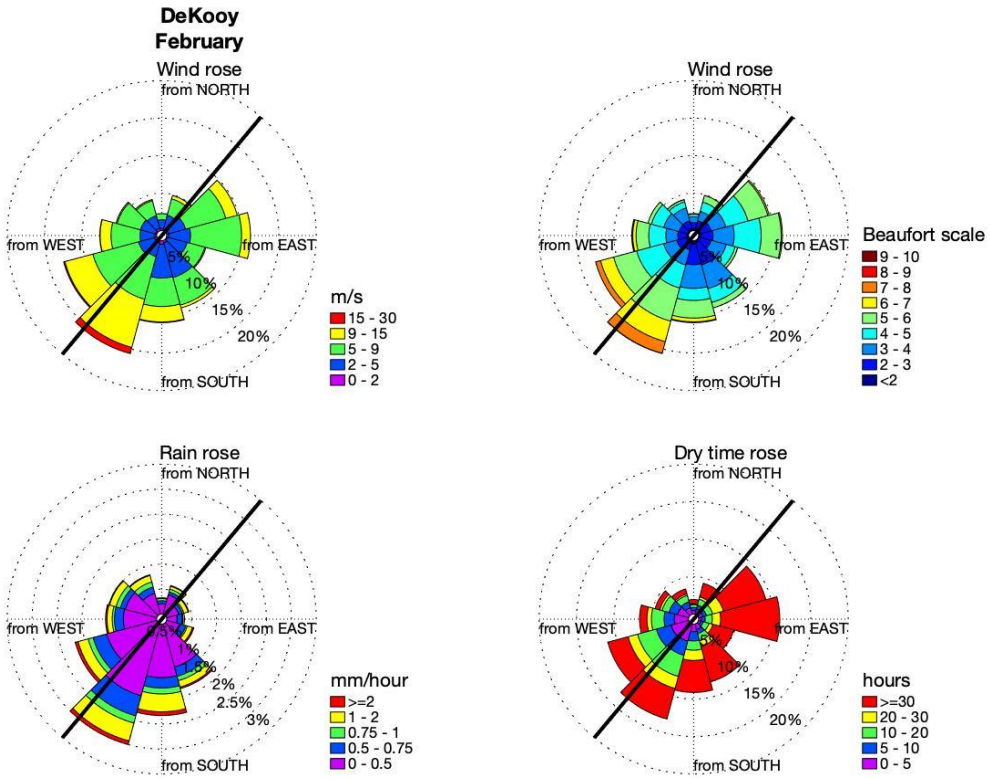

DeKooy
May

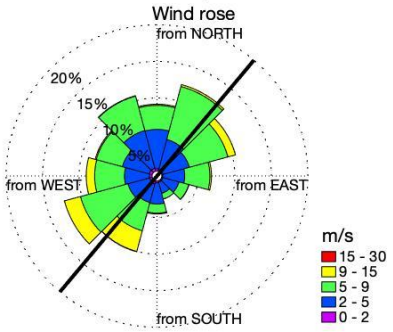
Wind rose
from NORTH
20%
15%
10%
5%
from WEST
from EAST
from SOUTH
m/s
15 - 30
9 - 15
5 - 9
2 - 5
0 - 2

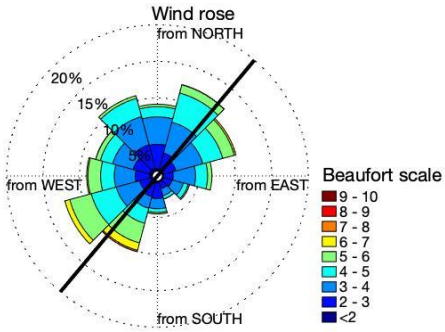
Wind rose
from NORTH
20%
15%
10%
5%
from WEST
from EAST
from SOUTH
Beaufort scale
9 - 10
8 - 9
7 - 8
6 - 7
5 - 6
4 - 5
3 - 4
2 - 3
<2

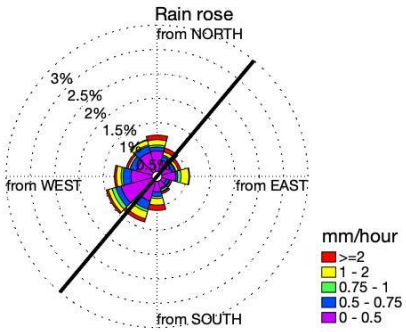
Rain rose
from NORTH
3%
2.5%
2%
1.5%
1%
from WEST
from EAST
from SOUTH
mm/hour
>=2
1 - 2
0.75 - 1
0.5 - 0.75
0 - 0.5

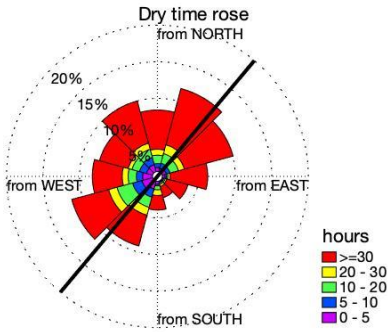
Dry time rose
from NORTH
20%
15%
10%
5%
from WEST
from EAST
from SOUTH
hours
>=30
20 - 30
10 - 20
5 - 10
0 - 5

DeKooy
August

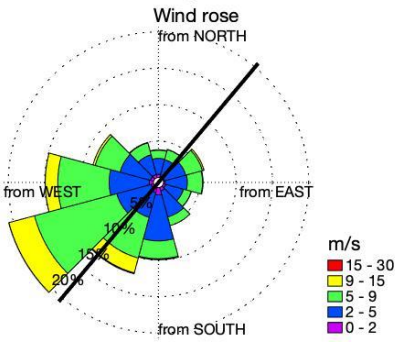

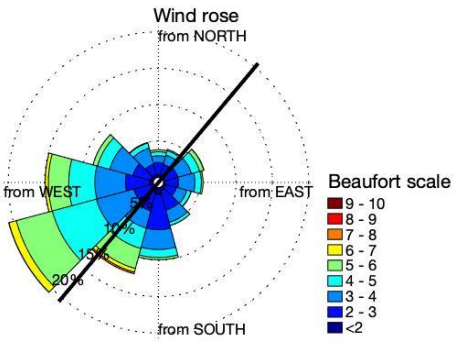

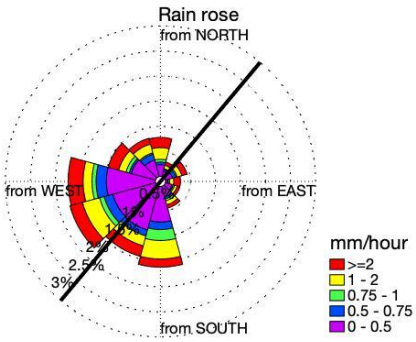

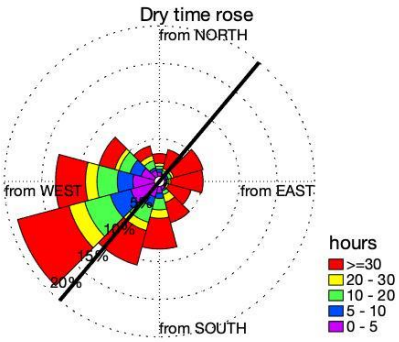

DeKooy
December

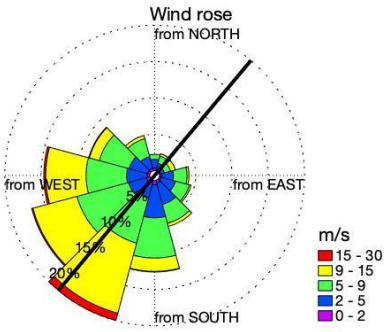

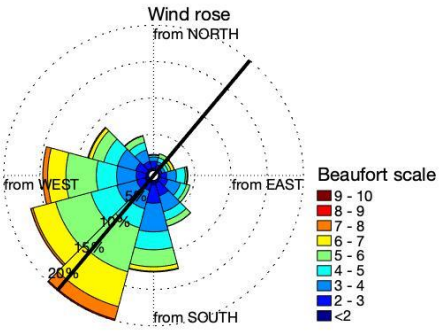

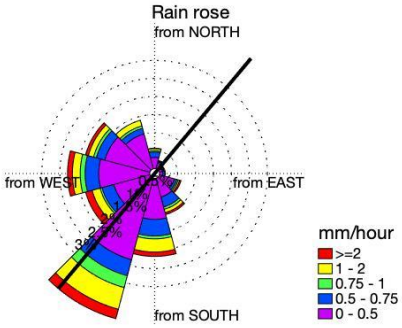

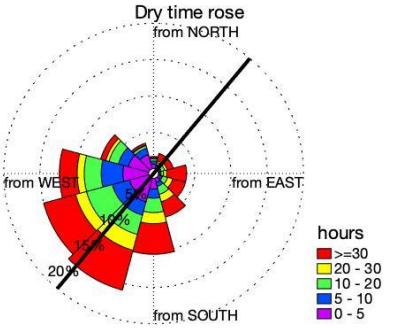

Annex B: *Data of wind speed, direction, rain periods, rain intensity and dry periods; Station De Kooy (2009-2019)*

De Kooy February

wind class->	0-2 m/s	2-5 m/s	5-9 m/s	9-15 m/s	>15 m/s	total
hours wind						
0-30	8.70	6.90	7.40	0.50	-	23.50
30-60	11.80	13.50	27.80	3.20	-	56.30
60-90	13.50	18.20	48.00	4.50	-	84.20
90-120	9.80	13.30	16.40	0.50	-	40.00
120-150	18.40	19.40	9.70	0.50	-	48.00
150-180	24.90	25.30	26.40	5.20	0.50	82.30
180-210	11.80	13.60	27.10	27.50	3.20	83.20
210-240	9.80	15.20	48.00	30.60	0.50	104.10
240-270	10.20	9.80	27.40	11.90	0.50	59.80
270-300	8.80	11.80	17.80	1.10	-	39.50
300-330	10.00	14.90	10.10	0.50	-	35.50
330-360	7.10	5.40	4.00	-	-	16.50
total	**144.80**	**167.30**	**270.10**	**86.00**	**4.70**	**672.90**
hours rain						
0-30	0.70	0.26	1.31	0.04	-	2.31
30-60	0.66	0.39	1.29	0.30	-	2.64
60-90	0.91	0.49	0.40	0.48	-	2.28
90-120	0.28	0.64	0.78	0.07	-	1.77
120-150	0.81	1.45	1.30	0.35	-	3.91
150-180	0.95	2.97	5.03	2.41	0.10	11.46
180-210	0.38	0.87	1.99	6.09	0.64	9.97
210-240	0.60	1.36	2.77	3.64	0.14	8.51
240-270	0.32	0.47	2.42	1.82	0.15	5.18
270-300	0.32	0.56	1.67	0.15	-	2.70
300-330	0.76	1.14	1.15	0.41	-	3.46
330-360	0.45	1.02	0.89	-	-	2.36
total	**7.14**	**11.62**	**21.00**	**15.76**	**1.03**	**56.55**
mm rain						
0-30	0.59	0.05	0.75	0.01	-	1.40
30-60	0.39	0.30	1.01	0.14	-	1.84
60-90	0.57	0.26	0.23	0.34	-	1.40
90-120	0.15	0.48	0.35	0.02	-	1.00
120-150	0.25	1.07	1.33	0.47	-	3.12
150-180	0.55	1.74	3.40	1.85	0.16	7.70
180-210	0.26	0.60	2.08	4.55	0.61	8.10
210-240	0.55	0.67	1.55	3.61	0.19	6.57
240-270	0.30	0.58	2.21	1.57	0.18	4.84
270-300	0.28	0.73	1.38	0.23	-	2.62
300-330	0.51	1.02	1.58	0.33	-	3.44
330-360	0.31	0.70	0.65	-	-	1.66
total	**4.71**	**8.20**	**16.52**	**13.12**	**1.14**	**43.69**
Dry > 30 hours						
0-30	3.30	1.90	2.10	-	-	7.30
30-60	6.70	6.90	15.00	1.90	-	30.50
60-90	7.70	11.50	34.00	3.00	-	56.20
90-120	4.70	7.80	11.80	0.10	-	24.40
120-150	11.30	8.50	5.30	-	-	25.10
150-180	13.10	12.00	9.00	0.80	-	34.90
180-210	4.70	4.40	6.80	3.40	0.10	19.40
210-240	4.20	4.80	13.10	7.10	-	29.20
240-270	2.30	0.80	2.10	2.40	-	7.60
270-300	2.00	0.70	1.40	0.20	-	4.30
300-330	3.00	1.60	0.60	-	-	5.20
330-360	1.80	0.30	1.20	-	-	3.30
total	**64.80**	**61.20**	**102.40**	**18.90**	**0.10**	**247.40**
Dry > 5 hours						
0-30	6.00	4.50	4.40	-	-	14.90
30-60	9.50	11.10	23.90	2.60	-	47.10
60-90	11.60	16.10	45.50	3.90	-	77.10
90-120	8.60	11.70	14.80	0.30	-	35.40
120-150	15.40	14.80	7.50	-	-	37.70
150-180	21.90	18.30	17.80	1.50	-	59.50
180-210	9.80	9.80	19.00	13.20	1.40	53.20
210-240	7.60	10.50	34.00	19.00	-	71.10
240-270	7.80	6.60	14.00	5.80	-	34.20
270-300	6.00	6.30	7.20	0.20	-	19.70
300-330	7.10	8.20	4.80	-	-	20.10
330-360	5.10	2.30	1.70	-	-	9.10
total	**116.40**	**120.20**	**194.60**	**46.50**	**1.40**	**479.10**

De Kooy May

wind class->	0-2 m/s	2-5 m/s	5-9 m/s	9-15 m/s	>15 m/s	total
hours wind						
0-30	21.90	30.50	26.40	-	-	78.80
30-60	16.80	31.50	42.00	3.00	-	93.30
60-90	12.10	23.50	19.20	1.10	-	55.90
90-120	9.90	16.80	9.30	-	-	36.00
120-150	9.60	6.20	3.30	-	-	19.10
150-180	12.50	10.90	3.10	0.50	-	27.00
180-210	18.90	10.10	15.00	5.90	-	49.90
210-240	14.00	21.20	51.40	17.60	-	104.20
240-270	17.10	23.30	28.70	3.90	-	73.00
270-300	16.80	17.50	17.80	0.70	-	52.80
300-330	27.70	31.40	22.40	-	-	81.50
330-360	25.70	25.10	14.00	-	-	64.80
total	**203.00**	**248.00**	**252.60**	**32.70**	**-**	**736.30**
hours rain						
0-30	0.24	0.39	2.70	-	-	3.33
30-60	0.23	0.31	1.64	0.09	-	2.27
60-90	0.36	0.32	2.56	0.10	-	3.34
90-120	0.09	0.50	0.63	-	-	1.22
120-150	0.41	0.25	0.32	-	-	0.98
150-180	0.33	1.37	0.69	0.10	-	2.49
180-210	0.89	0.73	1.64	0.84	-	4.10
210-240	0.80	0.55	2.22	0.85	-	4.42
240-270	0.48	0.71	1.81	0.47	-	3.47
270-300	0.48	0.89	0.90	0.48	-	2.75
300-330	0.76	0.82	0.73	-	-	2.31
330-360	0.30	1.49	1.38	-	-	3.17
total	**5.37**	**8.33**	**17.22**	**2.93**	**-**	**33.85**
mm rain						
0-30	0.25	0.33	3.30	-	-	3.88
30-60	0.84	0.45	0.90	0.04	-	2.23
60-90	0.68	0.53	2.20	0.10	-	3.51
90-120	0.08	0.63	0.51	-	-	1.22
120-150	0.44	0.21	0.61	-	-	1.26
150-180	0.65	1.38	0.81	0.35	-	3.19
180-210	1.48	0.65	1.74	1.06	-	4.93
210-240	0.56	0.37	3.59	0.96	-	5.48
240-270	0.57	0.48	1.49	0.40	-	2.94
270-300	1.19	0.96	1.02	0.23	-	3.40
300-330	0.48	0.99	0.79	-	-	2.26
330-360	0.51	2.14	1.06	-	-	3.71
total	**7.73**	**9.12**	**18.02**	**3.14**	**-**	**38.01**
Dry > 30 hours						
0-30	13.70	19.60	15.10	-	-	48.40
30-60	11.50	22.30	24.30	2.00	-	60.10
60-90	8.50	19.80	10.70	0.80	-	39.80
90-120	7.90	14.10	7.20	-	-	29.20
120-150	5.90	4.80	2.10	-	-	12.80
150-180	5.20	5.10	1.10	-	-	11.40
180-210	10.50	4.60	5.70	0.90	-	21.70
210-240	8.50	10.10	20.10	4.10	-	42.80
240-270	10.00	14.10	9.20	0.20	-	33.50
270-300	8.90	8.80	4.20	-	-	21.90
300-330	17.80	20.80	8.60	-	-	47.20
330-360	17.00	12.80	5.90	-	-	35.70
total	**125.40**	**156.90**	**114.20**	**8.00**	**-**	**404.50**
Dry > 5 hours						
0-30	20.30	28.90	20.90	-	-	70.10
30-60	15.50	29.10	37.20	2.30	-	84.10
60-90	10.30	22.40	14.10	1.00	-	47.80
90-120	9.20	15.50	8.00	-	-	32.70
120-150	8.40	5.30	2.50	-	-	16.20
150-180	10.60	8.10	1.60	-	-	20.30
180-210	16.50	8.30	10.00	3.20	-	38.00
210-240	11.30	18.10	40.50	11.60	-	81.50
240-270	15.30	20.00	18.90	1.20	-	55.40
270-300	14.50	13.80	10.20	-	-	38.50
300-330	25.40	27.70	15.50	-	-	68.60
330-360	24.20	20.00	9.70	-	-	53.90
total	**181.50**	**217.20**	**189.10**	**19.30**	**-**	**607.10**

Note: Aeolian transport measurements
Date: 22 December 2023

www.leovanrijn-sediment.com

De Kooy August

wind class->	0-2 m/s	2-5 m/s	5-9 m/s	9-15 m/s	>15 m/s	total
hours wind						
0-30	14.20	6.90	4.40	0.50	-	26.00
30-60	14.40	15.40	11.40	0.70	-	41.90
60-90	15.30	12.90	9.70	-	-	37.90
90-120	13.80	15.10	6.90	0.50	-	36.30
120-150	18.40	11.40	1.90	-	-	31.70
150-180	39.40	18.10	8.40	-	-	65.90
180-210	30.30	15.70	16.20	2.10	-	64.30
210-240	20.20	36.00	81.00	19.90	0.60	157.70
240-270	26.00	32.80	51.50	8.10	-	118.40
270-300	26.40	27.40	25.70	1.90	-	81.40
300-330	13.00	19.80	8.70	0.50	-	42.00
330-360	15.50	8.40	4.90	0.50	-	29.30
total	**246.90**	**219.90**	**230.70**	**34.70**	**0.60**	**732.80**
hours rain						
0-30	0.63	0.62	1.08	0.07	-	2.40
30-60	0.30	0.35	1.07	0.30	-	2.02
60-90	0.20	0.34	1.29	-	-	1.83
90-120	0.34	0.66	0.08	-	-	1.08
120-150	0.79	0.38	0.35	-	-	1.52
150-180	1.09	1.99	2.64	-	-	5.72
180-210	0.97	2.05	2.91	0.52	-	6.45
210-240	0.78	1.09	3.51	0.60	-	5.98
240-270	0.68	1.70	2.21	0.35	-	4.94
270-300	0.82	1.26	1.93	0.29	-	4.30
300-330	0.67	1.88	1.46	0.09	-	4.10
330-360	1.40	1.29	1.36	0.07	-	4.12
total	**8.67**	**13.61**	**19.89**	**2.29**	**-**	**44.46**
mm rain						
0-30	2.20	1.67	1.88	0.07	-	5.82
30-60	0.72	0.71	1.63	0.90	-	3.96
60-90	1.17	1.46	2.88	-	-	5.51
90-120	0.27	1.06	0.15	-	-	1.48
120-150	2.52	0.78	0.84	-	-	4.14
150-180	1.51	2.22	2.61	-	-	6.34
180-210	2.44	3.11	4.63	0.49	-	10.67
210-240	1.33	2.60	9.43	1.01	-	14.37
240-270	2.76	3.14	6.21	1.57	-	13.68
270-300	1.66	4.17	2.88	0.93	-	9.64
300-330	1.69	3.45	2.57	0.42	-	8.13
330-360	1.44	2.45	3.65	0.23	-	7.77
total	**19.71**	**26.82**	**39.36**	**5.62**	**-**	**91.51**
Dry > 30 hours						
0-30	8.10	4.00	1.40	-	-	13.50
30-60	11.30	10.80	6.00	-	-	28.10
60-90	11.80	10.60	5.10	-	-	27.50
90-120	10.10	12.70	6.60	0.30	-	29.70
120-150	10.70	5.60	0.60	-	-	16.90
150-180	20.10	7.00	2.10	-	-	29.20
180-210	15.90	4.80	3.00	-	-	23.70
210-240	10.30	15.30	28.80	3.20	-	57.60
240-270	12.60	12.70	7.50	0.50	-	33.30
270-300	9.30	7.10	2.10	0.10	-	18.60
300-330	5.70	4.40	1.00	-	-	11.10
330-360	6.10	1.60	0.40	-	-	8.10
total	**132.00**	**96.60**	**64.60**	**4.10**	**-**	**297.30**
Dry > 5 hours						
0-30	12.30	5.30	1.70	-	-	19.30
30-60	13.50	14.00	9.40	-	-	36.90
60-90	13.70	12.10	7.00	-	-	32.80
90-120	12.40	13.90	6.60	0.30	-	33.20
120-150	15.70	9.90	1.20	-	-	26.80
150-180	34.70	12.10	2.90	-	-	49.70
180-210	26.10	10.60	8.70	0.90	-	46.30
210-240	16.40	28.80	58.80	13.00	0.50	117.50
240-270	21.30	25.10	31.00	3.50	-	80.90
270-300	19.60	18.40	12.00	0.20	-	50.20
300-330	10.00	13.50	2.90	-	-	26.40
330-360	11.60	5.40	1.20	-	-	18.20
total	**207.30**	**169.10**	**143.40**	**17.90**	**0.50**	**538.20**

De Kooy December

wind class->	0-2 m/s	2-5 m/s	5-9 m/s	9-15 m/s	>15 m/s	total
hours wind						
0-30	8.00	2.60	5.20	0.50	-	16.30
30-60	4.00	2.60	6.30	2.80	-	15.70
60-90	7.00	8.60	11.90	3.00	-	30.50
90-120	7.50	10.80	8.10	0.80	-	27.20
120-150	15.40	16.30	8.90	0.70	-	41.30
150-180	20.90	26.40	29.90	5.90	0.50	83.60
180-210	16.30	20.90	40.90	50.00	3.30	131.40
210-240	11.10	21.40	62.80	35.50	0.60	131.40
240-270	13.20	18.70	46.90	34.10	1.00	113.90
270-300	14.50	20.10	30.10	12.40	0.70	77.80
300-330	10.10	15.60	19.50	3.90	-	49.10
330-360	9.70	7.10	4.50	0.50	-	21.80
total	**137.70**	**171.10**	**275.00**	**150.10**	**6.10**	**740.00**
hours rain						
0-30	0.35	0.15	0.59	0.07	-	1.16
30-60	0.17	-	0.20	0.52	-	0.89
60-90	0.25	0.05	0.39	0.20	-	0.89
90-120	0.08	0.43	1.65	0.17	-	2.33
120-150	0.62	1.92	2.63	0.39	-	5.56
150-180	0.64	2.26	5.29	1.41	0.10	9.70
180-210	0.71	1.93	4.55	8.92	1.29	17.40
210-240	1.05	1.14	3.92	4.97	0.13	11.21
240-270	0.35	1.08	3.22	2.27	0.03	6.95
270-300	0.65	0.97	2.96	1.28	0.06	5.92
300-330	1.09	1.03	1.71	0.47	-	4.30
330-360	1.10	0.70	0.95	0.20	-	2.95
total	**7.06**	**11.66**	**28.06**	**20.87**	**1.61**	**69.26**
mm rain						
0-30	0.35	0.27	0.62	0.01	-	1.25
30-60	0.31	-	0.07	0.27	-	0.65
60-90	0.28	0.03	0.20	0.10	-	0.61
90-120	0.05	0.28	0.60	0.21	-	1.14
120-150	0.62	1.86	1.85	0.50	-	4.83
150-180	0.79	1.93	4.14	1.22	0.25	8.33
180-210	0.59	1.18	4.66	8.83	1.09	16.35
210-240	0.85	0.80	5.81	5.21	0.17	12.84
240-270	0.59	1.12	5.05	3.94	0.01	10.71
270-300	0.72	0.98	3.87	2.33	0.20	8.10
300-330	0.88	1.57	1.75	0.73	-	4.93
330-360	0.99	0.80	0.84	0.18	-	2.81
total	**7.02**	**10.82**	**29.46**	**23.53**	**1.72**	**72.55**
Dry > 30 hours						
0-30	1.70	0.80	2.20	-	-	4.70
30-60	1.20	0.80	4.60	0.10	-	6.70
60-90	4.80	5.40	7.90	-	-	18.10
90-120	5.00	4.30	2.80	0.60	-	12.70
120-150	8.20	5.00	2.50	0.10	-	15.80
150-180	10.50	7.80	4.60	1.40	-	24.30
180-210	6.60	9.50	7.10	12.60	-	35.80
210-240	3.40	7.50	19.10	8.10	-	38.10
240-270	5.70	5.40	10.80	2.20	-	24.10
270-300	1.60	4.30	0.50	0.70	-	7.10
300-330	0.90	0.60	1.40	0.30	-	3.20
330-360	1.50	-	-	-	-	1.50
total	**51.10**	**51.40**	**63.50**	**26.10**	**-**	**192.10**
Dry > 5 hours						
0-30	5.90	1.10	2.90	-	-	9.90
30-60	2.90	2.40	5.60	2.00	-	12.90
60-90	6.10	8.00	11.00	1.90	-	27.00
90-120	7.30	9.30	4.80	0.60	-	22.00
120-150	14.00	12.40	5.00	0.10	-	31.50
150-180	18.10	17.20	18.60	3.80	-	57.70
180-210	12.80	14.40	24.90	26.50	0.40	79.00
210-240	8.20	15.30	47.20	20.20	0.20	91.10
240-270	10.40	13.00	30.40	15.70	0.20	69.70
270-300	8.30	11.90	10.40	4.50	0.50	35.60
300-330	4.50	4.20	4.20	1.80	-	14.70
330-360	4.60	1.50	0.60	-	-	6.70
total	**103.10**	**110.70**	**165.60**	**77.10**	**1.30**	**457.80**